Alanine/EPR dosimetry for low to medium energy X-ray radiation processing control

Abbas Nasreddine

Université de Strasbourg

École Doctorale de Physique et Chimie-Physique (ED182)

Institut Pluridisciplinaire Hubert Curien – UMR7178

THÈSE présentée par :

Abbas NASREDDINE

soutenue le : **25 Septembre 2020**

pour obtenir le grade de : **Docteur de l'Université de Strasbourg**

Discipline/ Spécialité : Physique des rayonnements ionisants

Alanine/EPR dosimetry for low to medium energy X-ray radiation processing control

THÈSE dirigée par :

Dr. Ziad EL BITAR	Directeur de Recherches, Université de Strasbourg

RAPPORTEURS :

Dr. Peter SHARPE	Principal Research Scientist, National Physical Laboratory
Pr. Michel FROMM	Professeur, Université Franche Comté

AUTRES MEMBRES DU JURY :

Dr. Marie-Claude BORDAGE	Chargée de Recherches, Université Paul Sabatier
Pr. Rémi BARILLON	Professeur, Université de Strasbourg
Dr. Florent KUNTZ	Chef de Projet, Aerial

Dedicated to my beloved late Grandfather...

Acknowledgements

Here I am standing, after three years of reading, learning, thinking and experimenting, at the end of a long path, leading only to the beginning of an even longer, yet, more exciting and more challenging path. Three years have passed like a glimpse, yet, at then end, I find self evolved. This is why, by these few words, I would like to thank you for being a part of this journey.

To Ziad, I am very grateful to have met you and especially to have had you as my Ph.D director. I still remember the day when I had just came back from my summer vacation, and I received a call from Florent asking to schedule a meeting to discuss my masters internship application. I was very surprised because I was absolutely sure that I did not apply to any internship openings at the time, but it was you who sent my CV to Florent. The meeting went good, well I guess, and this long journey began, thanks to you! Because of you, I am here today! Thank you a lot for everything that you taught me, for being always here for me and especially for giving me this beautiful chance.

To Florent, I could not have been here today without you. You were always there for me, even when you were at the other end of the Earth. Thank you a lot for all what you have taught me in dosimetry, radiation processing, a little bit about fishing, but mostly, I thank you for every interesting discussion that we had. I would like to thank you as well for trusting me in all the different projects that we worked on. This taught me a lot of things that will surely be of use in the future.

To Alain, thank you for hosting me at Aerial during my masters internship but also during my Ph.D. Your confidence in me and your support played a big role in the achievement of this long journey. I would like to thank Florent and you for giving me the opportunity of a lifetime by letting me take a big role in the construction, installation, qualification and operation of a one in the world irradiation installation. It was an extremely challenging, yet, a very exciting project. I hope I was at your expectations.

To Peter and Michel, I would like to thank you very much for accepting to take a part in judging my work as reporters. I would like to extend these thanks to Marie-Claude and Rémi as well for accepting to examine my work. Thank you all as well for all our previous interesting meetings.

To my parents, my sisters, no words in the entire world can be sufficient to thank you. You have been always by my side, holding my hands, accompanying me throughout the difficulties of life since I was a little boy. Thank you for all the love, care, faith and support that you always gave me. Without you too, I would have never been here today, so thank you enormously for standing by me and for helping me realize all my dreams...

I would like to thank a lot all of the members of Aerial. You are like family to me! Thank you for your warm welcome and for all the good times that we have spent together. To Laura, Lysiane and Raphaël, I would like to thank you a lot for letting me take part of the crapoussins

teams, for all the fun that we had in our office, for all the 4 o'clock snacks but mostly, for all your kindness. A special thanks goes to Eric, Sébastien and Thomas for all your help and support that you have showed me since day one. You have played a big role in this work as well, so thank you very much! To Nicolas, it has been just over a year since we started to share the same office, but a year was enough to make an amazing friend! Thank you for everything that you taught me in radiation chemistry, for filling in my place during the manuscript writing period, but mostly, thank you for being the amazing person you are!

To all my, present and former, colleges at the IPHC laboratory, to Nicolas. A, Addil, AbdelMjid, Lena, Emilien, Julien, Matthias, Nicolas S., Séverine, Youbba, Halima and Pierre, thank you all for your warm welcome, for your support, guidance and for all the good moments that we had together. I wish you all the best of luck in your future endeavours.

To Anna Subiel and Peter Sharpe, I would like to thank you very much for welcoming me at NPL. Our collaboration was very helpful to my work. I wish you both lots of success in your future works and hope that our collaboration grows even stronger.

To my dearest friends, Hassan, Hussein and Khaled, you guys have been a big support for me but more importantly, you were and still are brothers to me. I would like to thank you all for all the amazing moments that we had together, for all the adventures that we went through, but mostly, thank you for always being who you are!

On behalf of my supervisors and myself, we would like to thank the Association Nationale de Recherche et Technologie (ANRT) for financing this thesis.

Contents

List of Figures

List of Tables

List of Abbreviations

Abbreviation	Designation
7OH-3CCA	7-hydroxy-coumarin-3-carboxylic acid
$\dot{D}$	Absorbed dose rate
D_{alnine}	Absorbed dose to the alanine dosimeter
D_{dos}	Absorbed dose to the dosimeter
D_w	Absorbed dose to water
D	Absorbed dose, Diffusion coefficient
AIEA	Agence Internationale de l'Energie Atomique
Al	Aluminium
ASTM	American Society for Testing and Materials
AAMI	Association for the Advancement of Medical Instrumentation
A	Atomic mass
Z	Atomic number
E_{avg}	Average energy
Q	Beam quality index
BIPM	Bureau International des Poids et Mesures
^{137}Cs	Caesium 137
CTA	Cellulose Tri-Acetate
CPE	Charged Particle Equilibrium
^{60}Co	Cobalt 60
Cu	Copper
3CCA	Coumarin-3-carboxylic acid
σ	Cross section, 1 standard deviation
$G(X)$	Cross-linking G-value
DC	Direct Current
DUR	Dose Uniformity Ratio

E_{eff}	Effective energy
EB	Electron Beam
EPR	Electron Paramagnetic Resonance
E	Energy
μ_{att}	Energy attenuation coefficient
r	EPR response
FWT	Far West Technologies
FAO	Food and Agriculture Organization of the United States
G-value	Free radical creation yield
ν	Frequency
HVL	Half Value Layer
HPLC	High Performance Liquid Chromatography
HV	High voltage
IQ	Installation Qualification
IPEMB	Institute of Physics and Engineering in Medicine and Biology
IAEA	International Atomic Energy Agency
ISO	International Organization for Standardisation
IBA	Ion Beam Applications
K	Kerma
LET	Linear Energy Transfer
B_0	Magnetic field
μ_{tr}/ρ	Mass energy transfer coefficient
μ_{en}/ρ	Mass-energy absorption coefficient
NIST	National Institute of Standards and Technology
NPL	National Physical Laboratory
OQ	Operational Qualification
H_{pp}	Peak to peak height of the EPR signal
PQ	Performance Qualification
$\psi(E)$	Photon energy fluence distribution
$\phi(E)$	Photon fluence distribution
PTB	Physikalisch-Technische Bundesanstalt
PMMA	PolyMethyl MethAcrylate
PSDL	Primary Standard Dosimetry Laboratory
m_s	Projection of electron spin state
RF	Radio Frequency

Q_0	Reference beam quality index
RPE	Résonance Paramagnétique Electronique
θ	Scattering angle
$G(S)$	Scission G-value
SSDL	Secondary Standard Dosimetry Laboratory
Ω	Solid angle
c_p	Specific heat capacity
SAR	Stable Alanine Radical
SIT	Sterile Insect Technique
SAL	Sterility Assurance Level
Sn	Tin
UV	Ultra Violet
USFDA	United States Food and Drug Administration
λ	Wavelength
XRT	X-Ray Tube

Résumé en français

La dosimétrie Alanine/RPE pour le contrôle du procédé d'irradiation par des rayons X de faible à moyenne énergie

Introduction

L'irradiation par des rayons X de faible à moyenne énergie (jusqu'à 320 keV) devient de plus en plus une technique répandue qui remplace des irradiations réalisées par des sources radioactives (^{137}Cs ou ^{60}Co). Plusieurs applications sont concernées, telles que l'irradiation des poches de sang, la stérilisation de dispositifs médicaux, la décontamination des produits alimentaires ou encore la stérilisation de larves d'insectes.

Afin d'assurer que la bonne dose de rayonnement a été délivrée au produit, un dosimètre est placé sur celui-ci pendant l'irradiation. Un des types de dosimètres utilisés pour ces applications est le dosimètre à l'alanine. Ce dosimètre se présente sous forme d'une pastille cylindrique de 4 mm de diamètre et 2.3 mm d'épaisseur, avec une composition chimique d'environ 91.6 % d'alanine et de 8.4 % de liants. Le dosimètre alanine a des propriétés d'absorption d'énergie équivalentes à celles de l'eau, milieu de référence, pour des irradiations par des rayons X d'énergie supérieure à 200 keV. Dans le cas d'irradiations à des énergies inférieures à 200 keV, ce dosimètre perd son équivalence à l'eau et peut ainsi conduire à une sous-estimation de la vraie dose délivrée au produit[7, 50, 95, 122, 149, 150, 153].

Le but de cette thèse est de développer des méthodes et des protocoles expérimentaux permettant d'établir des facteurs correctifs à appliquer à la réponse du dosimètre alanine afin de pouvoir estimer la vraie dose déposée dans le produit traité par irradiation.

Problématique

Dans le cas des applications de l'irradiation aux rayons X de faible à moyenne énergie, une partie importante des rayons X possède une énergie inférieure à 200 keV, seuil à partir duquel la différence de coefficient d'absorption massique (μ_{en}/ρ) entre l'eau et la matière du dosimètre devient significative[54]. Un facteur de correction doit ainsi être déterminé pour chacun des spectres d'énergie générés par les équipement d'irradiation mis en œuvre.

L'alanine est une acide aminée. Suite à son exposition à des rayonnements ionisants, une création de différentes espèces radicalaires stables en fonction du temps a lieu au sein du dosimètre. La quantification des ces espèces radicalaires radio-induites se fait par Résonance Paramagnétique Électronique (RPE). Il s'agit dans la pratique de déterminer un coefficient correctif à appliquer à la réponse de la mesure RPE du dosimètre alanine converti en dose à travers une courbe d'étalonnage au ^{60}Co (énergie moyenne de 1250 keV), mais utilisée lors des irradiations par des champs de rayonnement X de faible à moyenne énergie. La réponse d'un dosimètre alanine est définie comme le rapport de la hauteur du pic central du signal RPE (H_{pp}), illustré dans la figure 1, et la masse du dosimètre.

Ainsi, une des barrières à surmonter est l'attribution, à chaque générateur de rayons X, d'une grandeur caractéristique de son spectre en énergie qui permettrait de définir le coefficient de correction à appliquer à la réponse des pastilles d'alanine. La figure 2 montre un diagramme qui récapitule la logique adoptée pour étudier la réponse relative de l'alanine aux rayons X d'une qualité Q comparée à sa réponse à une qualité de rayonnement de référence Q_0.

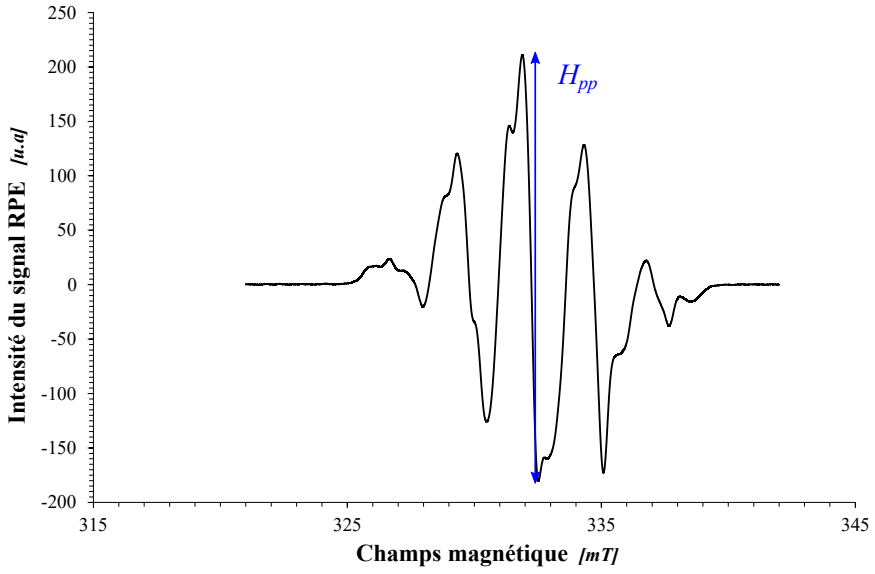

FIGURE 1: Le signal RPE d'un dosimètre alanine irradié à une dose de 100 Gy avec des rayons X générés avec un potentiel de 100 kV.

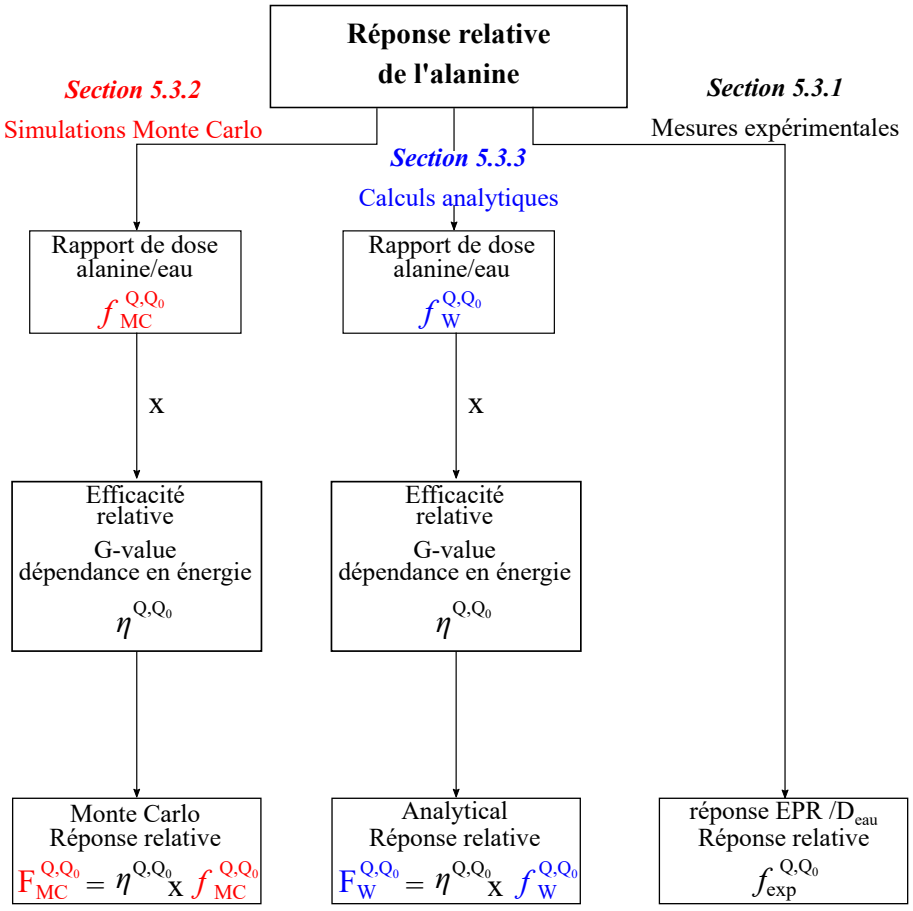

FIGURE 2: Diagramme qui montre la logique adoptée pour étudier la réponse relative de l'alanine aux rayons X de faible à moyenne énergie.

La détermination de la réponse relative des dosimètres alanine

La réponse du dosimètre alanine, en fonction de l'énergie des rayons X de faible à moyenne énergie, a été étudiée dans plusieurs travaux de recherche par Zeng et McCaffrey[153], Waldeland et al.[150], Waldeland et Malinen[149], Anton et Büermann[7], Khoury et al.[95], Nasreddine et al.[122], Hjørringgaard et al[50] et Soliman et al.[141].

Tous ces travaux ont bien montré que l'utilisation du dosimètre alanine, étalonné avec une source de ^{60}Co, dans le cadre des irradiations avec des rayons X de faible à moyenne énergie, pourrait induire jusqu'à 35% de sous-estimation de la vraie dose déposée dans l'eau.

L'énergie effective du spectre X est considérée comme qualité des faisceaux de rayons X, selon les recommandations de l'Agence Internationale de l'Energie Atomique (AIEA) dans le rapport technique TRS398[58]. Une liste de qualités de faisceaux de rayons X, détaillée dans le tableau 2, a été établie afin de déterminer la réponse relative du dosimètre alanine à ces qualités comparée à sa réponse aux rayons gamma d'une source d'étalonnage de ^{60}Co. Cette liste couvre des

énergies effectives allant de 27.5 keV à 168 keV. Des irradiations ont été réalisées à Aerial ainsi qu'au National Physical Laboratoty (NPL-Teddington, UK).

		Filtration externe					Spécificateur de qualité de faisceau	
Site d'irradiation	HV [kV]	Al [mm]	Cu [mm]	Sn [mm]	Solid Water [mm]	PMMA [mm]	HVL_1 [kV]	E_{eff} [keV]
Aerial	50	2.39	0	0	0	5	1.81	27.5
Aerial	70	2.88	0	0	0	5	2.65	31.9
Aerial	90	3.35	0	0	0	5	3.64	36.3
Aerial	100	1.43	0	0	0	5	2.57	31.5
Aerial	100	3.84	0	0	0	5	4.32	39.2
Aerial	100	4.95	0	0	0	5	4.93	41.7
Aerial	90	0.96	0	0	0	0	1.52	25.8
Aerial	100	1.43	0	0	0	0	2.18	29.5
Aerial	100	3.84	0	0	0	0	4.06	38.1
NPL	135	1.2	0.27	0	20	0	9.01	58.9
NPL	280	1	0.26	1.5	20	0	19.6	168

TABLE 2: Liste des différentes qualités de rayons X utilisées dans ce travail.

Afin d'aboutir à ce but, trois méthodes distinctes ont été développée durant ce travail de thèse. Ces méthodes servent à déterminer la réponse relative du dosimètre alanine aux rayons X de faible à moyenne énergie par différentes techniques. Le facteur correctif, à appliquer à la réponse du dosimètre d'alanine, peut être relié directement aux réponses relatives déterminées par cette relation:

$$k_{corr}^{Q,Q_0} = \frac{1}{f^{Q,Q_0}} \tag{1}$$

avec k_{corr}^{Q,Q_0} le facteur correctif à appliquer à la réponse du dosimètre alanine et f^{Q,Q_0} la réponse relative du dosimètre alanine aux rayons X de faible à moyenne énergie de qualité Q comparée à sa réponse à une qualité d'étalonnage Q_0. Ainsi, la vraie dose équivalente à l'eau pour une qualité de faisceau de référence Q_0, mesurée par l'alanine irradié aux rayons X de qualité Q, peut être écrite de cette façon:

$$D_w^{Q_0} = k_{corr}^{Q,Q_0} \times D_w^Q = \frac{D_w^Q}{f^{Q,Q_0}} \tag{2}$$

avec $D_w^{Q_0}$ la vraie dose équivalente à l'eau pour une qualité de faisceau de référence Q_0 et D_w^Q la dose mesurée par l'alanine irradié aux rayons X de qualité Q.

Mesures expérimentales

Cette méthode consiste à déterminer la réponse du dosimètre alanine, par unité de dose absorbée dans l'eau, irradié avec des rayons X, comparée à la même grandeur pour un dosimètre irradié à une qualité de référence telle que le ^{60}Co. Le facteur déterminé est le suivant :

$$f_{exp}^{Q,Q_0} = \frac{(r/D_w)^Q}{(r/D_w)^{Q_0}} \tag{3}$$

f_{exp}^{Q,Q_0} étant la réponse relative du dosimètre alanine déterminée par le mesures expérimentales, r la réponse du dosimètre alanine mesurée par RPE, D_w la dose déposée dans l'eau mesurée par une chambre d'ionisation étalonnée aux rayons X mais au ^{60}Co également, Q la qualité du faisceau de rayons X et Q_0 la qualité de faisceau de référence, ^{60}Co dans cette étude. Cette méthode de correction prend en compte l'interaction physique du rayonnement avec le dosimètre, mais aussi la création des radicaux libres à l'intérieur du dosimètre. Les résultats obtenus sont représentés dans la figure 3 et sont comparés aux résultats obtenus par différentes autres équipes.

Les résultats obtenus ont montré que la réponse relative du dosimètre alanine au rayons X de faible à moyenne énergie, varie de 0.68 à 0.95 pour des énergies effectives de 27 et 168 keV respectivement. Les résultats obtenus sont en bon accord avec les résultats publiés par différentes équipes. Un léger écart peut être levé entre les données obtenues durant ce travail et les données de littérature. Ceci est dû principalement à la différence de la composition chimique des dosimètres utilisés dans chaque étude, mais aussi à la différence des protocoles expérimentaux de mesure directe de la dose absorbée dans l'eau par des cambres d'ionisation.

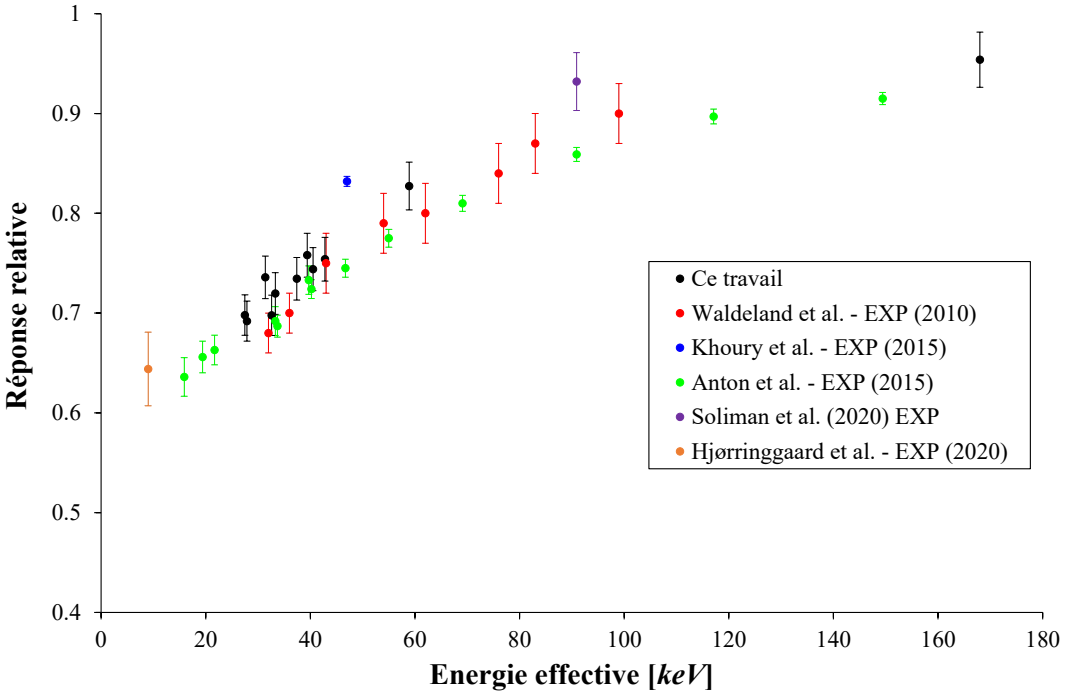

FIGURE 3: La réponse relative des dosimètres alanine pour des rayons X de faible à moyenne énergie, déterminée par des mesures expérimentales.

Simulations Monte Carlo

Des simulations Monte Carlo ont été mises en œuvre, en utilisant le code MCNPX[130], afin de déterminer la réponse relative de l'alanine aux rayons X de faible à moyenne énergie, pour les mêmes qualités de faisceaux listées dans le tableau 2. Les mêmes géométries d'irradiations expérimentales ont été reproduites dans les simulations. Le facteur déterminé est le ratio de la dose absorbée dans l'alanine par rapport à celle absorbée dans le même volume d'eau, pour une qualité Q de rayons X, comparé au même facteur déterminé pour la qualité de rayonnement de référence Q_0. Il s'écrit de la manière suivante:

$$f_{MC}^{Q,Q_0} = \frac{\left(\frac{D_{dos}}{D_w}\right)^{Q}}{\left(\frac{D_{dos}}{D_w}\right)^{Q_0}} \tag{4}$$

avec f_{MC}^{Q,Q_0} la réponse relative de l'alanine aux rayons X de faible à moyenne énergie, D_{dos} la dose absorbée dans l'alanine et D_w la dose absorbée dans l'eau. Le même facteur a été étudié par Waldeland et Malinen[149] ainsi que par Anton et Büermann[7]. La figure 4 montre la comparaison des résultats obtenus durant ce travail avec les résultats publiés par Waldeland et Anton.

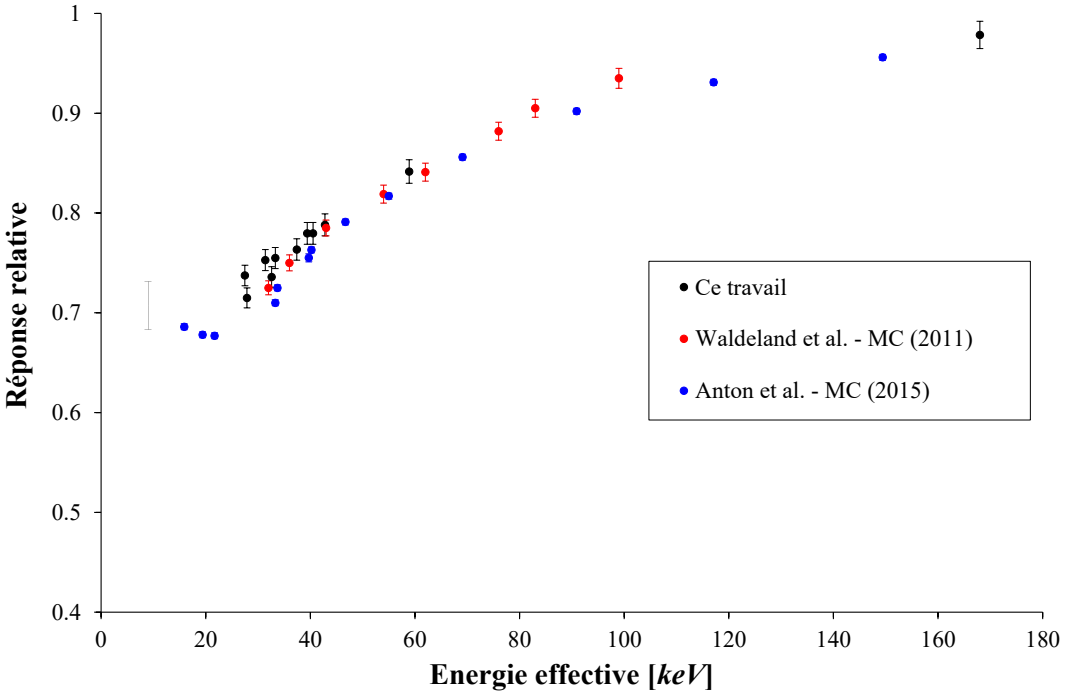

FIGURE 4: La réponse relative des dosimètres alanine pour des rayons X de faible à moyenne énergie déterminée par des simulations Monte Carlo.

Les résultats obtenus par les simulations Monte Carlo varient entre 0.737 à 0.978 pour des énergies effectives de 27.5 et 168 keV. Comparés aux résultats obtenus par des mesures expérimentales, les réponses relatives obtenues par des simulations Monte Carlo sont légèrement plus fortes. Un écart moyen de 3.82 % est décelé entre les résultats de simulations et l'expérience. Cet écart est dû au fait que les simulations Monte Carlo ne prennent pas en compte la dépendance en énergie du rendement de création des radicaux libres (G-value) dans l'alanine.

Les résultats obtenus dans cette étude sont en bon accord avec les résultats obtenus par Waldeland et Anton, comme le montre la figure 4. Un léger écart peut être discerné entre ces résultats pour des énergies effectives comprises entre 20 et 40 keV. L'origine de cet écart est dû à la différence de la composition chimique des dosimètres simulés dans chaque étude, mais aussi au choix du code Monte Carlo. Waldeland et Anton ont, en effet, utilisé le code EGSnrc[94] alors que le code MCNPX est utilisé dans ce travail.

Calculs analytiques

La nouveauté de ce travail de thèse réside dans l'élaboration et la validation de cette méthode de détermination de la réponse relative du dosimètre alanine. Cette méthode repose sur des calculs analytiques basés sur les facteurs d'absorption massique de l'énergie (μ_{en}/ρ) tabulés par le NIST[54]. Un code C++ est développé au cours de ce travail, qui prends comme entrée la distribution en énergie du spectre de rayons X à étudier, et ensuite pondère cette distribution d'énergie par les facteurs μ_{en}/ρ adéquats, comme le montre l'équation suivante:

$$f_W^Q = \frac{\int_0^{E_{max}} \left(\frac{\mu_{en}(E)}{\rho}\right)_{dos} . E . \phi(E) . dE}{\int_0^{E_{max}} \left(\frac{\mu_{en}(E)}{\rho}\right)_{w} . E . \phi(E) . dE} \times \frac{\left(e^{-\bar{\mu}_{att}^{Q} \cdot x}\right)_{dos}}{\left(e^{-\bar{\mu}_{att}^{Q} \cdot x}\right)_{w}} \tag{5}$$

avec f_W^Q la réponse relative de l'alanine pour une qualité Q de rayons X, E_{max} l'énergie maximale du spectre de rayons X en question, $\phi(E)$ est la fluence de photons ayant une énergie E, $\bar{\mu}_{att}^{Q}$ le coefficient moyen d'atténuation linéaire des rayons X de qualité Q et x l'épaisseur du dosimètre. Le premier terme du produit présenté dans l'équation ci dessus représente le ratio de la dose déposée dans le dosimètre alanine par rapport à la dose déposée dans l'eau. Le second terme du produit représente le ratio des pourcentages d'atténuation des rayons X dans une épaisseur x d'alanine ou d'eau.

Le facteur f_W^Q est ensuite divisé par la même grandeur mathématique mais qui est calculée pour une qualité de rayonnement de référence Q_0 telle qu'une qualité de rayons gamma issus d'une source de ^{60}Co. Ainsi, le facteur final calculé par ce code est le suivant:

$$f_W^{Q,Q_0} = \frac{f_W^Q}{f_W^{Q_0}} \tag{6}$$

La figure 5 montre les valeurs de la réponse relative du dosimètre alanine obtenues par les calculs analytiques ainsi que leur comparaison aux résultats obtenus par les mesures expérimentales et les simulations Monte Carlo.

On remarque que les résultats obtenus par les calculs analytiques sont très proches des résultats des simulations Monte Carlo (écart moyen de 0.7 %), ce qui justifie le remplacement des simulations Monte Carlo par ce type de calculs, surtout sachant que Le temps d'exécution moyen de ce code, pour une qualité de faisceau donnée, est de l'ordre de quelques secondes, alors que la durée d'un calcul Monte Carlo peut prendre quelques heures pour déterminer le ratio de dose de l'alanine par rapport à l'eau.

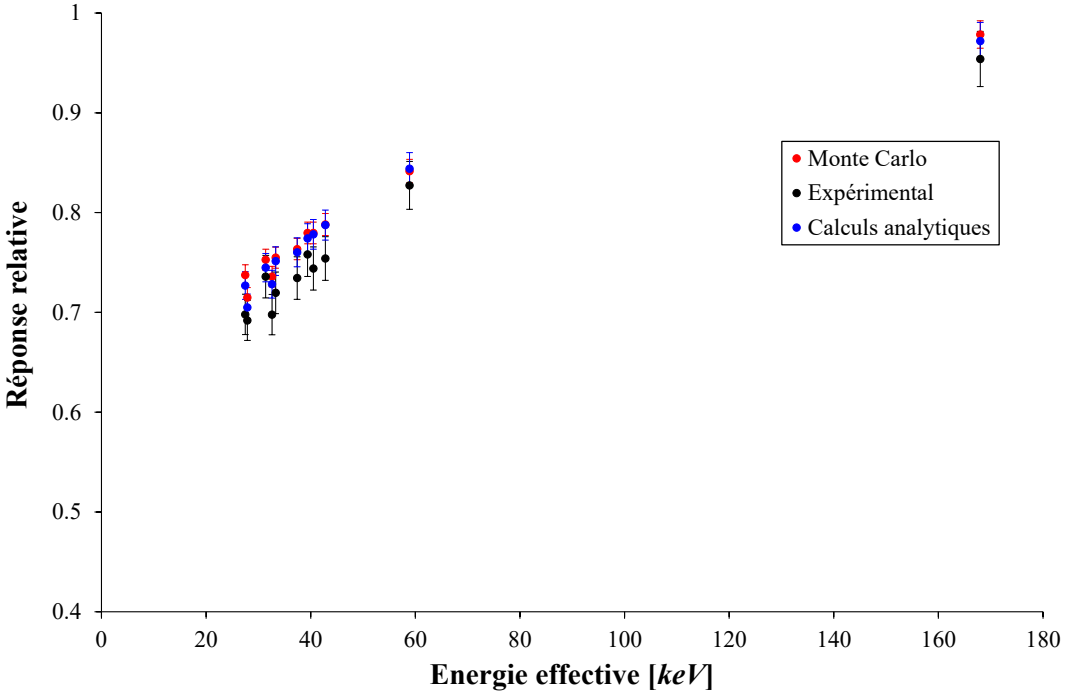

FIGURE 5: La réponse relative des dosimètres alanine pour des rayons X de faible à moyenne énergie déterminée par des calculs analytiques.

D'un autre côté, un écart de 3.15 % est observé entre les résultats obtenus par les calculs analytiques et ceux obtenus par des mesures expérimentales. Cet écart est dû au fait que la dépendance en énergie du rendement de création des radicaux libres n'est pas pris en compte dans les calculs.

L'étude de la dépendance en énergie du rendement de création des radicaux libres dans l'alanine

Le rendement de création des radicaux libres (G-value) est défini comme le nombre de radicaux libres créés dans l'alanine suite à un dépôt d'énergie égal à 100 eV. Cette valeur peut être assimilée la réponse du dosimètre alanine, qui est directement proportionnelle au nombre de radicaux libres radio-induits, par unité de dose absorbée, dans une gamme de dose allant de quelques grays jusqu'à 10 kGy.

Il a été mentionné plus haut que les résultats de la réponse relative du dosimètre alanine obtenus par les simulations Monte Carlo et les calculs analytiques présentent un écart par rapport aux résultats obtenus expérimentalement. Ceci est dû au fait que les simulations et les calculs ne tiennent pas compte des variations, en fonction de l'énergie des rayons X, de la création de radicaux libres dans le dosimètre alanine.

Formalisme adopté

Afin de mieux estimer la réponse relative des dosimètres alanine aux rayons X de faible à moyenne énergie, une étude a été menée pour déterminer la dépendance en énergie du rendement de création des radicaux libres dans l'alanine. Une approche relative a été abordée pour évaluer cette dépendance. Cette approche consiste à estimer l'efficacité relative du dosimètre alanine pour des rayons X de faible à moyenne énergie, comparée à son efficacité pour une qualité de rayonnement de référence telle que le ^{60}Co. Cette efficacité est définie comme:

$$\eta^{Q,Q_0} \;=\; \frac{G^Q}{G^{Q_0}} \tag{7}$$

avec η^{Q,Q_0} l'efficacité relative du dosimètre alanine pour une qualité Q de rayons X relative à celle pour une qualité Q_0 de référence et G^Q et G^{Q_0} les rendements de création des radicaux libres dans l'alanine pour une qualité Q de rayons X relative à celle pour une qualité Q_0 respectivement. Étant donné que la détermination expérimentale de la valeur absolue du G-value est très difficile, l'approche relative et le formalisme suivant ont été adoptés:

$$\frac{(r/D_w)^Q}{(r/D_w)^{Q_0}} \;=\; \frac{(r/D_{dos})^Q}{(r/D_{dos})^{Q_0}} \;\times\; \frac{(D_{dos}/D_w)^Q}{(D_{dos}/D_w)^{Q_0}} \tag{8}$$

ce qui équivaut à

$$f_{exp}^{Q,Q_0} \;=\; \eta^{Q,Q_0} \;\times\; f_{dose}^{Q,Q_0} \tag{9}$$

avec f_{dose}^{Q,Q_0} le rapport de la dose absorbée dans l'alanine par rapport à celle absorbée dans le même volume d'eau, pour une qualité Q de rayons X, comparé au même facteur déterminé

pour qualité de rayonnement de référence Q_0. Ainsi, f_{dose}^{Q,Q_0} peut être considéré comme f_{MC}^{Q,Q_0} ou f_W^{Q,Q_0}.

Résultats

Trois qualités de faisceaux de rayons X, couvrant la gamme d'énergie effective allant de 19 jusqu'à 49 keV, on été choisies pour étudier la dépendance en énergie du rendement de création des radicaux libres dans l'alanine. Des irradiations expérimentales ont été réalisées pour mesurer le facteur f_{exp}^{Q,Q_0}. En parallèle, des simulations Monte Carlo ainsi que des calculs analytiques permettent d'estimer le facteur f_{dose}^{Q,Q_0} par deux méthodes différentes.

Les valeurs de η^{Q,Q_0} obtenues en se basant sur les simulations Monte Carlo ainsi que sur les calculs analytiques sont en très bon accord avec un écart maximal de 0.57 %. Ce faible écart valide, encore une fois, la méthode de détermination de la réponse relative par des calculs analytiques.

La figure 6 montre les valeurs de η^{Q,Q_0} obtenues avec des simulations Monte Carlo, comparées à des valeurs présentées dans la littérature. Les résultats montrent un bon accord avec les données publiées, tenant en compte des incertitudes associées. Un écart est néanmoins observé entre les résultats obtenus et les résultats publiés. Ceci est dû à la différence dans la composition chimique des dosimètres étudiés, mais aussi aux méthodes adoptées.

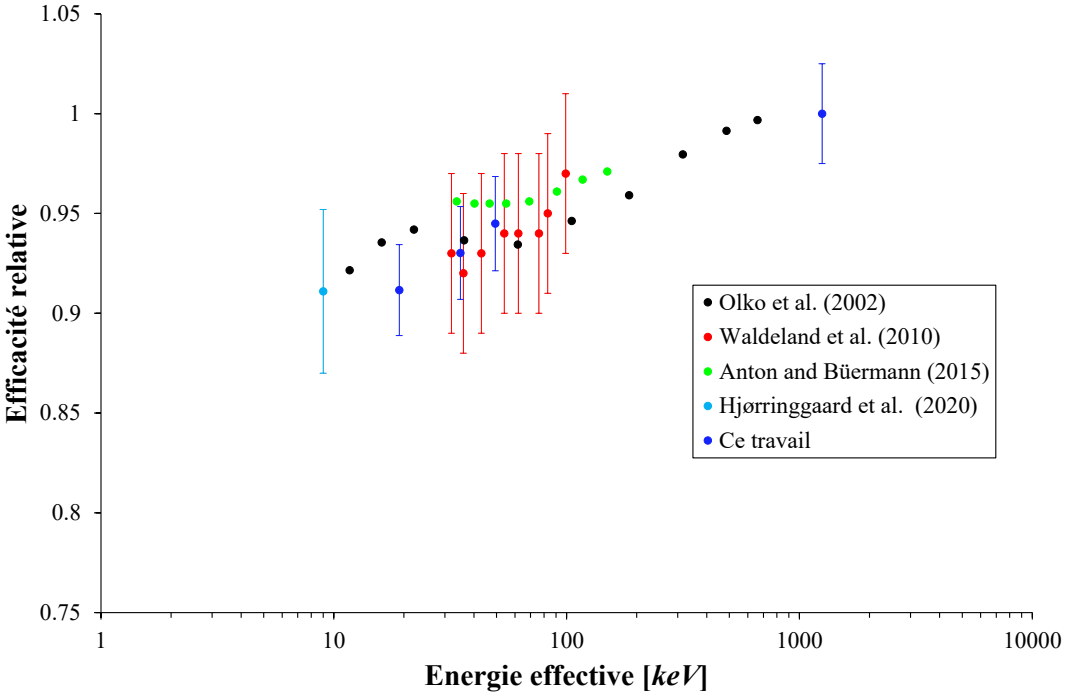

FIGURE 6: L'efficacité relative du dosimètre alanine d'Aerial.

Un ajustement mathématique des données représentées dans la figure 6 a permis de déterminer des valeurs d'efficacité relative η^{Q,Q_0} pour chacune des qualités de faisceaux listées dans le tableau 2. Ainsi, les valeurs des réponses relatives de l'alanine, déterminées par des simulations Monte Carlo et des calculs analytiques, ont été mis à jour en les corrigeant avec les valeurs de η^{Q,Q_0} adéquates. La figure 7 montre l'impacte de cette mise à jour sur valeurs de f_{MC}^{Q,Q_0} et f_W^{Q,Q_0}, ainsi que leur comparaison à la réponse relative déterminée par des mesures expérimentales.

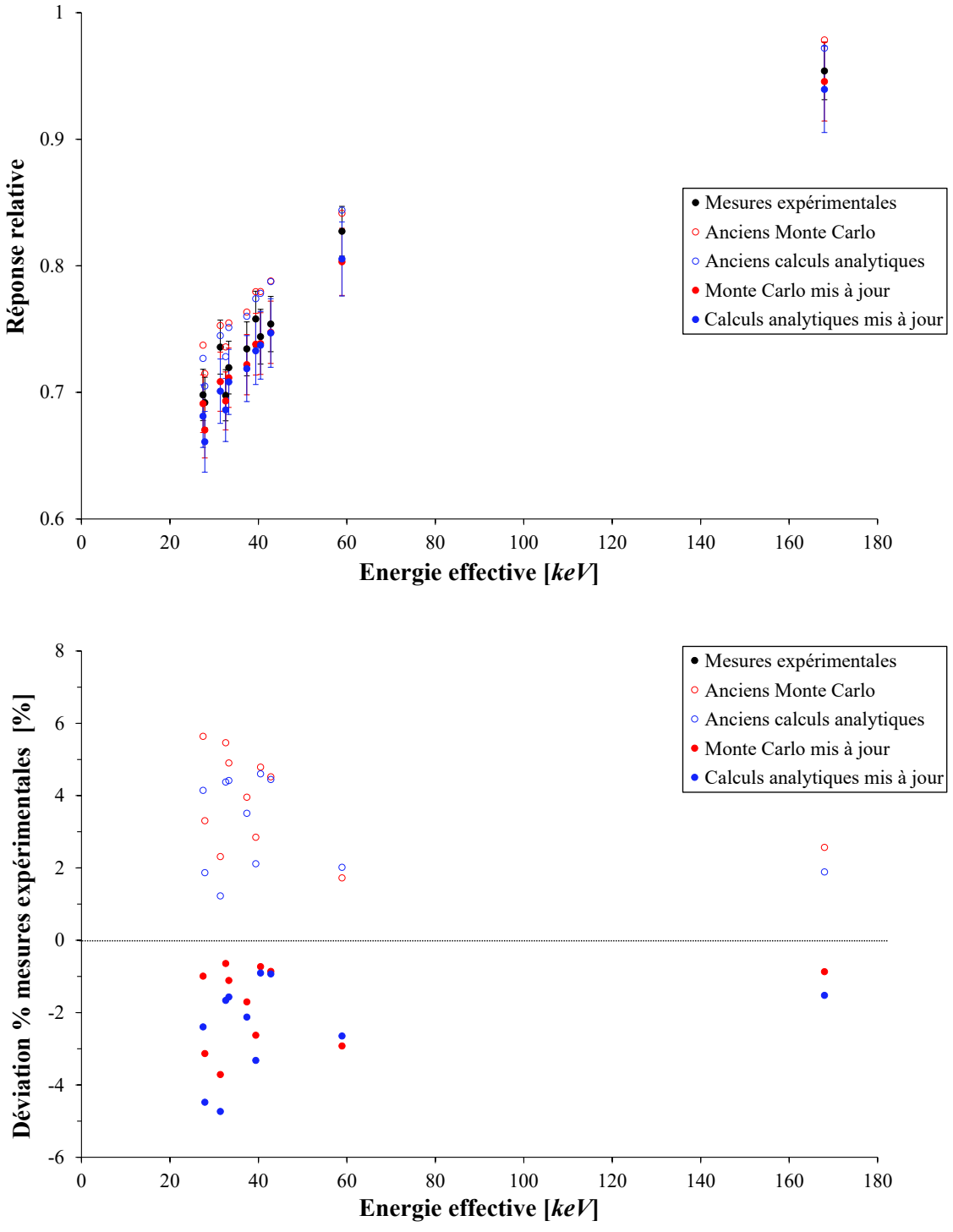

FIGURE 7: Comparaison des valeurs de f_{MC}^{Q,Q_0} et f_W^{Q,Q_0} mises à jour avec les valeurs de f_{exp}^{Q,Q_0}.

La mise à jour des valeurs de f_{MC}^{Q,Q_0} et f_W^{Q,Q_0} induit un meilleur accord avec les valeurs de f_{exp}^{Q,Q_0} où l'écart moyen entre les valeurs de f_{MC}^{Q,Q_0} et f_{exp}^{Q,Q_0} chute de 3.82 % à -1.75 %, et l'écart entre f_W^{Q,Q_0} et f_{exp}^{Q,Q_0} chute de 3.15 % à -2.39 %. Sur l'ensemble des résultats des trois différentes méthodes, le coefficient de variation moyen chute de 2.1 % à 1.3 %, suite à la correction des facteurs f_{MC}^{Q,Q_0} et f_W^{Q,Q_0} par les valeurs de η^{Q,Q_0}.

La détermination du rendement de création des radicaux $HO^\bullet$

Jusqu'à aujourd'hui, le seul matériau pour lequel le code GEANT4-DNA[16, 69–71] permet le calcul des rendements de création de radicaux libres est l'eau. Le but de cette deuxième partie des travaux de thèse était de valider le code de simulation GEANT4-DNA, en comparant les rendements de création du radical hydroxyle $HO^\bullet$ produit dans l'eau, obtenus par simulation et par mesure expérimentale, en premier lieu.

La deuxième étape de cette partie consiste à ajouter les sections efficaces d'ionisation de l'alanine, calculées par code développé dans le cadre de la thèse de Dr. Léna MOUAWAD[118] encadrée par Dr. Ziad EL BITAR, dans la base de données de GEANT4-DNA, pour ensuite comparer les rendements de création des radicaux libres dans l'alanine calculés par simulations et mesurés par des expériences.

Afin de valider le code de simulation GEANT4-DNA, une irradiation par faisceau d'électrons de 1 MeV de plusieurs volumes d'eau a été réalisée à Aerial en utilisant un accélérateur d'électrons de type *Van de Graaff*. La mesure de la concentration des radicaux $HO^\bullet$ était réalisée en mesurant l'absorbance du radical dans le domaine des UV, suite à sa capture par une molécule sélective: l'acide 3-coumarine carboxylique (3CCA). Les mesures d'absorbance ont été réalisées par le groupe *Radiochimie* de l'IPHC. La variation de la concentration initiale du 3CCA, ajoutée au volume étudié d'eau, détermine le temps de capture du radical $HO^\bullet$. Ainsi la variation de cette concentration permet d'étudier la cinétique de l'espère hydroxyle suite à la radiolyse de l'eau.

Le code de simulation Geant4-DNA a permis de calculer les rendements de création des radicaux $HO^\bullet$, en utilisant l'exemple *Chem5*, afin de les comparer aux valeurs expérimentales obtenues. Les mesures expérimentales ont montré que le rendement de création des radicaux $HO^\bullet$ chute dépend du débit de dose absorbée, où les rendements de création des radicaux $HO^\bullet$ augmentent en réduisant le débit de dose. La figure 8 montre la comparaison des résultats expérimentaux et des résultats de simulation à des données de la littérature.

A notre connaissance, aucun travail n'a réalisé les mêmes mesures pour des électrons d'énergie de 1 MeV. En revanche, des travaux ont été réalisé pour mesurer le rendement de création du radical $HO^\bullet$ suite à la radiolyse de l'eau par des rayons gamma[13, 99]. D'un autre côté, il existe plusieurs travaux de simulations qui ont étudié la cinétique du radical $HO^\bullet$ lors de la radiolyse de l'eau par des électrons d'énergie de 1 MeV[138, 147, 151].

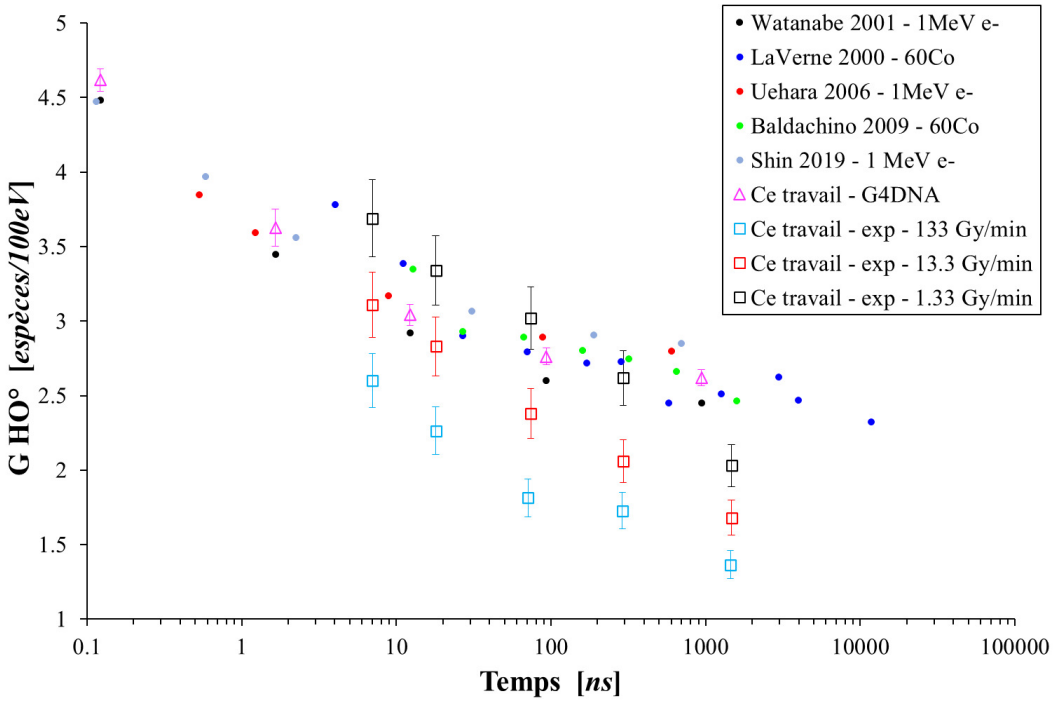

FIGURE 8: Comparaison des résultats expérimentaux et des résultats de simulation à des données de la littérature, pour le suivi temporel de la cinétique du radical $HO^{\bullet}$ radio-induit dans l'eau.

Les résultats obtenus par les simulations Monte Carlo varient entre 4.62 à 2.62 espèces/100 eV, pour des temps de capture de 0.1 et 939 ns respectivement. Ces résultats sont en bon accord avec les résultats publiés[13, 99, 138, 147, 151] pour les différents types des particules étudiés. En revanche, on remarque que les rendements de création des radicaux hydroxyle dépendent du débit de dose absorbée, où ces rendements augmentent en réduisant le débit de dose absorbée. Les résultats expérimentaux obtenus avec un débit de dose absorbée de 1.33 Gy/min sont en bon accord avec les résultats des simulations Geant4-DNA ainsi qu'avec les données de litérature[13, 99, 138, 147, 151].

Conclusion et perspectives

Ce travail a permis de déterminer, par trois méthodes différentes, la réponse relative du dosimètre alanine irradié par des rayons X de faible à moyenne énergie (jusqu'à 280 keV) comparée à une qualité de rayonnement de référence type ^{60}Co.

Des mesures expérimentales ont été réalisées à Aerial et au National Physical Laboratory (NPL, Royaume Uni) afin d'étudier la réponse du dosimètre alanine aux rayons X en comparaison à sa réponse aux rayons gamma d'une source de ^{60}Co. Les résultats obtenus sont en bon accord avec des résultats publiés dans la littérature.

Des simulations Monte Carlo et des calculs analytiques ont permis de déterminer les ratios des doses absorbées par le dosimètre alanine par rapport à l'eau. Les résultats obtenus sont en bon accords entre eux et avec des résultats déjà publiés, mais aussi en bon accord avec les résultats obtenus par des mesures expérimentales (écart moyen de 2.1 %).

L'intégration du modèle d'évaluation de l'efficacité relative du dosimètre alanine dans les méthodes de calcul de facteurs correctifs par simulations Monte Carlo et calculs analytiques a permis de réduire encore l'écart moyen sur les résultats des trois méthodes de 2.1 % à 1.3 %.

La nouveauté de ce travail réside dans la conception et la validation d'un modèle de calcul analytique qui permet d'estimer, à moins de 4 % près, la réponse relative du dosimètre alanine et ceci en quelques secondes, tout en s'affranchissant de la modélisation de la géométrie d'irradiation, ce qui est primordial dans le cas des simulations Monte Carlo et qui, en plus, requièrent quelques heures pour déterminer la réponse relative du dosimètre alanine.

La comparaison des rendements de création des radicaux $HO^{\bullet}$ dans l'eau, obtenus par simulation et par mesures expérimentales, montre une forte dépendance des rendements de création des radicaux $HO^{\bullet}$ avec le débit de dose absorbée, où la variation des rendements est inversement proportionnelle au débit de dose absorbée. Pour un débit de dose de l'ordre de 1.33 Gy/min, les mesures des rendements de création des radicaux $HO^{\bullet}$ sont en bon accord avec les résultats des simulations Monte Carlo ainsi qu'avec les données de litérature.

En perspectives de ce travail, une série d'irradiations expérimentales, avec des rayons X de faible à moyenne énergie, sera à réaliser au sein d'une installation industrielle afin de caractériser les qualités de faisceaux de rayons X d'intérêt. En se basant sur cette caractérisation, les réponses relatives de l'alanine seront déterminées par des calculs analytiques, pour ensuite appliquer les facteurs correctifs adéquats à la réponse RPE de l'alanine pour estimer au mieux la dose absorbée dans l'eau. Cette valeur estimée sera comparée à des mesures de dose absorbée dans l'eau par une chambre d'ionisation étalonnée. A l'issu de cette série d'irradiations, une validation finale de la méthode de calcul de la réponse relative des dosimètres alanine sera atteinte.

Une fois validé, le modèle de calcul des réponses relatives de l'alanine par des calculs analytiques sera intégré dans le logiciel de dosimétrie *AerEDE*, développé par Aerial, afin de pouvoir corriger systématiquement la réponse RPE d'un dosimètre alanine irradié avec des rayons X de faible à moyenne énergie. Cette correction sera appliquée dans le cas où spectromètre RPE, utilisé pour la mesure de la réponse de l'alanine, est étalonné avec une qualité de référence différente que les rayons X.

General Introduction

What if I tell you that you encounter irradiated products every single day of your life? Chocked, are you? We go through our lives mostly unaware of the use of radiation technologies that make things safer, more efficient, healthier and cleaner. When we travel by car or plane, get treated at hospital or even walk over a bridge, we may be experiencing the benefits of such technologies. Indeed, radiation technologies have been developed over the years for diverse applications such as the sterilization of medical devices, food decontamination, enhancing properties of polymers and plastics, de-pollution as well as for the restoration and the preservation of art pieces. All these effects are obtained by an operation known as *radiation processing*, that put in use different sources of ionizing radiation, such as radioactive sources like ^{60}Co and ^{137}Cs, high energy electron accelerators that are also capable to generate high energy X-rays, and smaller kilo-voltage electron beams or electrical X-ray sources.

Nowadays, a clear growth in switching from radioactive source-based (^{60}Co or ^{137}Cs) irradiators to kilo-voltage X-ray irradiators is observed[37, 144]. This switch is driven by the difficulty to purchase, transport and reload radioactive sources as well as dealing with potential radioactive wastes. On the other hand, kilo-voltage X-ray self-shielded irradiators show a very promising future for many applications that use radioactive source-based irradiators, such as blood irradiation, phytosanitary treatments and Sterile Insect Technique (SIT).

However, in order to attain the desired goal, a key parameter of radiation processing has to be well controlled. This parameter is the absorbed dose delivered to the product benefiting from the advances of radiation technologies. For example, a medical device could be non sterile if the required dose was not delivered to it, thus, potentially endangering the life of a patient. This is why, it is described, in many national and international standards, how to accurately measure an absorbed dose[89] and how to determine associated uncertainties[85].

A well calibrated dosimetry system is used during each irradiation process to ensure that the right amount of dose is delivered to a product, assuring the achievement of the desired goal. There exists many dosimetry systems that are used in radiation processing. This aspect is well detailed in chapter 3. One of the well renown dosimetry systems that is used for most radiation applications is the alanine/EPR dosimetry system, which is well reputed for being a dosimetry system of high metrological quality, used for calibration of dosimetry systems as well as for routine process control. Alanine/EPR dosimetry systems ensure an accurate and reproducible

dose measurement over a large absorbed dose range (10Gy – 100kGy). Yet, it has been reported in many studies[7, 50, 95, 122, 141, 149, 150] that absorbed dose to water, measured with alanine dosimeters irradiated with kilo-voltage X-rays, could be underestimated compared to the true delivered absorbed dose. This is the case when the dosimetry system is calibrated with a reference beam quality which is different from X-rays, such as ^{60}Co gamma rays or high energy X-ray or electron beams, which often happens. This non-equivalency to water mainly originates from the differences in the mass-energy absorption coefficients of alanine and water, for photon energies lower than 200 keV[54].

The main goal of this thesis is to study the relative response of alanine dosimeters to several kilo-voltage X-ray beam qualities, compared to a reference beam quality, such as ^{60}Co gamma rays, in order to determine later on correction factors to be applied to the alanine's EPR response, which enables us to estimate within reasonable uncertainty, the true absorbed dose to water that was delivered to the irradiated product. In order to achieve such goal, three different methods were investigated in this thesis. The novelty of this work resides in the development and validation of a novel method, that analytically calculates the relative response of alanine dosimeters in a few seconds with an uncertainty of less than 4 % (k = 1).

This thesis contains four main parts. The first part introduces and details physical notions that are important to understand, such as photon-matter interactions, dosimetric quantities and principals of X-ray generation and beam characterization. The second part of this thesis discusses different aspects of industrial radiation processing, from implemented ionizing radiation sources, to applications as well as generalities on industrial radiation dosimetry, where specifications of different dosimetry systems are discussed.

The third part of this thesis is more focused on alanine/EPR dosimetry. The first chapter of this part discusses basics of Electron Paramagnetic Resonance as well as its use in alanine dosimetry. Key parameters to take into account in alanine/EPR dosimetry are detailed in this chapter as well. The second chapter of this part details all the work that was carried out during this thesis to study the relative response of alanine dosimeters to kilo-voltage X-rays by three different methods: experimental measurements, Monte Carlo simulations and analytical calculations. A study of the photon energy dependence of the alanine free radical creation yield is also detailed in this chapter.

Finally, the fourth part of this thesis discusses aspects of water radiolysis as well as generalities on Geant4-DNA Monte Carlo simulation code. This code was used to determine the radiolytic yield of OH radicals that are generated in water after its irradiation by 1 MeV electrons. Experimental determination of radiolytic yields of OH radicals is also discussed in this part. Radiolitic yields of OH radicals obtained by Monte Carlo simulations are compared to ones measured during experimental irradiations. The main objective of this study was to take in hand the Geant4-DNA[**?**] Monte Carlo simulation code, and adapt it for calculations of free radical creation yields (G-value) of alanine molecules for electron irradiations, by adding ionization cross-sections of alanine, calculated by a code that was developed in another Ph.D thesis work. Unfortunately, due to the short amount of time left before the defense, the calculation of alanine's ionization cross-sections and their implementation in Geant4-DNA could not be achieved.

Part I

Generalities

Chapter 1

Physical principals

Contents

1.1 Photon - Matter interaction

Photons interact with matter via different interaction processes which can lead to a total or partial energy transfer from the photons to the electrons present in the matter. This depends mainly on the interaction probability, more specifically on the interaction's cross section which depends on many physical parameters like the incident photon's energy and the absorber's atomic number.

The probability of the occurrence of a photon-matter interaction is characterized by an interaction coefficient named "cross section" (σ) which unit is "barn" (b). Cross sections are additive, thus, if a photon can undergo different types of interactions, the total interaction cross section (σ) is the sum of each interaction type's individual cross section (σ_i):

$$\sigma = \sum_i \sigma_i \tag{1.1}$$

Photons are considered as indirectly ionizing particles. Their energy transfer in a media is due to generated secondary electrons. In this work, energy of studied photons range from few keV up to 300 keV. Only interaction processes that could occur in this energy range will be detailed, such as *Photoelectric effect, Compon scattering* and *Rayleigh scattering*. Thus, the equation 1.1 becomes:

$$\sigma = \sigma_{photoelectric} + \sigma_{Compton} + \sigma_{Rayleigh} \tag{1.2}$$

where $\sigma_{photoelectric}$, $\sigma_{Compton}$ and $\sigma_{Rayleigh}$ are the cross sections of the photoelectric effect, Compton scattering and Rayleigh scattering respectively.

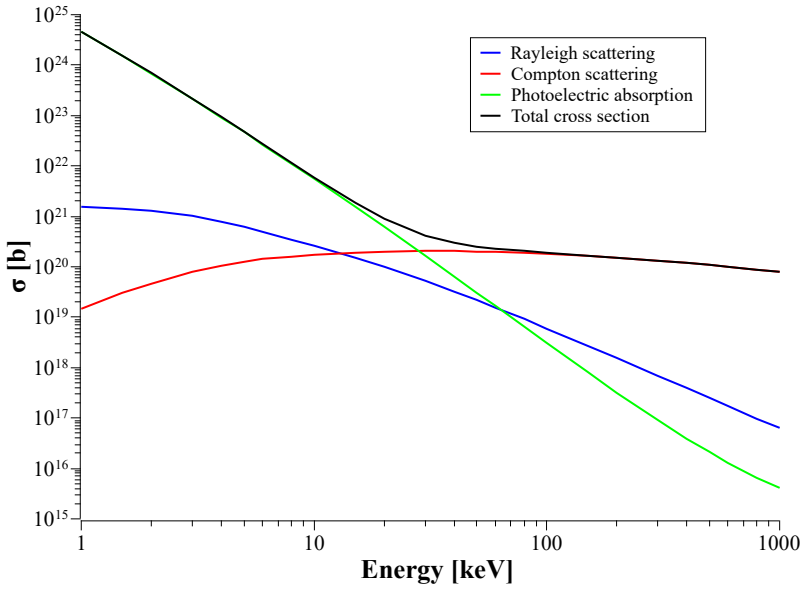

FIGURE 1.1: Photon interaction cross sections in water. [54]

1.1.1 Photoelectric effect

A photo-electron is ejected from the absorber atom's shell when the incident photon's energy is fully transferred to the ejected electron. The incident photon will be completely absorbed by matter and the energy of the ejected electron is given by:

$$E_{e^-} = h\nu - E_{binding} \tag{1.3}$$

where E_{e^-} is the ejected electron's kinetic energy, $h\nu$ represents the incident photon's energy with h being the Planck's constant ($6.626 \times 10^{-34}\ J.s$) and ν is the incident photon's frequency and $E_{binding}$ the electron's binding energy to the atom. This process is predominant in the case of low energy photons (lower than 100 keV), and its probability is enhanced for high atomic number elements. The photoelectric effect's cross section is approximated by this relation:

$$\sigma_{photoelectric} \cong k\frac{Z^n}{E^{3.5}} \tag{1.4}$$

k is a multiplicative constant, Z is the medium's atomic number, n varies between 4 and 5 depending on the incident photon's energy E. The high dependence of $\sigma_{photoelectric}$ on the atomic number explains why high Z materials, such as lead, are used in radiation shielding.

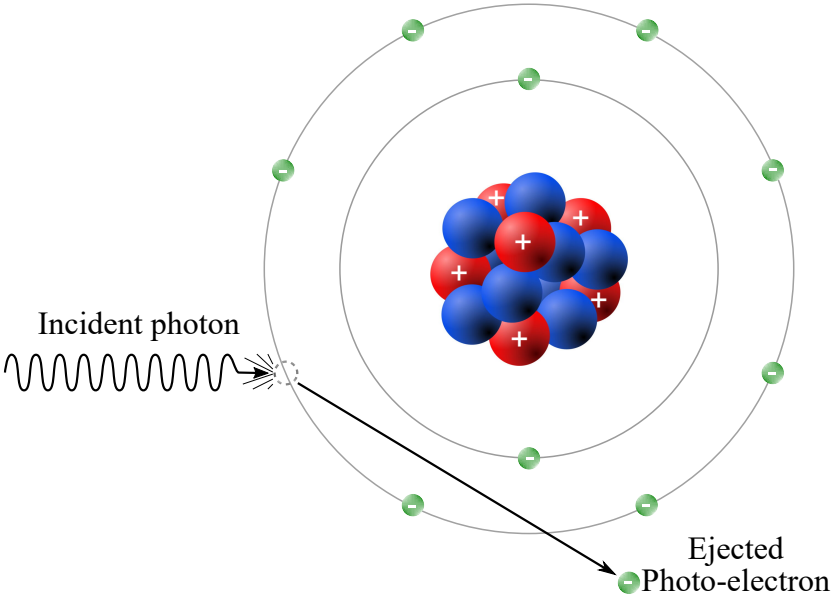

FIGURE 1.2: Photoelectric effect.

1.1.2 Compton scattering

Compton scattering, also called inelastic scattering, occurs when an incident photon interacts with an electron of the medium's atoms. A part of the incident photon's energy (E_i) is transferred to the electron, which is then ejected from its previously occupied state. After its interaction, the scattered photon changes its direction and carries the non-transferred energy,

as shown in the following equation:

$$E_s = \frac{E_i}{1 + \frac{E_i}{E_0}(1 - \cos(\theta))} \tag{1.5}$$

where E_s is the scattered photon's energy, E_i is the incident photon's energy, E_0 is the rest-mass energy of the electron ($511\ keV$) and θ is the scattering angle.

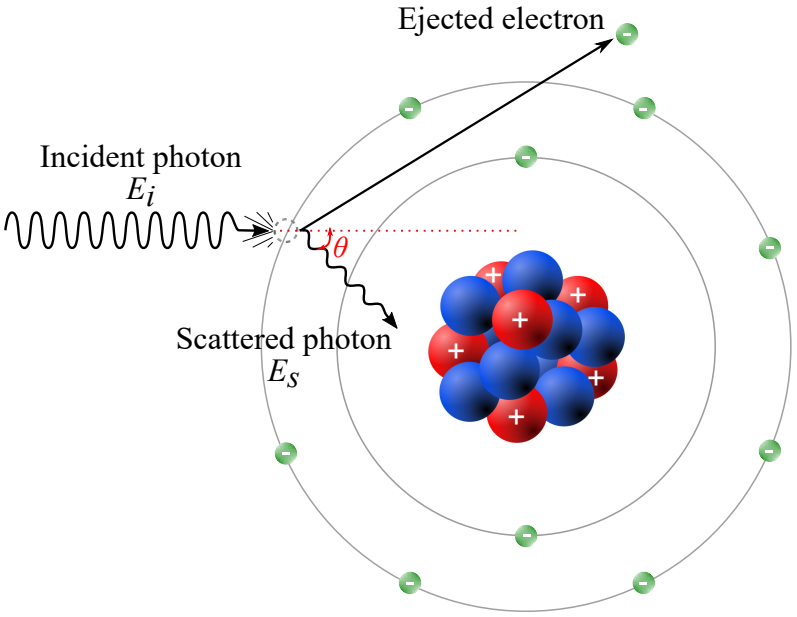

FIGURE 1.3: Compton scattering.

Knowing that the incident photon could scatter in all possible directions, the scattered photon's energy (E_s) can vary from $E_i/(1+E_i/E_0)$, if θ is close to π, to almost the energy of the incident photon (E_i) if the θ is close to 0. The angular distribution of scattered photons is predicted by the $Klein - Nishina$ model for the differential scattering cross-section $d\sigma/d\Omega$ [98] :

$$\frac{d\sigma_{Compton}}{d\Omega} = Z{r_0}^2 \left(\frac{1}{1+\alpha(1-\cos\theta)}\right)^2 \left(\frac{1+\cos^2\theta}{2}\right) \left(1 + \frac{\alpha^2(1-\cos\theta)^2}{(1+\cos^2\theta)[1+\alpha(1-\cos\theta)]}\right) \tag{1.6}$$

where Ω is the solid angle, Z is the medium's atomic number, r_0 is the classical electron radius ($2.8179\ fm$) and $\alpha \equiv E_i/E_0$. The total $\sigma_{Compton}$ can be calculated by integrating the equation 1.5 over all space and taking into account all surrounding electrons:

$$\sigma_{Compton} = Z \int_{\Omega} \frac{d\sigma_{Compton}}{d\Omega} d\Omega \tag{1.7}$$

1.1.3 Rayleigh scattering

Rayleigh scattering, also called coherent or elastic scattering, can occur when an incident photon interacts with all the electrons of the absorber material's atom. This process neither excites nor ionizes the atom. The electrons surrounding the nucleus start to oscillate, thus, creating

an electric dipole. The created dipole re-emits a photon having a similar energy to the incident photon's energy, but in a different direction.

1.1.4 Photon attenuation

1.1.4.1 Mass-attenuation coefficients

A monoenergetic photon beam with an initial intensity (I_0), traversing a material with a given mass-thickness (x) and a given density (ρ), emerges with a lower intensity (I) as describes the following equation:

$$I = I_0 e^{-\frac{\mu}{\rho}x} \tag{1.8}$$

Equation 1.8 can be also written as:

$$\frac{\mu}{\rho} = \frac{\ln(I_0/I)}{x} \tag{1.9}$$

where x is the mass-thickness which is the product of the true thickness t (expressed in cm) by the material's density ρ (expressed in g/cm^3). Actual tabulations [54] of mass-attenuation coefficients μ/ρ are based on theoretical calculations of the total interaction cross-section σ_{total}. Figure 1.4 shows mass-attenuation coefficients of photons traversing water medium. Values of μ/ρ can be related directly to tabulated values of σ_{total} by this relation:

$$\frac{\mu}{\rho} = \frac{N_A}{A}\,\sigma_{total} \tag{1.10}$$

where N_A is the *Avogadro's* constant (equal to $6.022 \times 10^{23}\ mol^{-1}$) and A is the material's atomic mass (expressed in g/mol). Thus, equation 1.1 can be written as follows:

$$\mu = \mu_{photoelectric} + \mu_{Compton} + \mu_{Rayleigh} \tag{1.11}$$

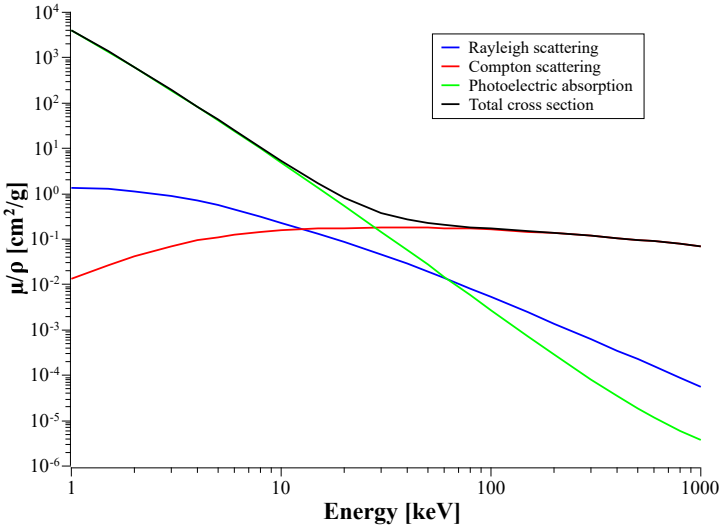

FIGURE 1.4: Mass-attenuation coefficients of photons interacting with water material. [54]

1.1.4.2 Mass-energy transfer coefficients

Mass-energy transfer coefficients μ_{tr}/ρ represent the average energy that is transferred from primary non charged particles (photons) to secondary charged particles created by photon-matter interactions. Multiplying mass-energy transfer coefficients by the photon energy fluence distribution ψ gives a dosimetric quantity called *kerma*. More details about *kerma* are presented in section 1.3.1. Mass-energy transfer coefficients are expressed in cm^2/g. According to NIST's data [54], mass-energy transfer coefficients can be expressed as such:

$$\frac{\mu_{tr}}{\rho} = (f_{photoelectric}\sigma_{photoelectric} + f_{Compton}\sigma_{Compton} + f_{Rayleigh}\sigma_{Rayleigh})\ \frac{N_A}{A} \tag{1.12}$$

where the f factors represent the average fractions of the photon energy E that is transferred to kinetic energy of charged particles in the remaining types of interactions.

1.1.4.3 Mass-energy absorption coefficients

Mass-energy absorption coefficients μ_{en}/ρ represent the average energy that is transferred, and not re-emitted by radiative processes (fluorescence or *Bremsstrahlung* emissions), from primary non charged particles (photons) to secondary charged particles created due to photon-matter interactions. Thus, mass-energy absorption coefficients can be related to mass-energy transfer coefficients [54, 66] by this equation:

$$\frac{\mu_{en}}{\rho} = (1-g)\ \frac{\mu_{tr}}{\rho} \tag{1.13}$$

where g is the fraction of the transferred energy that is re-emitted by secondary charged particles due to radiative processes.

1.2 X-rays

X-rays, by nature, are considered as both electromagnetic waves and non charged particles. Their energy can be expressed as such:

$$E = h\nu = h\frac{c}{\lambda} \tag{1.14}$$

where E is the X-ray photon's energy, h is the *Planck*'s constant ($h = 6.626 \times 10^{-34}\ J.s$), ν is the frequency expressed in Hz, c is the speed of light in vacuum ($c \approx 3 \times 10^8\ m/s$) and λ is the wavelength expressed in m.

1.2.1 X-ray tubes

An X-ray tube (XRT) is used to generate both characteristic and *Bremsstrahlung* X-rays. Figure 1.5 represents a scheme showing the general components of an XRT, which mainly consist

of an electron source and a high density and high Z target material. The electron source, also referred to as the cathode, is a tungsten filament that is heated by an electrical current that controls the thermionic emission of electrons [60]. An electrical field is created between the cathode and the anode by applying a high voltage, generated from an external source, between these two components. This accelerates the emitted electrons from the filament and increases their energy. For example, if a high voltage of 100 kV is applied between the anode and cathode, accelerated electrons gain 100 keV of energy. The accelerated electrons bombard the conversion target, thus, creating X-rays via already discussed processes in sections 1.2.2 and 1.2.3. X-rays are then generated in many directions. However, due to the XRT's external shielding, only X-rays passing through the thin exit window truly exit the XRT and are then used for different applications.

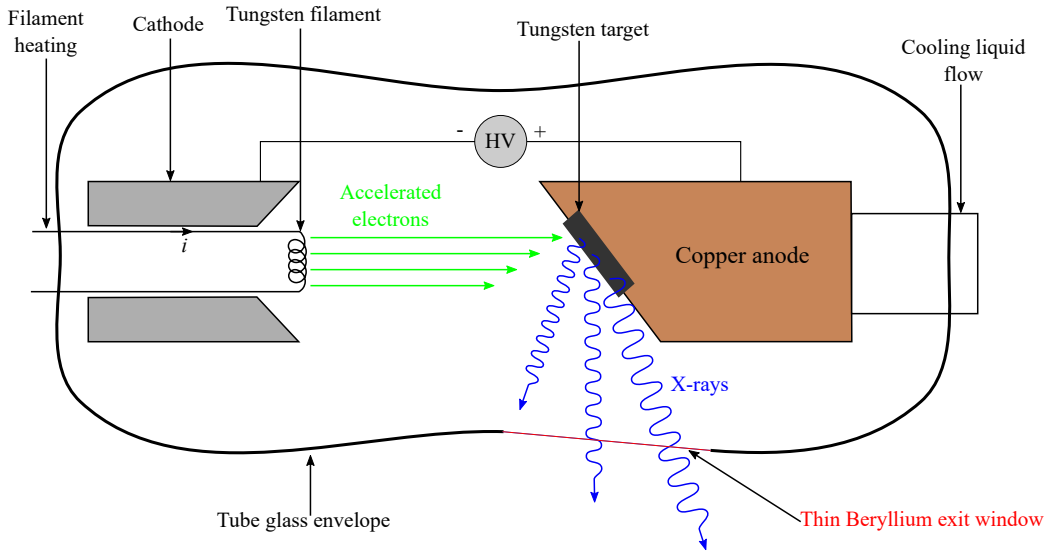

FIGURE 1.5: Classic X-ray Tube design[60]

Depending on the desired application as well as on the operating high voltage range, one needs to choose the optimal conversion target material. For example, a tungsten (Z=74) target is commonly used in different radiology applications as well in industrial radiation processing using low to medium energy X-rays (maximum high voltage of 300 kV[22, 97]). On the other hand, X-ray tubes with a molybdenum (Z=42) or rhodium (Z=45) target are commonly used in mammography [60].

1.2.2 Characteristic X-rays

A vacancy in a specific electronic shell is created when an electron of this shell is ejected after undergoing an ionizing interaction with an incident particle. The atom is hereby ionized, thus, to re-establish the atom's equilibrium, an electron from a higher energy state occupies the created vacancy by liberating energy in a the form of a photon, more precisely, a characteristic X-ray. Figure 1.8 represents this process.

Characteristic X-rays, also called fluorescence X-rays, have discrete energy values which correspond to the difference of the initial and final transition energy levels, and are present in the form of peaks when looking to X-rays energetic fluence distribution.

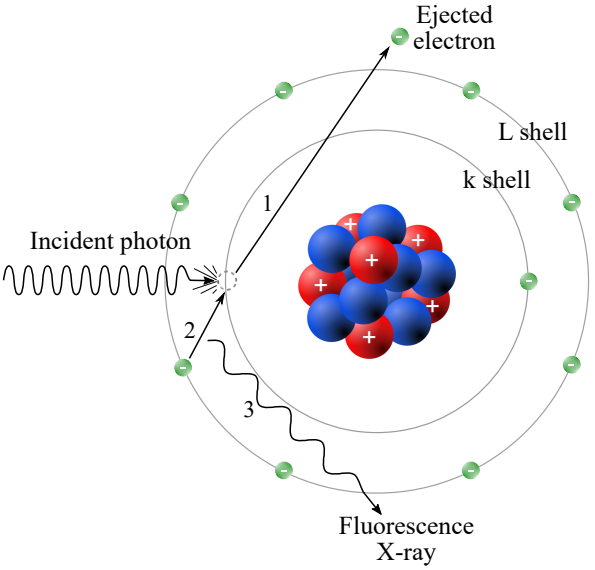

FIGURE 1.6: Characteristic X-ray generation. *The chronological order of processes is indicated by the numbers 1, 2 and 3*

1.2.3 Bremsstrahlung X-rays

An inelastic interaction, also known as a radiative interaction, can occur between an incident electron and an atom's nucleus. The negatively charged electron is passing through the coulombian electrical field created by the positively charged nucleus. The trajectory of the incident electron is deviated, as shown in figure 1.7, and the electron decelerates. In order to ensure the conservation of the electron's total mechanical energy, and according to classical mechanics, the deviated electron emits energy as a form of a braking X-ray, also known as *Bremsstrahlung X-ray*[11].

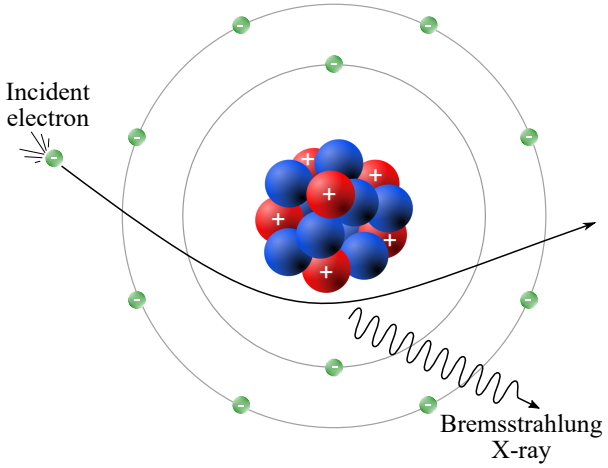

FIGURE 1.7: Bremsstrahlung X-ray generation.

The energy of an emitted X-ray varies from approximately the energy of the incident electron down to zero, depending on the magnitude of the deviation that undertook the incident electron. Thus, the *Bremsstrahlung X-rays* represent a continuum in the energetic fluence distribution, as shown in figure 1.8.

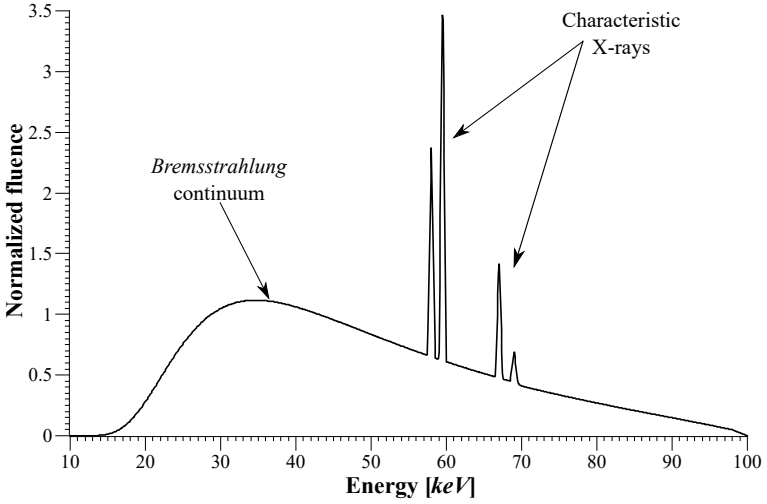

FIGURE 1.8: Energetic fluence of X-rays generated by an X-ray tube operating at 100 kV.[131]

1.2.4 X-ray beam quality

An X-ray beam quality is identified by the use of a sole or combined beam quality specifier. The best way to specify an X-ray beam quality is to measure the spectral energy fluence distribution as a function of the energy of photons that are emitted from an X-ray tube. However, knowing that this measurement could be difficult[49], different physical values were adopted as X-ray beam quality specifiers. These specifiers must somehow reflect the identity of emitted X-rays in order to make us able to distinguish beam qualities. The most commonly used X-ray beam specifier is the Half Value Layer (HVL)[61]. More details on HVL are discussed in section 1.2.4.2. It has been reported in many international codes of practice [22, 58, 61, 97] that the use of tube potential (kVp) alongside the HVL is more adequate, especially for clinical applications. Many beam quality specifiers are furthermore discussed in the following sections.

1.2.4.1 X-ray tube potential

The X-ray tube potential (kVp) is the high voltage that is delivered to the tube and used to accelerate electrons before bombarding the conversion target. This value gives the maximum energy of the spectral photon energy distribution. However, it is not recommended to use kVp as a sole beam specifier for kilo-voltage (kV) X-ray beams because the true beam quality is affected by many other parameters, such as added external filtration. Two X-ray spectra generated with the same high voltage can have a big difference in their photon energy fluence distribution, thus a big difference in beam quality, as shows figure 1.9.

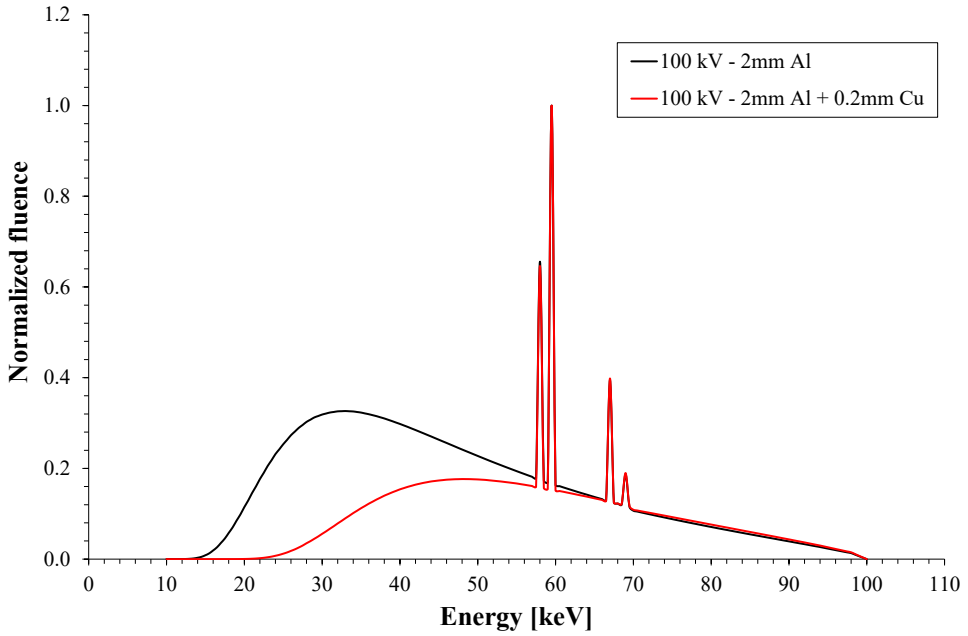

FIGURE 1.9: Energy fluence distribution of two X-ray beams having the same high voltage but different external filtration.

1.2.4.2 Half Value Layer

Until today, the first Half Value Layer (HVL_1) is the most commonly used beam quality specifier to characterize a kilo-voltage X-ray spectrum. It is defined as the thickness of an absorber (typically high purity aluminium or copper) that reduces air-kerma rate by half and is expressed in terms of *mm Al* or *mm Cu*. The thickness of an absorber that reduces air-kerma rate by a factor of 75% is defined as the second Half Value Layer (HVL_2) and the ratio of HVL_1/HVL_2 is defined as the Beam Homogeneity factor. Both HVLs give an idea on the hardness of the X-ray beam, in other words, on its penetration capacity in a certain material.

However, two different X-ray beams can have the same first HVL, thus, many dosimetry codes of practice [22, 58, 61, 97] suggest to use another beam specifier, such as the tube potential or the average energy, alongside the HVL_1 in order to have a better understanding of the beam quality of interest.

Air-kerma rate, or absorbed dose to water rate provided charged particle equilibrium is attained, is measured at a certain point of interest in the X-ray field as increasing thickness of a certain attenuator material (Al or Cu) is placed in the path of the beam. HVL is then deduced from the graphical representation of obtained dosimetric measurements as a function of absorber thickness. In order to have a precise measurement of the HVL, it is more suitable to do measurements in a scatter free environment, thus, it is recommended [61] to place the detector at least at 50 cm from the X-ray source and use a narrow beam in order to limit the scattering of X-rays.

1.2.4.3 Effective energy

The effective energy (E_{eff}) is defined as the energy of a mono-energetic photon beam having the same HVL_1 as its associated poly-energetic photon beam. Once the HVL_1 is determined for a certain X-ray beam quality, one can calculate its correspondent attenuation coefficient μ_{att}, using this equation:

$$\mu_{att} = \frac{ln(2)}{HVL_1} \tag{1.15}$$

and thus, we can estimate the effective energy using NIST's tabulated data on attenuation coefficients [54] based on the calculated μ_{att}.

1.3 Dosimetry

The effects of radiation on matter can be quantified by many physical quantities. These quantities take into account the different radiation-matter interaction processes, described in section 1.1, in order to estimate a physical value that is representative of the irradiation effects undergone by the irradiated material.

1.3.1 Kerma

Kerma, which is an acronym for *kinetic energy released in matter* [143], represents the amount of kinetic energy transferred, from primary non-charged particles (i.e. photons) to secondary generated charged particles (i.e. electrons) per mass unit, as described in the following equation.

$$K = \frac{dE_{tr}}{dm} \tag{1.16}$$

where K is kerma which is expressed in *Gray (1 Gy = 1 J/kg)*, dE_{tr} is the transferred energy from primary particles to secondary charged particles and dm is the interacting material's mass. kerma can be also related to mass-energy transfer coefficients (see section 1.1.4.2) by multiplying these coefficients with the energy fluence distribution ψ of incident photons, as shown in following equations [11], in the case of irradiations with mono-energetic and poly-energetic X-ray beams respectively:

$$K = \psi(E)\ \frac{\mu_{tr}(E)}{\rho} \tag{1.17}$$

$$K = \int_{E=0}^{E_{max}} \psi(E)\ \frac{\mu_{tr}(E)}{\rho}\ dE \tag{1.18}$$

where E is the photon energy, $\psi(E)$ is the photon energy fluence distribution, $\mu_{tr}(E)$ is the mass-energy transfer coefficient at the energy E and ρ is the material's density. These equations permit to determine kerma in a given medium. Air kerma is a dosimetric quantity which is widely used in many calibration protocols of dosimetric equipment [22, 58, 97].

1.3.2 Absorbed dose and dose rate

Absorbed dose D can be defined as the energy transferred to the material, but not re-emitted by secondary generated particles via any radiative interactions such as *Bremsstrahlung* radiation, per mass unit as shows the following equation [11, 66, 89, 143]:

$$D = \frac{dE}{dm} \tag{1.19}$$

where D is the absorbed dose expressed in $Gray(Gy)$, dE is the absorbed energy by the material expressed in J and dm is the material's mass expressed in kg. In the same way that kerma is related to mass-energy transfer coefficients μ_{tr}/ρ using equations 1.17 and 1.18, absorbed dose to a material can be related to mass-energy absorption coefficients by the following equations, in the case of irradiations with mono-energetic and poly-energetic X-ray beams respectively:

$$D = \psi(E)\ \frac{\mu_{en}(E)}{\rho} \tag{1.20}$$

$$D = \int_0^{E_{max}} \psi(E)\ \frac{\mu_{en}(E)}{\rho}\ dE \tag{1.21}$$

where D is the absorbed dose to the material, E is the incident photon's energy, E_{max} is the maximum photon energy in the case of a poly-energetic X-ray beam, $\psi(E)$ is the energy fluence distribution, $\mu_{en}(E)$ is the mass-energy absorption coefficient of an X-ray with an energy E traversing the material of density ρ. Thus, using equations 1.20 and 1.21, one can calculate the absorbed dose in a specific material based on the mass-energy absorption coefficients tabulated by NIST [54] and on the energy fluence distribution of incident X-rays.

In industrial radiation processing, absorbed dose to water D_w is a key parameter [79, 89]. D_w is monitored and evaluated during a routine irradiation process in order to ensure that the delivered dose to the product meets the required dose that guaranties the successfulness of the irradiation process, and hereby achieving the desired goal within the dosimetric acceptable limits.

Absorbed dose rate $\dot{D}$ is another physical value which is of interest when it comes to radiation processing. The dose rate plays an important role in the kinetics of chemical reactions that occur inside of the matter during and after its irradiation. Absorbed dose rate is the measurement of the absorbed dose by a material over a specific duration of exposure time, as shows the following equation:

$$\dot{D} = \frac{D}{t} \tag{1.22}$$

where $\dot{D}$ is the absorbed dose rate, D is the absorbed dose during the time-lapse of interest t.

1.3.3 Charged particle equilibrium

During the interaction of primary non charged particles with matter, secondary generated charged particles will undergo different trajectories inside of the material until their total energy is fully deposited. Thus, if a small volume of the irradiated volume is traversed by the a certain flux of incident secondary electrons that is equal to the flux of electrons exiting the same volume, this volume is considered in *charged particle equilibrium (CPE)* [11, 60].

Taking into account this definition, one can say that *CPE* is not attained at the surface of the material because not enough secondary electrons are generated in this region, yet, *CPE* is attained after a certain depth in the medium depending on the energy of incident particles as well as on the energy transfer inside of the material. The region that is situated between the material's surface and the beginning of *CPE* is called the *Build-up region*. Figure 1.10 shows the variation of collision kerma and absorbed dose as a function of depth in a certain material.

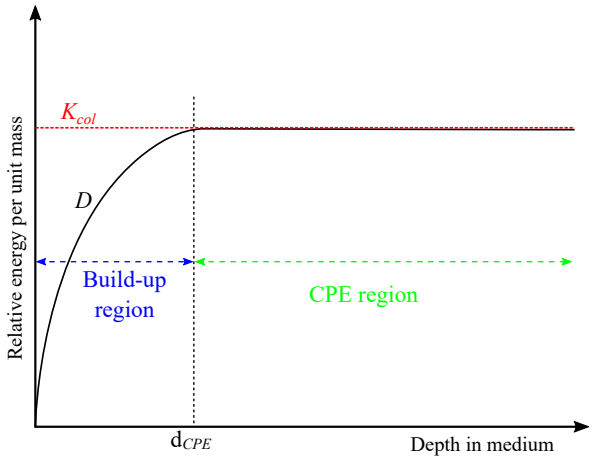

FIGURE 1.10: Variation of collision kerma (K_{col}) and absorbed dose (D) as a function of depth in material. d_{CPE} represents the depth from which the *CPE* region begins.

Absorbed dose can be also related to collision kerma. Kerma can be decomposed into two physical terms, as shows equation 1.23. The first term K_{col} represents the energy transferred, from incident photons to secondary charged particles, and then deposited in the material by collision processes, while the other term K_{rad} represents the energy lost by secondary charged particles due to radiative interactions.

$$K = K_{col} + K_{rad} \tag{1.23}$$

where K is kerma, K_{col} is named collision kerma and K_{rad} is named radiative kerma. K_{col} can be also expressed as such:

$$K_{col} = K\ (1 - g) \tag{1.24}$$

where g is the fraction of the transferred energy that is re-emitted by secondary charged particles due to radiative processes, as discussed in section 1.1.4.3. Looking at the relation between absorbed dose and mass-energy absorption coefficients $\mu en/\rho$ and taking into account equation

1.24, one can directly state that the absorbed dose D is equal to the collision kerma K_{col}. However, this is true only if CPE is attained in the irradiated volume as shown in figure 1.10.

Part II

Aspects of industrial radiation processing

Chapter 2

Ionizing radiation sources used in radiation processing and their applications

Contents

2.1 Introduction

The term "*radiation*" includes a wide variety of different electromagnetic waves that we encounter in our every day life, such as visible light, radio waves, microwaves and more energetic waves called ionizing radiation like gamma or X-rays. Due to increasing scientific and technological advances, man learned how to use different kinds of electromagnetic waves for his needs, especially ionizing radiation in different fields such as medicine, food and industry.

"*Radiation processing*" can be defined as a controlled application of ionizing radiations, such as gamma rays, accelerated electrons and X-rays, in the goal of achieving a desired effect on a certain object. Nowadays, a clear growth is witnessed in the use of ionizing radiation sources for different scientific as well as industrial applications, such as the sterilization of medical devices, food irradiation and enhancement of some material's properties.

This chapter presents different types of ionizing radiation sources that are used in radiation processing, as well as properties and modalities of different industrial radiation applications.

2.2 Radiation sources

2.2.1 Radioactive source-based irradiators

Two of the most commonly used radio-isotopes in radioactive source-based irradiators are Cobalt-60 (^{60}Co) and Caesium-137 (^{137}Cs). Their frequent use in radiation processing is due to the relatively high energy of their gamma rays (0.66 MeV for ^{137}Cs and 1.17 and 1.33 MeV in the case of ^{60}Co) and their long half-life (30.1 years for ^{137}Cs and 5.27 years for ^{60}Co). However, the use of ^{137}Cs has been limited to small self-shielded irradiators, used primarily for the irradiation of blood and for insect sterilization. Currently, a large number of industrial radiation processing facilities employ ^{60}Co as the gamma radiation source[110].

One of the key elements of a radioactive source-based installation is the activity of its radio-isotopes. The activity of a radioactive source is defined as the number of decays of radioactive nuclides per second. Its unit is the *Becquerel* (Bq). However, because of the very important activities of radioactive sources, another unit is more commonly used which is the *Curie* (Ci), where 1 Ci is equal to 3.7 10^{10} Bq. The activity of radioactive sources used in radiation processing ranges from few kCi up to few MCi.

For industrial radiation processing, there exists two types of radiation source-based installations: an irradiation plant or a small self-shielded cabinet. Very often, irradiation plants operate using racks of ^{60}Co pencil sources when self-shielded cabinets can rely on ^{137}Cs, and this is mainly due to the difference of the radiation applications that are put in practice. For applications that require a high production throughput, such as the sterilization of medical devices and food irradiation, irradiation plants are more suitable than self-shielded cabinets.

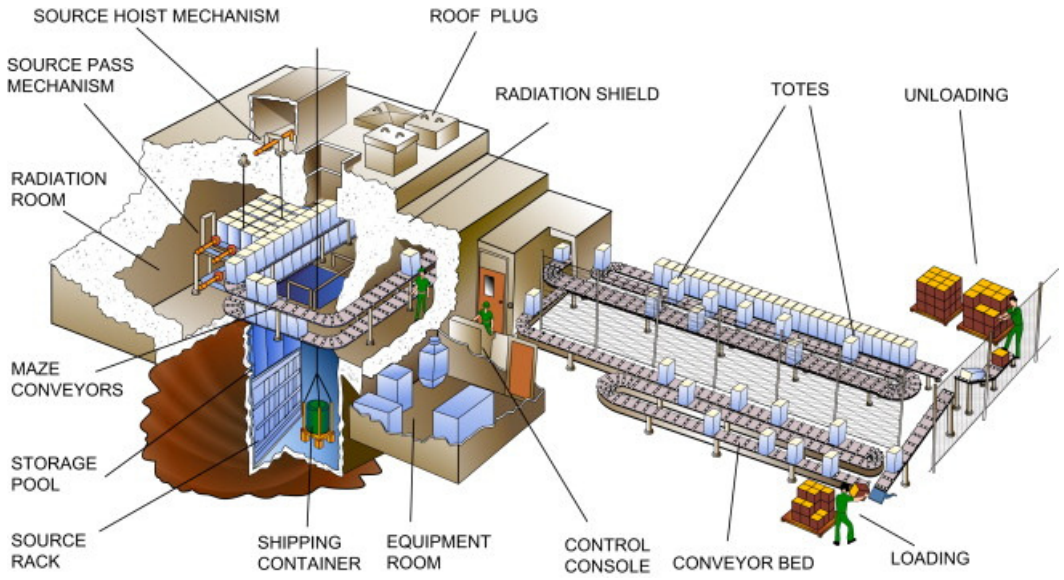

FIGURE 2.1: Drawing of an industrial gamma irradiation installation operating with ^{60}Co sources.

In an irradiation plant, the process begins by loading products to be irradiated in totes that will be then conveyed into the irradiation room. While products are conveyed into the irradiation room, the source racks are lifted from their storage pool, located beneath the irradiation room. This is the case of a "*wet storage*" irradiator. When not used for irradiation, source racks are always stored in a storage water pool that permits to absorb all radiation so that there will be no danger on human presence in the irradiation room, often for maintenance purposes. For radiation protection purposes, large thicknesses of concrete (up to 2 m) are put in place during the construction of an irradiation plant, in order to ensure that all radiation is contained in the irradiation room and that the staff operating in other areas is safe. This shielding is also called the "*Biological shield*".

During the irradiation, products are conveyed in front of or between the source racks in a certain way that ensures the best homogeneous dose distribution in the products. Double sided irradiations ensure the better homogeneity of dose distribution inside of the products. Once the irradiation is finished, the product is conveyed to the unloading area. The main advantages of such installations are the production throughput, the capacity of delivery of high doses in the kGy range and finally the dose homogeneity inside the products. The dose uniformity in an irradiation process is expressed using this factor:

$$DUR = \frac{D_{max}}{D_{min}} \tag{2.1}$$

where DUR is the Dose Uniformity Ratio and D_{max} and D_{min} are the maximum and minimum measured doses in the process in question respectively. For a very homogeneous irradiation, DUR is close to unity. Irradiations carried out in a gamma irradiation plant present a DUR in the range of 1.1 to 2.2, depending mainly on the product's density and volume. Irradiation is more homogeneous in the case of lower density products than it is for higher density product, and this is caused by the laws of attenuation of photons in matter.

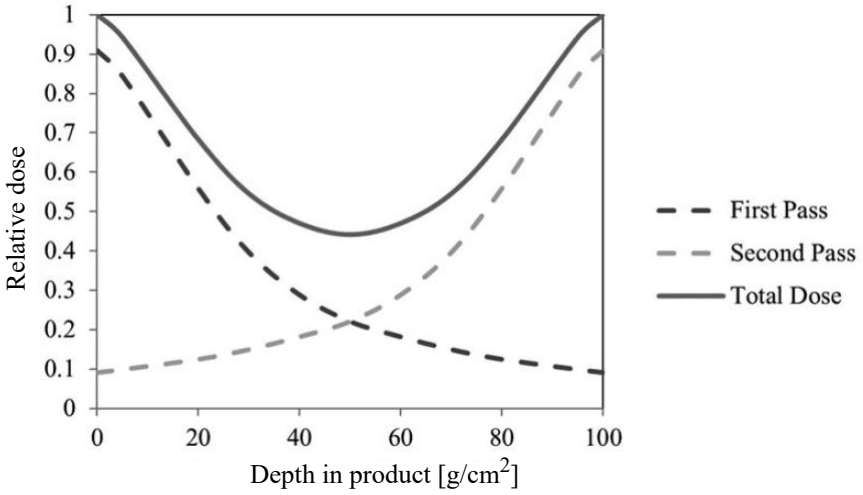

FIGURE 2.2: Dose distribution in a double-sided ^{60}Co irradiation[28].

Self-shielded irradiators are specially designed for research and for applications that need small doses, such as blood irradiation, reproductive sterilization of insects and irradiation processes with relatively small throughputs[110]. Irradiators house the radioactive sources within a protective shield, often made by lead. The product is firstly placed in the loading position and is then transferred to the irradiation position by a special mechanism. Knowing that the dose rate is very invariant, at certain position in the irradiation position, the main parameter of dose delivery to the product is the irradiation time. Radioactive source are placed in a way that they surround the product for all sides thus making the absorbed dose very uniform. Another advantage of such type of irradiators is that it is small and could be placed in a room without extra shielding.

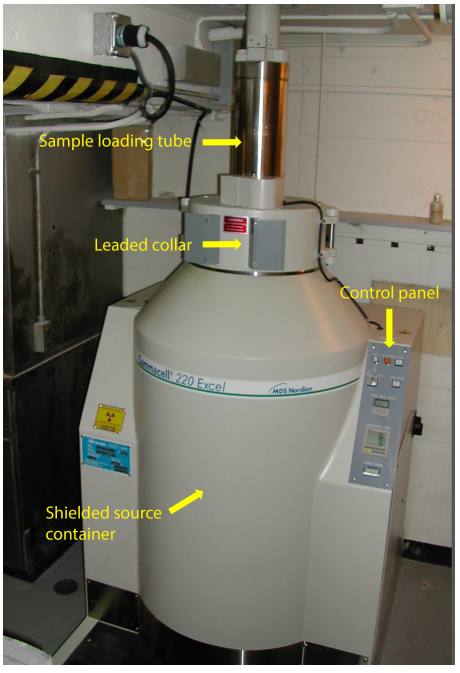

FIGURE 2.3: Gammacell200®, a self-shielded gamma irradiator.

2.2.2 Electron beam accelerators

There exists many types of electron beam (EB) accelerators that are currently being used in radiation processing. The choice of an EB accelerator depends on many parameters such as the desired radiation application, densities of treated products and desired doses and dose rates. Two key parameters control the efficiency of an EB irradiator: accelerating voltage and the beam current. Electrons that are emitted from the electron source into the accelerator will gain an amount of energy that is proportionate to the accelerating voltage that is applied in the acceleration phase, thus controlling the beam's penetration in the product. An electron subjected to a 1 MV accelerating voltage will gain 1 MeV in energy. On the other hand, the electron emission current regulates the number of electrons that are being accelerated and then delivered to the product, thus controlling the dose rate and the delivered dose hereafter.

Type	Energy range [MeV]	Penetration [g/cm^2]	Applications
Low energy	0.08 - 0.3	up to 0.085[83]	Surface decontamination
			Surface coating
			Surface crosslinking
Medium energy	0.3 - 5	up to 2.7[86]	Polymer crosslinking
			Medical device sterilization
High energy	5 - 10	up to 5[86]	Polymer crosslinking
			Medical device sterilization
			Food irradiation

TABLE 2.1: List of the properties of different types of EB accelerators.

For radiation processing, there exists two types of EB installations like gamma installations: irradiation plants and self-shielded irradiators. Self-shielded irradiators house a small EB source that could accelerate electrons of low to medium energy levels with a power of the order of few kW to few tens of kW. This type of installation is used in many radiation applications such as surface decontamination of food or packaging material, sterilization of pharma packaging, curing of inks, surface polymer crosslinking and radiation grafting. Nowadays, he highest EB energy that can be attained in a self-shielded installation is of 5 MeV. This facility is used for research and development purposes only. On he other hand, medium to high energy EB accelerators are installed in a bunker for radiation protection purposes just like the case of ^{60}Co irradiation plants.

Medium to high energy EB accelerator can be distinguished into three types: Direct Current (DC) type where a constant beam is extracted, microwave pulsed type (GHz) where the output beam is repeated at a low frequency and Radio-Frequency (RF) pulse or continuous wave type where lower RF (100–200 MHz) is used to accelerate electrons passing in a resonant cavity[103]. The difference between these three types of accelerators is the maximum acceleration voltage and the maximum electrical power that can be attained. DC accelerators can deliver electron beams with a maximal energy of 5 MeV with a power in the range of 25 to 300 kW[24]. Acceleration using DC acceleration is based on a high voltage applied to an acceleration tube that results in

the creation of an accelerating electrical field. The accelerated beam is then transported via a beam line to the scanning horn where it will be scanned on the surface of a passing product.

Microwave (MW) based EB accelerators can deliver electron beams at higher energies, up to 10 MeV but with maximum power of less than 100 kW. Manufacturers of such accelerators, such as MEVEX (Canada), are putting effort and technical improvements in current systems in order to raise this limit. Acceleration is obtained due to many small resonant cavities powered by pulsed microwaves. On the other hand, RF based EB accelerators offer both high energy (up to 10 MeV) and high power (up to 700 kW) electron beams. One of the most common RF systems is the Rhodotron® [30], designed by the Belgium company IBA.

An RF accelerator is based on a large, single cavity operating at a frequency between 100 MHz and 200 MHz. Emitted electrons undergo a first acceleration towards the inner cavity wall. Since the electric field is reversed when they emerge in the second part of the cavity, electrons are accelerated a second time, completing a crossing of the diameter. An external magnet then bends the accelerated beam and sends it back into the cavity for another acceleration cycle, until the desired energy is attained, then the beam is extracted from the accelerating cavity to the scanning horn via the beam transport line.

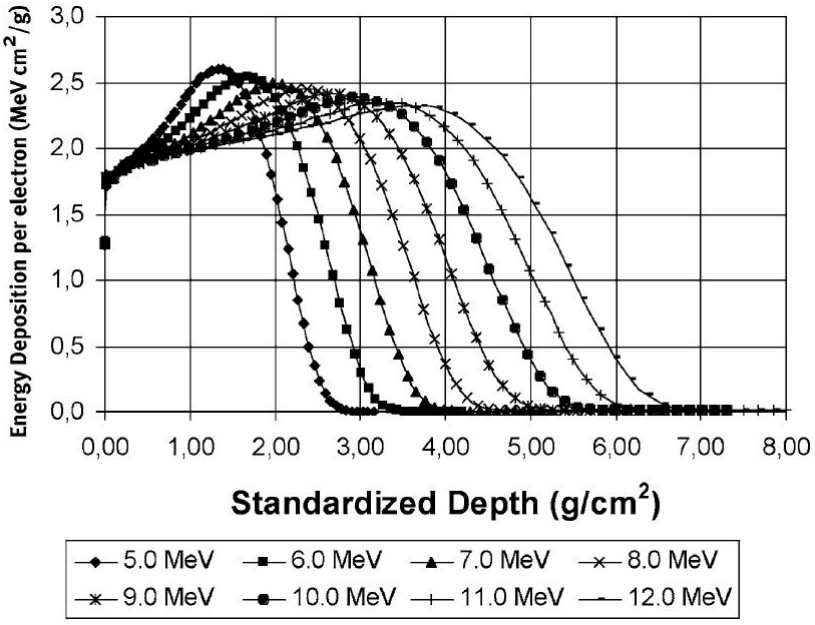

FIGURE 2.4: Depth doth curves of different EB energies[86].

Many parameters play an important role in dose delivery, such as beam energy, beam current, conveyor speed, scan width, beam length and the product's density, shape, geometry and thickness. All parameters that are related to the installation need to be well characterized during the installation and operational qualification (IQ/OQ). Thus, by knowing the dosimetric limits of a certain products, the irradiation operator can adapt the irradiation parameters in order to ensure that all requirements are fulfilled, such as absorbed dose and product DUR. The dose rate delivered by medium to high energy EB accelerators ranges from few kGy/s up to few

tens of kGy/s. This kind of installations offer many radiation applications such as the sterilization of medical devices, polymer crosslinking or degradation, food irradiation and surface decontamination.

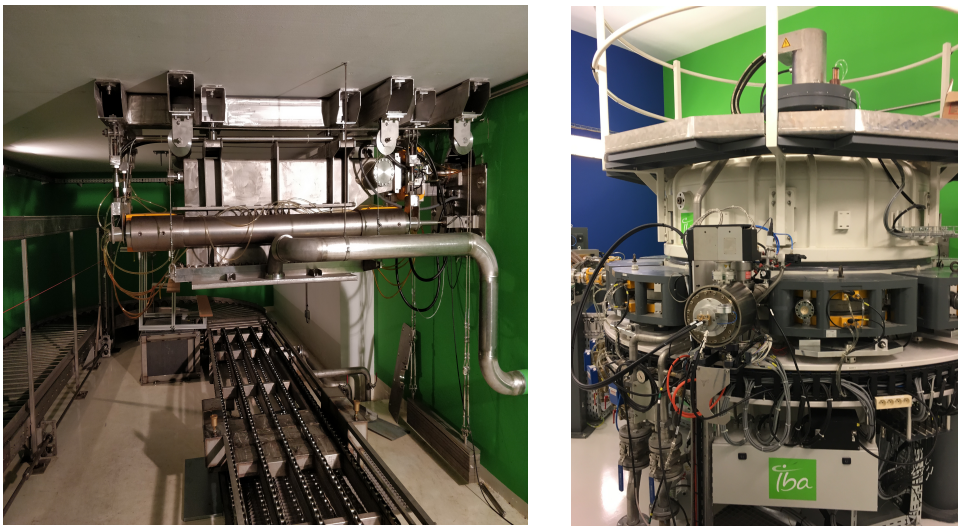

FIGURE 2.5: feerix® irradiation installation at Aerial, Strasbourg. On the right: TT200/300 Rhodotron® and on the left: 10 MeV electron beam scan horn and conveyor system.

2.2.3 X-ray irradiators

Although EB irradiations offer a very high dose rate, it could be inefficient in case of dense or thick product irradiation because of its low penetration, thus it was found more suitable to benefit from the electron beam and convert it into X-rays. Generation of X-rays begins by accelerating electrons towards a conversion target where X-rays will be generated due to electron interaction with the converter's material as discussed in Chapter 1. The X-ray production efficiency depends on both the incident electrons energy and the target's material and thickness, knowing that the maximum authorized X-ray energy, for radiation processing, is 5 or 7.5 MeV, depending on regulations of local authorities. These limits are set because of potential radio-induced activation of materials irradiated at higher energies[76]. For tungsten material, the X-ray production efficiency at 100 keV is in the order of 0.1% and increases to about 7 to 8% at 5 MeV[76].

For kV X-rays, targets made of tungsten are used for X-ray generation with high voltages going from few kV up to 300 kV, and are used for different applications whether in medicine, research or industry. Other X-ray generators house a molybdenum target and are used in mammography, operating with a high voltage in the range of 20 - 50 kV. A new 4π X-ray tube concept[96], based on a cylindrical gold X-ray target and an axial cathode, is used for many kV X-ray applications such as blood irradiations and Sterile Insect Technique (SIT) treatments. Almost all kV X-ray irradiators are self-shielded and ensure a homogeneous dose delivery to products in box sizes, while irradiation plants based on mega-voltage (MV) EB accelerators are able to treat industrial sized pallets.

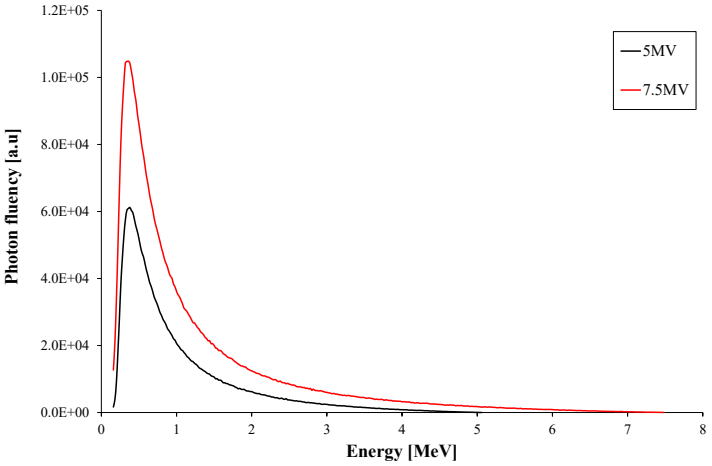

FIGURE 2.6: Geant4 Monte Carlo simulation of energy spectra of X-rays generated from a 1.2 mm thick tantalum conversion target at 5 and 7.5 MV.

The difference between MV and kV X-ray irradiators resides in the installation geometry and in many cases, in the choice of the converter's material. In the case of MV X-ray irradiators, X-ray generation relies on direct transmission where the incident EB is perpendicular to the X-ray target, which is often made of tantalum ($Z = 73$) and has a length of up to 2 m. In the case of kV X-ray generators on the other hand, the X-ray conversion target is often made of tungsten ($Z = 74$), with a length in the range of few centimetres, and is placed at a small angle with respect to incident electrons (10 to 30 degrees), in order to maximize the X-ray emission probability.

FIGURE 2.7: 5 or 7 MV X-ray scan horn and a pallet conveying system at the feerix® facility at Aerial. X-ray conversion target measures 2.2 m long and is made of tantalum.

X-rays interact less with matter compared to electrons, thus they are more penetrating. Figure 2.8 shows the percentage depth dose distribution of different photon beams in water. Delivered dose rates depend on many parameters such as high voltage, beam current, added filtration, scan width and source to product distance. MV X-rays are more penetrating in mater than ^{60}Co gamma rays, as shows figure 2.8, thus, MV X-ray irradiators can offer at least an equivalent, and in many cases a better dose homogeneity than radioactive source-based irradiators.

In order to deliver high dose rates, MV X-ray generators require a big amount of electrical power because of the low EB to X-ray conversion efficiency. Newly developed MV X-ray generators, such as the TT1000 Rhodotron, can deliver 7 MV X-ray with a power of up to 560 kW. This beam power is equivalent to a ^{60}Co gamma irradiator with a total source activity of 4.5 MCi[36].

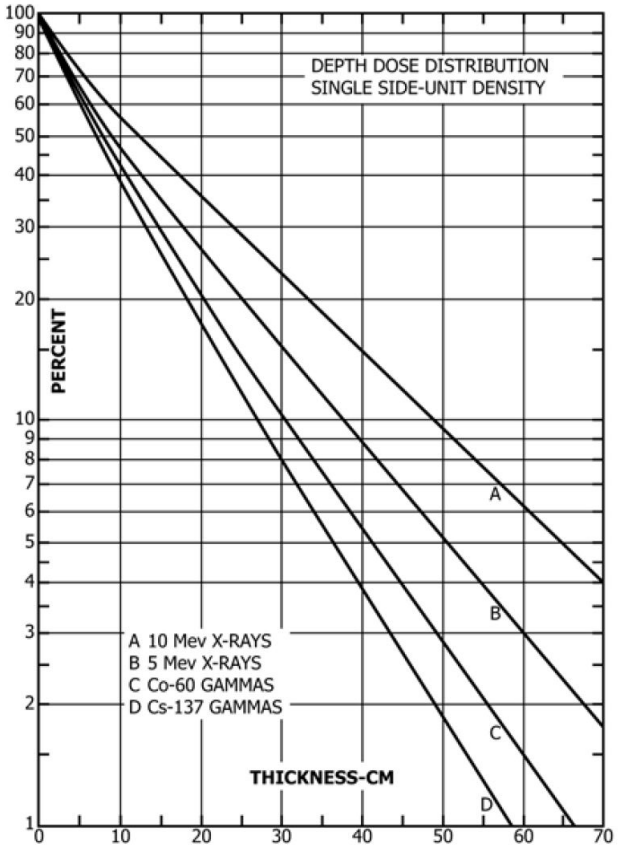

FIGURE 2.8: Percentage depth dose distribution in water for a single sided irradiation with different photon beams[76].

2.3 Radiation applications

2.3.1 Medical device sterilization

Sterility is defined as "*a state of being free of viable microorganisms*[72]". Nowadays, in order to ensure the safety of a patient, all medical devices, such as syringes, tubes, catheters, sutures and implants are required to be sterilized before being put into use. Over the past years, medical

devices have been sterilized by many techniques, including ethylene oxide, dry heat, hydrogen peroxide, steam and ionizing radiation. Radiation sterilization of medical devices remains one of the most efficient techniques because it does not put the end-use product in contact with any medium other than its own packaging system, thus avoiding all potential fixation of residues of the sterilizing agent.

The main goal of sterilization of medical devices it to reduce the quantity of pathogens to a certain level where the use of such medical device is considered to be safe in terms of microbial contamination. This goal should be achieved without damaging the product itself, thus, potentially compromising the device's effectiveness. Ionizing radiation kills bacterial cells due to both direct (ionization of DNA protein molecules) and indirect damage (radio-induced water radiolysis releasing free radicals that could break DNA protein molecules) to the DNA molecules. The effect of ionizing radiation on the inactivation of a certain bioburden can be determined using this equation[129]:

$$N = N_0 \, e^{-D/D_{10}} \tag{2.2}$$

where N is the number of surviving microorganismes at a dose D, N_0 is the original number of microorganismes and D_{10} is the absorbed dose value required to reduce the population of the considered microorganismes to 10%. D_{10} values depend mainly on the type of the microorganisme. For bacteria, typical D_{10} values are in the range of 1 to 4 kGy, whereas in the case of viruses, typical D_{10} values are within 3 to 8 kGy[129]. D_{10} values can be also dependant on the temperature of the microorganisme culture and water content.

Many standards have been developed by international organisms, such as the International Organization for Standardisation (ISO)[72–74] and the Association for the Advancement of Medical Instrumentation (AAMI)[1, 2], in order to: present requirements for the development, validation and control of sterilization process, give guidance on establishing maximum acceptable and sterilization doses and finally to discuss dosimetric aspects of mandatory installation, operation and performance qualifications. The most important requirement to be met during a radiation sterilization process is the Sterility Assurance Level (SAL) which is defined as the "*probability of a single viable microorganism occurring on an item after sterilization*[72]" and has a value of 10^{-6}, thus, meaning 1 in a million chance of survival of a colony forming unit on the irradiated medical device.

In order to sterilize while maintaining the efficiency of the medical device, standards[72–74] have established methods that permit to determine two key dose values: sterilization dose and the maximum acceptable dose. Other documents developed by the *Panel on Gamma and Electron Irradiation* give guidance on how to establish these dose levels[127, 128]. The sterilization dose (D_{ster}) is defined as the "*minimum dose to achieve the specified requirements for sterility*", and the maximum acceptable dose ($D_{max,acc}$) is defined as the "*dose given in the process specification as the highest dose that can be applied to a defined product without compromising safety, quality or performance*".

During a performance qualification (PQ), a dose mapping of the irradiated product is carried out in order to determine the zones having minimum and maximum dose. To validate an irradiation process, the operator needs to guarantee that the product is irradiated at dose levels

higher than D_{ster} and lower than $D_{max,acc}$, in other terms, to ensure that the process DUR, taking into account all uncertainties and variabilities, is lower than the ratio $D_{max_{acc}}/D_{ster}$. This is done by defining two new dose levels: minimum D_{min} and maximum D_{max} dose. These two dose levels take into account uncertainties and variabilities derived mainly from OQ and PQ. Limits of D_{min} and D_{max} are well defined in ISO standards 11137-3[74] and [75] as such:

$$D_{min}^{limit} = D_{ster} \times UF_{lower} \tag{2.3}$$

and

$$D_{max}^{limit} = D_{ster} \times UF_{upper} \tag{2.4}$$

where UF_{lower} and UF_{upper} are defined as the lower and upper limits of the process factor respectively. Process factors are calculated based on minimum and maximum values the standard deviation associated with the irradiation process used for setting process target doses ($\sigma_{process}$). They are expressed as such:

$$UF_{lower} = \frac{1}{1 + k \,.\, \sigma_{process}^{min}/100} \tag{2.5}$$

and

$$UF_{upper} = \frac{1}{1 + k \,.\, \sigma_{process}^{max}/100} \tag{2.6}$$

where k is the coverage factor, $\sigma_{process}^{min}$ is the standard deviation associated with the process minimum dose and $\sigma_{process}^{max}$ is the standard deviation associated with the process maximum dose.

2.3.2 Food irradiation

Food irradiation is the processing of food products by ionizing radiation in order to, among other goals, control food-borne pathogens, reduce microbial load and insect infestation, inhibit the germination of root crops, and extend the durable life of perishable produce[42]. The principal standard from an international perspective is the *Codex Alimentarius General Standard for Irradiated Food*[41]. According to this document, the radiation sources that are allowed to be used in food irradiation are: gamma rays from ^{60}Co and ^{137}Cs radionuclides, X-rays generated from machine sources operated at or below an energy level of 5 MeV and electrons generated from machine sources operated at or below an energy level of 10 MeV. However, because of the low x-ray generation efficiency, the IAEA (International Atomic Energy Agency) has recommended that the upper limit on electron energy for X-ray processing of food products be raised to 7.5 MeV, and the USFDA (United States Food and Drug Administration) has recently approved this limit[55, 116].

Dose range [kGy]	Desired effects	Treated foodstuff
0.1 - 1	Sprouting inhibition	Potato, garlic, onion
	Delay of ripening	Papaya, banana
	Phytosanitary treatment	Fresh produce
	Killing of insects	Dried fish, dried fruits
	Inactivation of parasites	Meats, fresh fruits and vegetables
1 - 10	Extension of shelf life	Strawberries
	Inactivation of non sporulating microorganisms	Frozen meats, seafood
	Reduce of microbial contamination	Spices, dried food
> 10	Sterilization	Hospital diets, food for astronauts

TABLE 2.2: Table of the different applications for food irradiation.

Sanitary applications of food irradiation, at doses ranging from 1 to 10 kGy, are based on the lethal effects of radiation on microorganisms such as those causing food-borne disease or reducing storage time or shelf life, parasites that can infest meats and insects that can cause post harvest losses. On the other hand, phytosanitary measures are more of preventive precautions that are taken in order to significantly reduce potential introduction or spread of harmful pests on food. Typical radiation doses used for phytosanitary treatments are in the range of 0.4 to 1 kGy. These somehow low doses of radiation can induce sterility or mortality of the pest, depending on its type.

Process validation for food irradiation is based on that for sterilization of health care products[57, 72]. After achieving installation and operation qualifications, the user should perform a performance qualification that consists in a dose mapping of each type of product in order to locate minimum and maximum dose zones, calculate a DUR and finally ensure that the delivered dose to the product falls within the range of minimum and maximum product dose limits.

Low radiation doses that phytosanitary treatments require, have made the use of small kV X-ray irradiators very interesting compared to large scale irradiation plants. Figure 2.9 shows a drawing of an installation based on four kV X-ray irradiators used for phytosanitary treatments. Use of small self-shielded irradiators ensures a DUR close to 1.4, depending on the box's density and the loading pattern inside of the box. The cost of installation of such system is in the order of one tenth the cost of the installation of a big scale irradiation plant, while having a smaller footprint, thus, products can be irradiated on the same day they are packaged and therefore reducing time and costs of transporting products to be irradiated at an external irradiation plant. This type of irradiators is witnessing an increasing demand compared to self-shielded radioactive source-based irradiators, and many users of small gamma irradiators are switching to alternative X-ray solutions because of the increasing difficulties in procuring, managing and transporting radioactive sources.

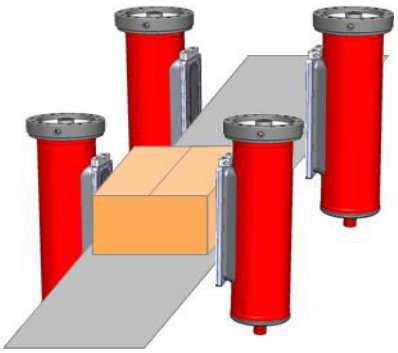

FIGURE 2.9: Drawing of 4 kV X-ray irradiators used for phytosanitary treatments.

2.3.3 Applications for polymer material

Physico-chemical properties of polymers can be altered by ionizing radiation. Electron beams are considered as the most efficient radiation sources that can be used to obtain different goals such as curing, grafting, crosslinking and chain scission of polymers. These radio-induced effects are of interest for many users and service providers such as cable wiring industry, ink and printing industries, automotive industries as well as companies that recycle plastics and polymer-based products.

2.3.3.1 Polymerization(curing)

Polymerization is the assembly, using absorbed energy, of repetitive units (monomers) in order to make a long monomers chain called a polymer. Low energy (up to 300 keV) electron beams are used to polymerize coatings, adhesives and inks. Irradiation is used in order to harden and solidify such material as radiation initiates and induces the formation of extra bonds between monomers that constitute the polymer chains[102]. Curing of such materials does not require the presence of solvents, where the irradiated material can be water based. In order to achieve such goals, the typical delivered dose is in the range 10–30 kGy[26]. Electron beams are the best choice of ionizing radiation source due to very high dose rates that permit to treat products on a large scale with a high throughput.

Composites made of fibres and resine benefit from an augmentation of their strength when exposed to ionizing radiation. They are usually cured with heat, but EB irradiation offers the best results with less time and costs. Curing of such materials require a dose in the rage of 150 to 250 kGy, depending on the material. At these doses, monomer polymerization is accompanied with polymer crosslinking. The main benefiters of such applications are the automotive industries and aerospace organizations that both require stronger and lighter materials.

2.3.3.2 Radiation grafting

Radiation grafting is the process of joining together two different polymer chains in order to form a copolymer. This technique can modify properties of polymers in order to make enhanced

materials. Such enhancements go from adding hydrophilic properties to hydrophobic polymers, improving biocompatibility of polymers for use in medicine[51], changing the permeability selectivity of a certain polymer, to making flame retardant materials[45]. Typically, electron beams are used for this type of application and delivered doses go up to 10 kGy[26].

2.3.3.3 Polymer crosslinking

Radiation-induced crosslinking is the phenomenon of creating chemical bonds between two or more polymers inside of a material due to absorbed energy given by ionizing radiation. Polymer crosslinking leads to the enhancement of mechanical (rigidity) and thermal (thermo-resistance) properties of irradiated materials. However, polymer crosslinking is accompanied by polymer chain scissions due to degradation caused by ionizing radiation. Yet, one phenomenon dominates the other depending on the intrinsic properties of the polymer as well as the absorbed dose range. Radio-induced yields of both crosslinking and scission are defined as the number of specific events per 100 eV of absorbed energy and are denoted *G(X)* and *G(S)* respectively. Polymers with values of $G(S)/G(X) < 1$ are considered as favorable for crosslinking applications, such as natural rubber and polyethylene. Values of *G(S)* and *G(X)* change with absorbed dose and irradiation temperature. Typical absorbed doses for crosslinking applications range from 50 to 250 kGy depending on the material, yet, using specific additives to enhance the crosslinking effect can reduce the required dose.

This technique is used to treat insulated wires and cables making them more resistant to high temperatures, thus inducing fire retardation, more resistive to abrasion and more resistant to some solvents. These cables and wires are used in cars, aircraft and spacecraft. Polyethylene thin plastic tubing is crosslinked to enhance the memory effect. Irradiation stabilizes the original dimensions of the tubing. When it is heated above the classical melting temperature, the irradiated tubing becomes elastic and can be expanded. When cooled, it keeps the expanded dimension but retains the memory of its original dimension, thus, when heated again, it contracts to its original dimension. Components of rubber tires, containing multiple layers of different materials, are irradiated at doses ranging from 30 to 50 kGy in order to obtain a partial crosslinking between layers before the tire assembly.

2.3.4 Blood irradiation

The risk of development of Transfusion-Associated Graft Versus Host Disease (TA-GVHD) following transfusion of blood components containing viable lymphocytes to susceptible individuals can be prevented by irradiation of such blood components[92, 134]. Blood components are usually irradiated to doses in the range of 15 to 50 Gy, using gamma rays, from ^{60}Co and ^{137}Cs radionuclides, or X-rays with energies in the range of 40 to 300 keV[87].

Blood irradiators house either a radioactive gamma source or an X-ray tube. Blood components are placed in special canisters that is then loaded inside of the irradiator to be irradiated. In order to maximize the dose homogeneity inside of the canister, new irradiator models offer the possibility to rotate the canister in front of the beam, or use many radiation sources to irradiate

blood components from different angles. Thus, to ensure that blood components have been properly irradiated, accurate dose measurements on the product or simulated product needs to be performed. ISO/ASTM 51939 standard[87] stipulates that "*For each blood irradiator, an absorbed-dose rate at a reference position within the canister is measured as part of irradiator acceptance testing using a reference-standard dosimetry system*". These absorbed dose measurements can be performed in blood equivalent volumes such as polystyrene phantoms.

Nowadays, a clear growth in switching from radioactive source-based irradiators to kV X-ray irradiators is observed. This switch is driven by the difficulty to purchase, transport and reload radioactive sources as well as dealing with potential radioactive wastes. On the other hand, it has been demonstrated that X-ray irradiations of blood offer same results as gamma irradiations[90, 139], while ensuring same capacities in terms of delivered dose rates and DURs.

FIGURE 2.10: RS3400 4pi X-ray irradiator[132].

Dosimetry for X-ray self-shielded irradiators however can be difficult knowing that response of most dosimeters has significant energy dependence at photon energies that are below 100 keV[87]. Alanine dosimeters are used in many radiation applications using kV X-rays[95] including blood irradiation due to their high dosimetric properties and for being used in both reference and routine dosimetry. This was one of the motives that lead us to study the alanine's relative response to kV X-rays in order to ensure a better and more precise dosimetry for this type of applications.

2.3.5 Sterile Insect Technique

In order to preserve locally grown produce and to reduce diseases that can be propagated by a certain type of pests, large scale control of the development of specific pest species is achieved by applying the Sterile Insect Technique (SIT). SIT is based on collecting big numbers of certain

male pests and then inducing their sterility using ionizing radiation. Once sterilized, male pests are released into their natural environment to mate with female pest. Because of radio-induced sterility, offspring hatching of harmful pests is significantly reduced or completely eliminated in some cases. Depending on the species of the pest to be controlled, delivered doses vary from 20 to 600 Gy[84].

Different types of ionizing radiation sources are used for SIT treatments, such as self-shielded gamma or X-ray irradiators as well as MV electron or X-ray beams[12]. However, a serious problem has arisen for new SIT projects as it is becoming almost impossible to acquire radioactive sources for insect sterilization[107]. Thus, just like in the case of blood irradiators, an increasing switch from radioactive source-based irradiators to X-ray irradiators is noticed. IAEA has approved in late 2019 the launch of a coordinated research project with the objective of promoting the innovation of in-line and in-house radiation processing of foods using low energy beams.

The key parameter for quality assurance in SIT treatments, as well as in other radiation applications, is the measurement of absorbed dose. A full dosimetric characterization of the RS-2400 X-ray irradiator, that is used in the Insect Pest Control Laboratory of the Joint FAO/IAEA Division of Nuclear Techniques in Food and Agriculture, was carried away using a Gafchromic® film dosimetry system[111]. This study showed that this X-ray irradiator is well suited for SIT treatments from a dosimetric point of view, where it was demonstrated that this system is capable of delivering the same performances (dose rate, dose homogeneity and DUR) as a gamma source-based irradiators. As for the efficiency of X-ray irradiators in ensuring same radio-induced biological outcomes as gamma irradiation, a study, that compared biological effects of the irradiation of two pest species with X-rays and gamma rays, showed that the use of X-rays for SIT treatments ensures the same desired biological effects that gamma rays induce in the studied pest species[107].

Dosimetry using alanine can be interesting for this type of applications, where the alanine dosimetry system ensures lower dose measurement uncertainties and less or correctable impact of influence quantities on the alanine dosimeter's response, compared to other dosimetry systems that are used in SIT such as the Gafchromic® film dosimetry system. Chapter 3 discusses and details more information about both dosimetry systems.

2.3.6 Other applications

Ionizing radiation is used in many other fields such as environmental applications where sewage sludge waste water or industrial flue gases are irradiated for de-pollution reasons. Radiation is also used to color or change the color of gemstones by applying very high doses in the range of MegaGrays. Electronic properties, such as conversion times of semi-conductors, can be improved by irradiation. Cultural heritage and monuments can be preserved from damage caused by insects or microorganismes by subjecting them to ionizing radiation that would kill any potential threat to these objects.

2.4 Conclusion

This chapter presented various types of ionizing radiation sources, from gamma-based irradiators, to electrical machines generating both electron or X-ray beams at different energy levels; as well as major applications that use these ionizing radiation sources in the benefit of humankind. Yet, in order to maintain a good quality of all irradiation processes, a key parameter needs to be well understood and most importantly well controlled. This parameter is the absorbed dose. This quantity might be difficult to measure and many precautions need to be taken into account to ensure the viability of any irradiation process. Chapter 3 will present these different aspects as well as dosimetry systems that are used in radiation processing and radiation research.

Chapter 3

Dosimetry in industrial radiation processing

Contents

3.1 Introduction

A continuous growth in the use of radiation sources, both radioactive sources or electrical machines, is observed since the start of industrial scaled radiation processing in the 1950's [67]. As discussed in chapter 2, industrial radiation processing plays an important role in protecting people's lives by applying radiation to daily used products, such as medical devices or food, in order to ensure sterility of a certain product or the decontamination of another, thus, all irradiation processes need to be properly established, validated and then routinely well performed.

Quality assurance of all irradiation processes relies on the use of efficient dosimetry systems [57] that are traceable to national or international standards, in order to perform proper process qualification and routine process control. Accurate dose measurement is therefore a key element in all irradiation processes. This accuracy must be maintained during the qualification of the irradiation facility as well as during process validation and routine monitoring.

It is the duty of the irradiation facility to demonstrate that the specified minimum dose was delivered to the product and to ensure that all dose points did not exceed the maximum acceptable dose. In general, the establishment of specified minimum dose is based on previous studies that show that the desired effect is achieved at a certain absorbed dose level. Maximum acceptable dose is the absorbed dose level from which irradiation changes some properties of the product in an acceptable manner. Thus, during a dose mapping (Performance Qualification) of a given product, the irradiation operator needs to prove that all dose points fall between specified minimum and maximum acceptable doses, within limits and uncertainties.

To summarize, accurate dosimetry is a key element in radiation processing, yet, the choice of an adequate dosimetry system is crucial and relies on many parameters such as the dose range, dose rate, desired uncertainty and potential influence quantities. This chapter presents the different families of dosimeters that are used in industrial radiation processing and discusses their usage pros and cons as well as influence quantities that could affect each dosimeter's reading.

3.2 Types of dosimeters and dosimetry systems

A dosimeter is defined as a "device that, when irradiated, exhibits a quantifiable change that can be related to a dosimetric quantity using appropriate measurement instrument(s) and procedures"[89]. A dosimetry system is defined as "interrelated elements used for measuring a dosimetric quantity, including dosimeters, instruments and their associated reference standards, and procedures for their use."[89].

Classification of dosimeters and dosimetry systems is based on two criteria: the inherent metrological properties of the dosimeter and the field of application of the dosimetry system [89]. Classification based on the inherent metrological properties of a certain dosimeter led to the distinction of two types of dosimetry systems: *Type I* and *Type II* dosimeters.

Type I dosimeters are considered as dosimeters of high metrological quality which response is affected by influence quantities, such as irradiation temperature, in very well known way that

can be overcome by applying independent correction factors to the dosimeter's reading. *Type II* dosimeters are dosimeters which response is affected by influence quantities in a complex way that cannot be taken into account in terms of independent correction factors to be applied to the dosimeter's reading.

External influence quantities such as irradiation temperature, storage temperature, relative humidity, exposure to Ultraviolet (UV) or ambient light, absorbed dose rate and oxygen content may have significant effects on the response of some dosimetry systems.

Classification of dosimetry systems according to their proper field of application distinguishes four types of dosimeters as described here-after. All four dosimeter types are linked by a chain of traceability that begins with BIPM (Bureau International des Poids et Mesures), located in Paris. The BIPM acts as the superior international reference that standards held by national laboratories are compared to. Primary standard dosimetry systems, held by Primary Standard Dosimetry Laboratories (PSDL), are directly related to the BIPM's standards, reference standard dosimeters, often delivered by Secondary Standard Dosimetry Laboratory (SSDL) are calibrated against primary or secondary standards, and are used as transfer standard dosimeters to calibrate routine dosimeters, as shows figure 3.1.

3.2.1 Primary standard dosimetry system

A primary standard dosimetry system is one that enables an absolute measurement of absorbed dose to be made with reference only to the SI base units(mass, length, time, electric current, etc.) and fundamental physical constants [67]. It is also defined as a dosimetry system that is designated or widely acknowledged as having the highest metrological qualities and whose value is accepted without reference to other standards of the same quantity [89]. This type of dosimetry system is generally operated by a national standards laboratory and Primary Standard Dosimetry Laboratories (PSDL), and is used to provide the primary standard for use in a particular country. Calorimeters and ionization chambers are the most frequently used dosimeters to establish the primary standard. Absorbed dose to water D_w is the quantity that is normally used in high dose dosimetry. Primary standard dosimetry systems ensure a maximum measurement uncertainty of $\pm$ 2% at a confidence level of 95% ($k = 2$).

3.2.2 Reference standard dosimetry system

A reference standard dosimetry system is defined as a dosimetry system of high metrological quality, which can be used as a reference standard to calibrate other dosimetry systems [67]. Both primary standard and reference standard dosimeters belong to the *Type I* dosimeter family. To be considered as a reference standard, the system in question must have an intrinsic signal that is accurately measurable, this signal must have a well-defined functional relationship with absorbed dose. The effect of external influence quantities, such as irradiation temperature or absorbed dose rate, should be well characterized and expressed in terms of independent correction factors. Commonly used reference standard dosimeters include Fricke, dichromate or ceric-cerous solutions, alanine pellets and calorimeters. Reference standard dosimetry systems ensure a maximum measurement uncertainty of $\pm$ 3% at a confidence level of 95% ($k = 2$).

Reference standard dosimeters can be created and handled by both a PSDL and accredited Secondary Standard Dosimetry Laboratory (SSDL).

3.2.3 Transfer standard dosimetry systems

Transfer standard dosimeters are used for transferring dose information from an accredited laboratory to an irradiation facility in order to establish traceability of their dosimetry system to the national or international standard. Many calibration laboratories operate mailed dosimetry services where dosimeters, sent from the laboratory to the irradiation facility, are irradiated at the facility and then sent back to the laboratory for readout and certification. They are usually considered as reference standard dosimeters [67] and are used to calibrate other dosimetry systems such as a routine dosimetry system. Alanine pellets as well as Fricke, dichromate and ceric-cerous chemical solutions are considered and used as transfer standard dosimeters.

3.2.4 Routine dosimetry systems

Compared to reference standard dosimeters, routine dosimeters may not have the same performance, yet, they present a cheap and easy to use solution that makes them suitable for a day to day routine use in radiation processing facilities. The effect of influence quantities can be complex to characterize and their expression is therefore difficult in terms of independent correction factors, thus, the calibration of routine dosimeters is usually done in the irradiation facility in order to reproduce the same environmental conditions. Radiochromic films, plastics as well as dyed plastics are dosimeters that are commonly used as routine dosimeters. Routine dosimetry systems ensure a measurement uncertainty of about $\pm$ 5% at a confidence level of 95% ($k = 2$). However, a growth in the use of other dosimeters such as alanine pellets in routine is observed. This is mainly due to the smaller measurement uncertainty that provides the alanine dosimetry system as well as the broad dose measurement range of few Gy to 100 kGy.

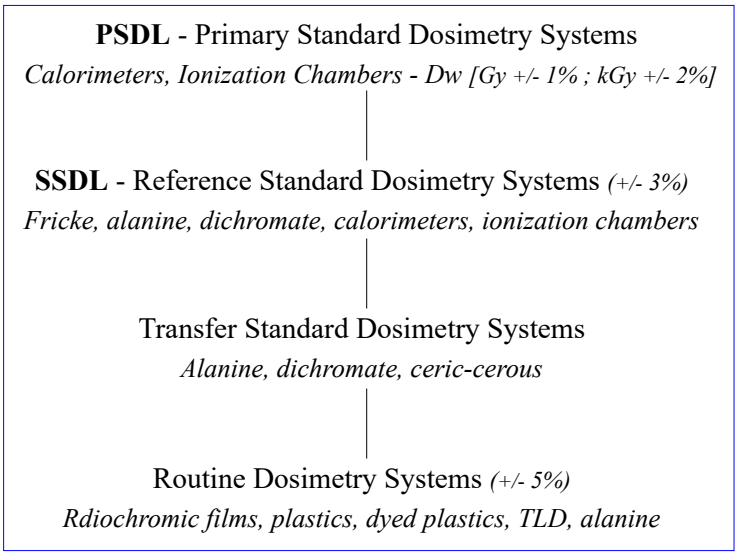

FIGURE 3.1: Chain of traceability between different dosimetry systems.

3.3 Dosimetry systems used for radiation processing control

This section presents different types of dosimetry systems that are commonly used in radiation processing as reference standard or routine dosimeters, as well as their reaction mechanisms, methods of measurement, dosimetric properties and influence quantities.

3.3.1 Alanine/EPR dosimetry system

The Alanine/EPR dosimetry system is based on the measurement of specific free radicals in crystalline α-alanine generated by ionizing radiation. It is used as reference standard, transfer standard as well as routine dosimetry system for different radiation applications such as medical device sterilization, food irradiation and polymer modifications [81]. Alanine was first used as a solid dosimeter by Bradshaw in 1962 [17] and improved for high precision measurements in the 1980's [133]. Alanine dosimeters and are manufactured in many forms such as thin films, rods and mostly pellets. Many studies [52, 53, 117] reported that ionizing radiation induces the formation of a stable alanine radical (SAR) which results from the deamination of the alanine molecule. Studies later on showed that two other radical species are created due to ionizing radiation but at lower quantities compared to the SAR [135]. The nature of different types of radicals is thoroughly discussed in chapter 4.

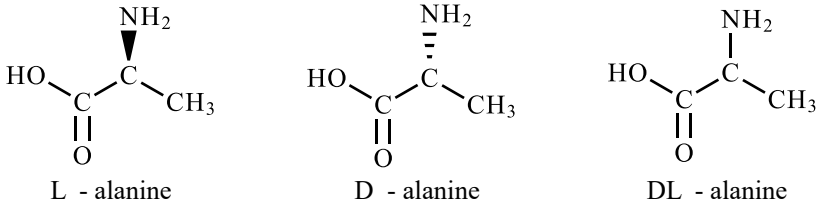

FIGURE 3.2: Chemical structures of different isomers used in fabrication of alanine dosimeters.

Alanine/EPR dosimetry is based on the measurement of the concentration of free radicals created inside the dosimeter due to ionizing radiation. This measurement is carried away using an EPR spectrometer that records the microwave power absorption while scanning over a given magnetic field range. The first derivative of this signal is plotted as a function of the magnetic field's magnitude, as shows figure 3.3. The value of absorbed dose is directly related to the peak to peak height (H_{pp}) of the central peak. This relation is established by a calibration curve that links the dosimeter's response, defined as the ration of the H_{pp} to the dosimeter's mass, to the absorbed dose.

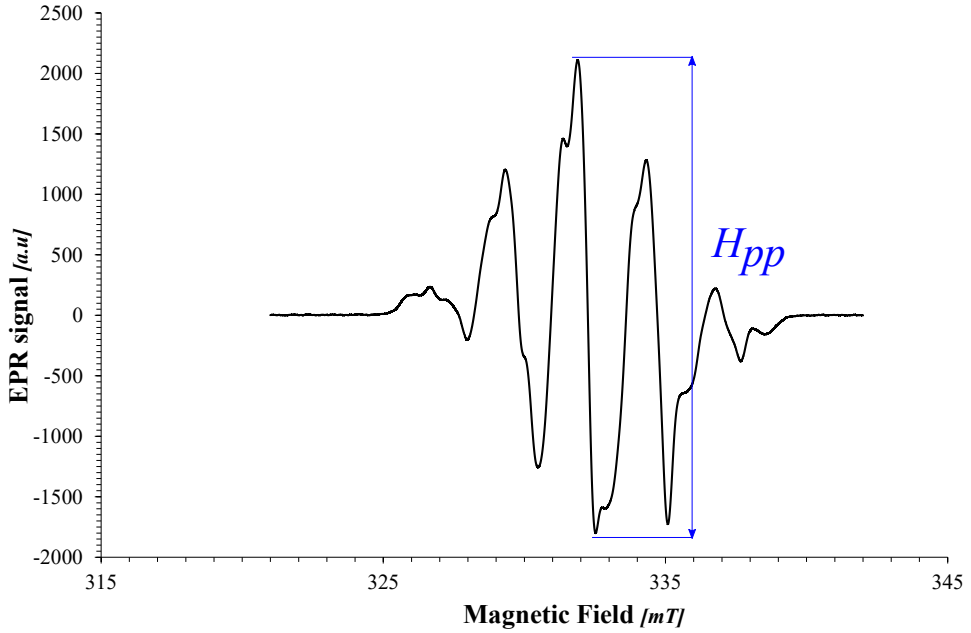

FIGURE 3.3: First derivative EPR signal of an irradiated alanine dosimeter.

Alanine dosimeters can be used for dose measurement in the dose range of $1Gy - 100kGy$[67] and even up to $150kGy$ according to the ISO/ASTM 51607 standard[81]. However, the linearity of the dosimeter's response in function of dose depends on the dose range. Figure 3.4 shows that alanine's response is linear for doses ranging from $1Gy$ up to less than $10kGy$ and it loses its linearity at higher doses. This is due to the saturation of the concentration of radio-induced alanine free radicals inside of the dosimeter, as the absorbed dose goes higher [44].

Alanine is considered as a *type I* dosimeter, thus, its response is affected by external influence quantities in a known way. The impact of such influence quantities can be corrected by applying independent correction factors to the dosimeter's reading. The major influence quantities that affect the alanine dosimeter's response are pre and post-irradiation storage relative humidity [9, 140], irradiation temperature, radiation energy and storage time [81]. Compared to other dosimetry systems, absorbed dose rate does not affect the response of alanine dosimeters [81] for both photon and electron irradiations.

The response of the alanine dosimeter increases with increasing irradiation temperature [67]. Correction factor accounting for irradiation temperature's influence can depend on the dosimeter's chemical composition. For dosimeters with L-alanine, reported data [33–35, 121, 137] showed that the irradiation temperature correction factor ranged from 0.1 %/°C up to 0.2 %/°C, for irradiations carried out at temperatures ranging from -10°C up to 70°C. EPR readout of alanine dosimeters is non destructive and ensures a dose measurement uncertainty of ± 2-4 % (k=2) for reference standard alanine, and ±4-6 % (k=2) for routine used alanine dosimeters[81]. However, due to continuous recent technological developments in EPR spectrometers, better uncertainties can be achieved using alanine/EPR dosimetry systems typically in the range of ± 2 to 3 % (k=2) for reference standard alanine, and ± 3 to 4 % (k=2) for routine used alanine dosimeters.

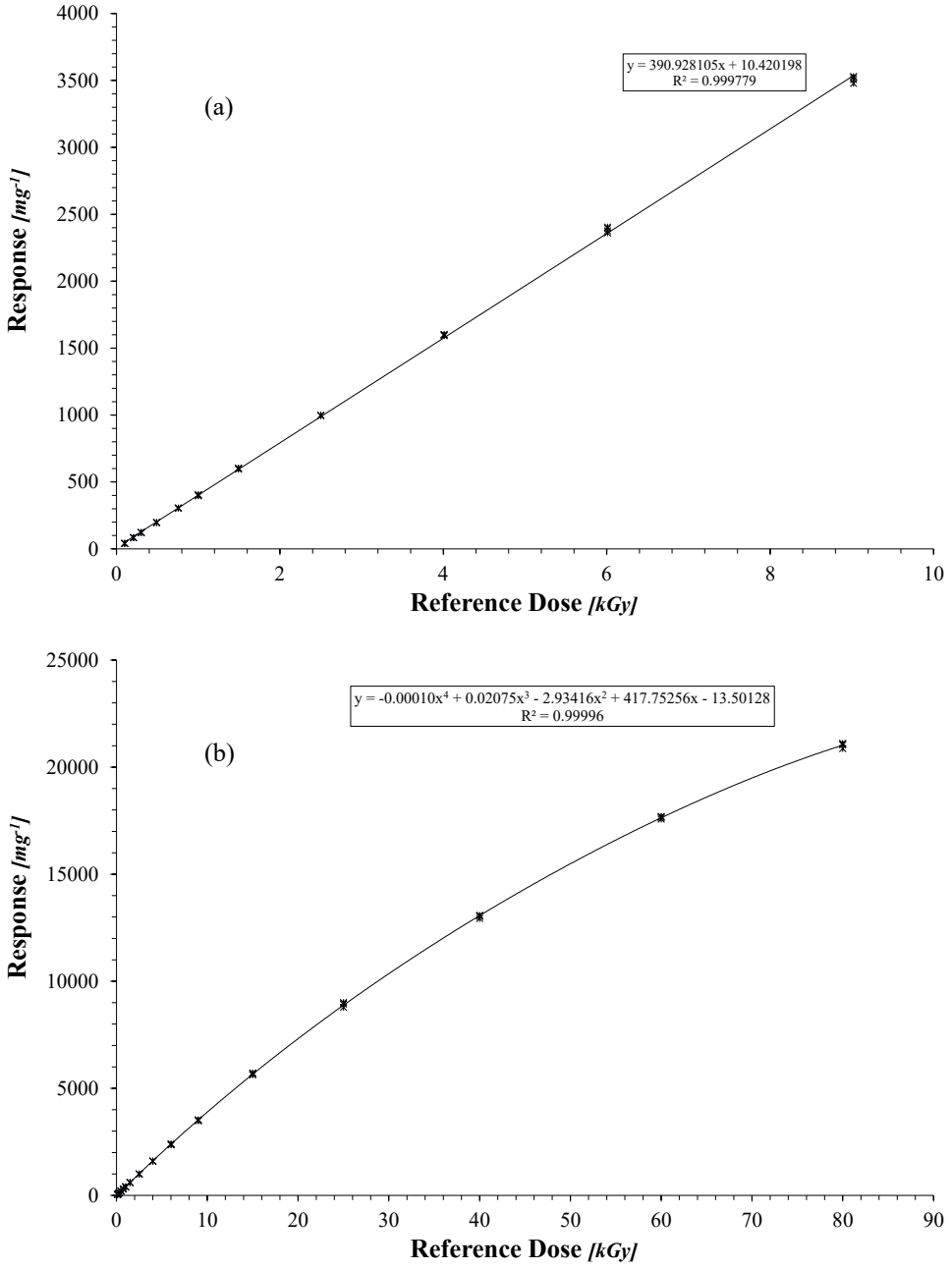

FIGURE 3.4: Calibration curve of an alanine dosimetry system for a dose range of (a) $100Gy - 10kGy$ (b) $100Gy - 80kGy$.

Alanine is considered as water equivalent, from a dosimetric point of view, for photon and electron irradiations at energies between 200 keV and 10 MeV, where the calculated absorbed dose in alanine with respect to absorbed dose in water varies by less than 4 % in this energy range [67]. However, it was reported in many studies [7, 50, 95, 122, 141, 149, 150, 153] that alanine's response drops down when irradiated with kilo-voltage X-rays. Alanine's relative response to kV X-rays, compared to its response to ^{60}Co is well studied in Chapter 5.

Many parameters can influence the post-irradiation stability of alanine's signal, such as storage temperature and relative humidity [67, 120], where fading rates ranging from 0.5% up to 5% per year were recorded for dose levels below 10 kGy, at storage temperatures and relative humidities

of 20-50°C and 40-60% respectively. Another influence parameter to take into account is the presence of ultraviolet (UV) light. It was shown [133] that long exposures to UV light, especially to light emitted by high pressure mercury lamps, can heavily influence on the EPR signal fading of irradiated dosimeters.

3.3.2 Calorimeters

Calorimetry is the measurement of a temperature variation inside of a specific irradiated volume. This technique is used by many national and international metrology laboratories to establish primary standard and reference standard and transfer standard dosimetry systems. The heart of calorimetry lies in the measurement of the temperature rise (ΔT) inside of the dosimeter (calorimeter core) due to ionizing radiation. Calorimeters, used in radiation processing, are considered *type II* dosimeters [88], where external influence quantities are difficult to control.

From a conception point of view, calorimeters used in radiation processing, for dose measurements in the range of kiloGrays, are quite simple compared to ones developed for radiotherapy dose level measurements [67]. They consist of an absorber, often made of polystyrene, placed in a heat insulating material, such as foam, with a temperature detector placed inside of the core for temperature measurement. The core's temperature can be measured during irradiation or before and after irradiation. For industrial radiation processing, temperature measurement during irradiation can be hard to achieve because wiring of the calorimeter for temperature readout can be difficult knowing that the calorimeter is conveyed to the beam delivery area.

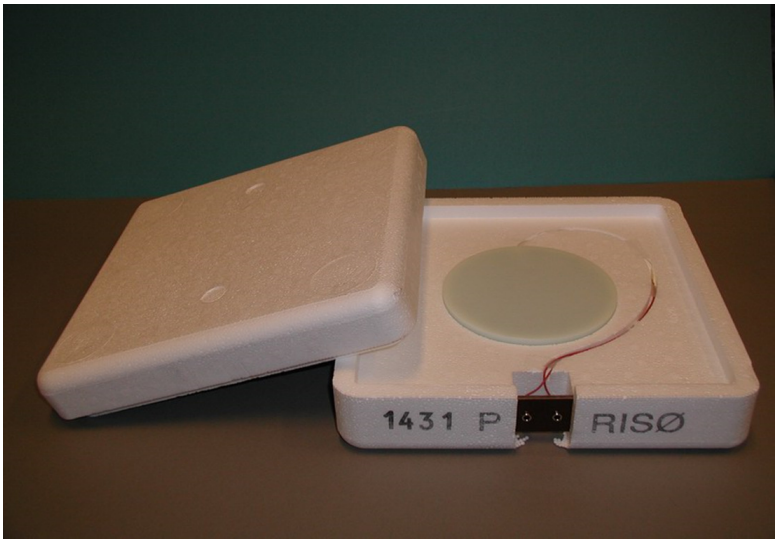

FIGURE 3.5: Polystyrene calorimeter developed by *Risφ* laboratory for routine dose measurements at a 10 MeV electron beam facility.

The use of such dosimetry systems is somehow exclusive to electron beam irradiations due to the limited stability of the radio-induced temperature rise inside of the calorimeter even though it is insulated. High dose rates delivered by electron beams, compared to gamma or X-ray beams, ensure that the desired dose is quickly delivered and the dose measurement is done in a short time frame compared to the stability of the dosimeter's response [112, 113]. Calorimeters can

be used for dose measurements in the range of 0.1 - 50 kGy [88], depending on their material (graphite: 15 kGy, polystyrene: 40 kGy, water: 50 kGy [67]). Calorimeters can be used in the electron energy range of 1.5 - 10 MeV [114, 115] or up to 12 MeV according to the ISO/ASTM 51631 standard[88].

The average absorbed dose in a calorimeter is determined as:

$$D = \frac{E}{m} \tag{3.1}$$

where D is the absorbed dose expressed in Gy, E is the absorbed energy by the calorimeter and m is its mass. Assuming that all absorbed energy is converted to heat, then the temperature rise can be expressed as such:

$$\Delta T = \frac{E}{c_p.m} \tag{3.2}$$

where c_p is the specific heat capacity of the calorimeter material expressed in $Jkg^{-1}K^{-1}$ or GyK^{-1}. Thus, by replacing absorbed energy deduced from equation 3.2 in equation 3.1, absorbed dose in the calorimeter can be expressed as such:

$$D = c_p.\Delta T \tag{3.3}$$

However, this calculation as easy as it appears, it is not directly used as such for dose measurements in radiation processing[67]. Temperature rise measurements are usually carried out using calibrated thermocouples or thermistors. For thermocouples, the temperature rise can be measured using a calibrated sensitive voltmeter where a small voltage variation is detected due to heat, however, voltage measurements can be affected by surrounding environment of the electron accelerator. For thermistors, the temperature rise induces a change of the resistance of the detectors that can be measured by a calibrated ohm meter.

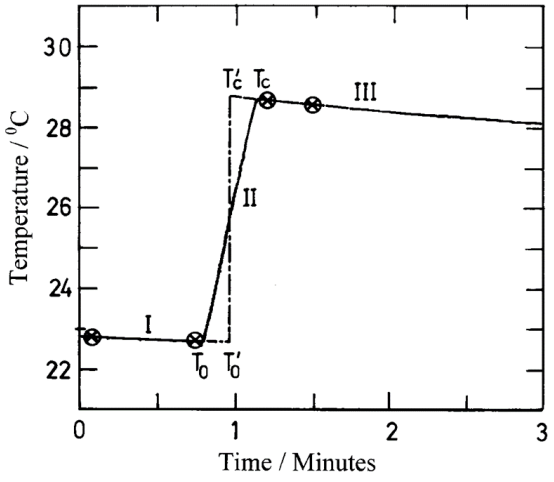

FIGURE 3.6: Calorimeter core temperature rise measurement as a function of time.[67]

In order to determine the radio-induced temperature rise in a calorimeter, one needs to determine the temperature drift before and after irradiation. This is done by extrapolating both pre and

post-irradiation temperatures to the midpoint of the irradiation time, as shows figure 3.6. The temperature difference between these two values is used as the temperature rise in equation 3.3.

Many external parameters can influence the response of a calorimeter. The ambient temperature can affect the calorimetric measurement in case the calorimeter is not in thermal equilibrium with its surroundings before being put to use. Response of calorimeters can be also affected by the radiation dose rate especially if the absorbed dose is delivered in a time frame that is in the order of magnitude of the cooling time of the calorimeter's core. Another influencing parameter is the electron energy variations, where a variation in the electron beam's energy could lead to a change of the dose distribution in the absorber.

3.3.3 Optical dosimetry systems

3.3.3.1 Radiochromic dye films / Spectrophotometer dosimetry system

A color formation or darkening on a radiochromic dye film dosimeter is observed due to electron or photon beam irradiation. Radiochromic films consist of a free-standing or coated polymeric foils that are flexible and transparent or slightly tinted, depending on the dosimeter type [67]. Figure 3.7 shows how the FWT-60 dosimeter's color darkens with absorbed dose. Nowadays, many radiochromic dye films can be found on the market. This type of dosimeters is often supplied in form of squares, strips or long rolled-up films which makes their use very convenient to dose mappings. In this section, two radiochromic dye film dosimeters will be discussed: FWT-60 and B3-Risø.

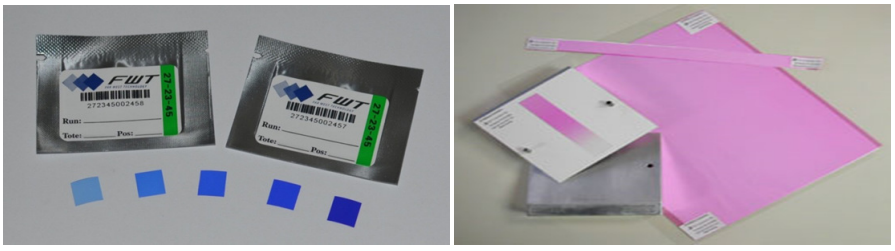

FIGURE 3.7: Two radochromic dye films used as routine dosimeters in radiation processing: FWT-60 (blue) and B3-Risø (pink).

Both FWT-60 and B3-Risø dosimeters are triphenylmethane-based films[46, 108, 109]. They are used for routine process control as well as irradiation plant qualifications (IQ, OQ and PQ). Readout for radiochromic dosimeters is usually carried out using a spectrophotometer, densitometer or a scanning microdensitometer[67]. Table 3.1 lists physical and dosimetric properties of three types of radiochromic dye dosimetry films. The overall dose measurement uncertainty of this type of dosimeter is within ±6 % (k=2)[80].

Dosimeter	Thickness [µm]	Measurement optical wavelength [nm]	Range of absorbed dose [kGy]
FWT-60	8, 10 or 50	510, 600 or 605	5 - 100
B3-Risø	18	552 ± 2	1 - 120
GafChromic HD-810	7	618 or 633 or 670	0.1 - 100

TABLE 3.1: List of the properties of three radiochromic dye film dosimeters used in radiation processing[80].

The response of a radiochromic dye film dosimeter is considered to be the ratio of the radio-induced increase of its absorbance to its thickness, and is expressed as such:

$$\Delta A = \frac{A - A_0}{t} \tag{3.4}$$

where ΔA is the radio-induced increase of the dosimeter's absorbance, A_0 and A are the absorbances measured before and after irradiation respectively and t is the dosimeter's thickness. The absorbed dose range in which radiochromic dye films can be useful depends on the dosimeter itself, as shows table 3.1. The lower dose limit is fixed according to absorbance increase at low doses[67]. On the other end, the high dose limit depends on the response saturation caused by the decrease of the radiation chemical yield at high doses.

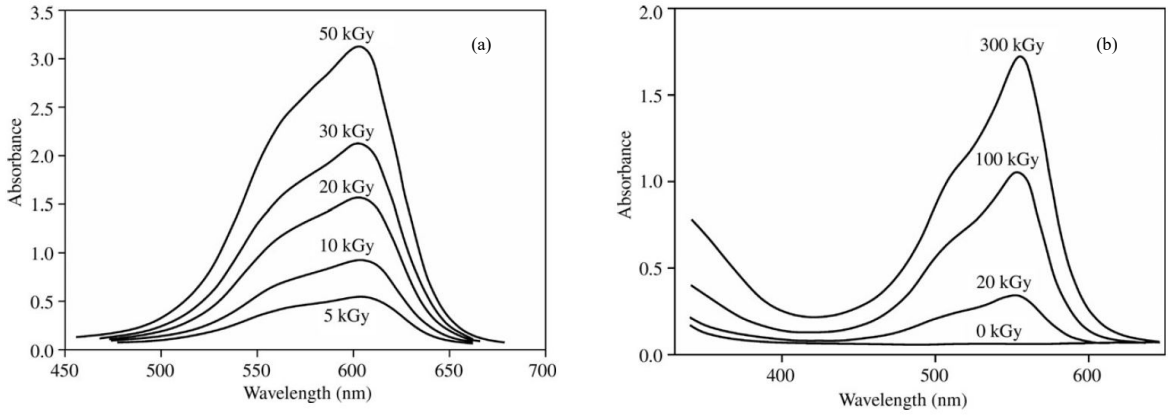

FIGURE 3.8: Typical measured absorbance spectra of both (a) FWT-60 and (b) B3-Risø dosimeters, as a function of wavelength.

The response of radiochromic dye films can be affected by many external influence quantities such as irradiation temperature, oxygen and water content and exposure to UV light [67, 80], thus, they are also sensitive to pre and post-irradiation relative humidity. Keeping the dosimeters in air and light tight pouches until readout reduces potential dose measurement error. Correction for all combined effects of these influence quantities is quite complex, which makes radiochromic dye film dosimeters *type II* dosimeters. The are no known dose or dose rate effects on this type of dosimeters [67], however, it is recommended to calibrate the dosimetry system in-house in order to avoid any potential environmental or dose-rate effects[80].

If stored in dark at ambient room temperatures, the response of B3-Risø dosimeters can be stable over long period of storage (around 3% over a year)[67]. However, this type of dosimeters present a short-term instability in the order of several hours after irradiation. The response

rises over time until its stabilisation. On the other hand, heating the dosimeters at 60°C for 5 minutes ensures the stabilisation of the dosimeter's color, and hereby its response.

For low dose measurements, Gafchromic® radiochromic films can be used. These films are polydiacetylene based dosimeters. When irradiated, a color formation is observed and it is due to the polymerization diacetylene monomers present in the film material[67]. These dosimeters are used in different radiation applications such as SIT treatments[59]. Dose determination is based on the measurement of optical density variation, carried away using an optical densitometer. After irradiation, the optical density of the film increases with time. An increase of 15 to 20 % of the initial optical density is observed 24 hours after irradiation. However, the optical density increase is dose dependant[31], where at low doses (10 Gy), the optical density stabilization could take up to 72 hours. Response of the Gafchromic® dosimeter is energy dependant where it was shown that its response to 4 MV X-rays decreases by 30 % in the case of 20 % in the case of 28 keV effective energy X-ray irradiation[3]. Uncertainty of dose measurement using Gafchromic® dosimetry system is about ±5 % (k = 2).

3.3.3.2 Cellulose Triacetate (CTA) films / Spectrophotometer dosimetry system

CTA films are used for high dose measurements, for both electron and photon beam irradiations, in the range of 10 - 300 kGy [67, 82]. Radio-induced chemical reactions occur in both CTA material and in the often present plasticizer material in the dosimeter. Absorbed dose is determined by absorbance measurements at a wavelength of 280 nm using a UV-spectrophotometer. CTA films can be used for electron beam irradiations at energies in the range of 0.2 - 50 MeV and photon beam irradiations at energies in the range of 0.1 - 50 MeV [82]. The response of CTA films is the ratio of their measured absorbance to their thickness, knowing that commercial CTA films have an average thickness of 125 µm. This response is then linked to absorbed dose based on a calibration curve. The response of this dosimetry system is almost linear and is dose rate and temperature dependent.

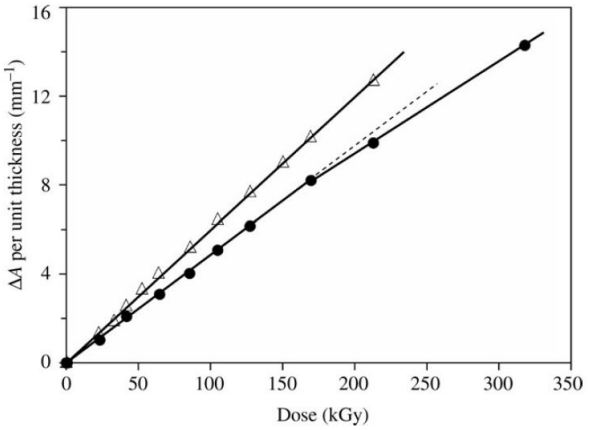

FIGURE 3.9: Response of CTA dosimeters as a function of absorbed dose for irradiations with electrons (filled circles) and gamma rays (triangles). [67]

CTA dosimeters are commonly used in radiation processing facilities for many purposes. Being commercialized in a film format makes their use for dose mapping and beam profile measurements very easy, especially when using a spectrophotometer with a motorized feeder. They are very used in electron beam facilities for the measurement and validation of the electron beam energy, where dosimeters are placed inside an aluminium wedge, irradiated and then measured. The measurement gives the dose distribution inside of aluminium and permits the determination of the range of electrons, and hereby the calculation of the electron beam's energy based of the estimated range.

CTA dosimeter is considered as *type II* dosimeter because of complex effects of influence quantities on its response [82]. Response of such dosimeters depends on the absorbed dose range. Their response to gamma rays at dose rates around 10 kGy/h was found to be up to 30 % higher than that of electron beam irradiations where the dose rate is around 10 MGy/h [67]. Irradiation temperature also affects the response of CTA films where a temperature coefficient of the dosimeter's response is about 0.5 %/°C for dose rates up to 10 kGy/h. At higher dose rates, the effect of irradiation temperature are negligible [145]. For each 10% increase in relative humidity, an increase of 2% of the CTA dosimeter's response was observed for irradiations at dose rates around 10 kGy/h[145] at temperatures ranging between 40 to 60°C. The response of CTA films is also sensitive to UV-light exposures which could increase the pre-irradiation absorbance of the film. Due to its complex behaviour to irradiation conditions, it is recommended to measure the dosimeter's absorbance 2 hours after irradiation[67]. Taking into account all these parameters, the CTA dosimetry system ensures a dose measurement reproducibility within 6% (2σ).

3.3.4 Dosimetry systems based on chemical solutions

3.3.4.1 Ferrous Sulfate (Fricke) solution

The conventional Fricke dosimeter consists of 1.0 mmol/L ferrous ammonium sulfate in an air saturated, aqueous solution of 0.4 mol/L of sulfuric acid[67]. Sodium chloride is usually added to reduce the effects of impurities that may be present in the prepared solution. It is used for low energy X-ray [64], high energy X-rays and gamma rays [62] and high energy electron [65] dosimetry. A 0.2% dose measurement accuracy can be achievable using Fricke solutions, when prepared in the best conditions and when very well handled[67]. However, the dose range in which Fricke solution can be used is narrow, ranging from 20 to 400 Gy [10]. Dosimetry using Fricke solution relies on the measurement of conversion of ferrous ions (Fe^{2+}) into ferric ions (Fe^{3+}) due to ionizing radiation. The measurement of the ferric ions concentration is done using a spectrophotometer operating in the range of 302 to 305 nm.

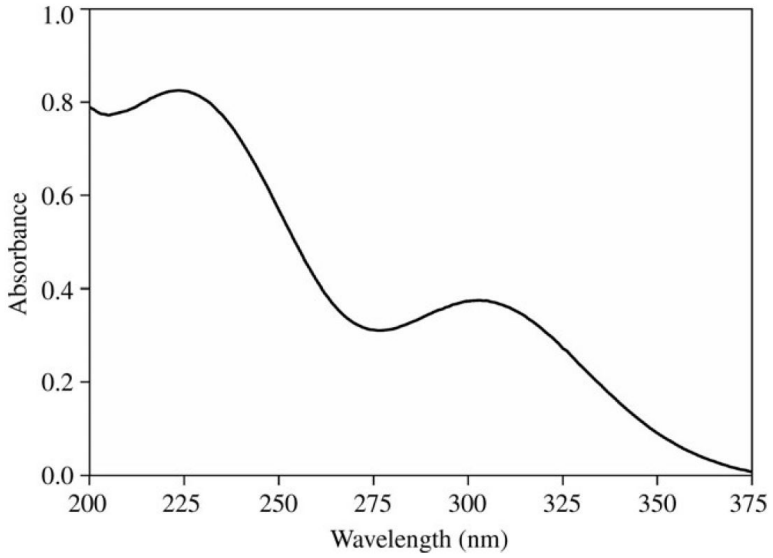

FIGURE 3.10: Absorption spectrum for a Fricke solution irradiated at 100Gy. (Optical path length = 1cm)[67]

Spectrophotometric measurements help determine both the radio-chemical creation yield of ferrous ions ($G(Fe^{3+})$) and their molar linear absorption coefficient ($\epsilon_\lambda(Fe^{3+})$). Both quantities could be also measured at a lower wavelength of 224 nm. However, potentially present impurities are more absorbent at 224 nm than they are at 305 nm. The absorbed dose determined by Fricke solution can be expressed as such:

$$D = \frac{\Delta A}{\epsilon \,.\, G(Fe^{3+}) \,.\, \rho \,.\, l} \tag{3.5}$$

where ρ is the density of the solution ($\rho \approx 1.023\ g/cm^3$) and l is the path length over which the absorbance is measured. For absorbed dose to water measurement, based on Fricke dosimetry, the dose determined by equation 3.5 needs to be multiplied by a conversion factor that takes into account differences in radiation absorption and densities between water and the dosimeter's material. For ^{60}Co γ-rays and high energy X-rays, this factor is equal to 1.0032[67]. On the other hand, although the Fricke dosimetry system is of high quality and that it is possible to estimate absorbed dose using equation 3.5, determined doses cannot be considered as traceable to national or international standards[10, 67].

The ferrous ions radio-chemical creation yield is dependent on many parameters such as temperature, absorbed dose rate, linear energy transfer (LET) and the material of the vessel containing the Fricke solution. ASTM recommends that the absorbed dose rate should not exceed $10^6 Gy/s$. Purity of the prepared solution plays an important role in the evolution of the ferrous ions radio-chemical creation yield. In order to test the purity of a solution, it is recommended to irradiate two solutions with and without sodium chloride. For the solution containing sodium chloride, absence of the decrease in $G(Fe^{3+})$ value ensures a good purity of the other solution. If the prepared solution is of great purity and is handled in the best conditions, such as in reference dosimetry laboratories, a measurement uncertainty of $\pm 3\%(k = 2)$ can be achieved.

3.3.4.2 Ceric-Cerous solution

Dosimetry using a ceric sulfate hydrate ($Ce(SO_4)_2.H_2O$) of ceric ammonium sulfate is somehow resembling to Fricke dosimetry, yet, in this case the dosimetric measurement relies on the reduction of ceric ions (Ce^{4+}) into cerous ions (Ce^{3+}) in acidic medium[67]. The dose range in which ceric solutions can be used ranges from 0.5 kGy to 50 kGy [67, 77], depending on the original concentration of the ceric ions (0.2 mmol/L to 50mmol/L).

The determination of the radio-chemical creation yield of cerous ions ($G(Ce^{3+})$) is done using UV/visible spectrophotometry. On the other hand, another type of dosimetry system, called ceric-cerous solution, is also used for radiation dosimetry. It contains approximately equal concentrations of ceric and cerous ions in order to reduce the effects of impurities that can be present in prepared solutions. Dose readout using ceric-cerous dosimeters can be made using potentiometric as well as spectrophotometric measurements. Measuring the electrical potential difference between irradiated and unirradiated dosimeters seems to be easier for the users because no dilution is needed for this type of measurement compared to spectrophotometric measurements, thus, making this dosimeter usable for routine dose monitoring in industrial radiation processing.

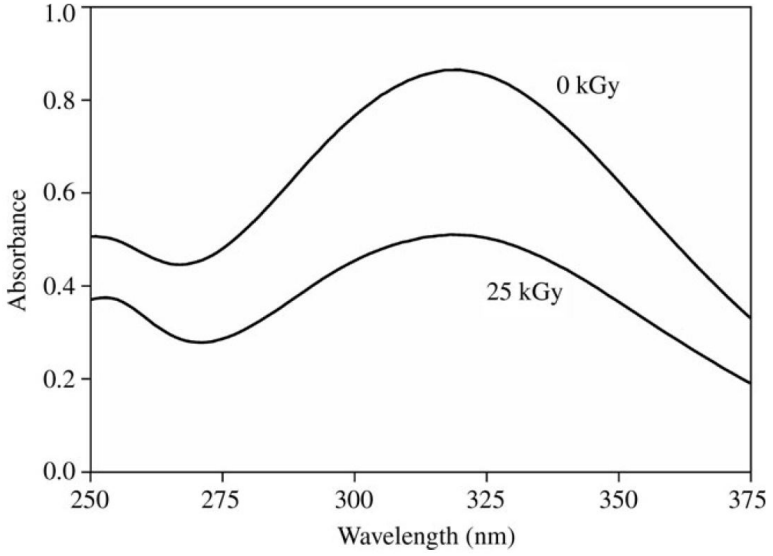

FIGURE 3.11: Absorption spectrum at 320nm of both irradiated and unirradiated ceric solutions. (Optical path length = 1cm)[67]

The absorbed dose range, in which ceric and ceric-cerous dosimeters can be used, depends on the initial concentrations of ions in the prepared solutions. For a dose range of 0.5 to 10 kGy, solutions are prepared by adding 3 mmol/L of $Ce(SO_4)_2.4H_2O$ with 3 mmol/L of $Ce_2(SO_4)_3.8H_2O$ into a 0.4 mol/L of H_2SO_4. For a dose range of 5 to 50 kGy, solutions are prepared by adding 15 mmol/L of $Ce(SO_4)_2.4H_2O$ with 15 mmol/L of $Ce_2(SO_4)_3.8H_2O$ into a 0.4 mol/L of H_2SO_4[67, 77].

The radio-chemical creation yield of ceric ions decreases with increasing temperature with a near constant temperature coefficient of -0.2%/°C, over the range of irradiation temperature of

10 to 60°C. Ceric ions can be also reduced because of ambient UV light, if not sealed in a glass ampoule. The effect of UV light is more significant on diluted solution that will be used in spectrophotometric measurements.

3.3.5 Plastics and dyed plastics / Spectrophotometer dosimetry system

One of the most commonly used plastic dosimeter is the polymethylmethacrylate (PMMA) dosimeter. PMMA dosimeters usually come in a sealed plaque format with a thickness of few millimeters, and they are also available in different colors depending on the absorbed dose range in which they shall be used. PMMA dosimeters can be used in both photon and electron beam irradiations[78].

Radiation induces the formation of unstable free radicals inside of the PMMA dosimeter which react and produce a more stable radiolytic product. Dose measurement is carried out using a spectrophotometer operating at different possible wavelengths depending on the type of the used PMMA dosimeter. Radio-induced radicals undergo complex reactions which are dependant on many parameters such as storage temperature, ambient light and oxygen or humidity presence[67].

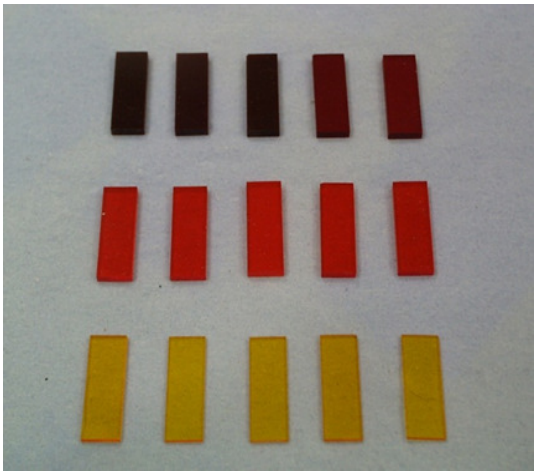

FIGURE 3.12: Different PMMA dosimeters (amber, red and yellow) used for different absorbed dose ranges.

More over, the response of PMMA dosimeters is affected by many influence quantities such as storage and irradiation temperature, storage humidity, light presence, dose rate and radiation type and energy. Effects of light and humidity can be significantly reduced due to the conditioning of the dosimeters in water and light-tight pouches. The response of such dosimeters is defined as the ratio of the measured absorbance at a specific wavelength to the dosimeter's thickness. The absorption of a dosimeter is measured using a UV/visible spectrophotometer. Table 3.2 lists physical and dosimetric properties of four different commercial PMMA dosimeter types.

Dosimeter	Thickness [mm]	Measurement optical wavelength [nm]	Range of absorbed dose [kGy]
Harwell Red 4034	3	640	5 - 50
Harwell Amber 3042	3	603 or 651	1 - 30
Harwell Gammachrome YR	2	530	0.1 - 3
Radix W	1.5	280 or 320	1 - 150

TABLE 3.2: List of the properties of four PMMA dosimeters used in radiation processing as routine dosimeters[78].

PMMA dosimeters should be calibrated in the same irradiation conditions as their future intended use, especially in terms of absorbed dose rate, radiation type and energy and irradiation temperature[67, 78]. All these combined effects are difficult to be taken into account and corrected by a simple correction factor, which makes the PMMA dosimeter a *type II* dosimeter.

3.4 Conclusion

This chapter presented many dosimeters and dosimetry systems that are currently commonly used, as reference standard or in routine dose monitoring, in different applications of industrial radiation processing. Different dose measurement techniques were presented as well as dosimeter's intrinsic properties, such as absorbed dose range, reaction mechanisms, measurement difficulties and the impact of external influence quantities.

This work is dedicated for kilo-voltage X-ray application, with maximum photon energies up to 280 keV, and for applications which absorbed dose ranges range from few tenths or hundreds of Grays up to tenths of kiloGrays. Thus, the choice alanine/EPR dosimetry system for this kind of industrial applications is well justified, especially when taking into account all the benefits that alanine/EPR dosimetry can ensure in the desired absorbed dose range, compared to other dosimetry systems. The most important blocking point in front of the use of alanine for kilo-voltage X-ray applications is its photon energy dependence which this work is dedicated to resolve, in order to ensure the best use of this dosimetry system at the least possible uncertainties. Another aspect that led us to choose alanine/EPR dosimetry system for this kind of applications, is the rapid growth in the demand of such dosimetry systems by many radiation installations operators all over the world, as well as by many research and medical teams.

Part III

Alanine/EPR dosimetry

Chapter 4

Aspects of alanine/EPR dosimetry

Contents

4.1 Introduction

When exposed to ionizing radiation, alanine molecules undergo different reactions leading to the formation of new chemical species called "*free radicals*". The evolution in time of some radio-generated radicals was found to be very stable and quantitatively dependent on absorbed doses of radiation, thus making alanine a good candidate for the use in radiation dosimetry. In order to estimate absorbed dose by the alanine dosimeter, one has to measure its response, which is a quantitative reflection of the concentration of created free radicals in alanine. This measurement is done by Electron Paramagnetic Resonance (EPR).

This chapter deals with the scientific aspects of EPR spectrometry and sheds a light on the use of the alanine/EPR dosimetry system for radiation dosimetry. The use of alanine as a solid state dosimeter was first introduced in 1962 by W. W. Bradshaw [17]. Since then, many studies have been conducted to better understand the effects of ionizing radiation on alanine from a radio-chemical point of view, while other studies were carried out to optimize the use of alanine for radiation dosimetry. Nowadays, due to continuous developments in EPR spectrometry, alanine dosimetry system is considered as one of many high metrological quality systems, and is used as reference standard, transfer standard as well as routine dosimetry system in many fields of radiation applications.

4.2 Electron Paramagnetic Resonance

4.2.1 Zeeman effect

Radio-generated free radicals have an unpaired electron in their electronic shells. When applying and external magnetic field (B_0) to the studied sample, electron's magnetic momentum tends to align with the direction of B_0, thus, they act like the needle of a compass that aligns itself with the terrestrial magnetic field. Since energies are quantized, the unpaired electron only has two allowed energy states: the lower state of energy when the moment of the electron (μ) is aligned with the magnetic field and a higher energy state when μ is aligned against the magnetic field as shows figure 4.1. In quantum physics, these two energy states are designated by the projection of the electron's spin (m_s) on the direction of the external magnetic field. Because the electron is 1/2 spin particle and is of negative electrical charge, the parallel state has $m_s = -1/2$ and the antiparallel state has $m_s = +1/2$. Electron spin state orientation is the opposite of proton's spin state orientation due to the negative charge of the electron. The splitting of the fundamental electron's energy state into two new energy states ($m_s = \pm 1/2$) due to the presence of an external magnetic field is called the *Zeeman effect*.

The energy difference between the parallel and antiparallel energy states of an unpaired electron present in an external magnetic field can be expressed as such:

$$\Delta E = h\nu = g \,.\, \mu_B \,.\, B_0 \,.\, \Delta m_s = g \,.\, \mu_B \,.\, B_0. \tag{4.1}$$

where ΔE is the energy difference between the two states, $h\nu$ is the energy of the electromagnetic wave generated by a microwave source inside of the EPR spectrometer, g is the *Lande* factor ($g \approx 2$), μ_B is the *Bohr*'s magneton ($\mu_B = 9.274 \ .10^{-24} \ J/T$), B_0 is the amplitude of the external magnetic field and Δm_s is the difference between the projections of the spin of the two energy states ($\Delta m_s = +1/2 - (-1/2) = 1$). When the unpaired electron absorbs an energy that is equal to ΔE due to present electromagnetic wave in the EPR spectrometer, a transition between the two energy levels occur, this is called resonance.

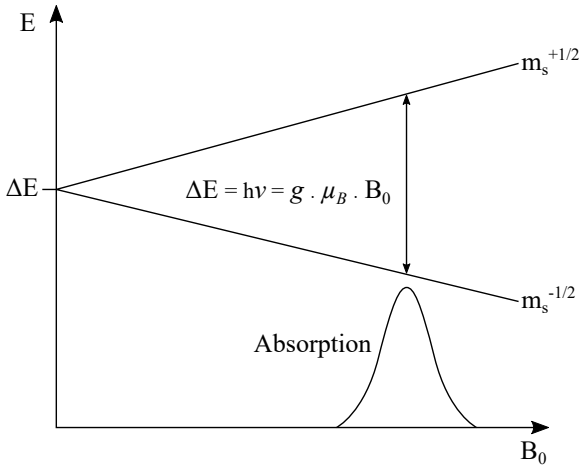

FIGURE 4.1: Representation of the unpaired electron's energy level splitting due to the Zeeman effect.

4.2.2 EPR spectrometry

EPR spectrometry is the measurement of resonance of different unpaired electrons of different radicals that are present inside of sample. To do so, the magnetic field applied in the EPR resonant cavity could be held constant while the frequency of the electromagnetic wave is scanned. From another point of view, the microwave frequency could be held constant while the magnetic field is scanned. Absorption of energy occurs when the magnetic field is at a defined magnitude that gives an energy ($g.\mu_B.B_0$) to the unpaired electron that is equal to the energy of the applied microwave ($h\nu$). Because of difficulties in scanning microwave frequencies and because of the use of a resonant cavity for signal detection, most EPR spectrometers operate at constant microwave frequency and scan the magnetic field in order to measure different resonances. This process is known as the magnetic field tuning.

An EPR spectrometer is composed of:

- Resonant cavity
- Microwave source and bridge
- Magnets and their control system
- Signal processor

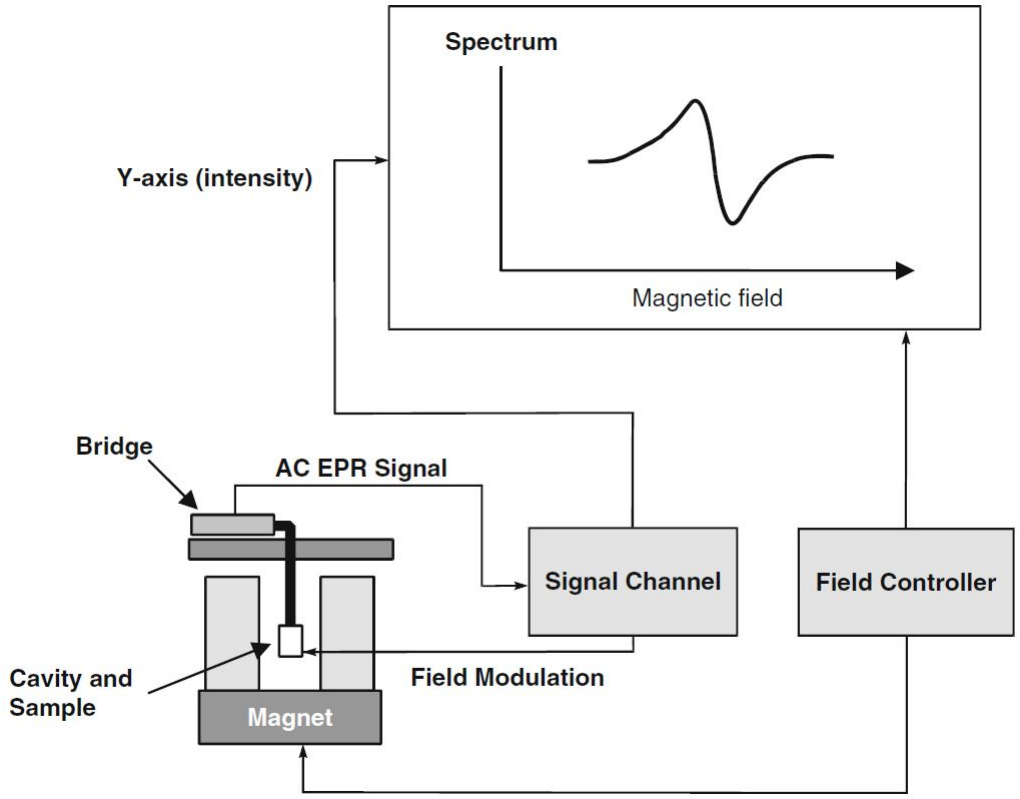

FIGURE 4.2: Block diagram of an EPR spectrometer[39].

4.2.2.1 The microwave bridge

Both microwave source and detector are placed inside the microwave bridge. The output of microwave source is difficult to control, thus after emission, the microwave passes through a wave attenuator that accurately controls its power in order to avoid signal saturation regimes. Most EPR spectrometers that are fabricated nowadays are called reflective spectrometers, meaning that they measure the amount of incident microwave that is reflected by the resonance cavity and the sample due to energy transitions. Thus, in order to have an accurate measurement of the microwave absorption by the sample, the microwave detector needs to measure only the contribution of the microwave that is being reflected from the cavity and not the one coming from the source. This is achieved by placing a device called a circulator that has different ports to channel, in a distinguished way, the source microwave to the cavity and sample, and on the other end, the microwave reflected from the cavity to the detector. Finally, the reflected microwave power is converted to an electrical signal via a diode.

Microwave band	Microwave frequency [GHz]
L	0.8 - 1.2
S	3.4 - 3.8
X	9 - 10
K	24
Q	34
W	94

TABLE 4.1: Microwave frequencies of different microwave sources.

4.2.2.2 The EPR cavity

EPR cavities, also named resonators, play an important role in amplifying weak signals from the studied sample. Cavities are often metallic boxes shaped as a cylinder or a rectangle. While sweeping the frequency of the generated microwave, both the sample and the cavity reflect a fraction of this microwave back to the microwave detector. However, at a certain microwave frequency, the microwave energy is stored inside of the cavity and is not reflected back to the detector. This frequency is defined as the resonance frequency (ν_{res})[39]. The more the cavity is able to retain microwave energy, the better the cavity's efficiency is. The quality of the EPR cavity, and therefore the EPR spectrometer, is known as the Q factor which can be expressed as such:

$$Q = \frac{2\pi \,.\, E_s}{E} \tag{4.2}$$

where E_s is the amount of microwave energy that is stored in the cavity at resonance regime and E is the microwave energy that is lost during a full cycle. However, this measurement technique can present some problems because a part of the microwave can be lost in the form of heat in the cavity, thus, the Q factor can be measured using this relation:

$$Q = \frac{\nu_{res}}{\Delta\nu} \tag{4.3}$$

where $\Delta\nu$ is the width at half height of the resonance signal, as shows figure 4.3. Due to the resonance, a standing electro-magnetic waves is present in the cavity. When the electrical component of the electro-magnetic wave is at is maximum, the magnetic component is at its minimum, and vice versa. These two components are spatially separated inside of the cavity. The microwave magnetic field component controls the energy absorption. Therefore, if the sample is placed in the minimum of the electric field, thus, in the maximum of the magnetic field , the highest sensitivity, and therefore the highest signal are obtained.

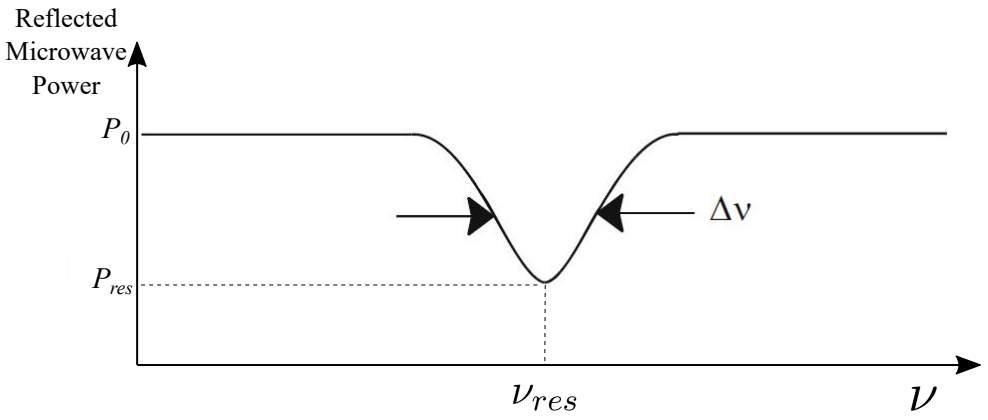

FIGURE 4.3: Representation of the microwave reflection by the EPR cavity.[39]

4.2.2.3 The magnetic field

Magnet systems used in EPR are composed of magnets, a power supply, a field sensor and a field regulator. This system generates a magnetic field that is swept over a certain range. When the microwave frequency and the swept magnetic field's amplitude fulfill the resonance conditions, a spin transition in the sample is induced and it is then detected by the detector due to a drop in the cavity's Q factor. The sweeping range of the magnetic field depends on both the microwave frequency and the sample properties. For example, for an organic solution, having a g value of 2, and for an X-band spectrometer (frequency 9.6 GHz), the required magnetic field is about 3430 G (343 mT) with a sweep range of 100 G[18].

The magnetic field controller defines the center field and sweeps the magnetic field for the scan. It consists of two parts: a digital component that defines the field values and the timing of the field sweep, and an analogue component that regulates the current in the magnet to vary the magnetic field value. The setting of the magnetic field and the timing of the magnetic field sweep are controlled by a microprocessor in the controller.

The magnetic field regulation occurs via a *Hall* probe, placed in the gap of the magnet, that produces a voltage that depends on the magnetic field component that is perpendicular to the probe. At each discrete step of the magnetic field scan, a comparison is made between the voltage from the Hall probe and the reference voltage given by the controller. If a difference between the two voltages exist, a correction voltage is sent to the magnet power supply that changes the amount of current flowing through the magnet, thus, correcting the magnetic field. After few iterations, this difference drops to zero and the magnetic field is "stable" or "locked"[39].

4.2.2.4 The signal channel and EPR spectra acquisition

In order to record the EPR signal, a magnetic field sweep needs to be put in place alongside a synchronised detection of the sample's response. The signal channel operates as the synchronizing system while driving the controller of the Hall probe. During a specified amount of time,

the signal channel accumulates the signal coming from the microwave bridge, for a specific value of magnetic field, and then, it advances the Hall probe controller to the next field value.

The signal channel contains a lock-in detector that measures a signal of known frequency with high sensitivity. In order to generate a signal of precise frequency, the method of field modulation is applied. It all begins with the generation of 100 kHz frequency by the lock-in module, that is then amplified by the modulation amplifier. The generated frequency is fed to a coil that adds a magnetic field oscillation (B_{mod}) parallel to the main magnetic field. When the main magnetic field is in resonance, the oscillating field modulates the resonance conditions, thus, the sample's response is also modulated at the same frequency of 100 kHz. Therefore, the signal that is going from the sample through the microwave bridge for detection is modulated as well. This signal is then processed by the lock-in detector to produce the EPR signal as a function of the magnetic field sweep. Due to the magnetic field modulation, a measurement of the EPR absorption slope, at a given magnetic field value, is measured as shows figure 4.4. This slope is non other the first derivative of the absorption EPR signal.

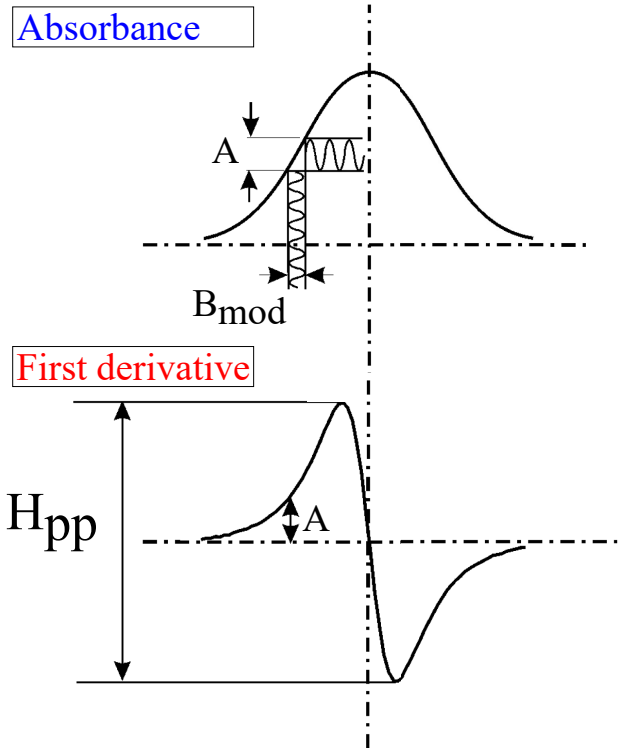

FIGURE 4.4: The magnetic field modulation process. A is the microwave absorbance by the cavity and sample, B_{mod} is the modulation magnetic field and H_{pp} is the peak to peak height of the first derivative signal.[18]

Modulation field has a very big impact on the desired resolution of the EPR spectrum. The smaller B_{mod} is, the higher is the resolution and vice versa. Thus, if the value of B_{mod} is very big, in a way that an important part of the absorption signal is covered, the derivative signal will no longer reflect true information about the sample, especially in terms of line shape and linewidth. At the end of the modulation process, an Analogue to Digital Converter (ADC) converts the EPR signal into a computer readable format.

4.3 Dosimetry based on alanine/EPR systems

Alanine/EPR dosimetry is based on the measurement of the quantity of the radio-induced free radicals inside an alanine dosimeter. This measurement is done using EPR spectrometers. In the early years, it was uncommon to use EPR spectrometry for radiation dosimetry, compared to optical dosimetry systems. However, due to the technological advances in the field of EPR spectrometry, alanine/EPR dosimetry continue to demonstrate its effectiveness as well as its superiority on optical dosimetry systems, thus, becoming more and more employed for radiation dosimetry in many sectors such as medical, research and industry. Alanine/EPR dosimetry systems as recognized as reference standard, transfer standard and routine dosimetry system due to its high metrological qualities.

4.3.1 Alanine dosimeters

Alanine ($C_3H_7NO_2$) is an amino acid that comes in many chemical forms such as: L-alanine, D-alanine and DL-alanine[133]. Nowadays, most alanine dosimeters use L-alanine as the main formulation component and take the form of cylindrical shaped pellets [32]. Raw alanine compound is sieved and ground into very small crystals of different sizes. Alanine pellets are made by mixing 90 to 93 % of small alanine crystals with the remaining percentage of a binding agent that is used to ensure a good physical coherence and strength of the dosimeter. Materials such as paraffin wax are used as a binding agent. The blend is then pressed into small alanine pellets with a diameter of 4 to 5 mm and a thickness of 2 to 3mm, depending on the manufacturer as well as the radiation type and energy.

Manufacturer	Average diameter [mm]	Average thickness [mm]	Composition
Aerial	4	2.3	91.63% alanine + 6.37% EUDRAGIT NE 30D + 2% MYVATEX[106]
Harwell	4.8	2.8	90.9% alanine + 9.1 paraffin
FWT	4.8	3	96% alanine + 4% binder

TABLE 4.2: Physical characteristics of different commercial alanine dosimeters.

4.3.2 Alanine radicals

Ionizing radiation induces the creation of different types of stable free radicals inside of the alanine dosimeter. The identity of such radicals have been investigated since the 1960's[117]. The first alanine radical that was confirmed experimentally is the de-aminated radical. The de-aminated radical, also known as the Stable Alanine Radical (SAR), was found to be the most preponderant radical. Another study [135] used L-α-alanine with different hydrogen compositions (using some deuterated molecules) as well as the Electron Nuclear DOuble Resonance (ENDOR) technique in order to further investigate the structural identities of radio-induced alanine radicals. Figure 4.5 shows the three different radio-induced alanine radical species that were presented in the work of E. Sagstuen et al.[135]. The second alanine radical is stabilized

by net hydrogen abstraction from the central carbon atom, and finally the third alanine radical is assumed to be an oxidation product[105].

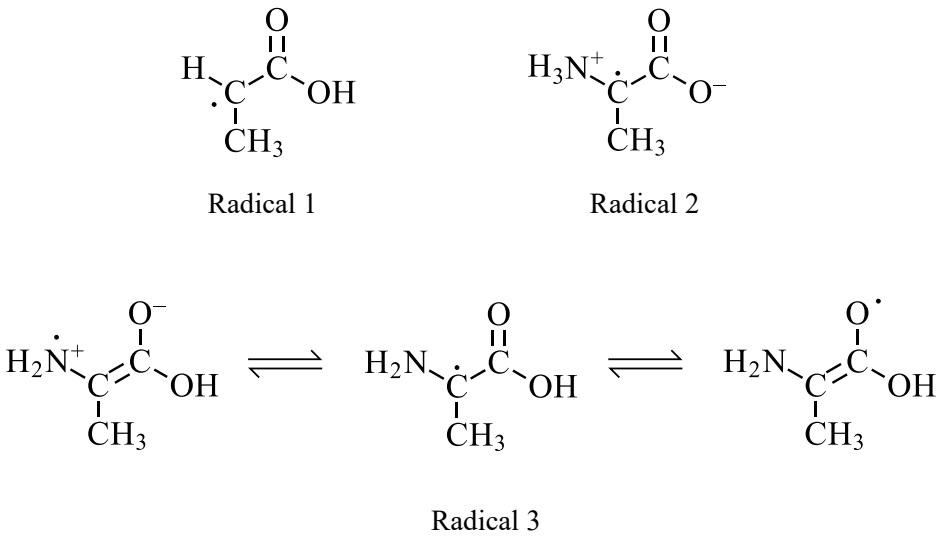

FIGURE 4.5: Structures of the three radio-induced alanine free radical species, presented by Sagstuen et al.[135]

Due to ionizing radiation, alanine radicals are generated with different fractions. Many studies suggested that de-aminated and the de-hydrogeniated radicals are created within the ratios of 55-60% for the SAR and 30-35% for the second radical, leaving a variable fraction of 5-10% for the third alanine radical[48, 104, 105]. These ratios depend on different parameters such as the ionizing radiation type and energy, the irradiation and measurement temperatures as well as the absorbed doses.

All different radicals contribute to the alanine EPR signal. A study by Heydari et al. [48] showed results of simulation calculations that estimated the contribution of each of the three radical species into the EPR signal. Experimental EPR signal was obtained by irradiating alanine with a 11 MeV electron beam at a dose of 10 Gy. Results of simulations showed that all three radical species contribute differently to the EPR signal over all the magnetic field sweep range, yet, the biggest contribution to the total EPR signal is the one resulting from the de-aminated free radical.

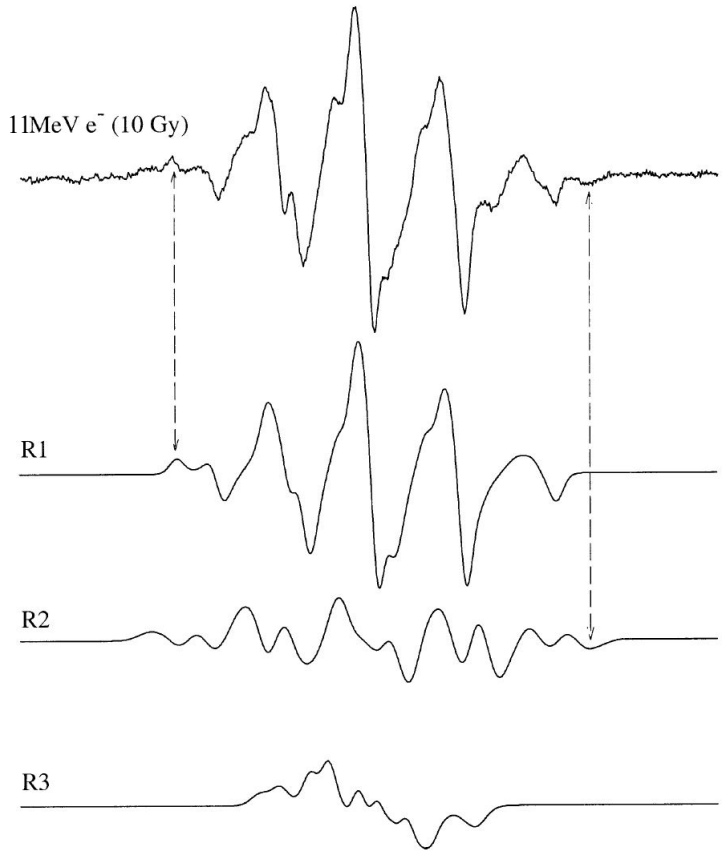

FIGURE 4.6: Contribution of the three different radical species in the total EPR signal[48].

4.3.3 Dose measurement using alanine/EPR dosimetry system

Dose measurement using alanine dosimeters is based on the determination of the peak to peak height (H_{pp}) of the central resonance line of the recorded EPR signal. Once the H_{pp} is determined, one can estimate the absorbed dose to the dosimeter based on a calibration curve of the dosimetry system. Very often, alanine dosimetry systems are calibrated with a ^{60}Co gamma reference beam. This curve shows the relation between the dosimeter's response (r), defined as the ratio of H_{pp} to the dosimeter's mass (m), and the absorbed dose to water (D_w). The peak to peak height of the alanine EPR signal is compared to the EPR signal of the spectrometer's internal ruby reference. This is done in order to take into account all variations and fluctuations in the EPR spectrometer parameters that can influence the EPR measurement. The ruby reference is a well characterized reference that is placed in a fix position inside of the EPR spectrometer near the analyzed samples.

The dosimeter's response should be corrected in order to take into account all the impact of influence quantities, and can be expressed as such:

$$r = \frac{H_{pp}}{m} . (1 + (T_{cal} - T_i).k_T) . k_{ruby} \tag{4.4}$$

where T_{cal} is the irradiation temperature of the alanine reference dosimeters used for creating the calibration curve, T_i is the irradiation temperature of the dosimeter that is being currently measured, k_T is the irradiation temperature correction factor and k_{ruby} is the EPR spectrometer correction factor.

The irradiation temperature correction factor is estimated by irradiating alanine dosimeters to different absorbed doses at different irradiation temperatures. The k_T coefficient for Aerial's alanine dosimeters is equal to 0.14 %/°C. The irradiation temperature can be estimated depending on the type of radiation. For photon irradiations, the irradiation temperature can be calculated as such:

$$T_i \;=\; T_0 \;+\; \frac{2}{3} \;.\; (T_{max} \;-\; T_0) \tag{4.5}$$

with T_0 being the dosimeter temperature measured just before the irradiation and T_{max} being the maximum temperature measured during the irradiation. In the case of electron beam irradiations, the irradiation temperature is dose dependant and is expressed as such:

$$T_i \;=\; T_0 \;+\; D_w \;.\; 0.7 \tag{4.6}$$

An internal study at Aerial showed that the dosimeter's temperature rises by 7 °C for each 10 kGy of absorbed dose. This depends on the calorific capacity of the dosimeter's material (alanine + binder).

k_{ruby} is obtained by comparing the peak to peak height values of the EPR spectrometer's internal reference that are recorded during the calibration of the dosimetry system and during the actual measurement of a random alanine dosimeter. It can expressed as such:

$$k_{ruby} \;=\; 1 \;+\; \frac{H_{pp}(cal) \;-\; H_{pp}(meas)}{f_{ruby}} \tag{4.7}$$

where $H_{pp}(cal)$ is the peak to peak height of the EPR signal of the ruby reference recorded during the calibration, $H_{pp}(meas)$ is the peak to peak height of the EPR signal of the ruby reference recorded during the ongoing measurement and f_{ruby} is the correction factor for the ruby holder. Once the dosimeter's response is calculated and corrected for the effects of influence quantities, the absorbed dose is calculated analytically by mathematically resolving the calibration curve model for the measured response.

4.3.4 Dose uncertainty estimation

Absorbed dose can be expressed as a function of different parameters, such as the dosimeter's response, irradiation temperature and other parameters, thus it can be expressed as such:

$$D \;=\; f(x_1,\; x_2,\; x_3,\; ...,\; x_n) \tag{4.8}$$

where D is the measured dose and each x_i is one of the parameters that are taken into account in the dose measurement. Dose measurement uncertainty estimation is well described in the ISO/ASTM 51707 standard [85], where it is clearly stated that two types (type A and type B) of

evaluation of uncertainties can be applied in order to establish the full dose measurement uncertainty budget. Type A evaluation of uncertainties are made by statistical analysis of a series of measurement results of a quantity value, such as the random scatter between dosimeters. This evaluation is often made by the user of the dosimetry system based on experimental data. Type B evaluation of the uncertainty is any evaluation of a component of measurement uncertainty by means, other than type A evaluation of measurement uncertainty[91]. These uncertainty components are very often given in a calibration certificate, or are obtained from limits deduced from personal experience. Based on equation 4.8, the combined dose measurement uncertainty ($u_c(D)$) can be determined by applying the variance propagation law as follows, knowing that all uncertainties are independent:

$$u_c(D) \;=\; \sqrt{\sum_i (\frac{\partial f}{\partial x_i})^2 \;.\; u^2(x_i)} \tag{4.9}$$

where $(\frac{\partial f}{\partial x_i})$ is the differential derivative of the dose function with respect to the x_i variable and $u^2(x_i)$ is the standard uncertainty of the x_i variable. Thus, the combined dose measurement uncertainty can be determined by this relation:

$$u_c(D) \;=\; \sqrt{u^2(cal) \;+\; [u(r) \;.\; slope(\frac{D}{r})]^2} \tag{4.10}$$

with $u(cal)$ being the calibration uncertainty, $u(r)$ the response measurement uncertainty and $slope(D/r)$ being the first derivative of the calibration curve at the point (D, r). $u(cal)$ is obtained from assessing the uncertainties of: the reference doses ($u(D_{ref})$), the fitting curve ($u(fit)$) and the reproducibility ($u(repro)$) that takes into account the dosimeter to dosimeter scatter as well as the irradiation homogeneity. $u(cal)$ can be expressed as such:

$$u(cal) \;=\; \sqrt{u^2(D_{ref}) \;+\; u^2(fit) \;+\; u^2(repro)} \tag{4.11}$$

$u(D_{ref})$ is given in the calibration certificate issued by the calibration laboratory. During a calibration, four alanine pellets are irradiated together at the same reference dose. The uncertainty of the calibration curve fit depends on the residuals of the average measured dose on the four alanine pellets compared the calibration curve fit. It is expressed as such:

$$u(fit) \;=\; \sqrt{\frac{\sum_i (average\ residual_i)^2}{n}} \tag{4.12}$$

with n being the number of dose points used in the calibration of the alanine dosimetry system. The uncertainty component covering the dosimeter to dosimeter scatter as well as the irradiation homogeneity is defined as:

$$u(repro) \;=\; \frac{Maxu(scatter); u(IH)}{\sqrt{N}} \tag{4.13}$$

with $u(scatter)$ being the uncertainty component taking into account the dosimeter to dosimeter scatter, $u(IH)$ is the uncertainty on the irradiation homogeneity and N being the number of

alanine pellets used per dose point. $u(scatter)$ and $u(IH)$ are expressed as such:

$$u(scatter) \;=\; \sqrt{\frac{\sum_i (residual_i)^2}{n_d \;-\; n_c}} \tag{4.14}$$

and

$$u(IH) \;=\; \frac{\sigma(D_1,\; ...,\; D_N)}{Average(D_1,\; ...,\; D_N)} \tag{4.15}$$

where $residual_i$ is the deviation of the measured dose compared to the calibration curve, n_d is the total number of alanine dosimeters used for calibration, n_c is the number of coefficients used in the calibration fit curve (in other terms, the degree of the calibration curve) and $\sigma(D_1,\; ...,\; D_N)$ is the standard deviation of dose measurements of all alanine pellets for each reference dose point.

The other major component to take into account for the combined dose measurement uncertainty is the EPR response measurement uncertainty ($u(r)$). This component takes into account the contribution of uncertainties of all physical quantities that influence the alanine EPR response such as the dosimeter's mass ($u(m)$), the irradiation temperature ($u(T_i)$), ambient environmental conditions ($u(T, RH)$) and the EPR measurement itself ($u(EPR)$). The EPR response measurement uncertainty can be expressed as such:

$$u(r) \;=\; \sqrt{u^2(m) \;+\; u^2(T_i) \;+\; u^2(EPR) \;+\; u^2(T, RH)} \tag{4.16}$$

4.3.5 Influence quantities

4.3.5.1 Irradiation temperature

The response of the alanine dosimeter increases with increasing irradiation temperature. Many studies reported values of the irradiation temperature correction factor, to be applied to the dosimeter's response, ranging from 0.1 to 0.3 %/°C, for irradiations carried out in the range of -10 to 55 °C, and for absorbed doses going up to 50 kGy[33–35, 67, 121, 137]. Sharpe et al. [137] investigated the irradiation temperature effect on Harwell alanine dosimeters at different absorbed doses ranging from 7 to 70 kGy, for both ^{60}Co gamma rays and 10 MeV electron beam irradiations. It was found that the effect of irradiation temperature on the response of the alanine dosimeters becomes non-linear and dose dependent at temperatures above 50 °C. It was also demonstrated that the irradiation temperature effects on the alanine response are similar for gamma and electron beam irradiations.

A series of 2.2 MeV electron beam irradiations was carried out at Aerial in order to determine the irradiation temperature influence on alanine dosimeters that are commercialized by Aerial. The studied irradiation temperatures ranged from -5 to 80 °C. Investigation was carried out for absorbed doses of 5 and 25 kGy. For each irradiation, 5 alanine pellets (lot 09/11 - pellets) were placed inside of a polyethylene holder and covered with a 1 mm thick polystyrene sheet. The dosimeter holder was placed on top of a temperature controlled device in order to maintain

irradiation temperature at a desired value. Figure 4.7 shows the EPR relative response (with respect to a 25 °C irradiation temperature) variation of irradiated dosimeters as a function of irradiation temperature. Results showed that irradiation temperature coefficient is equal to 0.128 %/°C at 5 kGy, and it was equal to 0.133 %/°C at 25 kGy.

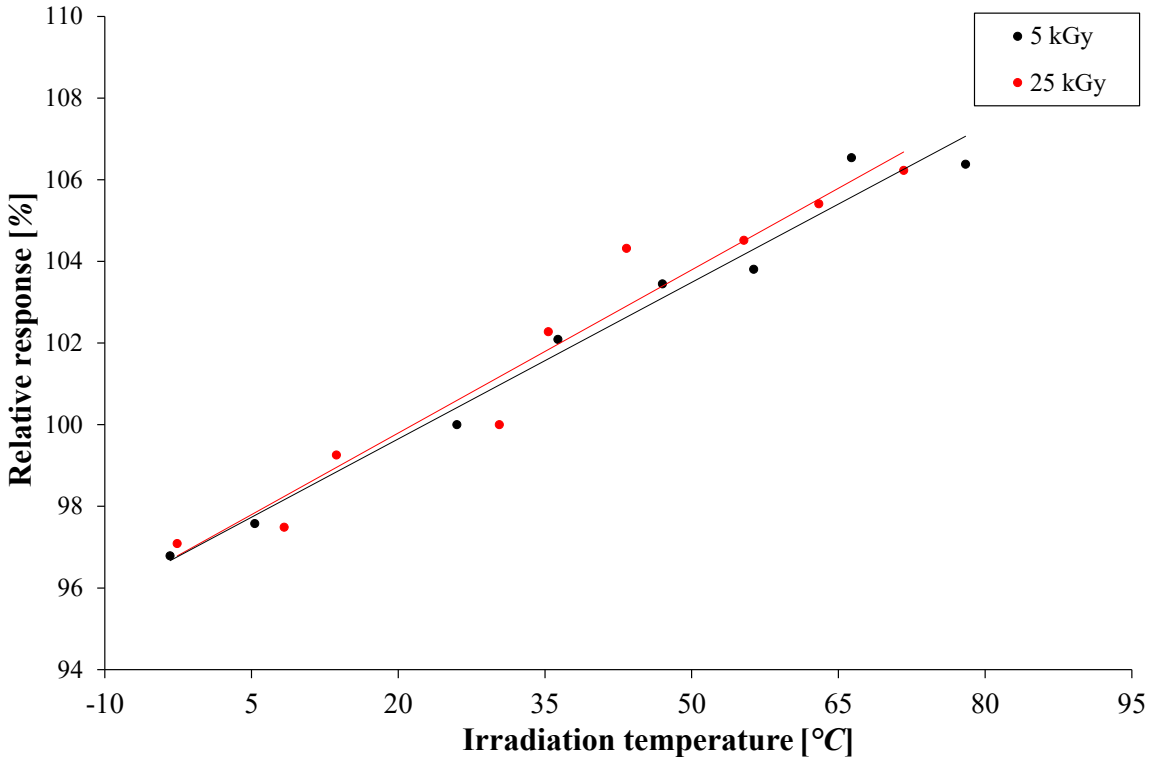

FIGURE 4.7: Aerial alanine dosimeters relative response variation as a function of irradiation temperature, at 5 and 25 kGy.

4.3.5.2 Relative humidity

The effect of relative humidity on Aerial's alanine dosimeters (lot 05/17 - packaged blisters) was studied for both pre and post-irradiation storage. Table 4.3 lists the relative humidity conditions that were put in place using different desiccators. For the study of pre-irradiation effect of relative humidity on alanine's response, dosimeters were stored for one week in separate desiccators with the conditions listed in table 4.3. They were all then irradiated simultaneously at a dose of 25 kGy with a 10 MeV electron beam and then put back in storage at 45 % of relative humidity. Dose readout was carried away two hours after irradiation. Obtained results showed that there was no significant effect of pre-irradiation storage humidity on the response of Aerial's alanine blister dosimeter after irradiation.

Storage temperature [°C]	Relative humidity [%]	Type of salt
20	23.1 ± 0.3	KCH_3CO_2
20	43.2 ± 0.3	K_2CO_3
20	75.5 ± 0.1	$NaCl$
20	85.1 ± 0.3	KCl

TABLE 4.3: Pre-irradiation storage condition of alanine blister dosimeters.

For the study on the post-irradiation storage relative humidity, dosimeters were stored at 20 °C and 45 % relative humidity during a weak before irradiation. Dosimeters were irradiated at 25 kGy with a 10 MeV electron beam and EPR readout was carried away two hours after irradiation. After first EPR readout, dosimeters were then placed in the same conditions as the ones listed in table 4.3. Three dosimeters were used for each level of relative humidity. Dosimeters were then taken out and measured periodically. Figure 4.8 shows obtained results. We can clearly see that the effect of post-irradiation storage relative humidity is very important especially at relative humidities that are higher than 70 %.

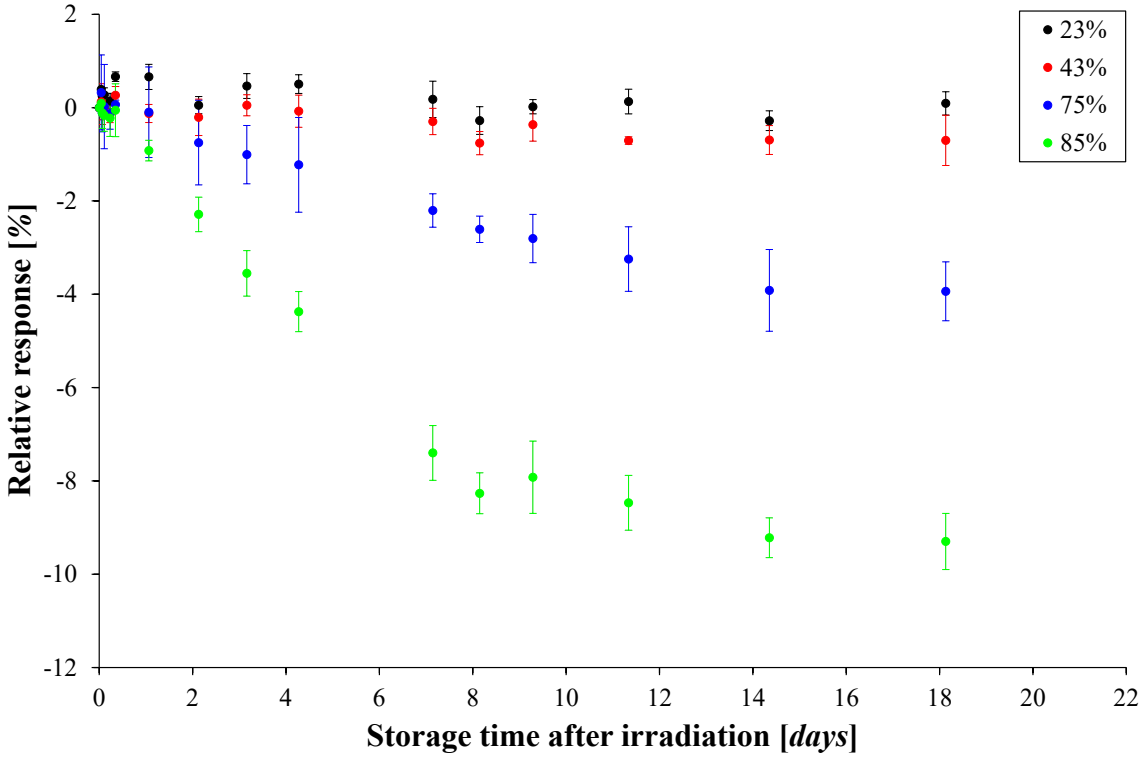

FIGURE 4.8: Aerial alanine dosimeters relative response variation as a function of storage time for relative humidities of 23, 43, 75 and 85 %.

4.3.5.3 EPR signal fading

Alanine dosimeters are considered some of the highly stable dosimeters in term of response evolution over periods of time up to few months[67, 81]. However, it is known that the alanine

EPR signal fades in times. Reported fading rates range from 0.5 up to 5 % per year, depending on many parameters such as the absorbed dose range, storage temperature and humidity and the dosimeter's composition. EPR measurements should be carried away in order to characterise short and long term fading of the alanine dosimeters.

A study was realized at Aerial in order to determine the short-term fading of alanine blisters (lot 05/17), with two different blister packagings, irradiated with a 10 MeV electron beam at doses of 5 and 25 kGy. Figure 4.9 represents the relative response of irradiated alanine dosimeters as a function of post-irradiation time. Results showed that the EPR signal of irradiated alanine pellets stabilises two hours after irradiation, in the case of both dose levels of 5 and 25 kGy. Thus, it was recommended in our dosimetry laboratory to wait for at least two hours after irradiation, before measuring absorbed doses. Results showed that the old packaging lead to a slightly lower response fading compared to the new packaging.

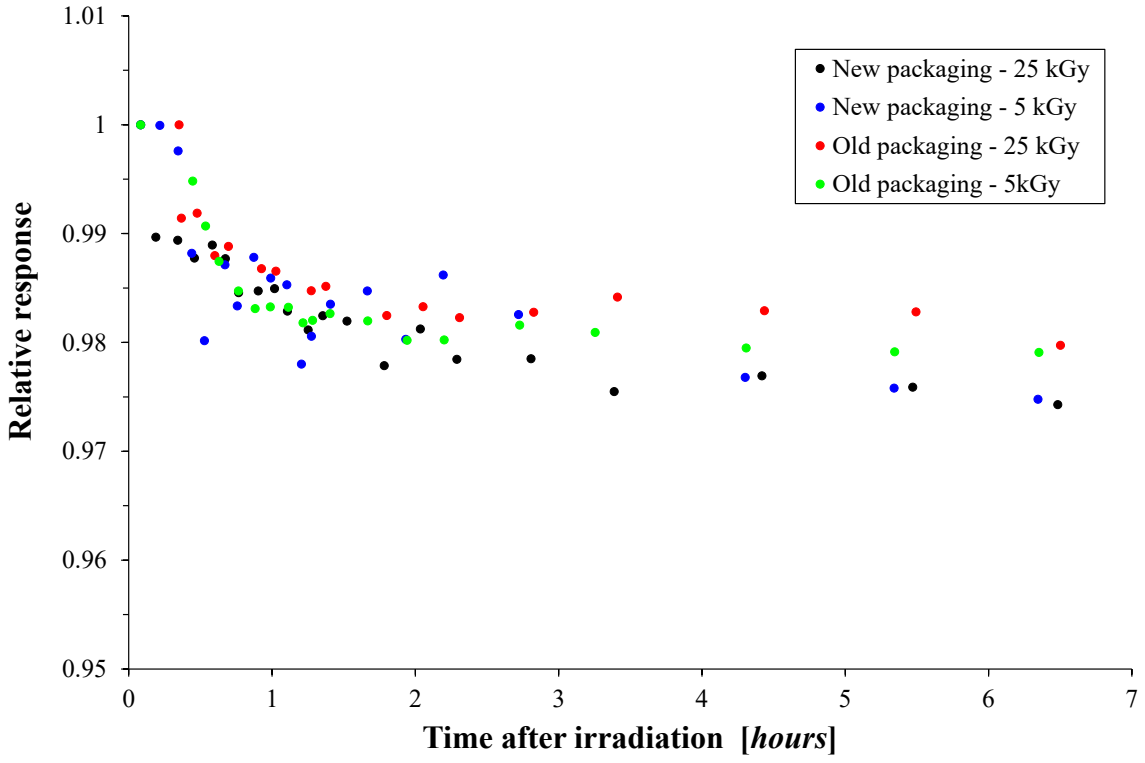

FIGURE 4.9: Aerial alanine dosimeters relative response variation as a function of post-irradiation time.

4.3.5.4 Energy dependence

According to ISO/ASTM 51607, alanine dosimeters can be used for photon and electron irradiations at energies ranging from 0.1 up to 30 MeV[81]. Many research projects studied alanine's response to different types and energies of ionizing radiation. It was found that alanine is nearly water equivalent when irradiated with photon or electron energies that range from 200 keV up to 10 MeV[8, 14, 15, 25, 47, 136, 154, 155].

Most of these studies compared the alanine's relative response to ^{60}Co gamma ray irradiation, which is well recognized internationally as a reference beam quality. For MeV electron beam irradiations, alanine's relative response ranged from 0.94 to 0.99 for irradiations at electron energies ranging from 6 to 22 MeV, when compared to ^{60}Co irradiations[15, 155]. In the case of MV X-rays, alanine's relative response ranged from 0.98 to 0.99 for irradiations with X-rays at nominal energies ranging from 4 to 30 MV compared to ^{60}Co irradiations [8, 14, 136, 154].

In the range of keV X-rays, the difference between mass-energy absorption coefficients of alanine and water becomes more significant compared to MeV X-rays, thus smaller and more variable relative responses of alanine were reported in many studies[7, 23, 50, 95, 122, 141, 149, 150, 153]. Reported results by different studies were in the range of 0.63 up to 0.95 for X-ray irradiations with tube potentials ranging from 40 up to 280 kV, when compared to ^{60}Co irradiations. A more detailed literature study as a full investigation of the alanine's response to kV X-rays is presented in chapter 5.

4.3.6 Use of alanine/EPR dosimetry systems

Benefiting from high metrological properties, alanine/EPR dosimetry systems are used in many calibration laboratories as reference standard dosimetry systems as well as a transfer standard and routine monitoring dosimetry systems. For many years, alanine dosimeters were used in many ionizing radiation fields such as electron and photon beams, as well as in many radiation applications such as polymer irradiation, medical device sterilization, food irradiation and radiotherapy.

4.4 Conclusion

This chapter presented different basics of Electron Paramagnetic Resonance spectrometry and described the roles and the function of major components of an EPR spectrometer. On the other hand, this chapter discussed the use of alanine as a dosimeter for ionizing radiation dose measurements, and presented the free radical creation mechanism in alanine as well as the contribution of different radical species in the EPR spectrum. Parameters that should be taken into account for dose measurement using alanine/EPR dosimetry systems were detailed as well as the standard relative uncertainties determination.

The response of the alanine dosimeter can be affected by different influence quantities such as the irradiation temperature, the storage conditions as well as the type and energy of ionizing radiation. Yet, the influence quantity that could have a major impact on alanine's response is the energy of the used radiation, especially kV X-rays. Thus, a study was carried away in this thesis in order to study the alanine dosimeter's relative response to different kV X-ray beam qualities compared to ^{60}Co reference beam quality.

Chapter 5

The relative response of Aerial's alanine dosimeters to kV X-rays

Contents

5.1 Introduction

Nowadays, a clear growth in switching from radioactive source-based (^{137}Cs or ^{60}Co) irradiators to kilo-voltage (kV) X-ray irradiators is observed. This switch is driven by the difficulty to purchase, transport and reload radioactive sources as well as dealing with potential radioactive wastes. On the other hand, kV X-ray self-shielded irradiators show a very promising future for many applications that use radioactive source-based irradiators, such as blood irradiation[90, 134, 139], phytosanitary treatments[43] and Sterile Insect Technique (SIT) applications[107, 111].

However, to maintain a performing irradiation process, adequate dosimetry system needs to be put in place, characterized and properly used for qualification and routine monitoring purposes. Alanine/EPR (Electron Paramagnetic Resonance) dosimetry systems ensure an accurate and reproducible dose measurement over a large dose range (10Gy – 100kGy). Yet, it has been showed in many studies[7, 23, 50, 95, 122, 141, 149, 150, 153] that absorbed dose to water (D_w), measured with alanine dosimeters irradiated with kV X-rays, could be underestimated compared to the true absorbed dose. This is the case when the dosimetry system is calibrated with a reference quality which is different from kV X-rays, such as ^{60}Co or high energy X-ray or electron beams, which is often the case. Thus, correction factors need to be applied to measurements done with alanine dosimeters, calibrated with different reference beam quality, in order to better estimate true absorbed dose to water.

This chapter presents approaches and results of different studies that investigated the alanine's relative response to kV X-rays, and details three different methods that were elaborated during this thesis to characterize the relative response of Aerial's alanine dosimeters to several kV X-ray beam qualities, compared to ^{60}Co reference beam quality.

Experimental measurements were carried out using different X-ray beam qualities to determine alanine's response per dose to water unit as a function of X-ray spectra's relative effective energies. The used beam qualities covered a range of high voltages going from 50 kV to 280 kV. Monte Carlo simulations were done, modelling the irradiation geometry and source to determine the relative dose ratio of alanine to water for different X-ray beam qualities. Finally, a C++ code was developed to analytically calculate the ratio of absorbed dose in alanine compared to water. These three methods permitted to study alanine's relative response to kV X-rays compared to ^{60}Co for different X-ray beam qualities. Once the beam quality specifier is determined (see section 1.2.4), correction factors for D_w measurements, done with alanine dosimeters, can be therefore determined and hereby applied.

5.2 Alanine's relative response to kV X-rays

5.2.1 Case of mono-energetic photon beams

Alanine dosimeters are considered as water equivalent in the case of photon irradiations at energies that are higher than 200 keV, where the difference between mass-energy absorption coefficients (μ_{en}/ρ) of alanine and water does not exceed 4 % in the energy range of 0.2 to 10 MeV [54]. However, for photons with energies below 200 keV, the difference between the mass-energy absorption coefficients of alanine and water increases, as shows figure 5.1.

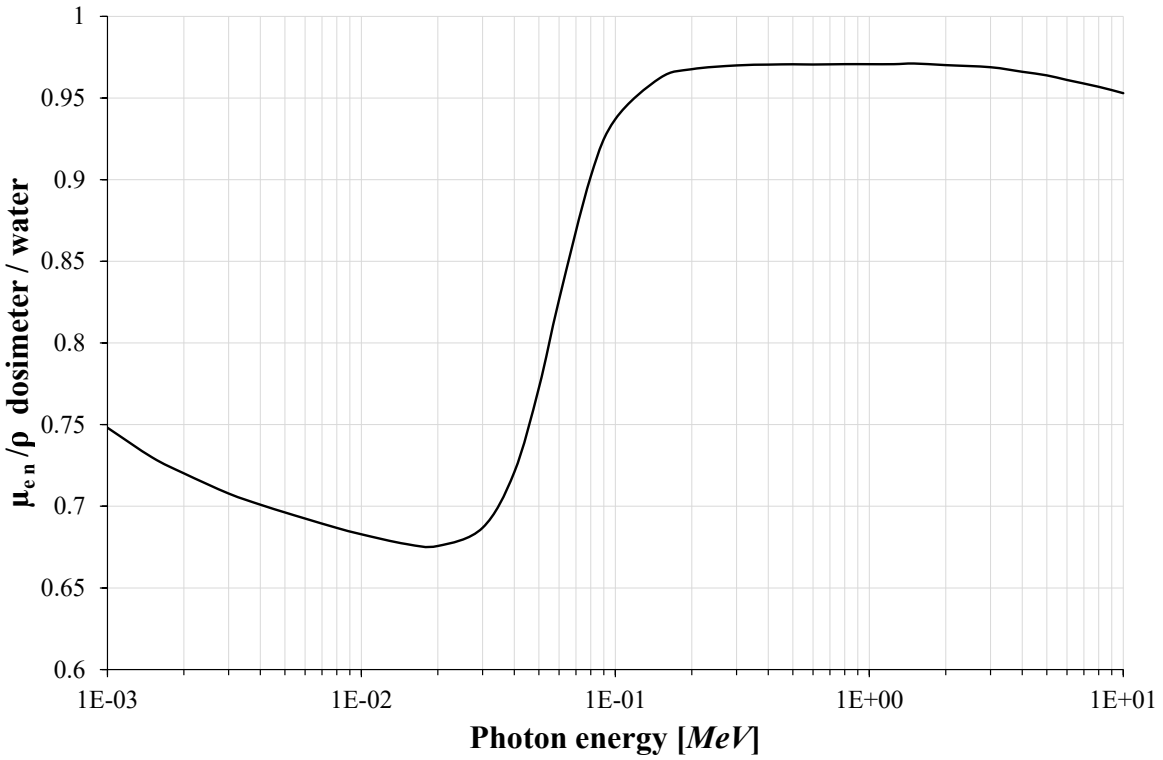

FIGURE 5.1: Ratio of mass-energy absorption coefficients of Aerial's alanine dosimeter and water[54].

Figure 5.1 shows that the ratio of the μ_{en}/ρ factors of alanine to water could decrease down to 0.68 in the energy range of 1 to 200 keV, thus, based on 1.21, this could induce a dose to water underestimation up to 32 % if the dose is measured using alanine/EPR dosimetry system that is calibrated with a reference beam quality of high energy photon or electron beams, such as ^{60}Co reference beam quality. This requires the application of a correction factor to the alanine dosimeter's EPR response in order to better estimate the true absorbed dose to water.

5.2.2 Case of poly-energetic photon beams

X-ray tubes generate a continuum of X-rays having different energies ,thus, it is more complicated to determine a correction factor to be applied to the alanine's response based of mass-energy absorption coefficients, compared to irradiations with mono-energetic photon irradiations. However, in this work, one of the studied methods that determines alanine's relative response to kV X-rays compared to ^{60}Co is based on mass-energy absorption coefficients (section 5.3.3).

From the beginning of the use of alanine in radiation dosimetry, many studies were carried out to determine alanine's relative response to different types of radiation fields. In 2005, Zeng and McCaffrey [153] studied the response of alanine to a 150 kV poly-energetic X-ray beam, compared to ^{60}Co reference beam in the case of air kerma measurements. Six alanine pellets were stacked in a 1 mm wall thick PMMA holder and were irradiated at air kerma points in the range of 20 to 70 Gy. Other sets of alanine pellets were placed inside the same PMMA holder which was then placed inside of a 4 mm thick PMMA cap for ^{60}Co irradiations. Monte Carlo calculations, using DOSRZnrc code of the EGSnrc system[94], were carried out in order to determine the absorbed dose to alanine per unit air kerma. Thus, to estimate the alanine's relative response to kV X-rays compared to ^{60}Co reference beam quality, this factor was calculated:

$$\frac{(r/D_{alanine})_Q}{(r/D_{alanine})_{Q_0}} = \frac{(r/K_a)_Q}{(r/K_a)_{Q_0}} \Big/ \frac{(D_{alanine}/K_a)_Q}{(D_{alanine}/K_a)_{Q_0}} \tag{5.1}$$

where r is the alanine's EPR response, $D_{alanine}$ is the absorbed dose to the alanine dosimeter, K_a is the air kerma and Q and Q_0 are the X-ray and reference beam qualities respectively. The first term of the right hand side of this equation represents the relative alanine/EPR air kerma response, and it can be obtained by the slope ratio of the air kerma response curves for the 150 kV X-ray quality to ^{60}Co gamma rays. The absorbed dose to alanine per unit air kerma ($D_{alanine}/K_a$) was calculated using Monte Carlo simulations. Results showed that the alanine air kerma response was 16.1 % lower for the 150 kV X-ray spectrum than for ^{60}Co gamma rays. Unfortunately, no data was provided in this study on the alanine's relative response for an absorbed dose to water (D_w) measurement. I was also found in this study that the same amount of absorbed X-ray energy in alanine produces 5.7 % fewer stable free radicals than the same amount of absorbed ^{60}Co energy, due to the higher Linear Energy Transfer (LET) of X-rays. This value was found to be in good agreement with published results[125].

Waldeland et al[149, 150] studied the energy dependence of alanine dosimeters for medium energy X-rays in the range of 50 to 200 kV. The energy dependence factor was determined as follows:

$$F_{Q,Q_0} = \frac{(r/D_w)_Q}{(r/D_w)_{Q_0}} = \frac{(r/D_{alanine})_Q}{(r/D_{alanine})_{Q_0}} \cdot \frac{(D_{alanine}/D_w)_Q}{(D_{alanine}/D_w)_{Q_0}} \tag{5.2}$$

where r is the alanine's EPR response, $D_{alanine}$ is the absorbed dose to the alanine dosimeter, D_w is the absorbed dose to water, Q is the studied X-ray beam quality and Q_0 is the reference beam quality. r/D_w represents also the slope of the calibration curve of the alanine/EPR dosimetry system. In the right hand side of the equation, the first fraction of the product is considered as the alanine dosimeter's relative effectiveness (or the relative radiation yield) and

was denoted G_{Q,Q_0}. The second term is the absorbed doses (alanine to water) ratio in a specific X-ray beam quality Q to the ratio in a reference beam quality Q_0, and was denoted H_{Q,Q_0}, thus the energy dependence factor can be expressed as such:

$$F_{Q,Q_0} = G_{Q,Q_0} \,.\, H_{Q,Q_0} \tag{5.3}$$

Irradiations were carried out for X-ray beam qualities with high voltages ranging from 50 to 200 kV (effective energies in the range of 32 to 99 keV). ^{60}Co gamma rays were used as reference beam quality. Absorbed dose to water was measured according to the IAEA TRS 277 protocol[56], using a FC65-G Farmer type ionization chamber (IBA Dosimetry, Germany). H_{Q,Q_0} factor was determined based on Monte Carlo simulations carried out using the EGSnrc code[94]. Experimental results showed that alanine's energy response F_{Q,Q_0} varied from 0.68 at 50 kV up to 0.9 at 200 kV. For Monte Carlo calculations, H_{Q,Q_0} values ranged from 0.725 up to 0.935 at high voltages of 50 and 200 kV respectively.

Khoury et al [95] studied the use of alanine/EPR as a transfer standard dosimetry system for low energy X-ray irradiations. Two different batches of alanine dosimeters (of different chemical composition), one of them being purchased from Aerial and was manufactured in-house, were irradiated with 125 kV X-ray, generated by a 4π RS2400 X-ray tube[111] at different doses ranging from 20 to 160 Gy. Absorbed dose to water was measured using a RadCal 0.6 cc free air ion chamber. A calibration curve was then determined in the studied dose range for both dosimeter batches. Results showed that both dosimeters present a very similar response to 125 kV X-rays, yet, lower than the response of alanine to ^{60}Co gamma rays. Authors calculated the ratio of calibration curves slopes of the alanine dosimetry system for ^{60}Co compared to 125 kV X-rays. This ratio was found to be equal to 1.2.

Figures 5.2 and 5.3 show the results of alanine's relative response obtained by different studies. Anton and Büermann [7] also studied the relative response of the alanine dosimeters to medium energy X-rays, where three sets of irradiations were carried out, at the Physikalisch-Technische Bundesanstalt (PTB) laboratory in Germany, using low energy X-rays (30 to 100 kV), medium energy X-rays (70 to 280 kV) and ^{60}Co gamma rays. The dosimeter's response was defined as:

$$R = \frac{D^c}{D} \tag{5.4}$$

where D^c is the determined dose by EPR spectrometry based on a ^{60}Co calibration and D is the known delivered dose. For low energy X-ray irradiations, a flat ion chamber was used to measure the delivered dose D and alanine dosimeters were placed at the same position as the ion chamber later on for irradiations. For medium energy X-rays, alanine pellets were placed in a PMMA phantom housing a watertight PMMA sleeve for an NE2561 Farmer ion chamber. The phantom and the sleeve were then positioned inside a water phantom at a depth of 5 cm. Delivered dose D was measured using a water calorimeter. This same geometry was also used for ^{60}Co irradiations. The dose to water response relative to ^{60}Co was also calculated by Monte Carlo calculations, using the EGSnrc simulation code, as follows:

$$R^{MC} = \frac{(D_{ala}/D_w)_Q}{(D_{ala}/D_w)_{^{60}Co}} \tag{5.5}$$

This factor is identical to the H_{Q,Q_0} factor calculated by Waldeland et al [149, 150]. Experimental results showed that alanine's relative response ranged from 0.636 up to 0.915 at high voltages of 30 and 280 kV respectively, while results of Monte Carlo calculations showed that the alanine's response varied from 0.686 up to 0.956 for the same high voltages. This difference in results between experimental irradiations and Monte Carlo simulations was noticed in both works of Anton[7] and Waldeland[149, 150]. Its origin is explained by the fact that Monte Carlo simulations do not take into account the contribution of the free radical creation yield $G-value$, which is a very important component in the alanine/EPR dose measurement.

Soliman et al[141] determined the alanine's relative response to X-rays generated by the beam line ID17 at the European Synchrotron Radiation Facility (ESRF), compared to ^{60}Co reference beam quality. The energy of generated X-rays ranged from 50 to 600 keV with less than 1 % of the photons having energies higher than 300 keV [29], and the mean energy of the X-ray spectrum is equal to 99 keV. The relative response was determined experimentally using the same approach presented in the work of Anton and Büermann[7], where the delivered dose was measured using a PTW pin point ion chamber and EPR measurements were carried out to determine the absorbed dose to water measured by alanine dosimeters. The relative response of the alanine dosimeters was found to be equal to 0.932, whereas values reported by Waldeland and Anton, for the same X-ray mean energy of 99 keV, were equal to 0.9 and 0.859 respectively. The better agreement with Waldeland's results is explained by the fact that the dosimeters used in both studies are identical from a chemical composition point of view (96 % alanine and 4 % binder), yet, the ones used in Anton's work present a different composition (91 % alanine and 9 % paraffin wax). The main cause of difference however is the difference in the X-ray energy spectrum where the synchrotron spectrum is "harder" (present photons at higher energies), thus, the relative response of alanine dosimeters to synchrotron X-rays is found to be closer to their response to ^{60}Co gamma rays.

Hjørringgaard et al[50] studied the EPR response of alanine dosimeters to 40 kV X-rays (9 keV effective energy). The method adopted in their study is the same as the one that was used by Waldeland et al[149, 150]. Dose to water was measured using a PTW 23344 soft X-ray ion chamber, and Monte Carlo simulations were carried out using the EGSnrc code. It was found that the alanine's relative response to 40 kV X-rays, compared to ^{60}Co reference beam quality, is equal to 0.644.

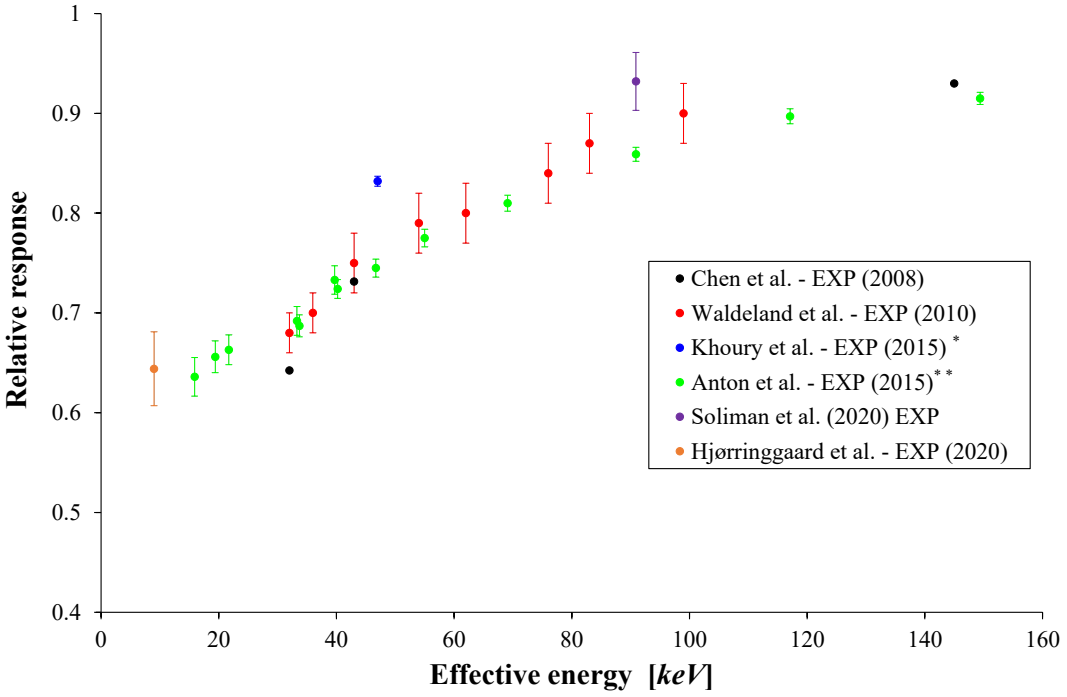

FIGURE 5.2: Published experimental results of alanine's relative response to kV X-ray beam qualities compared to ^{60}Co reference beam quality, as a function of X-ray spectra's effective energies. (* *Estimated effective energy,* ** *Butler et al[20] estimations of the effective energy.*)

Results, of different literature studies, plotted in figure 5.2, represent the alanine's relative response to different X-ray beam qualities as a function of effective energy. These results were obtained by experimental measurements as discussed before. A small fluctuation in plotted results can be noticed. This fluctuation is due to many parameters, such as the composition of the used dosimeters, the irradiation geometry, the calibration of the reference dosimetry material and the dosimetry protocol put into use. However, published data remain in a good agreement, taking into account overall uncertainties, over the studied effective energy range of 9 to 160 keV. We can see that the alanine's relative response rises from about 0.64 at 9 keV up to 0.93 at 160 keV, where a convergence to unity is noticed at high effective energies.

Figure 5.3 shows results of Monte Carlo simulations carried out by Waldeland and Malinen[149], Anton and Büermann[7] and Hjørringgaard et al[50]. All of the three studies calculated the same factor H_{Q,Q_0} as proposed by Waldeland. This factor represents the ratio of absorbed dose in alanine to water at a certain X-ray beam quality Q, relative to the same ratio for a ^{60}Co reference beam quality Q_0. The EGSnrc Monte Carlo simulation code was used in all three studies. One can notice that the result obtained by Hjørringgaard seems to follow the tendency of results obtained by Anton and Büermann at low energies (around 10 keV). Both teams used the same alanine dosimeters purchased from Harwell (UK) with a chemical composition of 91 % of L-α-alanine and 9 % paraffin wax. Results obtained by Waldeland et al are also in agreement with the results of Anton and Büermann, yet, a slight drift in results can be noticed around 100 keV. This can be explained by the difference of the chemical composition of the alanine dosimeters that were studied in each work.

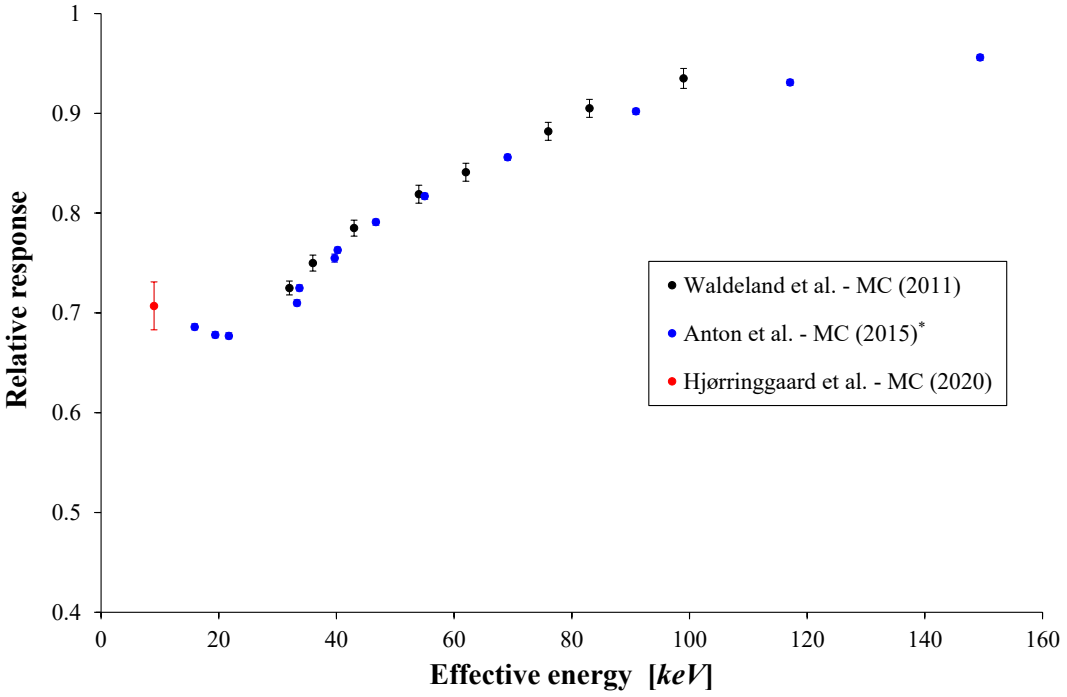

FIGURE 5.3: Published Monte Carlo simulations results of alanine's relative response to kV X-ray beam qualities compared to ^{60}Co reference beam quality, as a function of X-ray spectra's effective energies. (* *Butler et al[20] estimations of the effective energy.*)

5.3 Study of alanine's relative response

In order to adapt the use of Aerial's alanine/EPR dosimetry system for kV X-ray applications, the relative response of Aerial's alanine dosimeters needed to be well characterized, in order to determine correction factors that can be applied the alanine's EPR response for a precise absorbed dose to water measurement. Thus, three different methods were studied in this thesis to determine Aerial's alanine dosimeter response to different kV X-ray beam qualities, compared to ^{60}Co reference beam quality. Figure 5.4 shows a diagram that summarizes the logic that was adopted in each method to determine the relative response of alanine dosimeters to kV X-ray beam qualities Q compared to a reference beam quality Q_0.

The first method is based on direct experimental measurements, the second method is based on Monte Carlo calculations and the third method, which brings all the novelty to this thesis permitted to calculate analytically the alanine's relative response to kV X-rays, with results that were found to be in a good agreement with Monte Carlo simulations, yet, the analytical calculations are much faster (few seconds) than Monte Carlo simulations running time (few hours).

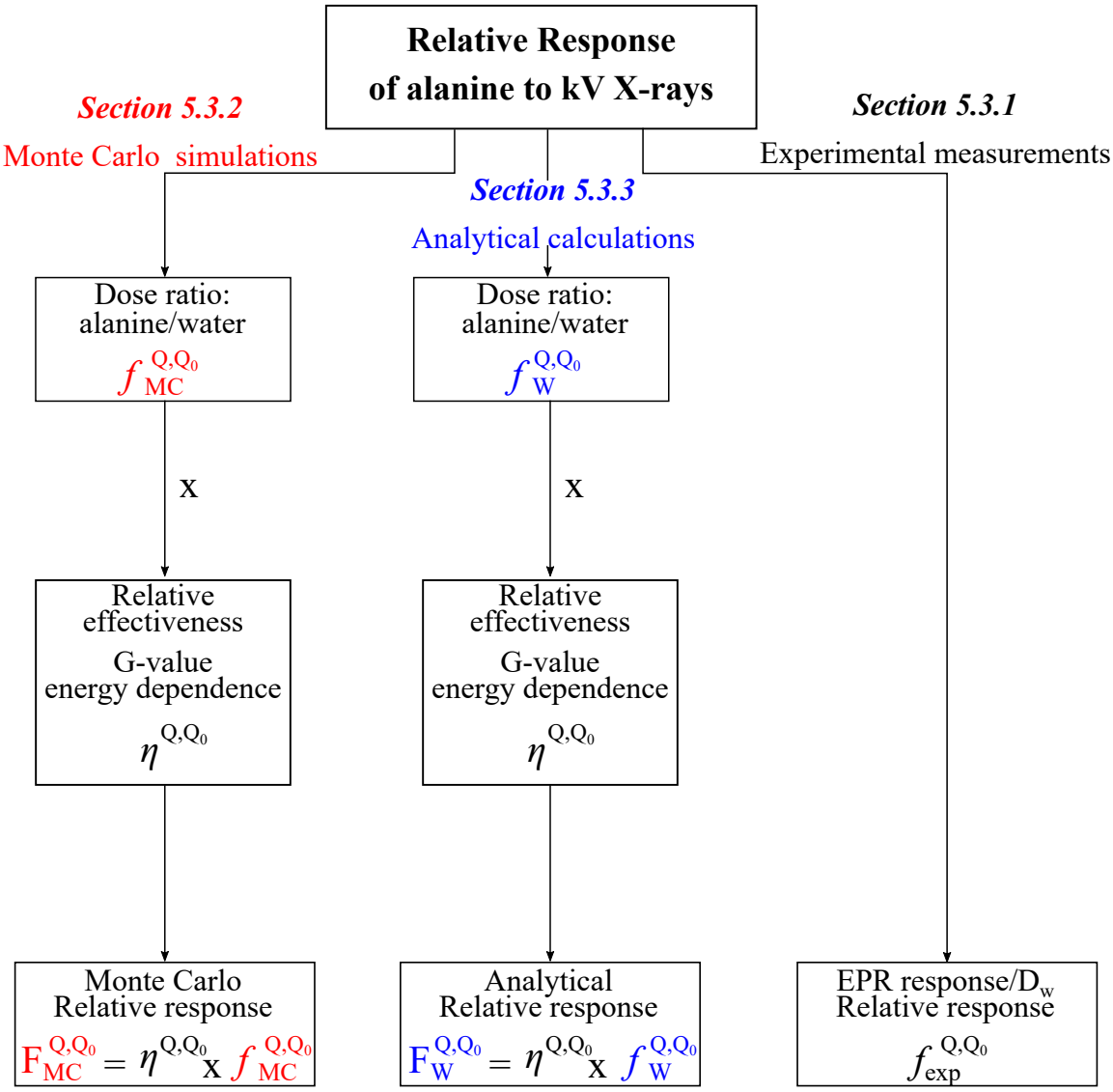

FIGURE 5.4: Diagram of the three studied methods to determine the relative response of alanine to kV X-rays.

5.3.1 Experimental measurements

In order to determine the relative response of Aerial's alanine dosimeters to kV X-rays, two different sets of irradiations were carried out at Aerial and at the National Physical Laboratory (NPL), using two different sets of geometries. Irradiations carried out at Aerial covered tube potentials ranging from 50 kV up to 100 kV, while irradiations carried out at NPL covered tube potentials of 135 and 280 kV.

5.3.1.1 General formalism

The alanine's relative response is defined as the ratio of the dosimeter's EPR response per unit of absorbed dose to water, for a specific X-ray beam quality compared to the same ratio for a

^{60}Co reference beam quality. It is expressed as such:

$$f_{exp}^{Q,Q_0} = \frac{(r/D_w)^Q}{(r/D_w)^{Q_0}} \tag{5.6}$$

where f_{exp}^{Q,Q_0} is the alanine's relative response to an X-ray beam quality Q compared to a reference beam quality Q_0, r is the dosimeter's EPR response and D_w is the absorbed dose to water delivered to the alanine dosimeter. The value of the delivered absorbed dose to water is determined by ion chamber measurements. The factor r/D_w also represents the slope of the calibration curve of the alanine system, in the linear dose range of few Grays up to 10 kGy. Thus, in order to better estimate the f_{exp}^{Q,Q_0} factor, a calibration curve was determined for each X-ray beam quality Q, as well as for Q_0 reference beam quality. In this work, ^{60}Co gamma rays were considered as the Q_0 reference beam quality. Alanine reference dosimeters, used for the calibration of Aerial's alanine/EPR dosimetry system, were used to establish the calibration curve for ^{60}Co reference beam quality. The reference dosimeters were irradiated at NPL.

5.3.1.2 X-ray irradiations

Aerial disposes of a low energy X-ray irradiator capable of generating X-ray spectra at potentials ranging from 5 up to 100 kV. A high voltage generator, with a maximum power of 3 kW, powers a BALTEAU-NDT TSD 160/0 X-ray tube that is housed in a self-shielded X-ray cabinet, as shows figure 5.5. The tube's anode is made of tungsten with an incline angle of 20°. The beam exit window consists of 0.8 mm thick beryllium window. Table 5.1 lists the beam qualities that were used in this study. For each beam quality, high voltage and external added filtration are listed, as well as two different beam specifiers: first half value layer (HVL_1) in aluminum, and the beam's effective energy (E_{eff}) in aluminum. The X-ray tube in dispose at NPL can deliver X-ray spectra at potentials of up to 280 kV. It is a bipolar X-ray tube with a tungsten anode having an incline angle of 20°. This facility is used for air-kerma calibration of different types of ion chambers against the NPL Free Air Chamber (FAC) primary standard.

Values of HVL and E_{eff} are calculated based on the SpekCalc software[131]. This software takes into account different parameters that are intrinsic to the X-ray tube such as the anode angle, the operational high voltage and inherent filtration, as well as external added filtration of different material such as aluminum and copper, and calculates the first and second HVL in aluminum and copper, the mean energy of the X-ray spectrum as well as the effective energy in aluminum and copper. It has been reported in many international dosimetry codes of practice [22, 58, 61, 97] that the use of tube potential alongside the HVL is adequate to reflect the X-ray beam quality. However, for the sake of comparison with different literature works, the effective energy in aluminum is chosen as the sole beam quality specifier in this work.

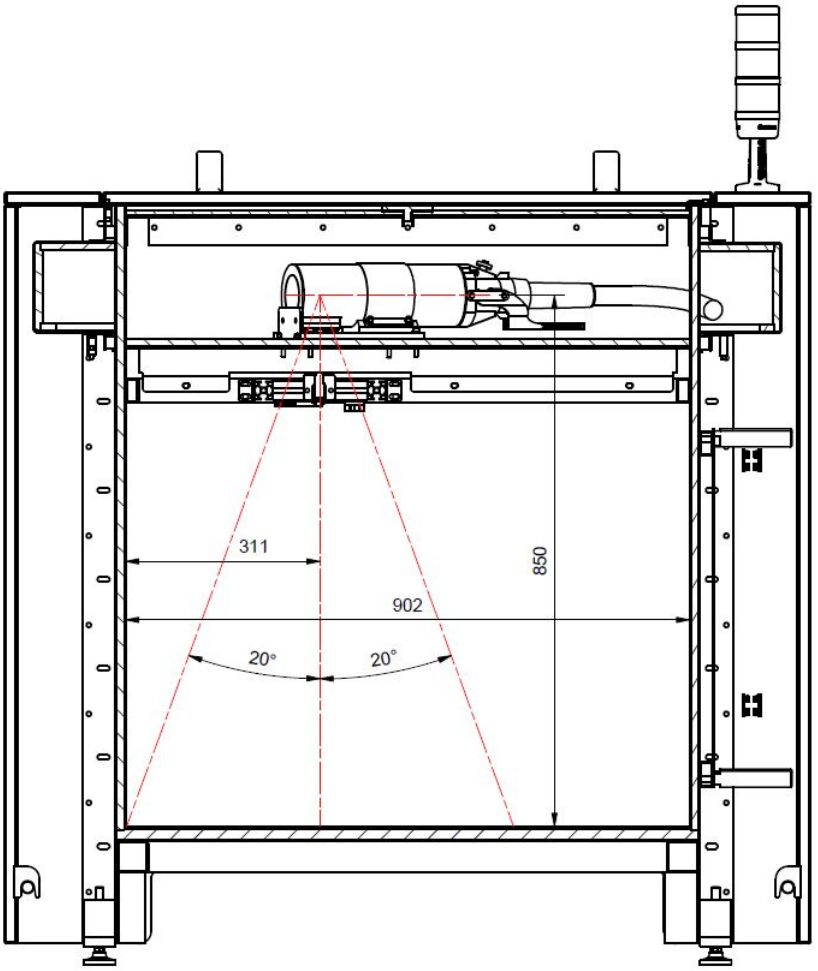

FIGURE 5.5: Drawing of the self-shielded X-ray cabinet used for X-ray irradiations carried out at Aerial.

		Added external filtration					Beam Quality specifier	
Irradiation site	HV [kV]	Al [mm]	Cu [mm]	Sn [mm]	Solid Water® [mm]	PMMA [mm]	HVL_1 [kV]	E_{eff} [keV]
Aerial	50	2.39	0	0	0	5	1.81	27.5
Aerial	70	2.88	0	0	0	5	2.65	31.9
Aerial	90	3.35	0	0	0	5	3.64	36.3
Aerial	100	1.43	0	0	0	5	2.57	31.5
Aerial	100	3.84	0	0	0	5	4.32	39.2
Aerial	100	4.95	0	0	0	5	4.93	41.7
Aerial	90	0.96	0	0	0	0	1.52	25.8
Aerial	100	1.43	0	0	0	0	2.18	29.5
Aerial	100	3.84	0	0	0	0	4.06	38.1
NPL	135	1.2	0.27	0	20	0	9.01	58.9
NPL	280	1	0.26	1.5	20	0	19.6	168

TABLE 5.1: List of the different X-ray beam qualities used in this work.

5.3.1.3 Alanine dosimeters and EPR readout

Aerial's commercial alanine dosimeters (Lot 09/11) were used in this work. Alanine pellets have a 4 mm diameter, a thickness of 2.35 mm and an average mass of 36.05 ± 0.05 mg, with a chemical composition of 91.63 % of pure L-α-alanine, 6.37 % of EUDRAGIT NE 30D and 2 % MYVATEX.

EPR readout was performed using a Freiberg Instruments Magnettech Miniscope MS5000 spectrometer (Freiberg, Germany)[101] using the following parameters: magnetic field sweep width of 2 mT, sweep time of 5 s, modulation amplitude and frequency of 0.7 mT and 100 kHz respectively, microwave power and frequency of 10 mW and 9.253 GHz respectively. Measured spectra were taken as input in the AerEDE2019 software, developed and commercialized by Aerial, in order to correct the dosimeter's response with irradiation temperature.

FIGURE 5.6: Aer'EDE219 software and the MS5000 EPR spetrometer used for alanine dosimeters readout.

5.3.1.4 Irradiation setups

For irradiations carried out at Aerial, the irradiation geometry consisted of 5 alanine dosimeters placed in a PMMA holder having a diameter of 10 cm, as shown in figure 5.7(a). Dosimeters were irradiated with a vertical photon beam. In addition, a thickness of PMMA was placed under the dosimeters, which were positioned in such a way that the distance between the X-ray tube's focal point and the surface of the dosimeters was equal to 80 cm. For some beam qualities, an additional 5 mm PMMA plate was added on top of the alanine pellets, as listed in table 5.1. Before irradiating the alanine dosimeters, the delivered absorbed dose rate to water was measured at the same reference point using a PTW 30013 Farmer waterproof ion chamber. Five dose rate measurements were carried out for 30 seconds of irradiation each, in order to determine the absorbed dose rate to water at the reference point. Alanine dosimeters were then positioned at the same reference point and irradiated for the right amount of time in order to receive the desired doses. The ion chamber is calibrated in terms of absorbed dose to water for

several X-ray radiation qualities as well as for ^{60}Co reference beam quality, with a traceability to PTB's water calorimetry secondary standard.

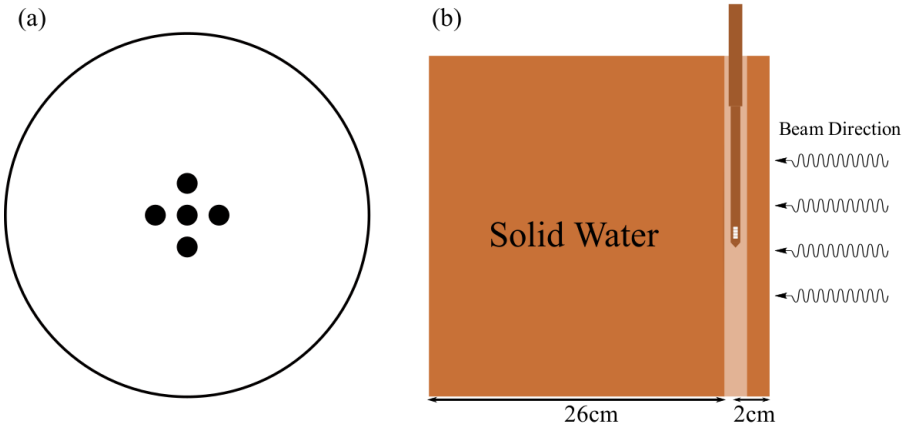

FIGURE 5.7: Different holders of alanine dosimeters: (a) irradiations at Aerial and (b) irradiations at NPL.

Irradiations carried out at NPL consisted of placing 4 alanine dosimeters inside a Solid Water® holder shaped as an ion chamber. This alanine holder was then placed in a 2 cm thick WT1 Solid Water® slab. Solid Water® slabs were purchased from Phoenix Dosimetry Ltd. Solid Water® plates were added between the beam exit window and the dosimeters in order to have the alanine pellets at a water equivalent depth of 2 cm. A total thickness of 26 cm of Solid Water® slabs was added behind the dosimeters to ensure full backscatter conditions as shown in figure 5.7(b). Dose output was measured using NPL's PTW 30012 Farmer ion chamber, which is calibrated in air-kerma, with a traceability to NPL's free air chamber primary standard. Absorbed dose rate to water was determined using the IPEMB (Institute of Physics and Engineering in Medicine and Biology)[97] code of practice using the in-phantom method for the determination of the absorbed dose to water. A comparison of ion chamber measurements of absorbed dose to water (Aerial PTW 30013 and NPL PTW 30012) was carried out beforehand in order to compare results obtained after irradiations at NPL, to the results of irradiations performed at Aerial. This is needed to ensure that the alanine's response is always compared to a dose unit measured by the same reference instrument, which, in this study, is Aerial's PTW 30013 ion chamber. Details of this comparison is presented in Appendix A (page 149).

5.3.1.5 Delivered absorbed dose to water measurements

In order to study the alanine's relative response to kV X-rays, as described in equation 5.6, the delivered absorbed dose to water needs to be well determined. This was done using a calibrated PTW 30013 Farmer ion chamber and a calibrated PTW UNIDOS-E electrometer. The measured absorbed dose to water can be expressed, according to the IAEA TRS 398 protocol[58], as follows:

$$D_w^Q = M^Q \cdot N_{D_w}^{Q_0} \cdot k^{Q,Q_0} \tag{5.7}$$

where D_w^Q is the measured absorbed dose to water for the beam quality Q, M^Q is the corrected ion chamber reading expressed in Coulomb $[C]$, $N_{D_w}^{Q_0}$ is the calibration coefficient of the ion chamber for a reference quality Q_0 and is equal to 5.351 $\times$ 10^7 Gy/C, and k^{Q,Q_0} is the beam quality correction factor given by the calibration laboratory.

The ion chamber reading M needs to be corrected for the influence quantities: temperature and pressure, polarity and the electrometer calibration. Thus, the corrected ion chamber reading, for a certain beam quality Q can be expressed as such:

$$M^Q \;=\; M \;.\; k_{T,P} \;.\; k_{pol} \;.\; k_{elec} \tag{5.8}$$

where $k_{T,P}$ is the temperature and pressure correction factor, k_{pol} is the polarity correction factor and k_{elec} is the electrometer calibration factor. These factors are expressed as:

$$k_{T,P} \;=\; \frac{(273.2 \;+\; T)}{(273.2 \;+\; T_0)} \;\times\; \frac{P_0}{P} \tag{5.9}$$

with T being the irradiation temperature, T_0 is the irradiation temperature during calibration, P is the ambient air pressure during the irradiation and P_0 is the ambient air pressure during calibration.

$$k_{pol} \;=\; \frac{|M_+| \;+\; |M_-|}{2M} \tag{5.10}$$

where M_+ is the ion chamber reading when the positive polarization voltage is applied and M_- is the ion chamber reading when the negative polarization voltage is applied. According to the calibration certificate of Aerial's PTW 30013 ion chamber, the polarity effect was found to be less than 0.2 %, thus it was not taken into account for ion chamber reading correction. k_{elec} is given by the calibration laboratory, and for Aerial's PTW 30013 ion chamber $k_{elec} \;=\; 1.000 \;\pm 0.5\%$.

For irradiations carried out at NPL, a PTW 30012 ion chamber, calibrated in terms of air-kerma, was used for absorbed dose to water readout, according to the IPEMB code of practice using the in-phantom method[97]. The absorbed dose is determined as follows:

$$D_{w,z=2cm} \;=\; M \;.\; N_k \;.\; k_{ch} \;.\; \left[\left(\frac{\bar{\mu}_{en}}{\rho}\right)_{w/air}\right]_{z=2,\phi} \tag{5.11}$$

where $D_{w,z=2cm}$ is the absorbed dose to water measured at a water depth of 2 cm for a beam quality Q, M is the ion chamber reading corrected for temperature and pressure differences, N_k is the air-kerma calibration coefficient for a beam quality Q, k_{ch} is the factor that accounts for the change in the response of the ion chamber between calibration in air and measurement in a water phantom and finally, $\left(\frac{\bar{\mu}_{en}}{\rho}\right)_{w/air}$ is the mass-energy absorption coefficient ratio, water to air, averaged over the photon spectrum at 2 cm depth of water and field diameter ϕ. The ion chamber reading is of course corrected for temperature and pressure, polarity and electrometer calibration as described before.

Two uncertainty budgets were established for each set of irradiations. Tables 5.2 and 5.3 presents the different components taken into account for the determination of the combined uncertainty on the alanine's relative response.

Symbol	Description	Uncertainty [%] - (k = 1) Type A	Type B
	Alanine - response measurement		
σ_r	Alanine response measurement by EPR spectrometery	0.5	
σ_m	Alanine dosimeters mass		0.2
σ_{EPR}	EPR spectrometer instability		0.35
σ_{air}	Small air gaps in PMMA holder		0.2
σ_{PMMA}	PMMA - Non equivalency to water		1.5
σ_T	Irradiation temperature correction	0.8	
	Total per type	0.94	1.57
	Total - alanine response measurement	1.83	
	Ion chamber measurement		
σ_M	Ion chamber - reading reproducibility	0.1	
$\sigma_{N_{Dw}^{Q_0}}$	Ion chamber - Dose to water conversion coefficient		0.7
$\sigma_{k^{Q,Q_0}}$	Ion chamber - beam quality correction factor		1.85
$\sigma_{k_{T,P}}$	Ion chamber - temperature and pressure correction factor	1	
σ_{elec}	Ion chamber - electrometer correction factor		0.25
σ_{recomb}	Ion chamber - recombination		0.2
σ_{pol}	Ion chamber - polarity effect		0.25
	Total per type	1	2.02
	Total - Ion chamber measurement	2.26	
	Total f_{exp}^{Q,Q_0} uncertainty	**2.91**	

TABLE 5.2: Uncertainty budget for alanine's relative response determined with irradiations carried out at Aerial.

Symbol	Description	Uncertainty [%] - (k = 1) Type A	Type B
	Alanine - response measurement		
σ_r	Alanine response measurement by EPR spectrometery	0.5	
σ_m	Alanine dosimeters mass		0.2
σ_{EPR}	EPR spectrometer instability		0.35
σ_{air}	Small air gaps in sleeve holder		0.2
σ_{SW}	Solid Water® - Non equivalency to water		0.5
σ_T	Irradiation temperature correction	0.3	
	Total per type	0.58	0.67
	Total - alanine response measurement	0.89	
	Ion chamber measurement		
σ_{N_k}	Air kerma calibration factor		0.6
$\sigma_{k_{ch}}$	Ion chamber correction factor		1.5
$\sigma_{\mu_{en}/\rho}$	Ratio of mass-energy absorption coefficient - air to water - at 2 cm water depth		1.5
	Total per type	0.00	2.2
	Total - Ion chamber measurement	2.2	
	Total f_{exp}^{Q,Q_0} uncertainty	**2.38**	

TABLE 5.3: Uncertainty budget for alanine's relative response determined with irradiations carried out at NPL.

5.3.1.6 Results and discussion

Alanine's response per absorbed dose to water (r/D_w) was determined for different X-ray qualities, listed in table 5.1, with respect to ^{60}Co reference beam quality. Obtained results are plotted in figure 5.8. Results are compared to ones reported by Anton and Büermann[7], Waldeland et al[150], Khoury et al[95], Soliman et al[141] and Hjørringgaard et al[50]. The main comparison is done with Anton and Waldeland's data that cover a large energy range. A good agreement is noticed between the three data series over all the energy range. Waldeland's data were studied as a function of effective energy, whereas Anton's data were published as a function of the X-ray spectra's average energy. A study done by Butler et al[20] using Anton's published data, showed a conversion of Anton's used average energies into effective energies. Error bars in figure 5.8 represent uncertainties (at k = 1). An overall uncertainty budget of 2.9 % (k = 1) was calculated in the case of irradiations carried at Aerial, and another budget of 2.38 % (k = 1) was calculated in the case of irradiations done at NPL. Anton mentioned in his work that alanine's relative response drops down to 64 % in case of low energy X-ray irradiations at an effective energy of 15.9 keV. Waldeland stated that the experimental relative response of alanine varied from 0.68 up to 0.9 over the studied effective energy range (32 keV up to 99 keV). Results obtained in this work are consistent with Anton and Waldeland's data over the studied effective energy range (27.5 keV up to 168 keV), yet, one can notice that results obtained in this work are higher than published data. This difference is mainly due to the difference in size and composition of the alanine dosimeters between the three studies, as well as the difference in the used experimental setup.

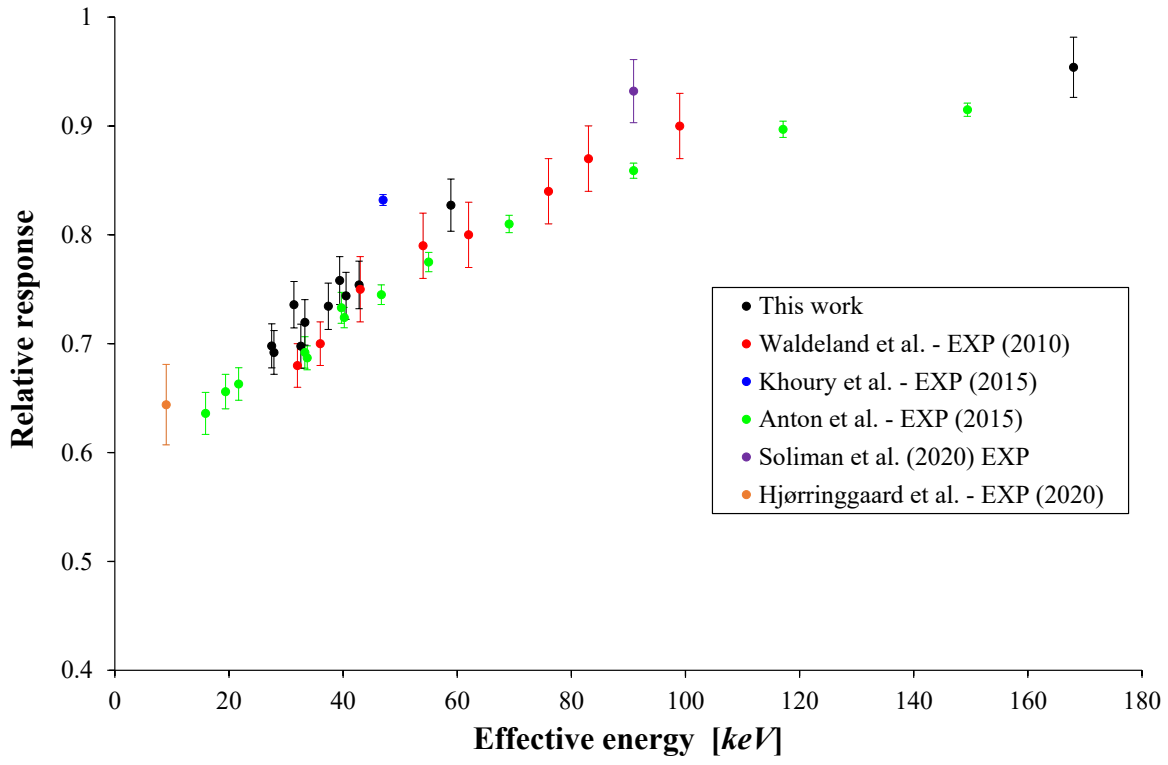

FIGURE 5.8: The relative response of Aerial's alanine dosimeters to kV X-rays, with respect to ^{60}Co reference beam quality, compared to results obtained different studies.

5.3.2 Monte Carlo simulations

5.3.2.1 General formalism

Monte Carlo simulations were carried out to determine the ratio of absorbed dose to the dosimeter with respect to water, for a certain X-ray beam quality Q compared to a reference beam quality Q_0 such as ^{60}Co gamma rays. The calculated actor is:

$$f_{MC}^{Q,Q_0} = \frac{\left(\frac{D_{dos}}{D_w}\right)^{Q}}{\left(\frac{D_{dos}}{D_w}\right)^{Q_0}} \tag{5.12}$$

where D_{dos} is the absorbed dose in the dosimeter and D_w is the absorbed dose to water. Knowing that Monte Carlo simulations do not take into account the free radical generation processes in the alanine dosimeter, this means that the obtained f_{MC}^{Q,Q_0} accounts only for the differences in physical interactions of X-rays and ^{60}Co gamma rays in alanine and water. The factor calculated in the equation 5.12 is identical to the one that was calculated by Waldeland and Malinen[149], Anton and Büermann[7] and Hjørringgaard et al[50]. However, the Monte Carlo code used in these studies is different than the ones used in this thesis.

5.3.2.2 Monte Carlo codes

The Monte Carlo method is a calculation technique based on the mathematical simulation of physical processes. The application of this technique requires a transcription of the variables of the physical processes in terms of probabilities. It is thus necessary to define probability and counting functions to decompose a complex problem into a series of random calculations of values for each variable based on a probability function.

In radiation physics, Monte Carlo calculations are done in order to estimate physical quantities, such as absorbed dose, particle position and particle energy. In this study, Monte Carlo calculations are done in order to follow the interactions of primary generated photons in the entire constructed geometry until their remaining energy falls below the energy cut-off limit, where the particle is killed. The transport phenomenon is governed by both probabilistic interactions and modelled physical quantities such as cross sections. The definition of a Monte Carlo simulation for particle transport is carried out in several steps:

1. Geometry definition: dimension, position and composition of each volume.
2. Source definition: particle type, particle energy, direction of generation and source position.
3. Sensitive volumes definitions: volumes of interest in which one would want to estimate a certain physical quantity such as deposited energy or particle fluence.
4. Physics definition: physics models and cut-off energies.
5. Number of primary particles to generate.

Many events (particles) are generated one by one in a desired way (described in source definition) into the constructed geometry. Each particle undergoes interaction with the material that it is crossing. The change in the energy and direction of the incident particle is governed by physics models based on different interaction cross sections. After each interaction, the Monte Carlo code assesses many parameters of the incident particle, such as its new energy and direction, as well as the parameters of secondary particles, if created. All interactions that occur in the defined sensitive volume are scored and are finally averaged and the statistical error is then calculated.

In radiation physics, there exists many Monte Carlo particle transportation codes, where each one is more suited for a certain type of application than others, and each one is often based on a different coding language, such as C++ or FORTRAN. Nowadays, the most commonly used Monte Carlo codes are:

- EGSnrc[94]: a version of the EGS (Electron Gamma Shower) code developed by the National Research Council of Canada (NRCC). This code is only used for electron and photon transportation.
- GEANT4[4–6]: Geometry ANd Tracking, developed by CERN. Mainly developed for high energy physics, but it was updated for almost all radiation applications. Its main flaw is the need of a good knowledge level of C++ coding.
- MCNP[130]: Monte Carlo N-Particle, developed by the Los Alamos National Laboratory in the USA. This code offers many statistical checks to validate obtained results, however, geometry visualization is difficult.
- GATE[40]: GEANT4 Application for Tomographic Emission, which is an upper layer based on GEANT4. It is more user friendly than GEANT4 and it is mainly used for medical radiation applications.

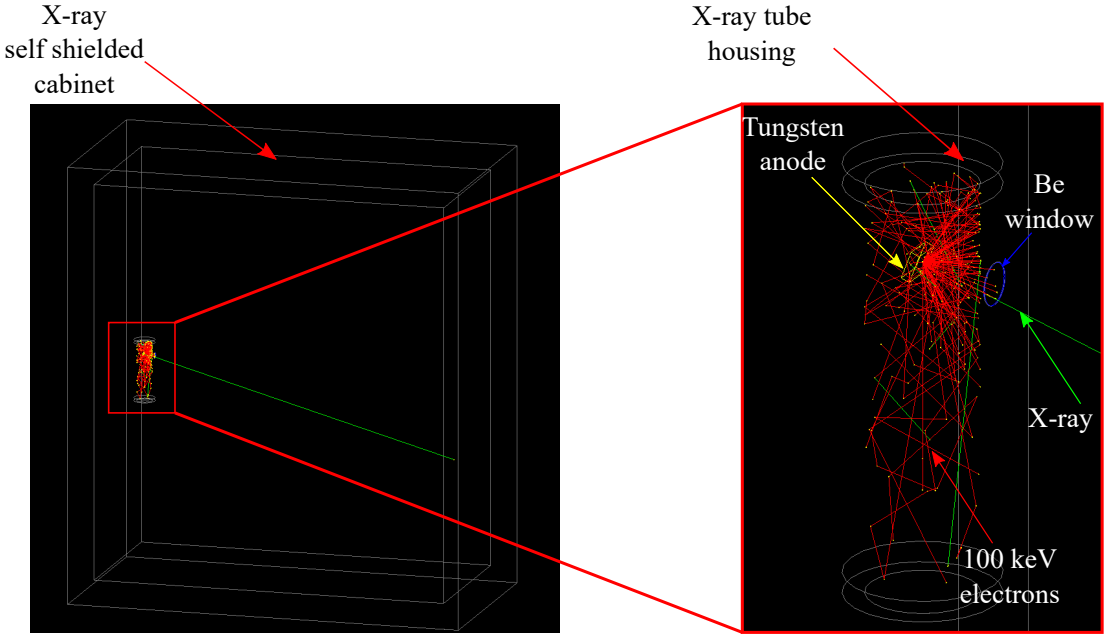

FIGURE 5.9: Geant4 simulation of Aerial's X-ray tube and self-shielded cabinet.

5.3.2.3 Results and discussion

Firstly, monoenergetic photon beams were simulated to compare the ratio of absorbed dose (alanine to water) to the mass-energy absorption coefficients displayed in figure 5.1. Simulations were carried out using both GEANT4 and MCNPX codes. Constructed geometry consisted of cylindrical pellets made of water and alanine dosimeter material that were placed in a PMMA holder. These sensitive volumes were irradiated separately with photons having energies in the range of 1 keV to 10 MeV. Both alanine and water cylinders had the dimensions of the Aerial alanine dosimeter. For GEANT4 simulations, both photon and electron energy cut-offs were set to 250 eV using the Livermore low energy physics model. MCNPX default physics limits the photon and electron energy cut-offs to a minimum of 1 keV. For each calculation, for both codes, 100 million photons were generated for each energy. Figure 5.10 shows the obtained results compared to NIST's data. A circular photon beam of 10 cm diameter was simulated with both simulation codes and was positioned at 75 cm from the surface of the sensitive volumes. Photons are generated at a perpendicular direction to the sensitive volumes surface.

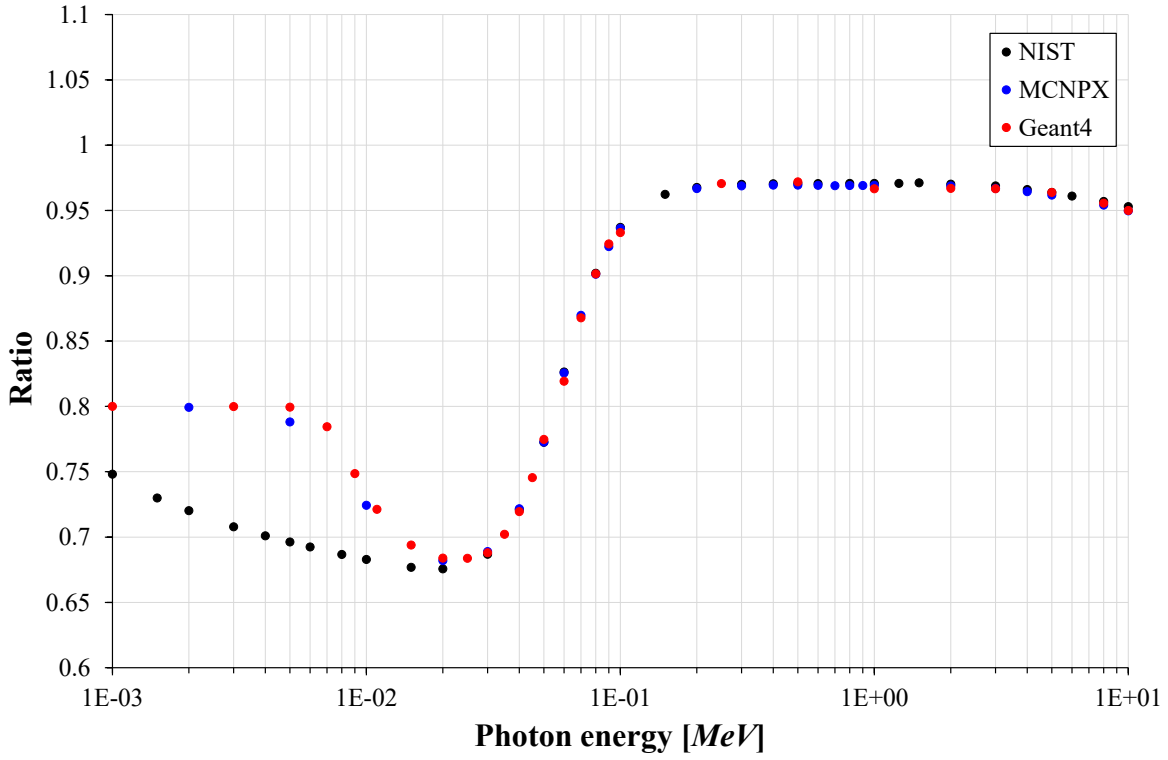

FIGURE 5.10: Ratio of absorbed dose in alanine to water compared to mass-energy absorption coefficients.

We can clearly notice that results obtained by both simulation codes are in good agreement over the energy range of 20 keV to 10 MeV. However, a difference is noticed between results obtained by Monte Carlo simulations and NIST data in the energy range of 1 to 20 keV. This is due to the fact that the penetration of low energy photons in matter is low, thus, it would have been more adequate to simulate thinner water and alanine volumes to have a better comparison. This hypothesis was tested by irradiating alanine and water volumes with a thickness of 500

µm. Alanine to water dose ratios were equal to 0.702 and 0.691 for photon energies of 7 and 10 keV respectively, for simulations carried out with Geant4 and MCNPX. Based on NIST's data the mass-energy absorption coefficients ratio are equal to 0.69 and 0.683 at photon energies of 7 and 10 keV respectively. At energies higher than 20 keV, results obtained by simulations are in very good agreement with NIST's data. In most cases of industrial irradiations using kV X-rays, filters are placed at the beam exit window to attenuate low energy X-rays (from 1 to 20 keV) and to ensure a more homogeneous irradiation due to induced scattering of photons.

For simulations using polyenergetic X-ray spectra, only the MCNPX code was used for its easiness of use compared to GEANT4. Irradiation geometries presented in figure 5.7 as well as the X-ray cabinet (figure 5.5) were simulated in the Monte Carlo code. For irradiations carried out at NPL, the irradiated geometry was placed inside a big bunker with dimensions of 5m x 15m x 2.5m and placed at the same distance from the X-ray source as in reality, to reproduce as much as possible the irradiation configuration. Figure 5.11 represents the logic diagram of carried out Monte Carlo simulations. For all simulations, a point source was defined, and photons were emitted in a cone angular distribution with an opening angle of 40°. The source was positioned at 80 cm above the sensitive volumes, for simulations that model irradiations carried out at Aerial. The same photon source type was positioned at 75 cm from the surface of the Solid Water® phantom, in the case of simulations modelling irradiations carried out at NPL. The default physics model was used for MCNPX simulations, where the photon mode was activated in order to take into account the generation of both secondary electrons and photons, as well as potential Bremsstrahlung photons. The energy cut-off values were set to 1 keV for both photons and electrons.

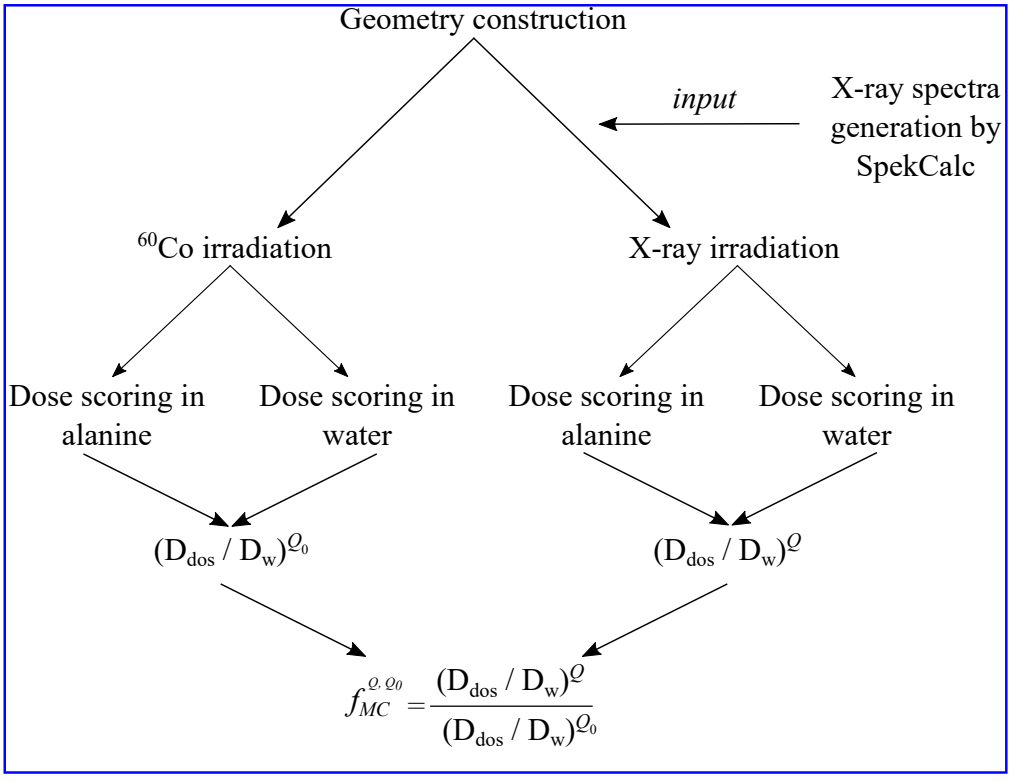

FIGURE 5.11: Logic diagram of carried out Monte Carlo simulations to determine the f_{MC}^{Q,Q_0} factor.

Once the geometry is defined, X-ray spectra generated by SpekCalc were taken as input for irradiation. Spectra are generated based on the real X-ray tubes configurations as well as added filtrations that lists table 5.1. Firstly, alanine pellets were placed inside the defined holders and deposited energy was scored via a "+F6" tally. A tally is an operator defined in MCNP that permits to calculate a certain physical quantity, such as energy fluence and energy deposition in a sensitive volume. Absorbed dose in alanine pellets was then calculated by dividing the deposited energy, converted to Joules, by the dosimeter's mass expressed in kilogram. After that, water pellets having the same volume as he alanine dosimeters were placed in the exact same positions in holders and were irradiated with the same X-ray spectra. Dose calculation for water volumes is identical to the one used for alanine pellets. For ^{60}Co reference beam irradiations, a punctual ^{60}Co gamma source was modelled emitting gamma rays isotropically. Alanine and water volumes were placed in the same configuration as the one reproducing X-ray irradiations carried out at NPL. For each simulation, 10^9 primary photons were generated in order to obtain a low statistical uncertainty on calculated doses. Figure 5.12 shows obtained results by Monte Carlo simulations and their comparison to experimentally obtained results.

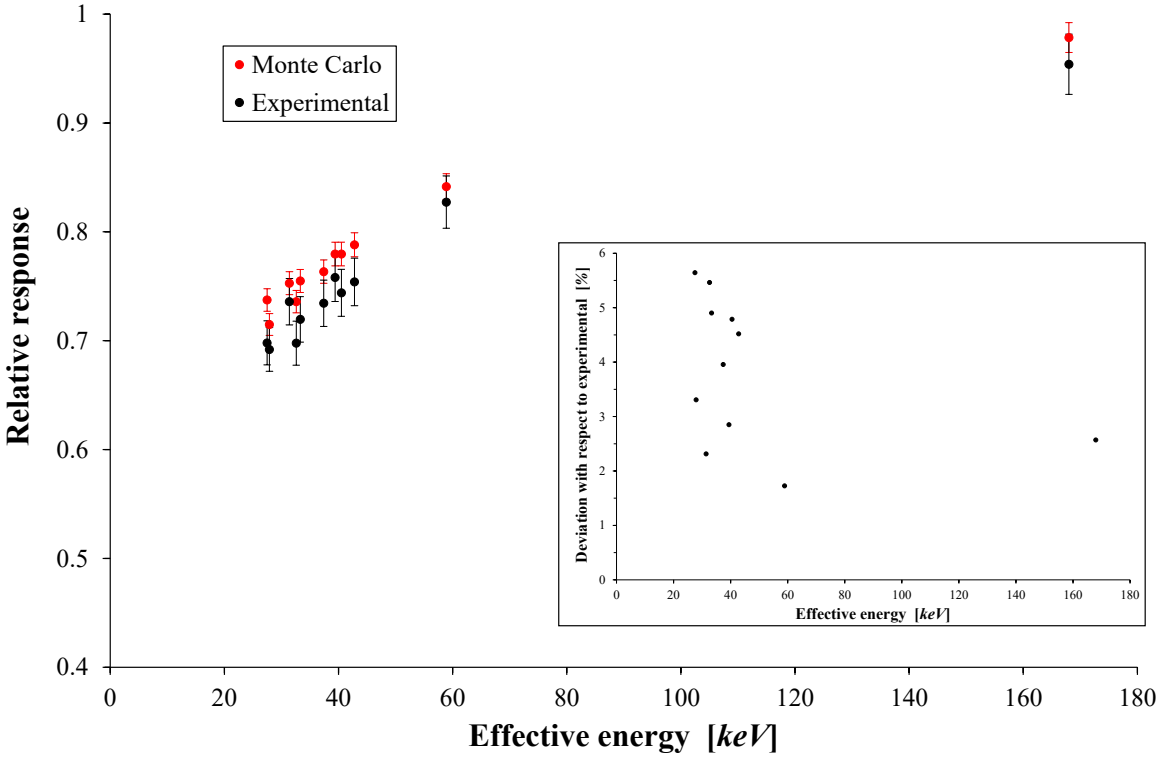

FIGURE 5.12: Values of f_{MC}^{Q,Q_0} factor obtained by MCNPX Monte Carlo simulations compared to the experimentally determined alanine relative response f_{exp}^{Q,Q_0}.

Obtained results showed that the f_{MC}^{Q,Q_0} factor follows the same tendency as the f_{exp}^{Q,Q_0} factor over the studied energy range. However, a difference between results obtained by Monte Carlo simulations and experimental measurements is clearly noticed, where Monte Carlo results are always higher than experimental results. This is due to the fact that Monte Carlo simulations do not model the free radical creation process in alanine dosimeters, thus, the photon energy dependence of the free radical creation yield (G-value) is not taken into account. Section 5.4

details a study that was carried out during this thesis to determine the variation of alanine radicals G-value as a function of the X-ray effective energies, compared to ^{60}Co gamma rays. Many studies[7, 50, 124–126, 150] showed that the alanine G-value is energy dependant for photon energies below 200 keV. Thus, it is necessary to determine the relative G-value of Aerial's alanine dosimeters and apply them to f_{MC}^{Q,Q_0} in order to have a better comparison of the results of experimental and Monte Carlo methods.

The average deviation between results obtained by Monte Carlo calculations and experimentally measured results is 3.82 %. An uncertainty budget, presented in table 5.4, of 1.41 % (k = 1) was determined for Monte Carlo simulations. This budget can be split into two components: σ_{stat} and σ_{model}. σ_{stat} represents the statistical uncertainty of the Monte Carlo calculations and can be simply minimized by increasing the number of simulated particles. σ_{model} takes into account all differences between the realistic and simulated irradiation geometries as well as chemical composition of all geometry elements.

		Uncertainty [%] - (k = 1)	
Symbol	**Description**	**Type A**	**Type B**
σ_{stat}	Statistical uncertainty	1	
σ_{model}	Geometry and material modelling uncertainty		1
	Total f_{MC}^{Q,Q_0} uncertainty	1.41	

TABLE 5.4: Uncertainty budget for the calculation of the f_{MC}^{Q,Q_0} factor (k = 1).

Figure 5.13 shows the comparison of results obtained in this work by Monte Carlo simulations, and the ones obtained by Waldeland and Malinen[149] and Anton and Büermann[7]. One can notice that all results follow the same tendency over the energy range of 27.5 to 168 keV. Yet, results obtained in this work are found to be slightly higher than published results. This is due to three factors: the difference in the chemical composition of the alanine dosimeters of each study, the difference in the irradiation geometry and finally the difference of the chosen Monte Carlo simulation codes where Waldeland and Anton used EGSnrc while MCNPX was used in this study.

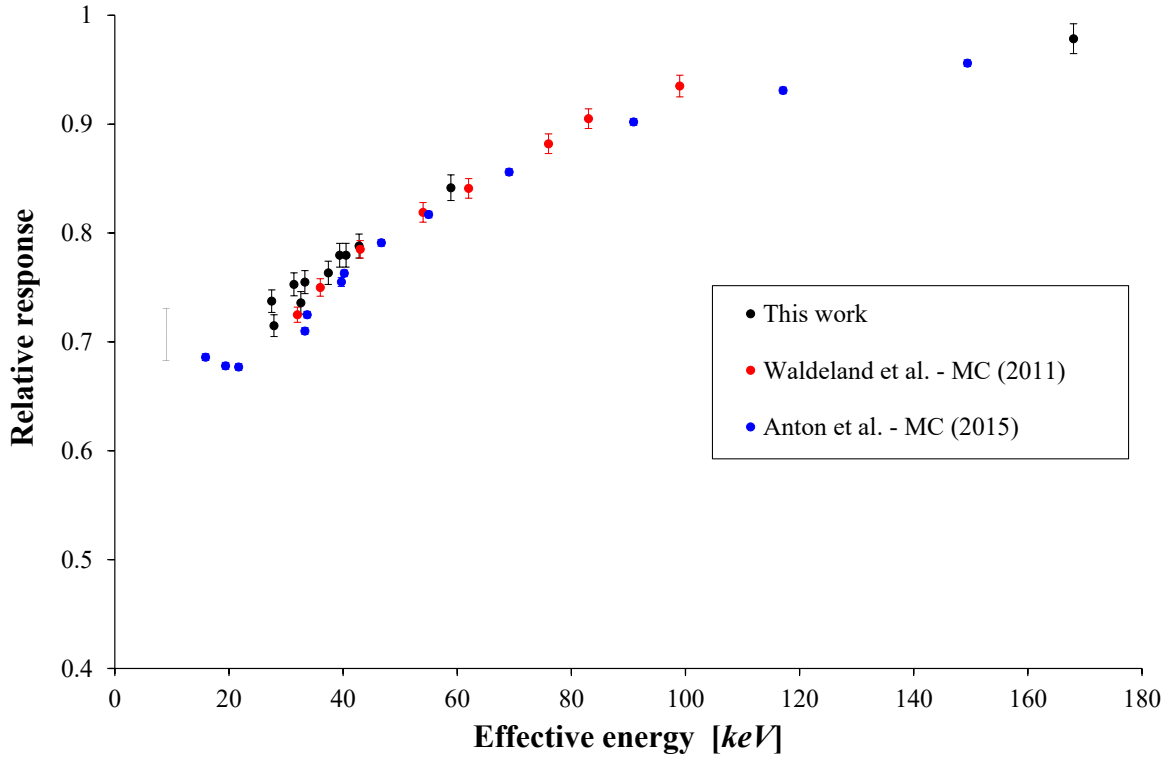

FIGURE 5.13: Values of f_{MC}^{Q,Q_0} factor obtained by MCNPX Monte Carlo simulations compared to the same calculated factor by Waldeland et al[149] and Anton and Büermann[7].

5.3.3 Analytical calculations

Alanine's relative response to kV X-rays was characterized by experimental measurements and Monte Carlo simulations in various studies[7, 50, 95, 122, 149, 150, 153], as well as during this thesis. The novelty of this thesis work resides in establishing and validating a new method that estimates Alanine's relative response to kV X-rays, by running analytical calculations based on mass-energy absorption and attenuation coefficients tabulated by NIST[54]. This method was proven to be reliable, accurate and very low-time consuming.

5.3.3.1 General formalism

This method relies on the calculation of the ratio of absorbed dose in alanine dosimeter to absorbed dose in water, for a specific X-ray spectrum, compared to the same ratio for a reference beam quality irradiation. This calculation is based on mass-energy absorption coefficients tabulated by NIST[54]. Energy spectra of all beam qualities, listed in table 5.1, were calculated by SpekCalc. Each spectrum was weighted by mass-energy absorption coefficients given by NIST. The following three equations represent the alanine to water dose ratio calculated for: an X-ray beam quality Q (f_W^Q), a ^{60}Co reference beam quality ($f_W^{Q_0}$) and the final calculated factor f_W^{Q,Q_0}, respectively.

$$f_W^Q = \frac{\int_0^{E_{max}} \left(\frac{\mu_{en}(E)}{\rho}\right)_{dos} . E . \phi(E) . dE}{\int_0^{E_{max}} \left(\frac{\mu_{en}(E)}{\rho}\right)_w . E . \phi(E) . dE} \times \frac{\left(e^{-\bar{\mu}_{att}^Q . x}\right)_{dos}}{\left(e^{-\bar{\mu}_{att}^Q . x}\right)_w} \tag{5.13}$$

$$f_W^{Q_0} = \frac{\left(\frac{\mu_{en}(^{60}Co)}{\rho}\right)_{dos}}{\left(\frac{\mu_{en}(^{60}Co)}{\rho}\right)_w} \times \frac{\left(e^{-\mu_{att}(^{60}Co) . x}\right)_{dos}}{\left(e^{-\mu_{att}(^{60}Co) . x}\right)_w} \tag{5.14}$$

$$f_W^{Q,Q_0} = \frac{f_W^Q}{f_W^{Q_0}} \tag{5.15}$$

where E_{max} is the maximum energy of the X-ray spectrum, $\mu_{en}(E)/\rho$ are the mass-energy absorption coefficients given by NIST at the photon energy E for the dosimeter or water materials, $\phi(E)$ is the photon spatial fluence value at the photon energy E, $\bar{\mu}_{att}$ is the average attenuation coefficient of the X-ray spectrum of quality Q and x is the dosimeter thickness.

In order to better simulate the photon interaction probability in the dosimeter and water volumes, the contribution of photon attenuation in 2.35 mm of dosimeter or water thickness was taken into account, by adding the second fraction present in both equations 5.13 and 5.14. This factor calculates the ratio of the attenuation percentage of incident photons in the dosimeter and water material, thus better representing the interaction probability of photons in these media.

5.3.3.2 NIST data modelling

NIST's mass-energy absorption coefficients and energy attenuation coefficients, in the energy range of 1 to 500 keV, were fitted using different mathematical models, in order to calculate the factors presented in 5.13 and 5.14. Figures 5.14 and 5.15 show NIST's data and the fitted data. For confidentiality reasons, the parameters of chosen mathematical fit models can not be divulged.

The non-equivalency of the alanine dosimeter to water, from a dosimetric point of view, can be clearly observed in figure 5.14 for photon energies between 1 and 200 keV, where a big difference between mass-energy absorption coefficients of both materials is noticed. Table 5.5 shows the uncertainty budget that was established for the calculation of the f_W^{Q,Q_0} factor. The combined uncertainty on the calculation of the f_W^{Q,Q_0} factor is equal to 2.17 %. For the calculation of $f_W^{Q_0}$ factor, relative to a ^{60}Co reference beam irradiation, mass-energy absorption coefficients and energy absorption coefficients were calculated for the mean gamma energy of 1.25 MeV, directly from NSIT data.

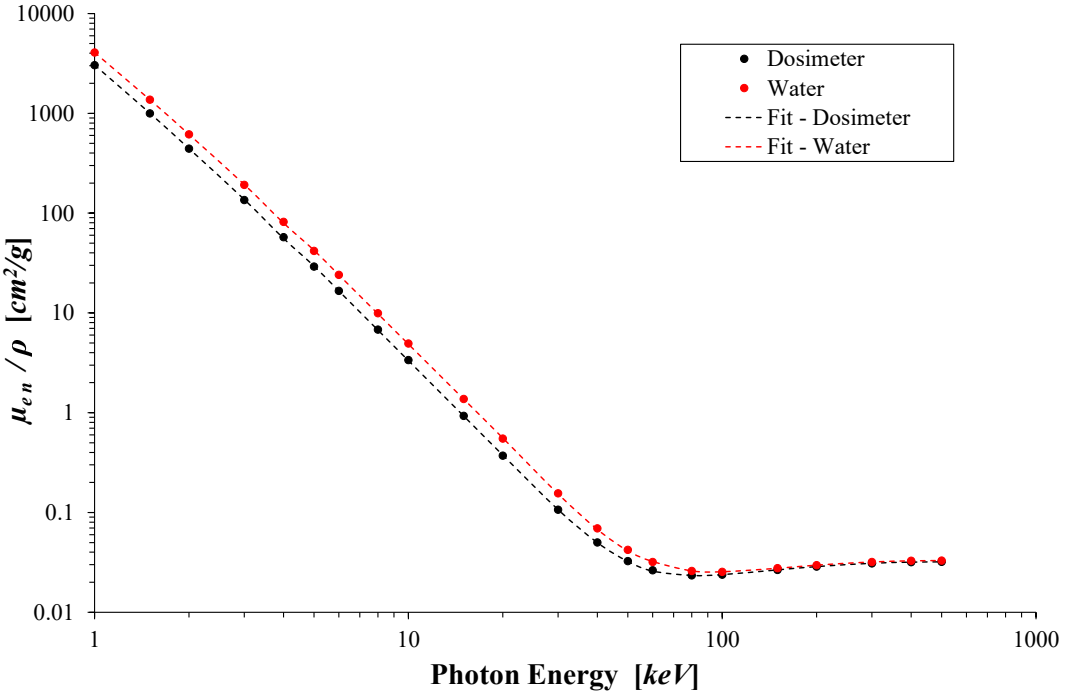

FIGURE 5.14: Modelling NIST's mass-energy absorption coefficients of both dosimeter and water material.

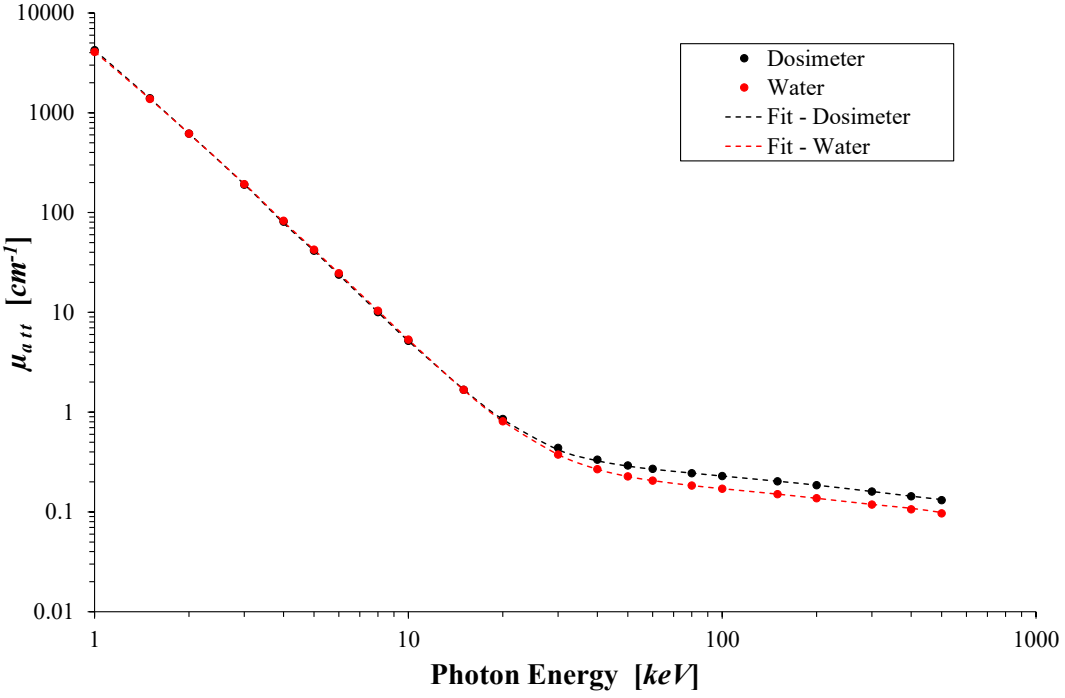

FIGURE 5.15: Modelling NIST's energy attenuation coefficients of both dosimeter and water material.

Symbol	Description	Uncertainty [%] - (k = 1) Type A	Type B
$\sigma_{\mu_{en}/\rho}$	Fit uncertainty - NIST μ_{en}/ρ data	1.48	
$\sigma_{\mu_{att}}$	Fit uncertainty - NIST μ_{att} data	1.59	
	Total f_W^{Q,Q_0} uncertainty	2.17	

TABLE 5.5: Uncertainty budget for the calculation of the f_W^{Q,Q_0} factor (k = 1).

5.3.3.3 Results and discussion

Absorbed dose ratio in the alanine dosimeter to water, for an X-ray beam quality Q irradiation compared to a ^{60}Co reference beam irradiation, was calculated using a C++ code that was developed in this thesis. The code takes as input X-ray spectra generated by SpekCalc and weighs each spectrum by calculated mass-energy absorption coefficients, based on NIST's tabulated data. The average energy attenuation coefficient of each X-ray spectrum is also calculated by the code in order to take into account the interaction probability of photons in the dosimeter and water materials. Figure 5.16 shows obtained results of the f_W^{Q,Q_0} factor compared to results obtained by experimental measurements and Monte Carlo simulations.

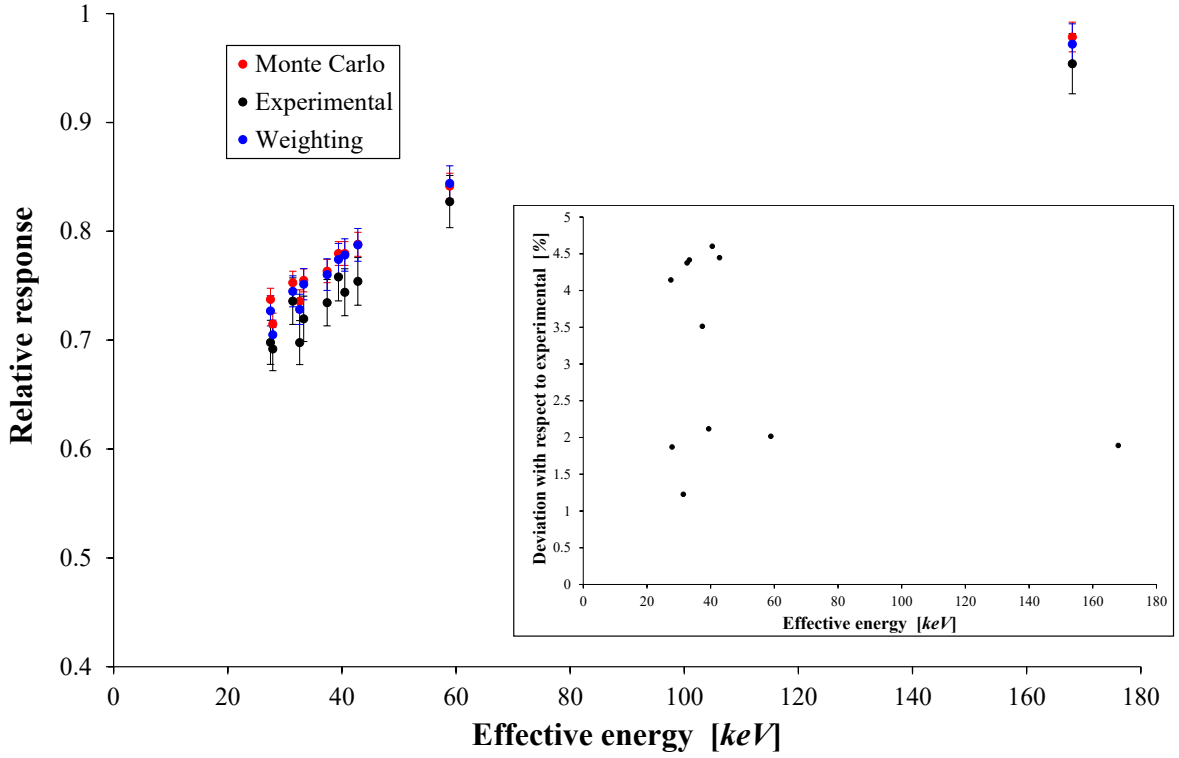

FIGURE 5.16: Comparison of the f_W^{Q,Q_0} calculated factors to factors determined by experimental measurements and Monte Carlo simulations.

Obtained results showed that the f_W^{Q,Q_0} factor follows the same tendency as the f_{exp}^{Q,Q_0} factor over the studied energy range of 27.5 to 168 keV. Yet, a difference between results obtained by analytical calculations and experimental measurements is clearly noticed, where calculation results are always higher then experimental results. This is due to the fact that analytical calculations do not model the free radical creation process in alanine dosimeters, thus, the effect of the energy dependence of the free radical creation yield (G-value) is not taken into account, just like the case of Monte Carlo simulations. The average deviation between results obtained by analytical calculations and ones measured experimentally is equal to 3.15 %. On the other hand, a great agreement is found between results obtained by Monte Carlo simulations and analytical calculations, where the average deviation between results was equal to 0.7 %. This small deviation justifies the use of analytical calculations as a replacement to Monte Carlo simulations, especially when the C++ execution time does not exceed 5 seconds, while Monte Carlo simulations can take up to few hours to calculated statistically trustworthy results.

5.4 Energy dependence of the alanine free radicals creation yield

5.4.1 Literature review

The free radical creation yield (G-value) is defined as the number of free radicals created inside the alanine dosimeter per unit of absorbed dose. The energy dependence of the alanine free radical creation yield (G-value) was studied by Olko[124, 125], Olko and Waligorski[126], Waldeland et al[150], Anton and Büermann[7] and Hjørringgaard et al[50], where different kV X-ray irradiations were carried out in order to determine the alanine's relative response to these beam qualities, compared to ^{60}Co reference beam quality. In parallel, Monte Carlo simulations were conducted to calculate the ratio absorbed dose in the dosimeter to water, for kV X-rays with respect to ^{60}Co gamma rays. Results of both campaigns permitted to evaluate the energy dependence of alanine G-value.

Olko constructed a model named "*The microdosimetric one hit detector model*", and it permitted to calculate the dose response, energy response and the relative efficiency of different dosimeters, alanine being one of the studied dosimeters. The model describes the locally deposited dose by means of energy deposition distributions in the volume of interest. The one hit term represents the interaction of one single incident particle with the target volume. Interactions of this incident particle, such as ionisations and excitations, with the target were modelled using Monte Carlo simulations in order to obtain the energy deposition distribution inside of the volume. Obtained statistical distributions were then used to calculate the alanine's relative efficiency (the energy dependence of the free radical creation yield) using the one hit detector model. This model uses two free parameters: the target diameter and the dose saturation parameter. Olko calculated relative efficiency values for kV X-ray irradiations compared to ^{137}Cs gamma irradiations. Figure 5.17 shows obtained results by Olko[126]. Results showed that the alanine's relative efficiency to kV X-rays, compared to ^{137}Cs gamma rays, does not heavily depend on the photon energy, where values of the relative efficiency ranged from 0.92 to

1 for effective photon energies of 11.7 and 662 keV respectively. Results published by Olko were a function of the X-ray spectra's mean energies. A conversion of mean energy into aluminum effective energy was applied in order to have a better comparison with other data.

Waldeland et al defined the alanine radicals G-value as the "*relative effectiveness*" and expressed it as such:

$$G_{Q,Q_0} = \frac{(r/D_{dos})_Q}{(r/D_{dos})_{Q_0}} \tag{5.16}$$

with r being the alanine dosimeter's EPR response, D_{dos} is the absorbed dose by the dosimeter and Q and Q_0 are the kV-ray and ^{60}Co reference beam qualities respectively. Values of the alanine's relative effectiveness were obtained based on the experimental determination of the F_{Q,Q_0} factor (equation 5.2) and calculation of the H_{Q,Q_0} factor (equation 5.2) by Monte Carlo simulations. Results showed that the relative effectiveness of the alanine dosimeter slightly varies between 0.92 and 0.94 for effective energies ranging from 32 to 99 keV, compared to ^{60}Co gamma rays. The formalism used by Waldeland is somehow identical to the one used by Zeng et al[153], yet, Zeng studied alanine's relative response to kV X-rays in term of air kerma measurements and not absorbed dose to water.

Anton and Bürmann also presented results of the energy dependence of the free radical creation yield. It was referred to as the "*relative intrinsic efficiency* η", as presented by Olko [124, 125] and Olko and Waligorski[126]. Anton convolved Olko's results using X-ray spectra of only the medium energy X-ray qualities (70 to 280 kV) in order to interpolate values of the relative intrinsic efficiency η. Obtained values ranged from 0.956 up to 0.971 for X-ray potentials of 70 and 280 kV respectively. However, no uncertainty was calculated for obtained results. A good agreement was noticed between experimental results of alanine's relative response and Monte Carlo results of absorbed dose ratio of alanine to water, when Monte Carlo results (r^{MC}) were multiplied by values of η.

Hjørringgaard et al[50] were also interested in determining the alanine dosimeter's relative effectiveness to a 40 kV X-ray beam quality. Hjørringgaard used the same formalism proposed by Waldeland et al[150]. Due to low X-ray energy, a correction of the dose gradient in the alanine dosimeter was taken into account in order to obtain more valid data. It was found that the relative effectiveness of studied alanine dosimeter is equal to 0.911, in the case of 40 kV (9 keV effective energy) X-ray irradiation, compared to ^{60}Co reference beam quality.

Figure 5.17 shows that all obtained results of the alanine dosimeter's relative radiation effectiveness are in good agreement over the studied photon energy range. Results ranged from 0.911 at 9 keV[50] up to unity at 662 keV gamma rays[124–126]. However, a small difference can be noticed in obtained results. This can be explained by many parameters such as the difference in the chemical composition of studied alanine dosimeters as well as the differences in adopted approaches. Yet, results still show good agreement, taking into account all uncertainties.

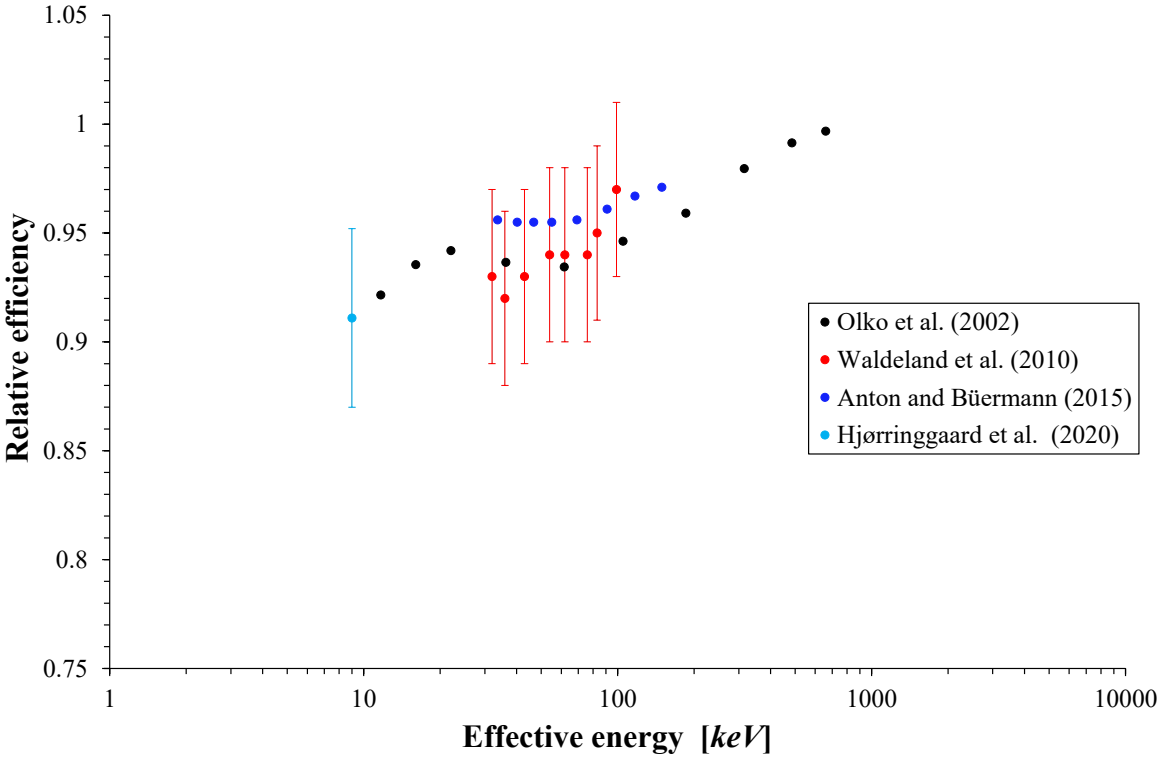

FIGURE 5.17: Literature results of the energy dependence of the alanine free radical creation yield.

5.4.2 Adopted formalism

In this thesis, two approaches were tested to study the energy dependence of the G-value of Aerial's alanine dosimeters for kV X-ray irradiations. The main idea was to separate the alanine's relative response into two terms, the first that depends only on the EPR response of the dosimeter, per unit of absorbed dose to the dosimeter, and the second term depends only on energy deposition differences between alanine and water material, in other words, the absorbed physical dose to alanine or water material. This approach can be mathematically represented by this relation:

$$\frac{(r/D_w)^Q}{(r/D_w)^{Q_0}} = \frac{(r/D_{dos})^Q}{(r/D_{dos})^{Q_0}} \times \frac{(D_{dos}/D_w)^Q}{(D_{dos}/D_w)^{Q_0}} \tag{5.17}$$

The left hand side of this equation represents the relative response of alanine to kV X-rays of quality Q compared to a Q_0 reference beam quality, and is equal to the f_{exp}^{Q,Q_0} factor that is experimentally determined in this work. The right hand side of this equation can be divided into two terms: the first term represents the relative effectiveness of the alanine dosimeter, and the second term is the ratio of absorbed dose in the dosimeter to water, for an X-ray beam quality Q compared to a Q_0 reference beam quality. This relation is identical to the one adopted by Zeng et al[153], Waldeland et al[150] and Hjørringgaard et al[50], and is equivalent to the formalism proposed by Anton and Büermann[7] and Olko et al[124–126].

Based on equations 5.6, 5.12 and 5.15, we can express equation 5.17 in two ways, as such:

$$f_{exp}^{Q,Q_0} = \eta^{Q,Q_0} \cdot f_{MC}^{Q,Q_0} \tag{5.18}$$

and

$$f_{exp}^{Q,Q_0} = \eta^{Q,Q_0} \cdot f_{W}^{Q,Q_0} \tag{5.19}$$

with η^{Q,Q_0} being the relative effectiveness of alanine radicals creation for an X-ray beam quality Q compared to a Q_0 reference beam quality. In this study, the reference beam quality is ^{60}Co gamma rays. Based on these two equations, values of η^{Q,Q_0} can be determined by two distinct approaches where the first one relies on Monte Carlo simulations to determine the dose in alanine to water ratio, and the other method relies on the weighting of X-ray spectra by mass-energy absorption coefficients given by NIST as discussed in section 5.3.3.

5.4.3 X-ray irradiations

In order to study the energy dependence of the relative effectiveness to kV X-rays of Aerial's alanine dosimeters, three different X-ray beam qualities where chosen. Table 5.6 lists the characteristics of used beam qualities. Values of HVLs and effective and average energies given in table 5.6 are calculated by SpekCalc[131]. Irradiations were carried out at Aerial using the kV X-ray installation presented in figure 5.5.

HV [kV]	Al filtration [mm]	HVL_1 [mm]	HVL_2 [mm]	E_{eff} [keV]	E_{avg} [keV]
50	0.47	0.65	1.11	19.1	26.9
90	2.88	3.33	5	35	47.3
100	9.9	6.83	8.25	49.4	58.2

TABLE 5.6: List of the three X-ray beam qualities used in the study of the energy dependence of the relative effectiveness of Aerial's alanine dosimeters.

For each X-ray beam quality, 16 alanine dosimeters (lot 09/11) were placed in a polyethylene holder and irradiated at the same time. The distance between two adjacent pellets is 5 mm, from center to center. The holder was placed in a homogeneous dose zone (dose homogeneity of $\pm$ 2 %). For each X-ray beam quality, delivered absorbed dose to water was estimated using the PTW 30013 Farmer ion chamber. An absorbed dose to water of 100 Gy was delivered to all dosimeters for all three X-ray beam qualities. This was done in order to exclude any effect that could arise from differences in delivered doses.

5.4.4 EPR spectrometry

EPR measurements were carried out using the Magnettech MS5000 X EPR spectrometer[101], which is an upgraded version of the standard MS5000 spectrometer. The upgrade if focused mainly on increasing the signal to noise ratio in the new spectrometer, in order to adapt it for low dose measurements (sub 10 Gy doses). The table below lists the EPR measurements recipe parameters.

Parameter	Unit	Value
Magnetic field range	mT	320 to 355
Sweep time	s	30
Magnetic field modulation	mT	0.01
Modulation frequency	kHz	100
Microwave power	mW	10
Number of scans		10

TABLE 5.7: Recipe parameters for EPR measurements carried out using the MS5000X EPR spectrometer.

For each EPR measurement, the peak to peak height of each EPR peak, present in the first derivative signal, was noted in order to determine an average peak to peak height and study its evolution with photon energy. EPR signals of four alanine dosimeters irradiated by a ^{60}Co gamma source were also measured using the same EPR recipe parameters. These dosimeters were provided by NPL and were previously used for the calibration of Aerial's alanine/EPR dosimetry system. The ^{60}Co irradiated dosimeters received the same absorbed dose to water of 100 Gy, as the ones that were irradiateed at Aerial using kV X-rays. Figure 5.18 shows an EPR spectrum of an alanine dosimeter irradiated at 100 Gy with 100 kV X-rays, measured with EPR parameters that are listed in table 5.7.

All dosimeters were measured one day after irradiation. Before the start of each set of EPR measurements, an empty quartz tube, that is used as the dosimeter holder, was inserted in the EPR spectrometer's cavity in order to measure the baseline EPR signal, so that it will be deduced from the alanine's EPR signal. This is done in order to eliminate all potential contribution of the quartz tube in the alanine EPR signal.

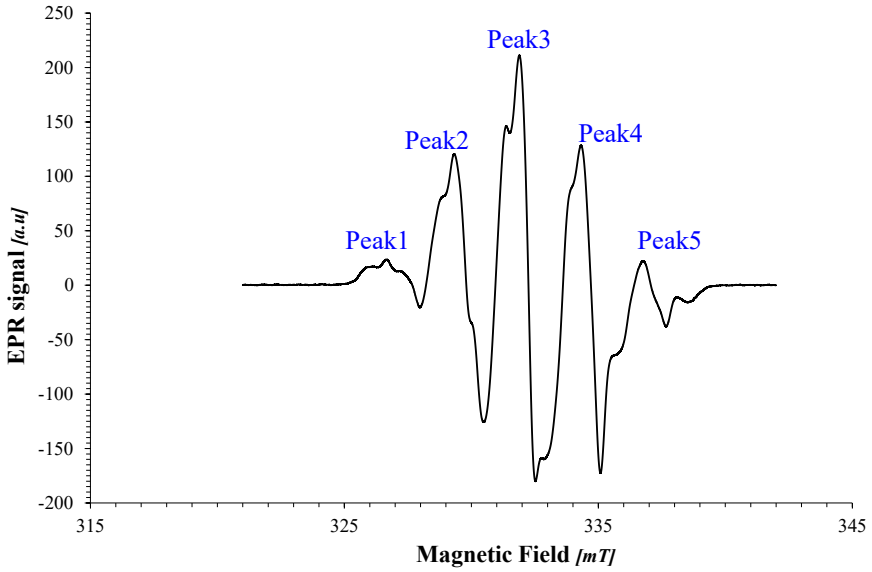

FIGURE 5.18: EPR spectrum of an alanine dosimeter irradiated at 100 Gy with 100 kV X-rays measured with the MS5000X EPR spectrometer.

5.4.5 Results and discussion

After X-ray irradiations, the peak to peak height of each peak presented in figure 5.18 was measured using EPR spectrometry. For each X-ray beam quality, the average peak to peak height of each peak was averaged on the 16 irradiated dosimeters. Figure 5.19 shows the evolution of peak to peak heights with photon effective energy. One can clearly notice that all peak to peak heights increase with increasing energy, although all dosimeters were irradiated at the same dose level. Thus, implying that the free radical creation yield of alanine radicals is energy dependent, in the studied effective energy range. Yet, in order to better quantify this variation, the relative effectiveness of alanine dosimeters was determined based on the formalism that was detailed in section 5.4.2.

Tables 5.8 and 5.9 detail the estimated uncertainty budget for the determination of the relative effectiveness of alanine dosimeters. For each beam quality, the average dosimeters response was determined based on the average measurements of the 16 dosimeters mass and average peak to peak height of the central peak. Thus, the alanine relative response (f_{exp}^{Q,Q_0}) can be hereby determined. Monte Carlo simulations were carried out to determine the ratio of absorbed dose (f_{MC}^{Q,Q_0}) in alanine to water, for X-ray beam qualities compared to ^{60}Co reference beam quality. This dose ratio was also calculated using the X-ray spectra weighting method with mass-energy absorption coefficients (f_{W}^{Q,Q_0}). Finally, to determine the relative effectiveness (η^{Q,Q_0}) of Aerial's alanine dosimeters, the ratios $f_{exp}^{Q,Q_0}/f_{MC}^{Q,Q_0}$ and $f_{exp}^{Q,Q_0}/f_{W}^{Q,Q_0}$ were calculated. Results are plotted in figure 5.20.

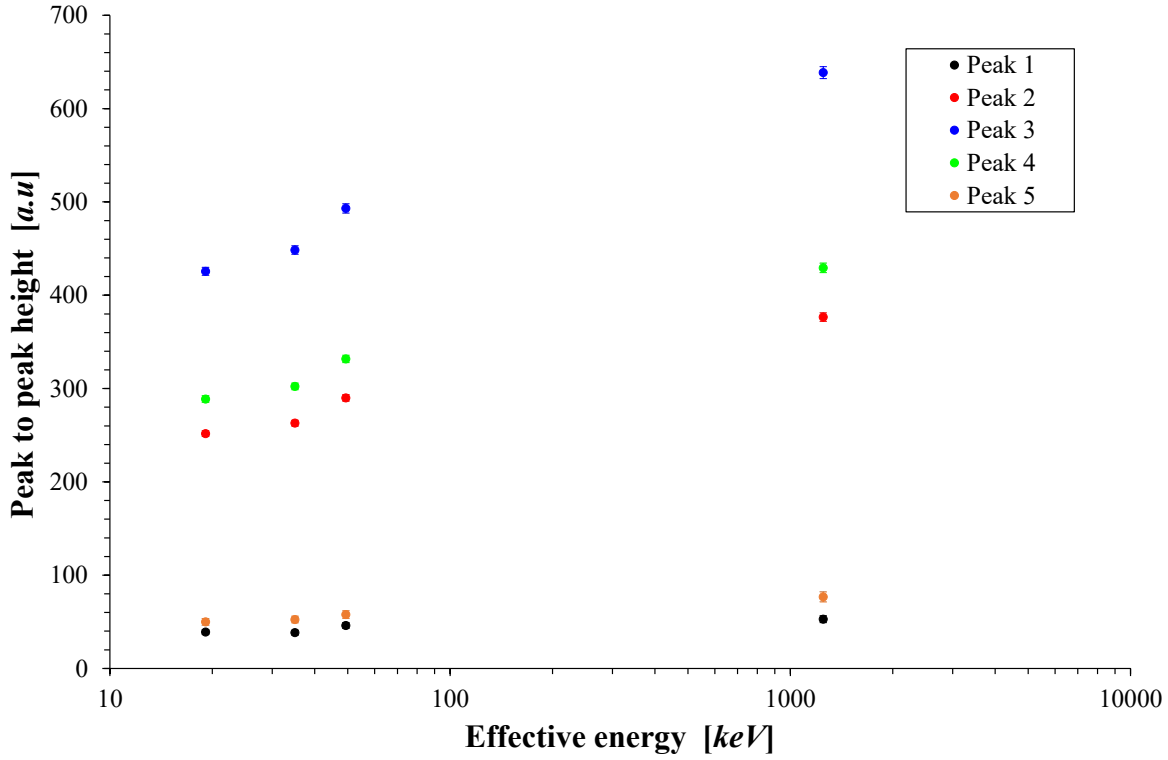

FIGURE 5.19: Peak to peak heights variation as a function of photon energy.

Symbol	Description	Uncertainty [%] - (k = 1) Type A	Type B
	Alanine - response measurement		
σ_r	Alanine response measurement by EPR spectrometery	0.5	
σ_m	Alanine dosimeters mass		0.2
σ_{EPR}	EPR spectrometer instability		0.35
σ_{PS}	Polystyrene - Non equivalency to water		1.3
σ_T	Alanine irradiation temperature correction	0.8	
σ_{stat}	Statistical uncertainty	0.95	
	Total per type	1.34	1.36
	Total - alanine response measurement	1.91	
	MC modeling		
σ_{stat}	Statistical uncertainty	1	
σ_{model}	Geometry and material modelling uncertainty		1
	Total per type	1	1
	Total - MC modelling	1.41	
	Total η^{Q,Q_0} uncertainty	2.38	

TABLE 5.8: Uncertainty budget for the determination of the alanine relative effectiveness $\eta^{Q,Q0}$ using Monte Carlo simulations.

Symbol	Description	Uncertainty [%] - (k = 1) Type A	Type B
	Alanine - response measurement		
σ_r	Alanine response measurement by EPR spectrometery	0.5	
σ_m	Alanine dosimeters mass		0.2
σ_{EPR}	EPR spectrometer instability		0.35
σ_{PS}	Polystyrene - Non equivalency to water		1.3
σ_T	Alanine irradiation temperature correction	0.8	
σ_{stat}	Statistical uncertainty	0.95	
	Total per type	1.34	1.36
	Total - alanine response measurement	1.91	
	Analytical calculations		
$\sigma_{\mu_{en}\rho}$	Fit uncertainty - NIST $\mu_{en}\rho$ data	1.48	
$\sigma_{\mu_{att}}$	Fit uncertainty - NIST μ_{att} data	1.59	
	Total per type	2.17	0
	Total - analytical calculations	2.17	
	Total η^{Q,Q_0} uncertainty - Analytical calculations	2.89	

TABLE 5.9: Uncertainty budget for the determination of the alanine relative effectiveness η^{Q,Q_0} using analytical calculations.

Results, presented in figure 5.20, show that both adopted approaches give results with a very good agreement over the studied photon energy range. This, again, confirms and proves that the developed analytical calculation method could replace Monte Carlo simulations. Results of the relative effectiveness η^{Q,Q_0} of Aerial's alanine dosimeter ranged from 0.906 up to unity for effective photon energies of 19.1 kev and 1250 keV (^{60}Co gamma rays average energy) respectively. Obtained results are compared to already published results, for different alanine dosimeter compositions, in figure 5.21. For the sake of visual simplicity, only η^{Q,Q_0} values obtained by Monte Carlo simulations are plotted in figure 5.21.

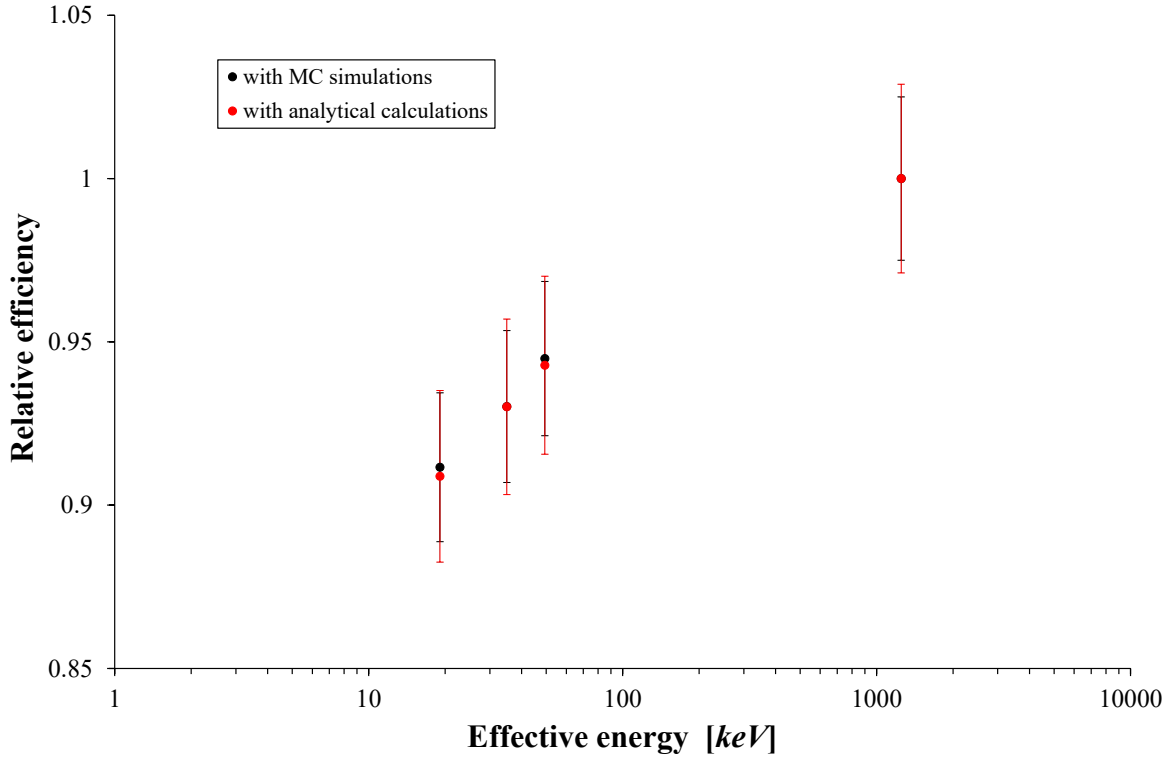

FIGURE 5.20: Comparison of η^{Q,Q_0} values obtained with Monte Carlo (MC) simulations and analytical calculations.

Values of the relative effectiveness of Aerial's alanine dosimeter are found to be in good agreement with already published data, as shows figure 5.21. However, even by taking account of all uncertainties and variabilities, one can notice that general tendencies are different between the results of cited works. This can be caused mainly by the differences in the chemical composition of studied dosimeters, where Olko et al used experimental data published by Regulla and Defner[133] which were obtained by irradiating dosimeters containing 90 % alanine and 10 % paraffin, Anton and Büermann and Hjørringgaard et al used dosimeters manufactured by Harwell (UK) containing 91 % alanine and 9 % paraffin wax and Waldeland et al used dosimeters that were purchased from Gamma Service Produktbestrahlung GmbH (Germany) that contain 96 % alanine and 4 % of unknown binder.

Other reasons leading to differences between results are the adopted formalism and method for the determination of the dosimeter's relative effectiveness, where Olko et al and Anton and Büermann obtained their results using experimental measurements in parallel with Olko's *one hit detector model* whereas experimental measurements accompanied by Monte Carlo simulations were used in this work as well as in the work of Waldeland et al and Hjørringgaard et al.

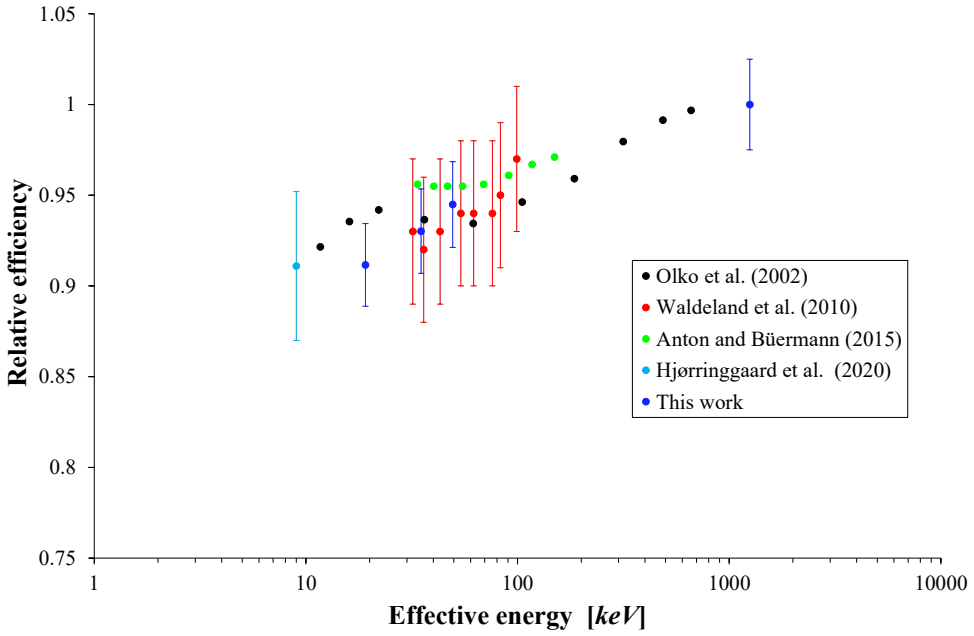

FIGURE 5.21: Comparison of η^{Q,Q_0} values obtained with Monte Carlo (MC) simulations with published data.

The main goal of this study was to evaluate the energy dependence of the relative free radical creation yield of alanine, in order to integrate it in both Monte Carlo simulations and analytical calculations that were used to determine the relative response of Aerial's alanine dosimeter. Figure 5.22 shows the fitting of η^{Q,Q_0} values for the results obtained by both Monte Carlo simulations and analytical calculations approaches, as well as fit residuals. The determined fit uncertainties were equal to 0.3 % and 0.21 % for results obtained by Monte Carlo simulations and analytical calculations respectively. Table 5.10 presents obtained results of η^{Q,Q_0} values as well as calculated values using established model fit curves presented in figure 5.22. The mathematical fit model, that was determined for values of η^{Q,Q_0} obtained with analytical calculations, was used to estimate the relative effectiveness values of alanine dosimeters for each beam quality that was used in the study of the alanine's relative response to kV X-rays, listed in table 5.1. Estimated relative effectiveness values were then applied to relative responses obtained by Monte Carlo simulations (f_{MC}^{Q,Q_0}) and analytical calculations (f_W^{Q,Q_0}). Updated results are compared to experimentally determined values of the alanine's relative response to kV X-rays (f_{exp}^{Q,Q_0}).

	Monte Carlo simulations			**Analytical calculations**		
E_{eff} **[keV]**	η_{MC}^{Q,Q_0}	**Fit value**	**Fit residus [%]**	η_W^{Q,Q_0}	**Fit value**	**Fit residus [%]**
19.1	0.9116	0.9110	-0.064	0.9088	0.9065	-0.260
35	0.9302	0.9338	0.391	0.9301	0.9321	0.215
49.4	0.9449	0.9421	-0.292	0.9429	0.9414	-0.157
1250	1.0000	1.0000	0.002	1.0000	1.0000	0.001

TABLE 5.10: Comparison of obtained and fitted η^{Q,Q_0} values.

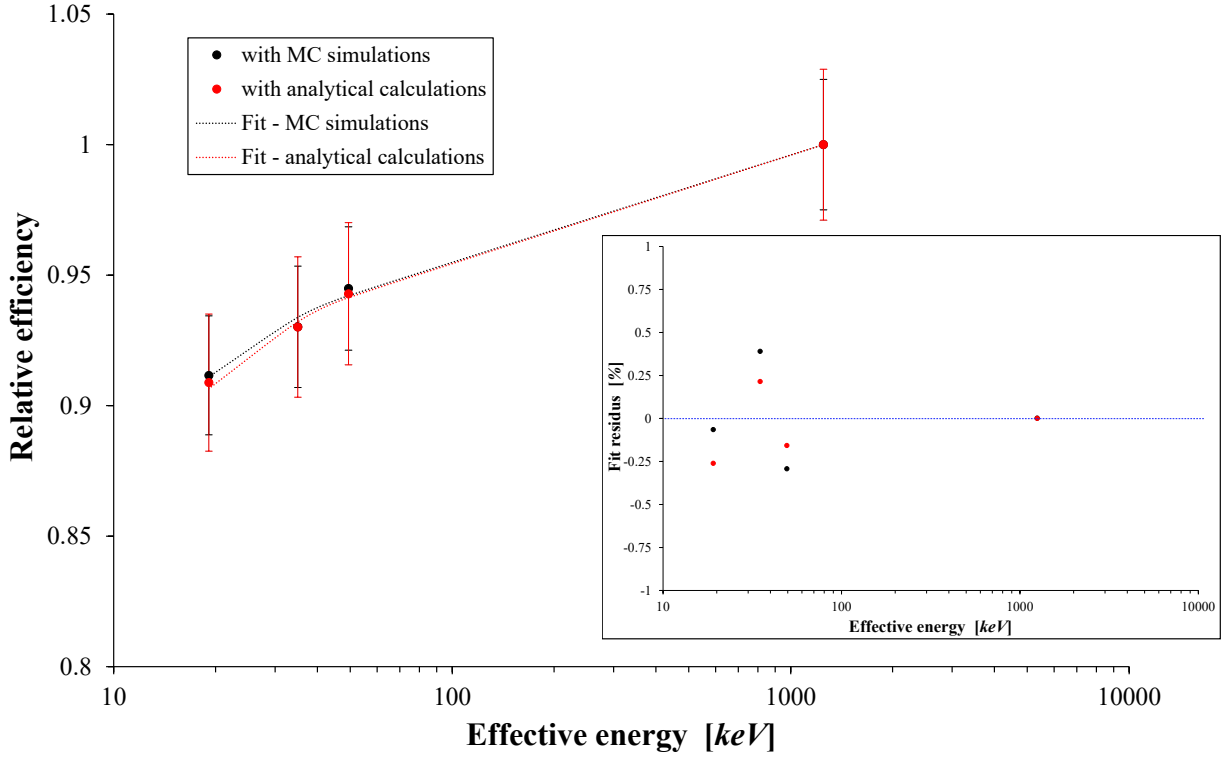

FIGURE 5.22: Mathematical fitting of obtained η^{Q,Q_0} values.

Taking into account the fit uncertainties, the total uncertainty for the determination of the relative effectiveness η_W^{Q,Q_0} rises up to 2.9 % (k = 1), which by consequence rises the combined uncertainties on f_{MC}^{Q,Q_0} and f_W^{Q,Q_0} factors up to 3.3 % and 3.63 % respectively. Figure 5.23 shows the preliminary and updated values of f_{MC}^{Q,Q_0} and f_W^{Q,Q_0} factors, as well as their comparison to the experimentally determined relative response to kV X-rays (f_{exp}^{Q,Q_0}). For the sake of visual simplicity, only uncertainty bars of updated values and experimental results are displayed in figure 5.23. Updated values of f_{MC}^{Q,Q_0} and f_W^{Q,Q_0} factors that are presented in figure 5.23 can be expressed as such:

$$F_{MC}^{Q,Q_0} = \eta_W^{Q,Q_0} \times f_{MC}^{Q,Q_0} \tag{5.20}$$

and

$$F_W^{Q,Q_0} = \eta_W^{Q,Q_0} \times f_W^{Q,Q_0} \tag{5.21}$$

Updating the relative responses of alanine, obtained by Monte Carlo simulations and analytical calculations, with estimated relative effectiveness values, lead to a better agreement with experimentally measured relative response of alanine dosimeters. The average deviation of preliminary Monte Carlo results to experimental results dropped from 3.82 % to -1.75 %, whereas the average deviation of preliminary analytical calculation results to experimental results dropped from 3.15 % to -2.39 %. The average variation coefficient of the results of all three methods (experimental, Monte Carlo and calculations) dropped from 2.1 % down to 1.3 %, after updating preliminary relative responses determined by Monte Carlo simulations and analytical calculations, with estimated values of the relative effectiveness of alanine dosimeters.

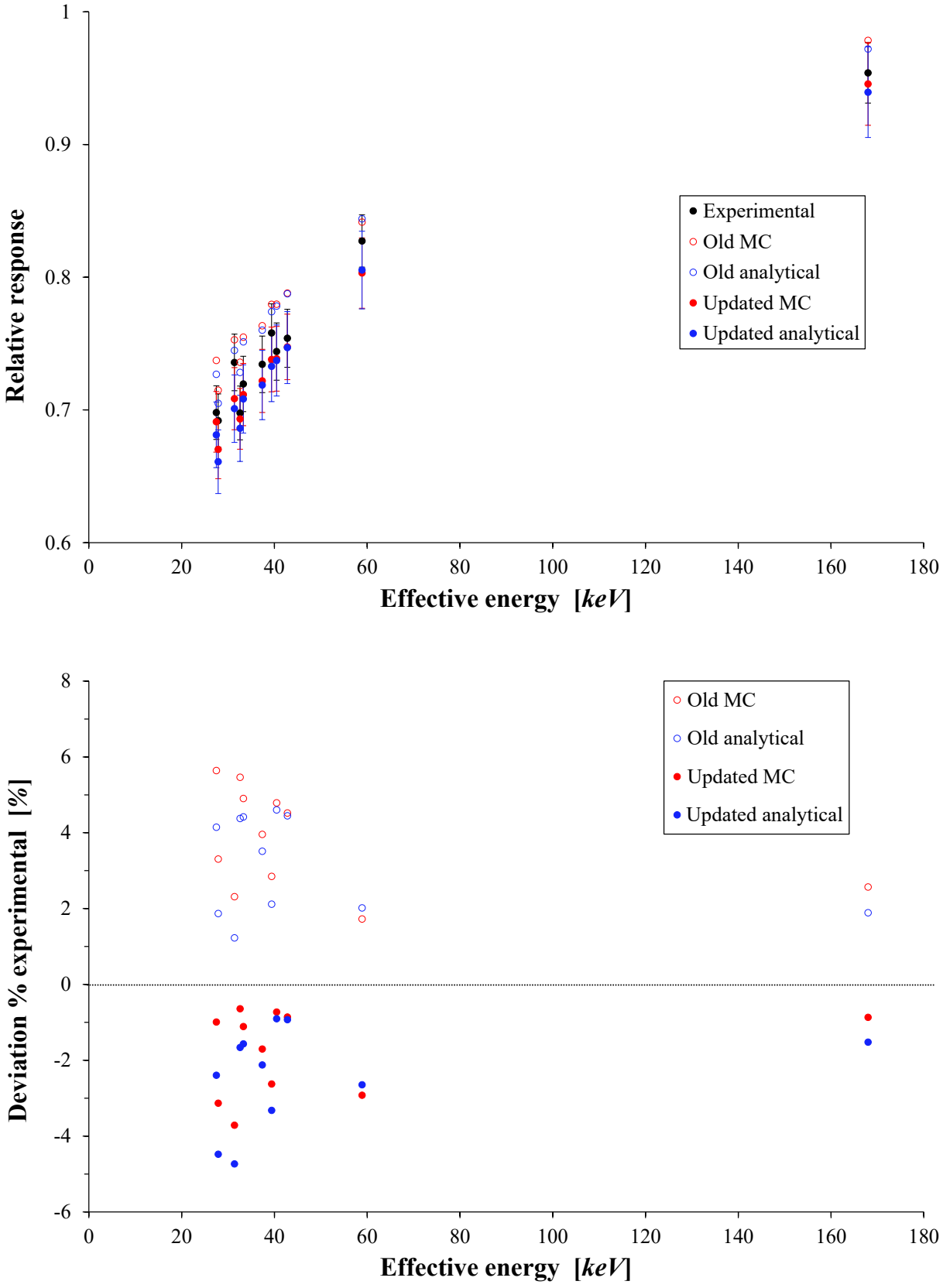

FIGURE 5.23: Comparison of preliminary and updated f_{MC}^{Q,Q_0} and f_W^{Q,Q_0} factors with experimental f_{exp}^{Q,Q_0} values.

Results presented in figure 5.23 show that the use of Monte Carlo simulations, as well as analytical calculations, taking into account the energy dependence of the free radical creation yields of alanine radicals, are well adapted to determine the relative response of alanine dosimeters to kV X-rays compared to ^{60}Co reference beam quality. Results also confirmed that the use of analytical calculations for this goal is well justified, were this method permitted to obtain results that are in good agreement with experimentally measured results. It is clear that analytical calculations are able to obtain results, with comparable uncertainties, in a much shorter calculation time (few seconds), compared to Monte Carlo simulations (few hours).

5.5 Conclusion

Many works[7, 23, 50, 95, 122, 141, 149, 150, 153] studied the relative response of alanine dosimeters to kV X-rays with different energy ranges and irradiation configurations, using experimental measurements and Monte Carlo simulations. This section presented obtained results of different methods, developed in this thesis, to determine the relative response of Aerial's alanine to different kV X-ray beam qualities, compared to its response to ^{60}Co reference beam quality.

Experimental irradiations lead to the measurement of the EPR response of Aerial's alanine dosimeters after X-ray irradiations, via EPR spectrometry, as well as the true absorbed dose to water via calibrated ion chamber measurements. This permitted to experimentally estimate the relative response of Aerial's alanine dosimeters over the effective energy range of 27 to 168 keV. Obtained values showed a good agreement with already published data of Waldeland et al[150] and Anton and Büermann[7]. Due to the difference in the chemical compositions of dosimeters used in this thesis, and the ones used in published studies, a slight difference in the relative responses was noticed.

Monte Carlo simulations, using MCNPX code, determined the ratio of absorbed dose in alanine to water for different kV X-ray spectra compared to ^{60}Co gamma rays. Obtained results were in a good agreement with experimental results (average deviation of 3.82 %) as well as published data. However, a small difference between experimental and Monte Carlo results was noticed in the effective energies below 200 keV. This is due to the fact that Monte Carlo simulations do not take into account the free radical creation process in alanine.

The novelty of this work resides in the elaboration and validation of a C++ code that analytically calculates the ratio of absorbed dose in alanine with respect to water for different kV X-ray beam qualities, based on the modelling of mass-energy absorption coefficients and energy attenuation coefficients tabulated by NIST[54]. Obtained results showed a good agreement with experimental results (average deviation of 3.15 %) as well as with Monte Carlo results (average deviation of 0.7 %). The larger deviation with experimental results is also explained by the fact that calculations did not take into account the contribution of the alanine radicals G-values, that vary with X-ray energies in the range of few to 200 keV. On the other hand, compared to Monte Carlo simulations, analytical calculations were found to be easier to put in place than simulations that require precise geometry definitions, and the code execution time is considerably smaller than the time that could take a Monte Carlo simulation, thus, analytical

calculations consist an easy, efficient and trustworthy method to determine the dose ratio of alanine to water. Table 5.11 presents all obtained results of the relative response of Aerial's alanine dosimeters for kV X-rays.

E_{eff} **[keV]**	f_{exp}^{Q,Q_0}	$u_{f_{exp}}$	f_{MC}^{Q,Q_0}	$u_{f_{MC}}$	**Deviation MC/exp** [%]	f_W^{Q,Q_0}	u_{f_W}	**Deviation W/exp** [%]
27.5	0.698	0.020	0.737	0.010	5.64	0.727	0.016	4.14
27.9	0.692	0.020	0.715	0.010	3.31	0.705	0.015	1.87
31.4	0.736	0.021	0.753	0.011	2.31	0.745	0.016	1.23
32.6	0.698	0.020	0.736	0.010	5.46	0.728	0.016	4.38
33.3	0.720	0.021	0.755	0.011	4.90	0.751	0.016	4.42
37.4	0.734	0.021	0.763	0.011	3.96	0.760	0.016	3.51
39.4	0.758	0.022	0.780	0.011	2.85	0.774	0.017	2.12
40.5	0.744	0.022	0.780	0.011	4.79	0.778	0.017	4.60
42.8	0.754	0.022	0.788	0.011	4.52	0.788	0.017	4.45
58.9	0.827	0.024	0.842	0.012	1.73	0.844	0.018	2.02
168	0.954	0.028	0.978	0.014	2.57	0.972	0.021	1.89

TABLE 5.11: The relative response of Aerial's alanine dosimeters to different kV X-ray beam qualities.

Another study was carried out in this thesis in order to evaluate the energy dependence of the alanine free radicals creation yield, also defined as the dosimeter's relative effectiveness η^{Q,Q_0}. For this goal, three X-ray beam qualities were chosen for alanine dosimeters irradiations. Experimental measurements accompanied by Monte Carlo simulations and analytical calculations showed that the relative effectiveness of Aerial's alanine dosimeters ranges from 0.906 up to 0.943 for effective energies of 19.1 and 49.4 keV respectively. Results were found to be in agreement with published data for other types of alanine dosimeters[7, 50, 124–126, 150].

Obtained values of the relative effectiveness of Aerial's alanine dosimeter were fitted using a mathematical model that permitted to estimate values of η^{Q,Q_0} for alanine dosimeters that were irradiated with X-ray beam qualities listed in table 5.1. These beam qualities were used to determine the relative response of alanine dosimeters to kV X-rays. Multiplying η^{Q,Q_0} values by f_{MC}^{Q,Q_0} or f_W^{Q,Q_0} values, led to a better comparison of relative responses measured experimentally against ones determined with Monte Carlo simulations and analytical calculations, where these two methods did not originally account for the free radical creation process in alanine. Updating relative responses determined by simulations and calculations with adequate relative effectiveness values led to a better agreement between determined results, where the variation coefficient dropped from 2.1 to 1.3 % over the effective energy range of 27.5 to 168 keV. Table 5.12 shows updated results of f_{MC}^{Q,Q_0} and f_W^{Q,Q_0} factors with determined relative effectiveness values η^{Q,Q_0}.

Updated results of analytical calculations were, again, in very good agreement with updated results of Monte Carlo simulations. All this validates the newly developed method, based on analytical calculations, and justifies its use instead of Monte Carlo simulations to determine the relative response of alanine dosimeters to kV X-rays, all while having reasonable uncertainty of 3.63 % (k = 1).

E_{eff} **[keV]**	f_{exp}^{Q,Q_0}	$u_{f_{exp}}$	f_{MC}^{Q,Q_0}	$u_{f_{MC}}$	**Deviation MC/exp** [%]	f_W^{Q,Q_0}	u_{f_W}	**Deviation W/exp** [%]
27.5	0.698	0.020	0.691	0.023	-0.99	0.681	0.025	-2.39
27.9	0.692	0.020	0.670	0.022	-3.13	0.661	0.024	-4.48
31.4	0.736	0.021	0.708	0.023	-3.71	0.701	0.025	-4.73
32.6	0.698	0.020	0.693	0.023	-0.64	0.686	0.025	-1.66
33.3	0.720	0.021	0.712	0.023	-1.11	0.708	0.026	-1.57
37.4	0.734	0.021	0.722	0.024	-1.70	0.719	0.026	-2.12
39.4	0.758	0.022	0.738	0.024	-2.63	0.733	0.027	-3.32
40.5	0.744	0.022	0.739	0.024	-0.73	0.737	0.027	-0.90
42.8	0.754	0.022	0.748	0.025	-0.86	0.747	0.027	-0.93
58.9	0.827	0.024	0.803	0.027	-2.92	0.805	0.029	-2.65
168	0.954	0.028	0.946	0.031	-0.87	0.939	0.034	-1.52

TABLE 5.12: The updated relative response of Aerial's alanine dosimeters to different kV X-ray beam qualities.

Part IV

Hydroxyl radical G-value determination

Chapter 6

Experimental and Monte Carlo determination of the hydroxyl radical G-value

Contents

6.1 Introduction

The main goal of the second part of this thesis was to take in hand the Geant4-DNA[16, 69–71] Monte Carlo simulation code, and adapt it for calculations of free radical creation yields (G-value) of alanine molecules for electron irradiations. For the moment, the kinetics of free radical generation is only allowed to be simulated in water material, using the Geant4-DNA code.

The first approach in this study was to get familiarized with the Geant4-DNA simulation code, by running simulations that are able to study the time evolution of the hydroxyl radical ($HO^{\bullet}$) G-value for 1 MeV electron irradiations, and then validate the constructed model by experimental measurements.

Once familiarized with the Geant4-DNA simulation code, the second task was to determine the cross-sections of different radio chemical interactions (ionization and excitation), between ionizing radiation and alanine molecule. The use of a mathematical calculation code, developed during the thesis of Dr. Lena MOUAWAD[118], would lead to the determination of ionization cross-section of alanine due to interactions with incident electrons. Once determined, these cross-sections were to be added to the existing cross-section models of Geant4-DNA, thus, enabling the study of free radicals generation in alanine medium.

Unfortunately, due to the short amount of time left before the defense, only the first part of this study was accomplished. Thus, this chapter will present the main aspects of water radiolysis, the logic of the Geant4-DNA simulation code and results of Monte Carlo simulations that were carried out to study the time evolution of the $HO^{\bullet}$ G-values as well its comparison to experimentally obtained results of water irradiation with 1 MeV electron beam.

6.2 Water radiolysis

Water radiolysis is the dissociation of water molecules due to the impact of ionizing radiation. This dissociation leads to the creation of new chemical species. This phenomenon is divided into different stages, depending on the occurrence time-scale of relative events, as described here below.

6.2.1 The physical stage

The first stage of water radiolysis consists of energy deposition of primary and secondary generated particles in water. The energy deposition leads to two possible reactions with water molecules: excitation and ionization. Excitation of H_2O molecules leads to the creation of H_2O^* species, while ionization leads to the generation of a water positive radical ion $H_2O^{\bullet+}$ and an electron, as describe the equations 6.1 and 6.2 respectively[142]. If enough energy is transferred to the electron, this will lead to the ejection of this electron in the medium and its interaction with other present chemical species. Figure 6.1 shows a drawing of different potential electron tracks in water.

$$H_2O \xrightarrow{h\nu} H_2O^* \tag{6.1}$$

and

$$H_2O \xrightarrow{h\nu} H_2O^{\bullet+} + e^- \tag{6.2}$$

These physical interactions happen in a time-frame of about 10^{-16} s[21]. Depending on the energy deposition (E) of the primary ionizing particle, different scenarios can occur:

1. E < 100 eV : The secondary electron, not having an important amount of energy, deposits locally all of its energy. This leads to the creation of 2 to 3 nm diameter zones called "*spurs*". A spur regroups 2 to 3 excited and ionized water molecules with their associated electrons[21].

2. E ≈ 100 to 500 eV : This leads to the creation of "*blobs*" which contain many spurs that are spatially close one to another.

3. E ≈ 0.5 to 5 keV : This leads to the creation of "*short tracks*" which consist of many overlapping spurs.

4. E > 5 keV : This leads to the creation of "*branch tracks*". A branch track is a track generated by secondary electrons of sufficiently high energy, so high that they might generate non-overlapping spurs just like the primary[119].

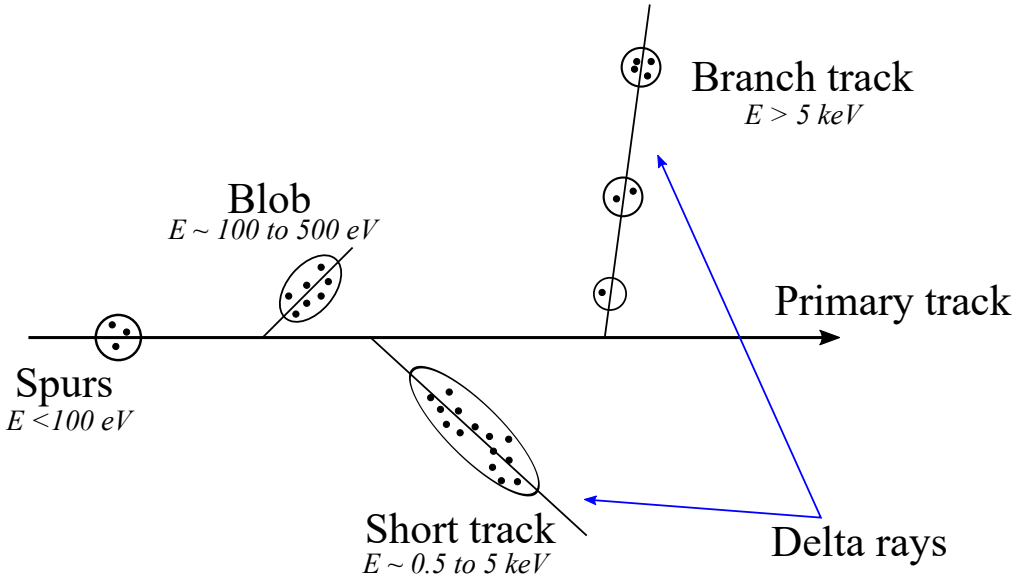

FIGURE 6.1: Drawing of electron tracks in dense medium. Adapted from the works of Mozumder and Magee[119] and Burton[19].

6.2.2 The physico-chemical stage

The physico-chemical stage consists of events that lead to the establishment of the system's thermal equilibrium[38]. These events have a duration of about 10^{-12} s[21]. Ejected electrons by the ionization of water molecules continue to interact with surrounding matter until they lose a significant amount of energy, after which, these electrons are considered as "*thermalized electrons*" (e^-_{th}). After this stage, a thermalized electron can be solvated (e^-_{aq}) by surrounding water molecules, as shows equation 6.3. The following equations represent the dominant processes that happen during the physico-chemical stage[21].

$$e^- \longrightarrow e^-_{th} \longrightarrow e^-_{aq} \tag{6.3}$$

$$H_2O^{\bullet +} + H_2O \longrightarrow OH^{\bullet} + H_3O^+ \tag{6.4}$$

$$H_2O^* \longrightarrow HO^{\bullet} + H^{\bullet} \tag{6.5}$$

The water positive radical ion ($H_2O^{\bullet +}$) undergoes a proton transfer with surrounding water molecules. This generates a hydroxyl radical and a hydronium ion (H_3O^+), as shows equation 6.4. The excited water molecules (H_2O^*) can undergo two different paths: de-excitation or dissociation. The de-excitation of this molecule leads to its return to a stable state accompanied by a liberation of thermal energy in the medium, while dissociation path leads to the formation of a hydroxyl radical and a hydrogen radical, as shows equation 6.5.

6.2.3 The non-homogeneous chemical stage

This stage represents the diffusion of radio-induced species during both physical and physico-chemical stages, located in agglomerations of spurs and blobs that are generated near the trajectory of the primary ionizing particle. The diffusion of these species leads eventually to the chemical equilibrium of the medium in a time frame of about 10^{-12} to 10^{-6} s after irradiation. In this time-lapse, and due to proximity, a part of the radio-induced species diffuse randomly leading to the creation of molecules and other radical species. On the other hand, the remaining part of radio-induced species manage to escape into other zones of the liquid due to diffusion. Table 6.1 lists some of the chemical reactions that occur during the chemical stage and their associated reaction rate constants (k).

By looking into chemical equations listed in table 6.1, one can deduce that the reactions of some chemical species, such as $HO^{\bullet}$, e^-_{aq} and $H^{\bullet}$, will induce the creation of other chemical species, such as H_2O_2 and H_2. This can be also expressed in terms of radiolytic yields (G-values) that are defined as the number of species that are created by an energy deposit of 100 eV. Thus, we can say that the G-values of $HO^{\bullet}$, e^-_{aq} and $H^{\bullet}$ species decrease in time leading, partially, to the increase of G-values of H_2O_2 and H_2 molecules. The water radiolysis, for radiation having LET of 0.23 keV/µm, can be presented by the following reaction[21]

$$H_2O \xrightarrow{h\nu} 0.28\ e^-_{aq},\ 0.062\ H^{\bullet},\ 0.28\ HO^{\bullet},\ 0.047\ H_2,\ 0.073\ H_2O_2,\ 0.28\ H_3O^+ \tag{6.6}$$

Numbers indicated in this equation represent radiolytic yields of each cited specie, expressed in µmol/J (1 specie/100 eV = 0.1036 µmol/J), at 10^{-7} s[21].

Reaction	k [10^{10} L/mol/s]
$e^-_{aq} + e^-_{aq} + 2H_2O \longrightarrow H_2 + 2OH^-$	0.54
$e^-_{aq} + HO^\bullet \longrightarrow OH^-$	3
$e^-_{aq} + H_3O^+ \longrightarrow H^\bullet + H_2O$	2.3
$e^-_{aq} + H^\bullet + H_2O \longrightarrow H_2 + OH^-$	2.5
$H^\bullet + H^\bullet \longrightarrow H_2$	1.3
$HO^\bullet + HO^\bullet \longrightarrow H_2O_2$	0.53
$HO^\bullet + H^\bullet \longrightarrow H_2O$	3.2
$H_3O^+ + OH^- \longrightarrow 2H_2O$	14.3

TABLE 6.1: List of chemical reactions that occur during the non-homogeneous chemical stage of water radiolysis[21].

6.3 The Geant4-DNA Monte Carlo simulation code

Geant4-DNA Monte Carlo simulation code[16, 69–71] is an extension of the basic Geant4 code[4–6]. It is also an open source code that is mainly dedicated for simulations of radio-induced biological damages at the cellular and sub-cellular levels. This code can be also used for micro-dosimetry calculations, simulations of DNA geometries as well as their radio-induced damages, and for the simulation of chemical processes such as water radiolysis.

The Geant4-DNA project was initiated in 2001 by Dr. P. Nieminen (European Space Agency). The main goal was to develop a computing platform enables the estimation of the biological effects of ionizing radiation using the Geant4 toolkit, in the perspective of future space exploration missions. Thus, a set of physical processes (down to eV energy scale), that are adapted to microdosimetry in water material, was added to the Geant4 code in late 2007. Currently, the project is entirely developed and managed by the Geant4-DNA collaboration.

6.3.1 Geant4-DNA Physics

In order to simulate processes that occur at very small space and energy scales, the Geant4 basic toolkit had to be updated with physics models that are validated for very low interaction energies in the order of the eV. Each event is modelled in a step-by-step tracking mode. Figure 6.2 visualizes the interaction of 240 MeV Carbon ions in water, based on two different physics models: Geant4 Standard Electromagnetic physics and Geant4-DNA physics. The lowest accurate energy cut off proposed by Geant4 electromagnetic physics goes down to 100 eV using the PENELOPE low energy model, while the standard Geant4-DNA physics lists are validated for energies that are in the order of few eV. This is reflected in figure 6.2, where we can clearly notice a much bigger number of interactions (yellow dots) when using the Geant4-DNA physics list, compared to the number of interactions of the same primary particle with matter when

using standard electromagnetic physics models. Red lines represent the track of primary and secondary particles. Table 6.2 lists the different types of electron interactions along with corresponding process and model classes and the minimum and maximum energies that each model offers.

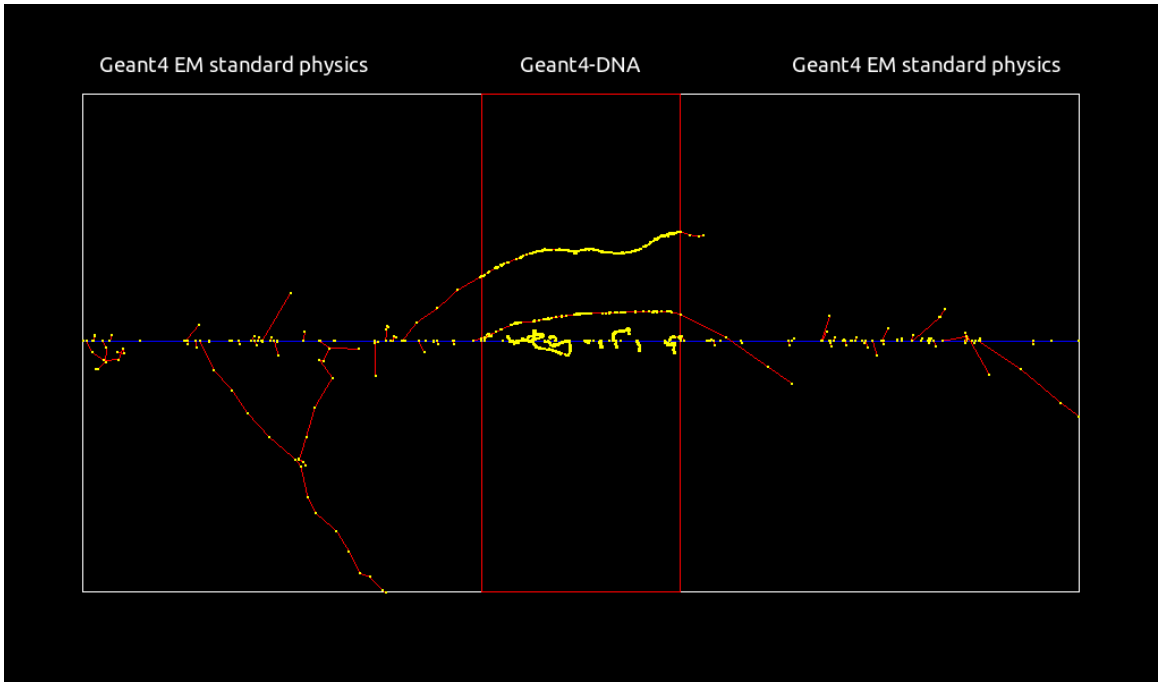

FIGURE 6.2: Mixed physics lists simulation showing the differences of interactions of 240 MeV Carbon ions in water[68].

Interaction	**Process class**	**Model class**	E_{min}	E_{max}
Elastic scattering	G4DNAElastic	G4DNAChampionElasticModel	7.4 eV	1 MeV
		G4DNAScreenedRutherfordElasticModel	0 eV	1 MeV
		G4DNAUeharaScreenedRutherfordElasticModel	9 eV	10 keV
		G4DNACPA100ElasticModel	11 eV	256 keV
Electronic excitation	G4DNAExcitation	G4DNABornExcitationModel	9 eV	1 MeV
		G4DNAEmfietzoglouExcitationModel	8 eV	10 keV
		G4DNACPA100ExcitationModel	11 eV	255 keV
Ionisation	G4DNAIonisation	G4DNABornIonisationModel	11 eV	1 MeV
		G4DNAEmfietzoglouIonisationModel	10 eV	10 keV
		G4DNACPA100IonisationModel	11 eV	255 keV
Vibrational excitation	G4DNAVibExcitation	G4DNASancheExcitationModel	2 eV	100 eV
Attachment	G4DNAAttachment	G4DNAMeltonAttachmentModel	4 eV	13 eV

TABLE 6.2: List of different physics models that offer the Geant4-DNA code for electron interactions[27].

6.3.2 Geant4-DNA Chemistry

The radiation chemistry in Geant4-DNA models the three stages that are described in section 6.2. The physical stage simulates all interactions of primary generated particles as well as the secondary generated particles and scores the energy depositions in the medium. For example, in case of electrons, all ionization and excitation processes are simulated.

During the physico-chemical stage, ionisation, excitation and dissociation events are simulated in the time-frame of 10^{-15} s to 10^{-12} s[93]. This leads to the formation of free radicals as well as different ions in the water medium. All dissociation channels are defined in the *G4EmDNAChemistry* files. During this stage, electrons are thermalized to an energy of 25 meV and are then solvated. A branching fraction is defined for each dissociation channel as shows table 6.3. Dissociation channels fractions are free parameters, thus, the user can set his own dissociation scheme.

Electronic state	**Dissociation channels**	**Fraction [%]**
All single ionization states	$H_3O^+ + HO^\bullet$	100
Excitation state $A1B1$ ($1b1 \rightarrow (4a1/3s)$	$HO^\bullet + H^\bullet$	65
	$H_2O + \Delta E$	35
Excitation state $B1A1$ ($3a1 \rightarrow (4a1/3s)$	$H_3O^+ + HO^\bullet + e^-_{aq}$ (AI)	55
	$HO^\bullet + HO^\bullet + H_2$	15
	$H_2O + \Delta E$	30
Excitation state (Rydberg, diffusion bands)	$H_3O^+ + HO^\bullet + e^-_{aq}$ (AI)	50
	$H_2O + \Delta E$	50
Dissociative attachment	$HO^\bullet + OH^- + H_2$	100

TABLE 6.3: List of different dissociation channels that are simulated during the physico-chemical stage by the Geant4-DNA code[16] (*AI : Auto-Ionization).*

Finally, the chemical stage is simulated in the time-frame of 10^{-12} s to 10^{-6} s. In this stage, chemical species that were created in previous stages can diffuse in the medium and interact with each other, according to tabulated values of diffusion coefficients of each specie. The simulation begins with the positions of radio-induced species that are scored at the end of the physico-chemical stage. These species are created according to the defined branching ratios.

The change of position of a certain specie is random and is governed by the following relation[93]

$$R = \sqrt{6.D.\Delta t} \tag{6.7}$$

with R is the geometrical step that is taken by the specie of interest, D is the diffusion coefficient and Δt is the time step value. Values of diffusion coefficients, used by the standard *G4EmDNAChemistry* constructor, are listed in table 6.4. During diffusion, if the distance between two molecules is smaller than the calculated interaction radius, based on the chemical reaction rate of a certain reaction, the reaction of interest will occur. Table 6.5 lists the reaction rates that are used by the standard *G4EmDNAChemistry* constructor. Default values of Δt can be changed by the user.

Species	**Diffusion coefficient - D [10^{-9} m^2 s^{-1}]**
e^-_{aq}	4.9
$HO^\bullet$	2.8
$H^\bullet$	7
H_3O^+	9
H_2	4.8
OH^-	5
H_2O_2	2.3

TABLE 6.4: Values of diffusion coefficients of listed species that are used in the standard *G4EmDNAChemistry* constructor.

Reactions	**Reaction rate constant - k [10^{10} M^{-1} s^{-1}]**
$H^\bullet + e^-_{aq} + H_2O \rightarrow OH^- + H_2$	2.65
$H^\bullet + HO^\bullet \rightarrow H_2O$	1.44
$H^\bullet + H^\bullet \rightarrow H_2$	1.2
$H_2O_2 + e^-_{aq} \rightarrow HO^\bullet + OH^-$	1.41
$H_3O^+ + e^-_{aq} \rightarrow H^\bullet + H_2O$	2.11
$H_3O^+ + OH^- \rightarrow 2H_2O$	14.3
$HO^\bullet + e^-_{aq} \rightarrow OH^-$	2.95
$HO^\bullet + HO^\bullet \rightarrow H_2O2$	0.44
$e^-_{aq} + e^-_{aq} + 2H_2O \rightarrow 2OH^- + H_2$	0.5

TABLE 6.5: Reaction rates of listed reactions that occur during the chemical stage, as used in the standard *G4EmDNAChemistry* constructor.

After the simulation of all events that happen during the three different stages of water radiolysis, the total deposited energy is scored as well as the time dependent number of created species of interest. This leads finally to the calculation of the time dependent radiolytic yield of the species of interest as shows the following equation:

$$G_X(t) = \frac{N_X(t) \,.\, 100}{E_d \; [eV]} \tag{6.8}$$

where $G(t)$ is the radiolytic yield of the X chemical specie calculated at the time t, $N_X(t)$ is the number of molecules of the specie X at the time t and E_d is the deposited energy expressed in eV.

6.4 OH radical creation yield determination

This section presents the results of some works concerning the determination of the radiolytic yields of hydroxyl radical ($HO^{\bullet}$) that is generated during the water radiolysis for different particle types and energies. Details and results of Monte Carlo simulations carried out, during this thesis, to study the time evolution of the G-value of $HO^{\bullet}$ radicals, for 1 MeV electrons irradiations, will be presented, as well as results of experimental measurements of the radiolytic yield of the hydroxyl radical.

6.4.1 Literature study

LaVerne[99] studied the OH radicals and oxidizing products in the gamma radiolysis of water. Solutions containing water and formic acid, that acts as a radical scavenger, were irradiated with a ^{60}Co gamma source. The $HO^{\bullet}$ radical produced by water decomposition extract hydrogen atoms from the formic acid to give a radical that quickly reacts with oxygen and then leads to the production of carbon dioxide, where its concentration was measured in order to estimate the radiolytic yields of $HO^{\bullet}$ radicals. G-values of $HO^{\bullet}$ radicals, generated by ^{60}Co gamma radiolysis of water, decreased from 4.5 radicals/100 eV at 200 ns down to 2.4 radicals/100 eV at the end of the reaction.

Watanabe and Saito[151] carried out Monte Carlo simulations, using the DBREAK code[146], to study the water radiolysis for monoenergetic electron irradiations. Simulated electron beams had energies of 100 eV, 1 keV, 10 keV and 1 MeV. During the physical stage, electrons were transported until their energy falls below 7.4 eV, which is equivalent to the threshold of electronic excitation of water. All chemical stage processes were simulated in the time interval of 10^{-12} s down to 10^{-6} s, just like the case of Geant4-DNA code. The chemical species considered in the diffusion process are $H^{\bullet}$, $HO^{\bullet}$, H^{+}_{aq}, e^{-}_{aq}, OH^{-}, H_2O_2, O, O_2, O^{-}_{2}, HO_2 and HO^{-}_{2}. A list of 33 chemical reactions were simulated during the chemical stage. The whole kinetic energy of primary electrons was absorbed in the cube, where an electron track exiting from one side of the defined water cube was forced to enter the same cube from the opposite side. For 1 MeV electron irradiations, G-values of OH radicals were found to decrease from 5.8 species/100 eV at 1 ps down to 2.45 species/100 eV at 1µs.

Monte Carlo simulations were also carried out, by Uehara and Nikjoo[147], to study the water radiolysis for low energy charged particle, such as electrons (200 eV - 1 MeV), protons (3 keV/u - 1 MeV/u) and alpha particles (3 keV/u - 1 MeV/u). They used the KURBUC Monte Carlo simulation code[148] to simulate the particles transport in water medium. Tracks can be simulated in the energy range of 7.4 eV up to 10 MeV. The evolution of species that were created at the end of the physical stage (e^{-}, H_2O^{+} and H_2O^{*}) is simulated during the physico-chemical stage (named prechemical stage in their work). This stage covers events that occur in the time interval of 10^{-15} s to 10^{-12} s. Branching ratios of the dissociation channels of excitation states, that are defined in this work, are slightly different that the ones that are defined in Geant4-DNA. Finally, the chemical stage simulates al events in the time interval of 10^{-12} s down to 10^{-6} s. Diffusion coefficients of defined chemical species are very close to the ones that are

defined in Geant4-DNA. Radiolytic yields were calculated only for the first 10 keV electron tracks. G-values of OH radicals, for 1 MeV electron irradiations, were found to be equal to 5.2 species/100 eV at 1 ps and decrease to 2.8 at 1 µs.

Irradiation and experimental measurements were carried out in a study of Baldacchino et al[13] to study the time dependent OH radicals yield using a fluorescent probe. Irradiations were performed with ^{60}Co gamma rays as well as heavy ions (4.8 GeV $^{12}C^{6+}$ and 20 GeV $^{40}C^{18+}$ nuclei). Radio-induced OH radicals were scavenged by coumarin molecules (coumarin-3-carboxylic acid, or 3CCA). This scavenger was also used in experimental measurements that were carried out during this thesis. Its reaction mechanism is detailed in section 6.4.3.1. The scavenging of OH radicals by the coumarin leads to the formation of the 7-hydroxy-coumarin-3-carboxylic acid (7OH-3CCA), which is a fluorescent stable product. Measurements were performed by using High Performance Liquid Chromatography (HPLC) and fluorescence spectroscopy. Measurements showed that G-values of OH radicals are with good agreement with published data, as shows figure 6.3.

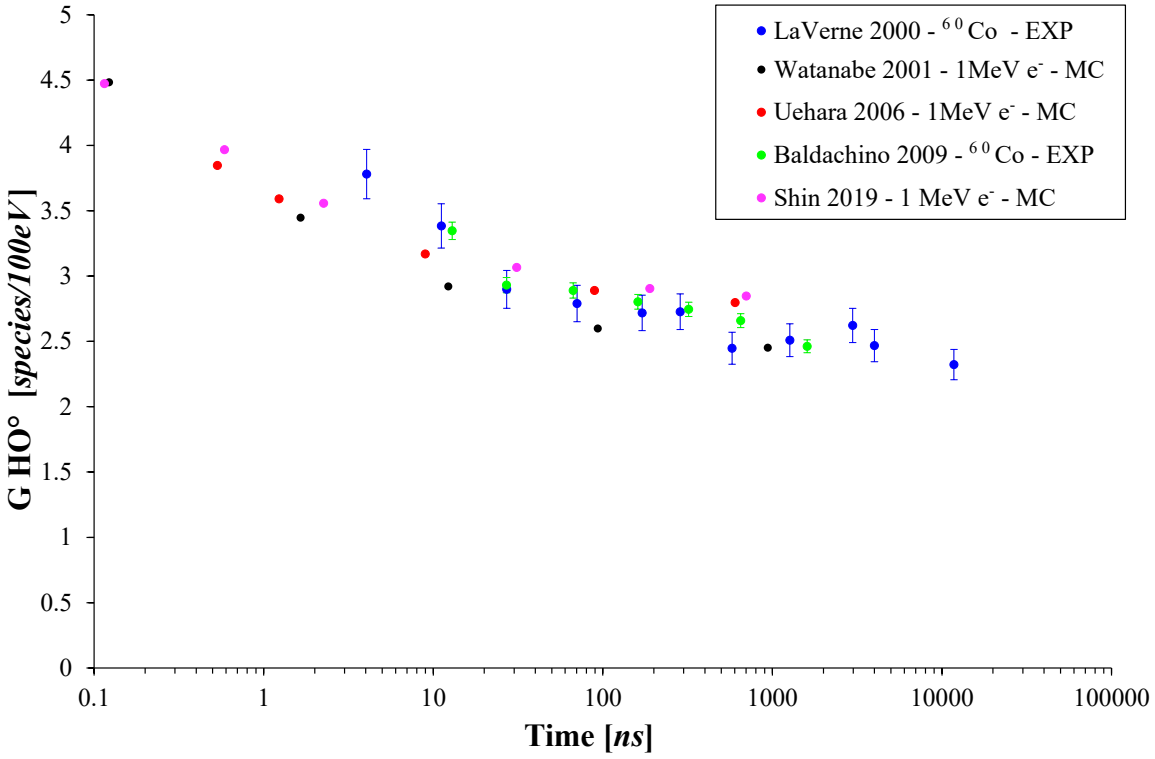

FIGURE 6.3: Comparison of G-values of OH radicals reported in literature.

Shin et al[138] studied the impact of different physics and chemistry models on the calculation of G-values of different species generated during water radiolysis for different electron energies. The *chem6* example of the Geant4-DNA Monte Carlo simulation code was used (version 10.5.p01) for radiolytic yields calculation. Three different physics models were used, combined with the default chemistry model to calculate G-values of different chemical species. In the case of 1 MeV electrons simulations, only the first 10 keV of the track were simulated. A slight

difference was noticed between obtained results, based on the three physics models, where results obtained with the *G4EmDNAPhysics_option2* model were found to be higher than results obtained with the *G4EmDNAPhysics_option8* model over the time interval of 1 ps to 1 µs. The three implemented physics models use the same excitation, ionization, vibrational excitation and dissociative attachment models. However, the main difference between these physics models resides in the chosen electron elastic scattering model where the *G4EmDNAPhysics_option2* model is based on the *Champion* model and the *G4EmDNAPhysics_option8* model is based on the *CPA100* model for energies below 256 keV, and relies on the *Champion* model for higher energies. The effect of the chemistry model was also studied by running the same simulation with the two possible chemistry models: the default model and the option 1 model. In their conclusion, it was recommended to use the *G4EmDNAPhysics_option2* physics model, although results obtained with *G4EmDNAPhysics_option8* physics model showed better agreement with literature data. It was also recommended to use the option 1 chemistry model.

It is clearly noticed in figure 6.3 that literature results are in good agreement over the showed time scale for both 1 MeV electron simulations and ^{60}Co gamma ray experimental measurements. G-values of OH radicals obtained in the case of water irradiations with 1 MeV electrons and ^{60}Co gamma rays can be compared with each other due to their similar Linear Energy Transfer (LET) values. LET of 1 MeV electrons is found to be in the range of to 0.2 keV/µm[151] to 0.3 keV/µm[147], while the LET of ^{60}Co gamma rays is found to be equal to 0.23 keV/µm[63].

6.4.2 Monte Carlo simulations

The *chem5* example of the Geant4-DNA code (version 10.05.p01) was used to determine the time dependency of G-values of OH radicals that are created during the water radiolysis induced by 1 MeV electron irradiation. The following sections detail the selected physics and chemistry constructors as well as the simulation parameters. A constructor is a class that attributes physics or chemistry models for specific physical interactions and chemical parameters (dissociation branching ratios, rate constants of reactions and diffusion coefficients).

6.4.2.1 Physics constructor

The *chem5* example uses by default the *G4EmDNAPhysics_option8* physics constructor. Table 6.6 lists the physical interaction models that are used by the chosen physics constructor. Chosen models will be used for the simulation of primary and secondary particles interactions with the medium during the physical stage of the water radiolysis. The option 8 physics constructor was chosen based on results that were obtained by Shin et al[138], where G-values of OH radicals, for 1 MeV simulations, were found to be the closest to literature data.

Physical process	**Geant4-DNA Physics models**	E_{min}	E_{max}
Electronic excitation	G4DNABornExcitationModel	9 eV	1 MeV
Ionisation	G4DNABornIonisationModel	11 eV	1 MeV
Vibrational excitation	G4DNASancheExcitationModel	2 eV	100 eV
Attachment	G4DNAMeltonAttachmentModel	4 eV	13 eV
Elastic scattering	G4DNACPA100ElasticModel	11 eV	256 keV
	G4DNAChampionElasticModel	256 keV	1 MeV

TABLE 6.6: List of physics models that are used by the *G4EmDNAPhysics_option8* physics constructor.

6.4.2.2 Chemistry constructor

The chemistry constructor that was used in this study is the *G4EmDNAChemistry_option1* constructor, which is selected by default in the *chem5* example, as recommended by Shin et al[138]. The branching ratios of the dissociation channels used in this model are the same ones that are defined in the standard chemistry constructor. Branching ratios are listed in table 6.3.

The differences between the option 1 constructor and the standard constructor are found in the diffusion coefficients as well as in the rate constants of some reactions. Tables 6.7 and 6.8 list values of diffusion coefficients and rate constants, respectively, for both *G4EmDNAChemistry* and *G4EmDNAChemistry_option1* chemistry constructors. It was noticed, in the work of Shin et al[138], that radiolytic yields of OH radicals, obtained using the *G4EmDNAChemistry_option1* chemistry constructor, were in better agreement with published data, compared to radiolytic yields obtained using the standard *G4EmDNAChemistry* constructor.

	D [10^{-9} m^2 s^{-1}]	
Species	*G4EmDNAChemistry*	*G4EmDNAChemistry_option1*
e^-_{aq}	4.9	4.9
$HO^\bullet$	2.8	2.2
$H^\bullet$	7	7
H_3O	9	9.46
H_2	4.8	4.8
OH^-	5	5.3
H_2O_2	2.3	2.3

TABLE 6.7: Values of diffusion coefficients of chemical species that are used in the standard *G4EmDNAChemistry* constructor and the *G4EmDNAChemistry_option1* constructor.

	Reaction rate constant - k [10^{10} M^{-1} s^{-1}]	
Reactions	*G4EmDNAChemistry*	*G4EmDNAChemistry_option1*
$H^\bullet + e^-_{aq} + H_2O \rightarrow OH^- + H_2$	2.65	2.5
$H^\bullet + HO^\bullet \rightarrow H_2O$	1.44	1.55
$H^\bullet + H^\bullet \rightarrow H_2$	1.2	0.503
$H_2O_2 + e^-_{aq} \rightarrow HO^\bullet + OH^-$	1.41	1.1
$H_3O^+ + e^-_{aq} \rightarrow H^\bullet + H_2O$	2.11	2.11
$H_3O^+ + OH^- \rightarrow 2H_2O$	14.3	11.3
$HO^\bullet + e^-_{aq} \rightarrow OH^-$	2.95	2.95
$HO^\bullet + HO^\bullet \rightarrow H_2O2$	0.44	0.55
$e^-_{aq} + e^-_{aq} + 2H_2O \rightarrow 2OH^- + H_2$	0.5	0.636

TABLE 6.8: Comparison of reaction rates of listed reactions that occur during the chemical stage, as defined in the standard *G4EmDNAChemistry* constructor and the used *G4EmDNAChemistry_option1* constructor.

6.4.2.3 Simulation parameters

Water radiolysis simulation codes often use a small segment of the entire physical track in order to simulate large numbers of tracks in reasonable calculation times. Yet, a *PrimaryKiller* class is defined in the *chem5* example to restrict the energy deposition of primary electrons, instead of restricting the geometry volume. This is done by defining two energy thresholds: T_1 and T_2. T_1 is the minimum energy deposition threshold, which, when the deposited energy by the primary track is higher than T_1, this track is killed, but its daughter tracks are simulated, until the total energy deposition of primary and associated secondary tracks exceed the T_2 maximum energy threshold. If this happens, the whole event is aborted (primary + associated secondary tracks). For 1 MeV electrons simulations, Shin et al[138] defined T_1 and T_2 at 10 and 10.1 keV respectively.

However, in the simulation that was carried out in this work, we wanted to reproduce a more realistic irradiation. Thus, the used logic consisted of letting the primary track deposit a big amount of energy, before being killed, and all daughter tracks will be simulated until total energy deposition. Thus, T_1 was set to 200 keV and T_2 was set to 1 MeV. This choice however is more time consuming. Fourteen primary events (14 $\times$ 1 MeV electrons) were simulated using 14 threads of an *Intel Xeon E5-2620* CPU (central processing unit) having a base processing frequency of 2.1 GHz. The calculation time took about two and a half days, yet, obtained results showed a maximal statistical error of 3.5 %. Figure 6.4 shows obtained results and their comparison to literature. Time values at which G-values of OH radicals were calculated have been set to the same time instants used by Watanabe and Saito[151] for better comparison.

Radiolytic yield of OH radicals decrease from 4.62 species/100 eV at 0.12 ns, down to 2.62 species/100 eV at 939 ns. As shows figure 6.4, results obtained in this work are in very good agreement with published data. An average deviation of 5 % is observed between results obtain in this work and results reported by Watanabe and Saito[151]. This agreement also validates the more realistic approach that is used in this work.

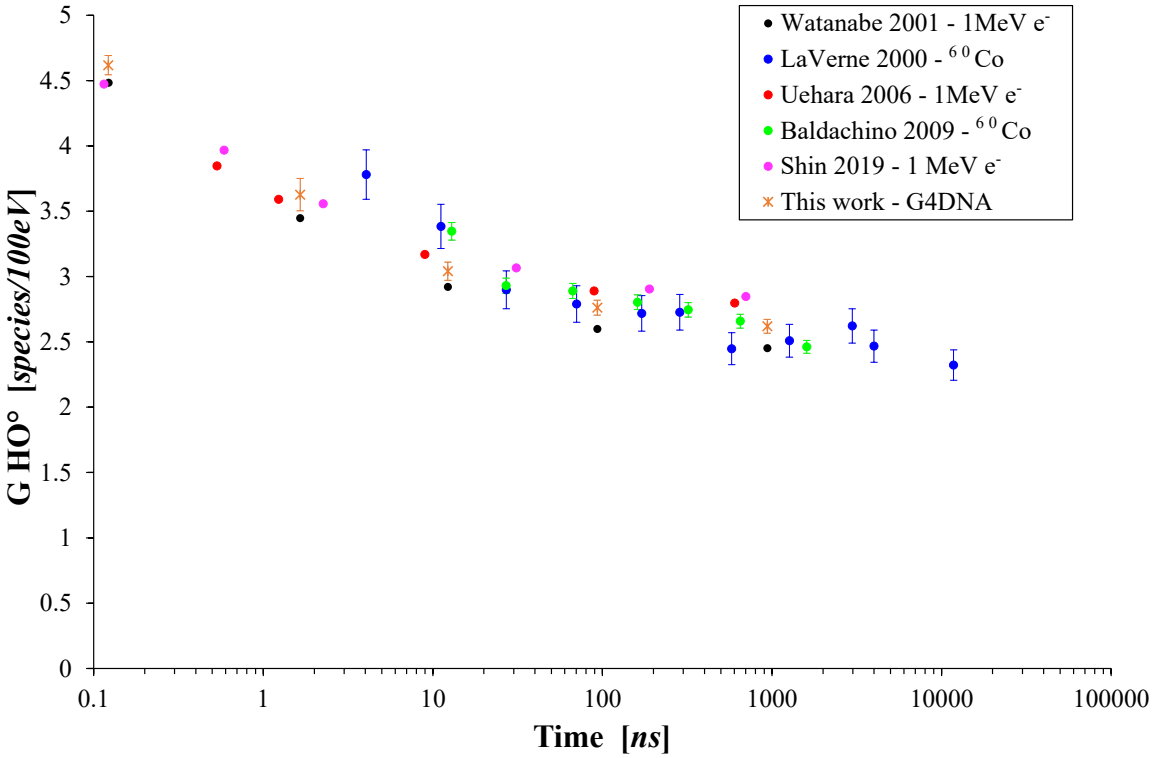

FIGURE 6.4: Comparison of G-values of OH radicals obtained in this work with values reported in literature.

6.4.3 Experimental measurements

Water samples were irradiated with a 1 MeV electron beam, at different doses, in order to measure the time dependence of the radiolytic yield of OH radicals. This work was done in collaboration with members of the *Radiochimie* team of the National Center for Scientific Research (CNRS) of Strasbourg, namely, Dr. Quentin Raffy, Dr. Catherine Galindo and Ing. Philippe Peaupardin. This section discusses the physical and chemical aspects of carried out experimental measurements, a presents obtained results as well as their comparison to Geant4-DNA simulation results and literature.

6.4.3.1 Coumarin scavenger

It is difficult to study the production process of free radicals by direct measurements in radiation chemistry. In the case of OH radicals, direct measurements are hard to realize because of the radical's high reactivity, and hereby, its short lifetime in water. Thus, indirect measurements of the OH radical concentration have been developed over time. Indirect measurements rely on the use of molecular probes that will react with OH radicals during the chemical stage of the water radiolysis, in competition with other possible chemical reaction that might undergo the OH radical.

The choice of the probe, also known as *scavenger*, is very important for this type of measurements, where the selected probe has to ensure good selectivity for OH radicals, and the resulting reaction has to lead to the formation of a stable chemical specie which is important for its detection, thus, being able to determine the concentrations of OH radicals in the solution. Other important factors to take into account in the selection of the scavenger are, firstly, the reactivity of the scavenger with OH radicals which needs to be very high, and secondly, the creation yield of the stable chemical specie that is measured at the end of the experiment. All these parameters are important to determine the concentrations of OH radicals at different instants. The scavenging time is related to the scavenger solution concentration by this equation:

$$t = \frac{1}{k \times C} \tag{6.9}$$

where t is the scavenging time expressed in s, k is the rate constant of the reaction between the scavenger and OH radicals expressed in $M^{-1}s^{-1}$ and C is the scavenger solution concentration expressed in M. Thus, by irradiating solutions having different scavenger concentrations, one should be able to determine the radiolytic yields of OH radicals at different times after irradiation.

The scavenger that was used in this study is the *coumarin-3-carboxylic-acid* (3CCA), which reaction with OH radicals lead to the production of a single stable fluorescent specie: *7-hydroxy-coumarin-3-carboxylic-acid* (7OH-3CCA)[123, 152], as shows figure 6.5. The rate constant of this reaction is $k = 6.8 \times 10^9\ M^{-1}s^{-1}$. The choice of this scavenger is due to its specificity to OH radicals as well as to the low fluorescence detection limit of the final stable 7OH-3CCA molecule. The production yield of the 7OH-3CCA is equal to 4.7 % ± 0.6 % [100, 123].

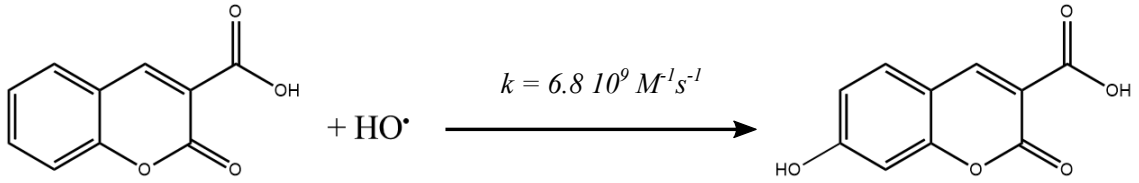

3CCA 7OH-3CCA

FIGURE 6.5: Reaction of the 3CCA molecule with OH radials, leading to the formation of the fluorescent 7OH-3CCA molecule.

6.4.3.2 G-value measurements

Seven 3CCA solutions, with different concentrations were prepared in order to measure the G-value of OH radicals at 5 different scavenging times. Table 6.9 lists the used 3CCA concentrations and the resulting scavenging times. After irradiation of water and 3CCA mixtures, concentrations of 7OH-3CCA were measured using HPLC coupled to fluorescence detector. The use of HPLC is due to the dependence of the fluorescence signal intensity, of the 7OH-3CCA molecules, on the concentration of 3CCA in the solution. Thus, in order to have valid measurements, a separation of both molecules is needed and is achieved by the use of the HPLC.

Once the concentration of 7OH-3CCA is measured by HPLC-fluorescence, the radiolytic yields of OH radicals can be estimated based on this relation:

$$G_{HO\bullet}(t) \;=\; \frac{1}{\alpha} \;\times\; \frac{[7OH-3CCA](t)}{D} \tag{6.10}$$

where $G_{HO\bullet}(t)$ is the radiolytic yield of OH radicals, expressed in mol/J, at the scavenging time t, α is the production yield of the 7OH-3CCA ($\alpha = 0.047$), $[7OH-3CCA](t)$ is the concentration of the 7OH-3CCA molecule, expressed in mol/L, at the scavenging time t and D is the absorbed dose expressed in Gy (or J/kg). The unit of G-values can be converted from mol/J into species/100 eV by using this relation:

$$G_{HO\bullet}(species/100eV) \;=\; 9.63\times10^{6}\; G_{HO\bullet}(mol/J) \tag{6.11}$$

3CCA concentration [M]	Scavenging time [ns]
2×10^{-2}	7
8×10^{-3}	18
2×10^{-3}	71
5×10^{-4}	290
1×10^{-4}	1449

TABLE 6.9: Used 3CCA concentrations and equivalent scavenging times.

6.4.3.3 Irradiations

Irradiations of water solutions, containing different concentrations of 3CCA molecules, were carried out at Aerial. Aerial's Van de Graaff electron accelerator was used to generate a 1 MeV electron beam. Water and 3CCA solutions were placed inside small petri dishes (5.5 cm diameter) and were then placed on the conveyor tray that is then conveyed to the irradiation room, through the generated electron beam. Different thicknesses of water and 3CCA solutions (2, 2.5, 3, 4 and 7 mm) were studied to investigate if the solution's thickness had an impact on the obtained results. For each thickness, 5 solutions were prepared by mixing water with different concentrations of 3CCA, as listed in table 6.9. Thus, we can determine G-values of OH radicals for each thickness. In total, 25 water and 3CCA solutions were prepared and irradiated.

The first step of the irradiations was to determine the depth dose profile in water equivalent material. Thus, 2 B3 radiochromic dye film dosimeters (18 µm thickness) were placed at the surface as well as between each of the 10 polystyrene plates ($\rho = 1.04$ g/cm^3 - dimensions:$10cm \times 10cm \times 0.05cm$) that were used to build an homogeneous water equivalent stack. Figure 6.7 shows obtained results. This measurement was used later on to determine the deposited energy in the irradiated water solutions by calculating the area under the fit model and converting the obtained result from kGy to eV.

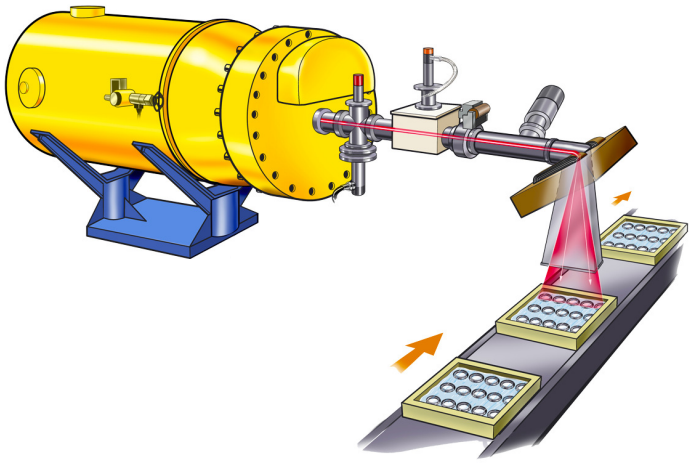

FIGURE 6.6: Sketch of Aerial's Van de Graaff electron accelerator.

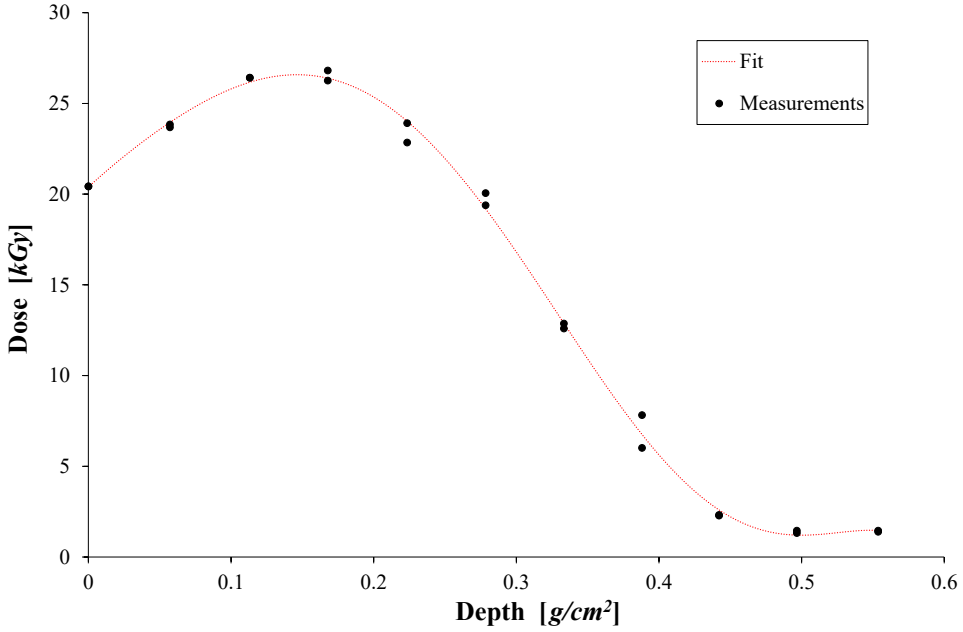

FIGURE 6.7: Depth dose distribution of 1 MeV electrons in water equivalent material.

The electrons energy can be also verified, based on the depth dose curve. The following relation, defined in the ISO/ASTM standard 51649[86], permits to estimate the electron beam energy at the water surface based on the determined practical electron range R_p.

$$E_p = 1.972 \times R_p + 0.245 \tag{6.12}$$

where E_p is the most probable electron beam energy, expressed in MeV. Value of R_p is determined graphically based on the depth dose curve showed in figure 6.7, and was found to be equal to 0.42 g/cm^2. The most probable electron beam energy is $E_p = 1.07$ MeV. Based on the surface dose measurement on the polystyrene stack, irradiation parameters (beam current and conveyor speed) were adapted to irradiate samples at doses of 20.4, 40.8 and 81.6 Gy.

Samples irradiated at 20.4 and 40.8 Gy were irradiated with the same dose rate of about 62.1 Gy/s, while samples that were irradiated at 81.6 Gy were irradiated with a dose rate of 124.2 Gy/s. Table 6.10 shows dose values converted into deposited energy, for each sample thickness.

	Deposited energy [MeV]		
Thickness [mm]	**20.4 Gy**	**40.8 Gy**	**81.6 Gy**
2	7.367E+11	1.473E+12	2.947E+12
2.5	9.134E+11	1.827E+12	3.654E+12
3	1.058E+12	2.116E+12	4.232E+12
4	1.222E+12	2.443E+12	4.886E+12
7	1.261E+12	2.521E+12	5.042E+12

TABLE 6.10: Conversion of absorbed doses into deposited energies for each solution thickness.

6.4.4 Results comparison and discussion

After to irradiations, HPLC-fluorescence measurements of irradiated solutions were carried out by the participating members of the *Radiochimie* team in their laboratory. Table 6.11 lists G-values of OH radicals that were measured for each solution thickness. Averaged results are compared to results obtained by Geant4-DNA Monte Carlo simulations as well as literature, in figure 6.8.

	$G_{HO\bullet}$ **[species/100eV]**				
Thickness [mm]	**1449 ns**	**290 ns**	**71 ns**	**18 ns**	**7 ns**
2	1.426	1.614	1.900	2.268	2.802
2.5	1.303	1.777	1.723	2.182	2.436
3	1.298	1.595	1.744	2.111	2.465
4	1.434	1.782	1.892	2.263	2.740
7	1.368	1.872	1.815	2.501	2.567
Average $G_{HO\bullet}$ [species/100eV]	1.366	1.728	1.815	2.265	2.602

TABLE 6.11: G-values of OH radicals that were measured for each solution thickness.

For each scavenging time, G-values were found to be in agreement for the five studied solution thicknesses, with an average variability of about 6 %. However, results obtained by experimental irradiations were found to be significantly lower than results obtained by Geant4-DNA simulations, as well as results reported in literature. The origin of such difference is currently being investigated.

This difference can originate from different physical parameters, mainly, the absorbed dose, the LET of incident particles and the absorbed dose rate. ^{60}Co gamma rays, that were used in the studies of La Verne[99] and Baldacchino et al[13], have an LET of 0.23 keV/µm[63]. LET of 1 MeV electrons was estimated to be in the range of 0.2 to 0.3 keV/µm which is very close to the LET of ^{60}Co gamma rays. Thus, the difference between experimental results and results of La Verne and Baldacchino can not be caused by LET effect.

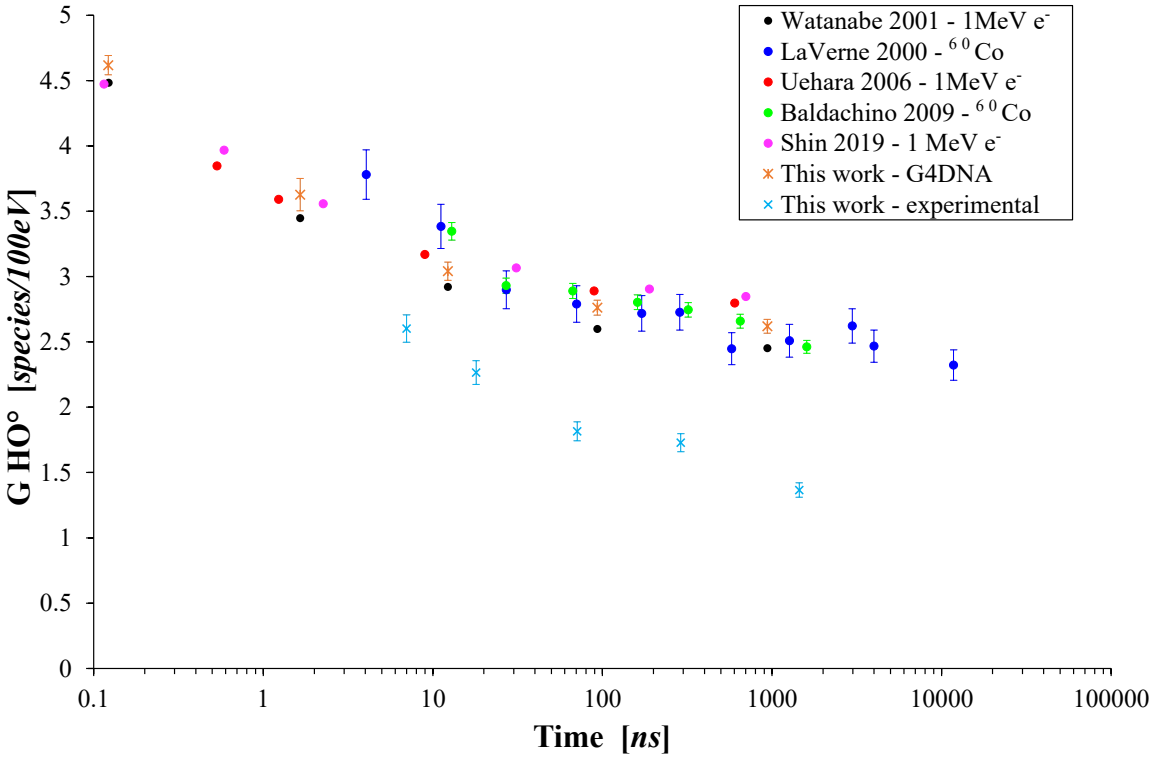

FIGURE 6.8: Comparison of experimentally measured OH radiolytic yields with results obtained by Geant4-DNA simulations and literature.

Secondly, in this study, water and 3CCA solutions were irradiated at a maximum dose of 81.6 Gy, which is slightly higher than the maximum dose that was delivered in the work of Baldacchino et al[13], however, the number of OH radicals was found to be very linear as a function of absorbed dose for all scavenging times and for all solution thicknesses. This eliminates the hypothesis that the absorbed dose caused such difference between experimentally measured and published results. The last hypothesis that should be investigated is the influence of the absorbed dose rate on the efficiency of the scavenging mechanism of OH radicals by the coumarin molecules.

High dose rates can increase the recombination probability of radicals that are created near the primary track, i.e. the recombination of OH radicals, thus reducing the efficiency of the 3CCA molecule to interact with all OH radicals. This hypothesis was investigated through irradiations carried out at different dose rates. Three absorbed dose rates were studied: 133, 13.3 and 1.33 Gy/min. The highest dose rate is identical to the one used in the first set of irradiations and it was selected to validate the previously obtained results. Absorbed dose rate was varied by varying the electron beam current.

The same irradiation configuration, described in section 6.4.3.3, was used. Yet, for each absorbed dose rate, 3 mm thick solutions of water and 3CCA molecules were irradiated at absorbed doses of 20, 40 and 60 Gy, where the absorbed dose was incremented gradually by 20 Gy after each irradiation of the same samples whilst keeping the absorbed dose rate fixed. Figure 6.9 shows the obtained results.

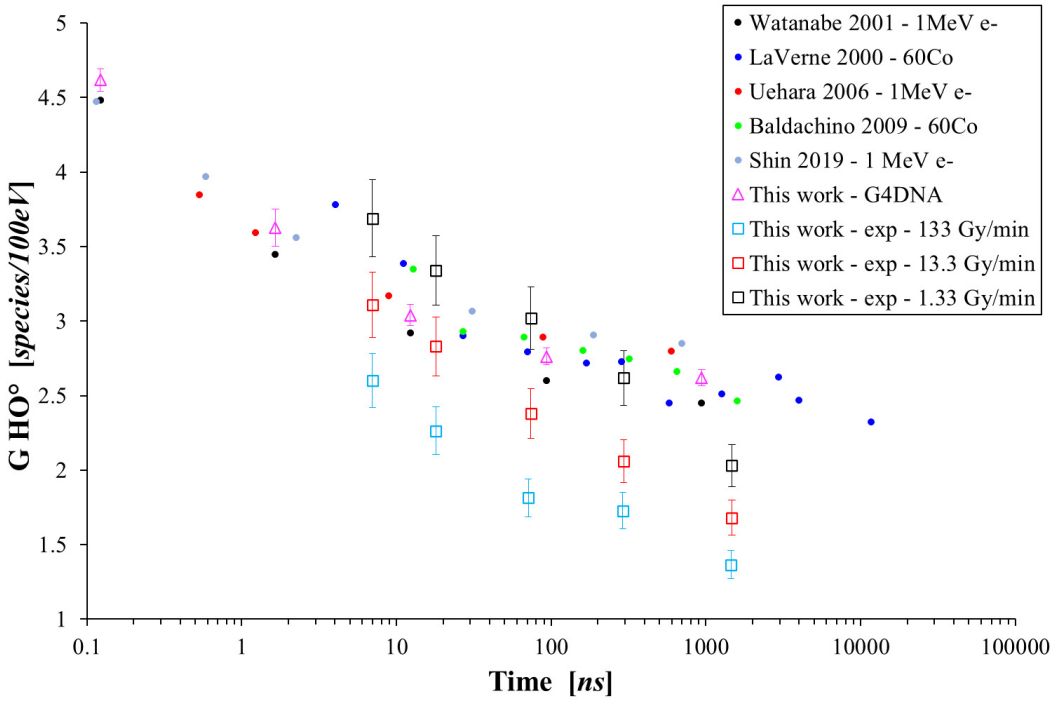

FIGURE 6.9: Study of the effect of absorbed dose rate on the radiolytic yields of OH radicals.

Obtained results show that G values of OH radicals increase with decreasing absorbed dose rate, where radiolytic yields of OH radicals that were measured with an absorbed dose rate of 1.33 Gy/min are found to be in good agreement with results obtained with Geant4-DNA simulations, as well as different literature data[13, 99, 138, 147, 151]. In order to validate these results, another set of irradiations of water solutions with a different scavenger are to be carried out to see if there is a dependence of G-values of OH radicals on the scavenging mechanism.

The absorbed dose rate of 1.33 Gy/min is close to the absorbed dose rate that a gamma source can provide, hence the good agreement between results obtained in this study and ones that are reported in LaVerne's work[99]. On the other hand, one can notice that the G-value of OH radicals at 1449 ns is found to be always diverging from the general tendency of the radiolytic yields. This can be explained by the fact that at high scavenging time, the concentration of the scavenger molecule is low, thus, the uncertainty on the concentration measurement is high. This hypothesis can be also validated by using a different scavenger and comparing obtained results.

6.5 Conclusion

This chapter presented both physical and chemical aspects of water radiolysis, by describing the different processes that occur during the physical, physico-chemical and chemical stages of the water radiolysis. The main goal of this part was to take in hand the Geant4-DNA Monte Carlo simulation code, validate it with experimental measurements and finally, try to adapt the simulation code to model the free radicals creation in Alanine molecules. Unfortunately, the calculation of alanine's ionization cross-sections and their integration in the Geant4-DNA code could not be achieved.

However, Geant4-DNA simulations of water radiolysis by 1 MeV electrons permitted to determine the time dependence of the radiolytic yield of OH radicals. Results were found to be in very good agreement with already published data. Experimental trials were carried out at Aerial where water and 3CCA solutions were irradiated with a 1 MeV electron beam. OH radicals were scavenged by the 3CCA molecules present in water, leading to the formation of a stable fluorescent molecule (7OH-3CCA). Measurement of the concentration of 7OH-3CCA molecules lead to the determination of radiolytic yields of OH radicals.

Experimental results were found to be significantly lower than the ones obtained by Geant4-DNA simulations as well as published data. This difference originates from the absorbed dose rate dependence of the radiolytic yields of OH radicals. This hypothesis was tested by irradiating water and 3CCA solutions at lower absorbed dose rates. Obtained results at an absorbed dose rate of 1.33 Gy/min were found to be in a good agreement with MC simulations results as well as literature.

Part V

General conclusion

General Conclusion

Alanine/EPR dosimetry system is a trustworthy, efficient and robust tool for qualifications (IQ/OQ/PQ) as well as for routine process control. It disposes of high metrological quality making it one of the many important reference as well as transfer standard dosimetry systems[81]. Yet, the easiness of use, the excellent measurement reproducibility as well as the low associated uncertainty make from the alanine/EPR dosimetry system a very interesting system for routine dose monitoring. Due to all advantages that offer the alanine/EPR dosimetry system, a significant growth in its use have been noticed during the last decade. This motivated Aerial to ensure the optimal use of its developed dosimetry system for most radiation application fields. Thus, many investigations and developments were carried out by Aerial to understand and optimize the effect of all influence quantities that take part in alanine/EPR dosimetry, and that may jeopardize its readout accuracy. One of the major influencers on the alanine dosimeter's EPR response is the photon energy, especially in the sub 200 keV energy range, where alanine loses its dosimetric equivalency to water[54].

On the other hand, a growing shift from radioactive source-based irradiators to electrical kilo-voltage X-ray irradiators is observed, especially in applications such as blood irradiation, Sterile Insect Technique treatments and phytosanitary irradiation of fresh produce[37, 144]. Yet, a great number of photons generated by kilo-voltage X-ray irradiators have an energy lower than 200 keV. Thus, use of alanine dosimeters for kilo-voltage X-ray irradiations can lead to a false estimation of the true delivered absorbed dose to water, only if the dosimetry system is calibrated with a reference beam quality that is different from kilo-voltage X-rays, which is often the case where the calibration of the dosimetry system is done with a ^{60}Co gamma rays or high energy electron or X-ray beams. This lead Aerial to start this Ph.D thesis, in collaboration with the National Center for Scientific Research (CNRS) of Strasbourg, inscribed in a Coordinated Research Program (CRP) piloted by the IAEA, to study the effect of low to medium energy photons on the EPR response of the alanine dosimeter.

During this thesis, many studies have been carried out to understand the effect of photon energy on the EPR response of Aerial's alanine dosimeters, by investigating the photon energy dependence of the relative response of alanine to several kilo-voltage X-ray beam qualities, compared to its EPR response to a ^{60}Co gamma source. Experimental measurements were carried out at Aerial as well as at the NPL in order to study the energy dependence of the alanine's EPR response per absorbed dose to water unit. This was done by irradiating alanine dosimeters at different dose levels with several X-ray beam qualities over an effective energy range of 27.5 to 168 keV. The response of alanine dosimeters was measured by EPR spectrometry

and values of delivered absorbed dose to water were measured using calibrated ion chambers. Results showed that the relative response of alanine dosimeters to kilo-voltage X-rays ranges from 0.698 to 0.954 at X-ray effective energies of 27.5 and 168 keV respectively. These results were found to be in good agreement with literature[7, 50, 95, 150]. Results obtained during this thesis were slightly higher than published data. This is mainly due to the differences of the chemical composition between alanine dosimeters that were studied in each work.

The absorbed dose ratio of alanine with respect to water, for several X-ray beam qualities, compared to a ^{60}Co reference beam quality, was determined using Monte Carlo simulations based on the MCNPX code. The irradiation geometries as well as the X-ray source parameters were reproduced in the simulations. X-ray spectra calculated by the SpekCalc program were taken as input by the simulation code. Results showed that the alanine to water dose ratio ranges from 0.737 to 0.978 for effective energies of 27.5 and 168 keV respectively. Results obtained by Monte Carlo simulations were found to be higher than results obtained by experimental measurements. Thus the average deviation between results obtained by Monte Carlo simulations and experimental measurements was found to be equal to 3.82 %. This significant deviation originates from the fact the energy dependence of the free radical creation yield in alanine is not taken into account in Monte Carlo simulations. On the other hand, results obtained by Monte Carlo simulations were in good agreement with published data over the studied effective energy range, despite slight differences that are due, again, to the difference of the chemical composition of studied alanine dosimeters, as well as the difference of the used Monte Carlo codes.

The novelty of this thesis resides in the elaboration, testing and validation of a C++ code that permits to calculate the absorbed dose ratio of alanine to water, for several X-ray beam qualities, compared to a ^{60}Co reference beam quality. The calculations consisted on weighting X-ray spectra, generated by SpekCalc, with mass-energy absorption coefficients and energy coefficients tabulated by NIST[54]. These coefficients were modelled using mathematical fits. Results were obtained within few seconds, where Monte Carlo simulations take few hours to calculate the alanine to water dose ratio. Analytical calculations showed that the alanine to water dose ratio ranged from 0.727 to 0.972 for effective energies of 27.5 and 168 keV respectively. Results obtained by analytical calculations were in very good agreement with results obtained by Monte Carlo simulations, with an average deviation of 0.7 %. This small deviation justifies and validates the use of this calculation code as a replacement to time consuming and geometry dependent Monte Carlo simulations. On the other hand, results obtained by analytical calculations were found to be in a good agreement with values of alanine's relative response measured experimentally, where the average deviation between results of both methods was equal to 3.15 %. This deviation is due to the fact that the energy dependence of alanine's free radical creation yield was not taken into account in analytical calculations neither. The average standard deviation of results of the three developed methods was equal to 2.1 %.

To account for the influence of the energy dependence of alanine's free radicals creation yield in the determination of the relative response of alanine dosimeters, by both Monte Carlo simulations and analytical calculations, a study was carried out in parallel. Alanine dosimeters were irradiated with three different X-ray beam qualities covering the effective energy range of 19.1

to 49.4 keV. For each X-ray beam quality, the relative efficiency of alanine dosimeters, defined as the ratio of alanine G-value for X-rays compared to ^{60}Co gamma rays, was determined based on experimental measurements of the alanine's relative response to each X-ray beam quality, and on Monte Carlo simulations leading to the determination of the absorbed dose ratio of alanine to water for each X-ray beam quality compared to a ^{60}Co reference beam quality. Values of the relative efficiency of Aerial's alanine dosimeters ranged from 0.91 to unity for X-ray effective energy of 19.1 keV and the energies of a ^{60}Co gamma source respectively. Obtained results were found to be in agreement with published data[7, 50, 124–126, 149]. A variability within determined and published results is observed. This is due to the differences in the chemical composition between studied dosimeters as well as differences in formalisms used to determine the relative efficiency. Alanine to water dose ratios, obtained by Monte Carlo simulations and analytical calculations, were updated with corresponding values of relative efficiencies determined by the mathematically modelling estimated values of the relative efficiency of alanine. This update lead to a better agreement of results of both simulations and calculations with experimentally measured relative responses of alanine, where the average standard deviation of updated results and measurements dropped from 2.1 % to 1.3 %. The overall uncertainty associated to the determination of the relative response based on the analytical calculation mathematical model is less than 4 % (k = 1).

During this thesis, it was programmed to update current cross-sections of the Geant4-DNA Monte Carlo simulation code with calculated ionization cross-sections of alanine, in order to make the Geant4-DNA code able to simulate the free radical creation process in alanine. Firstly, it was important to get familiarized with this code, thus, a pre-configured example was used for this purpose. The simulation example consisted in calculating the time evolution of radiolytic yields of OH radicals created during water radiolysis by 1 MeV electrons. After running multiple simulations, obtained results were found to be in good agreement with published data[13, 99, 138, 147, 151]. In order to validate the simulation code, it was evident that results obtained by simulations had to be compared to experimentally measured radiolytic yields of OH radicals. Therefore, experimental irradiations were carried out at Aerial with 1 MeV electrons. Solutions containing water and several concentrations of 3CCA molecules (a radical scavenger) were irradiated at different doses. HPLC coupled to fluorescence measurements of the concentration of the 7OH-3CCA molecule lead to the determination of radiolytic yields of OH radicals at different scavenging times. Experimental results were found to be lower than all published data as well as simulations carried out during this study. An investigation on the absorbed dose rate dependence of radiolytic yields of OH radicals were carried out using three different absorbed dose rates. Results showed that G-values of OH radicals increase with decreasing absorbed dose rate. Results were found to be in good agreement with Geant4-DNA MC simulation results as well as literature, for an absorbed dose rate of 1.33 Gy/min. Unfortunately, due to the lack of remaining time before the thesis defense, the calculation of alanine ionization cross-sections and their implementation in Geant4-DNA could not be achieved.

The next step to conclude this work consists of a final validation of the mathematical model that was put in place based on analytical calculations of the relative response of Aerial's alanine dosimeters. This validation can be achieved by carrying out alanine irradiations at external irradiation facilities in order to characterize their X-ray beam qualities, then compare calculated adequate relative response to the one that is measured using both EPR readout of the dosimeter's response and ion chamber measurements of delivered absorbed dose to water. Once validated, the defined model will be integrated in Aerial's dosimetry software *Aer'EDE*. This update will ensure a better absorbed dose to water measurement using alanine dosimeters, irradiated with kilo-voltage X-rays, mainly when the dosimetry system is calibrated with a different reference beam quality.

Bibliography

[1] AAMI. *AAMI TIR29: Guide for process characterization and control in radiation sterilization of medical devices.* AAMI, 2012.

[2] AAMI. *AAMI TIR37: Sterilization of health care products — Radiation — Guidance on sterilization of biologics and tissue-based products.* AAMI, 2013.

[3] AAPM. *Radiochromic film dosimetry: Recommendations of AAPM Radiation Therapy Committee Task Group 55.* Medical Physics, 1998. doi: https://doi.org/10.1118/1.598407.

[4] S. Agostinelli and al. *Geant4—a simulation toolkit.* Nuclear Instruments and Methods in Physics Research Section A: Accelerators, Spectrometers, Detectors and Associated Equipment, 2003.

[5] J. Allison and al. *Geant4 developments and applications.* IEEE Transactions on Nuclear Science, 2006. doi: http://dx.doi.org/10.1109/TNS.2006.869826.

[6] J. Allison and al. *Recent developments in Geant4.* Nuclear Instruments and Methods in Physics Research Section A: Accelerators, Spectrometers, Detectors and Associated Equipment, 2016. doi: https://doi.org/10.1016/j.nima.2016.06.125.

[7] M. Anton and L. Büermann. *Relative response of the alanine dosimeter to medium energy x-rays.* Physics in Medicine and Biology, 2015. doi: https://doi.org/10.1088/0031-9155/60/15/6113.

[8] M. Anton, R. P. Kapsch, M. Krystek, and F. Renner. *Response of the alanine/ESR dosimetry system to MV x-rays relative to 60Co radiation.* Physics in Medicine and Biology, 2008. doi: 10.1088/0031-9155/53/10/020.

[9] J. M. Arber and P. H. G. Sharpe. *Fading Characteristics of Irradiated Alanine Pellets: The Importance of Pre-irradiation Conditioning.* Applied Radiation and Isotopes, 1993. doi: https://doi.org/10.1016/0969-8043(93)90190-L.

[10] ASTM. *ASTM standard E1026: Standard Practice for Using the Fricke Dosimetry System.* ASTM, 2013.

[11] F. H. Attix. *Introduction to Radiological Physics and Radiation Dosimetry.* Wiley-VCH, 1986. ISBN 9780471011460.

[12] A. Bakri, K. Mehta, and D. R. Lance. *Chapter 3.3: Sterelizing Insects with Ionizing Radiation, from the book: Sterile Insect Technique Principles and Practice in Area-Wide Integrated Pest Management.* Springer, 2005. ISBN 978-1-4020-4051-1.

[13] G. Baldacchino, T. Maeyama, S. Yamashita, M. Taguchi, A. Kimura, Y. Katsumura, and T. Murakami. *Determination of the time-dependent OH-yield by using a fluorescent probe. Application to heavy ion irradiation.* Chemical Physics Letters, 2009. doi: https://doi.org/10.1016/j.cplett.2008.12.006.

[14] E. S. Bergstrand, K. R. Shortt, C. K. Ross, and E. O. Hole. *An investigation of the photon energy dependence of the EPR alanine dosimetry system.* Physics in Medicine and Biology, 2003. doi: https://doi.org/10.1088/2F0031-9155/2F48/2F12/2F306.

[15] E. S. Bergstrand, H. Bjerke, and E. O. Hole. *An experimental investigation of the electron energy dependence of the EPR alanine dosimetry system.* Radiation Measurements, 2005. doi: https://doi.org/10.1016/j.radmeas.2004.05.010.

[16] M. A. Bernal and al. *Track structure modeling in liquid water: A review of the Geant4-DNA very low energy extension of the Geant4 Monte Carlo simulation toolkit.* Physica Medica, 2015. doi: https://doi.org/10.1016/j.ejmp.2015.10.087.

[17] W. W. Bradshaw, D. G. C. JR., G. W. Crawford, and H. A. Spetzler. *The Use of Alanine as a Solid Dosimeter.* Radiation Research, 1962.

[18] M. Brustolon and E. Giamello. *Electron Paramagnetic Resonance A Practiotionner's Toolkit.* Wiley, 2009. ISBN 9780470432235.

[19] M. Burton. *Radiation Chemistry - A God fatherly look at its history and its relation to liquids.* Chemical and Engineering News, 1969.

[20] D. J. Butler, J. E. Lye, T. E. Wright, D. Crossley, P. H. G. Sharpe, A. W. Stevenson, J. Livingstone, and J. C. Crosbie. *Absorbed dose determination in kilovoltage X-ray synchrotron radiation using alanine dosimeters.* Australasian Physical and Engineering Sciences in Medicine, 2016. doi: https://doi.org/10.1007/s13246-016-0479-1.

[21] G. V. Buxton. *Chapter 1: An overview of the radiation chemistry of liquids, from the book: Radiation Chemistry - From Basics to Applications in Material and Life Sciences.* EDP SCIENCES, 2008. ISBN 9782759800247.

[22] C. M. M. Chair, C. W. Coffey, L. A. DeWerd, C. Liu, R. Nath, S. M. Seltzer, and J. P. Seuntjens. *AAPM protocol for 40–300 kV X-ray beam dosimetry in radiotherapy and radiobiology.* Medical Physics, 2001. doi: https://doi.org/10.1118/1.1374247.

[23] F. Chen, P. Nicolucci, and O. Baffa. *Enhanced sensitivity of alanine dosimeters to low-energy X-rays: Preliminary results.* Radiation Measurements, 2008. doi: https://doi.org/10.1016/j.radmeas.2007.11.066.

[24] A. Chmielewski, T. Sadat, and Z. Zimek. *Chapter 3: Gamma Irradiators for Radiation Sterilization, from the book: Trends in Radiation Sterilization of Health Care Products.* International Atomic Energy Agency, 2008. ISBN 978–92–0–111007–7.

[25] S. Chu, A. Wieser, H. Feist, and D. F. Regulla. *ESR/Alanine Dosimetry of High-energy Electrons in Radiotherapy.* Radiation Application and Instruments Part A, 1989. doi: https://doi.org/10.1016/0883-2889(89)90030-0.

[26] M. R. Cleland, L. A. Parks, and S. Cheng. *Applications for radiation processing of materials.* Nuclear Instruments and Methods in Physics Research B, 2003. doi: https://doi.org/10.1016/S0168-583X(03)00655-4.

[27] G.-D. collaboration. *Geant4-DNA website.* 2020. URL http://geant4-dna.org/.

[28] E. Craven, J. Schlecht, and R. Stein. *Chapter 3: Gamma Irradiation Plants, from the book: Food Irradiation Technologies Concepts, Applications and Outcomes.* The Royal Society of Chemistry, 2017. doi: https://doi.org/10.1039/9781788010252.

[29] J. C. Crosbie, P. Fournier, S. Bartzsch, M. Donzelli, I. Cornelius, A. W. Stevenson, H. Requardt, and E. Bräuer-Krisch. *Energy spectra considerations for synchrotron radiotherapy trials on the ID17 bio-medical beamline at the European synchrotron radiation facility.* Synchrotron Radiation, 2015. doi: https://doi.org/10.1107/s1600577515008115.

[30] D. Defrise, M. Abs, F. Genin, and Y. Jongen. *Technical Status of the First Industrial Unit of the 10 MeV, 100 kW Rhodotron.* Radiation Physics and Chemistry, 1995. doi: https://doi.org/10.1016/0969-806X(95)00197-6.

[31] J. F. Dempsey, D. A. Low, S. Mutic, J. Markman, A. S. Kirov, G. H. Nussbaum, and J. F. Williamson. *Validation of a precision radiochromic film dosimetry systemfor quantitative two-dimensional imaging of acute exposuredose distributions.* Medical Physics, 2000. doi: https://doi.org/10.1118/1.1290488.

[32] M. F. Desrosiers. *Chapter 13: Alanine-EPR High-Dose Radiation Metrology, from the book: Applications of EPR in Radiation Research.* Springer, 2014. ISBN 978-3-319-09216-4.

[33] M. F. Desrosiers, T. Ostapenko, and J. M. Puhl. *The Impact of Irradiation Temperature Estimations on the Accuracy of Dosimetry.* Radiation Physics and Chemistry, 2009.

[34] M. F. Desrosiers, M. Peters, and J. M. Puhl. *A Study of the Alanine Dosimeter Irradiation Temperature Coefficient from 25 to 80 ˚C.* Radiation Physics and Chemistry, 2009. doi: https://doi.org/10.1016/j.radphyschem.2009.03.026.

[35] M. F. Desrosiers, A. M. Forney, and J. M. Puhl. *A Comparison of Harwell and FWT Alanine Temperature Coefficients from 25 ˚C to 80 ˚C.* NIST Journal of Research, 2012. doi: https://dx.doi.org/10.6028%2Fjres.117.007.

[36] P. Dethier. *Industrial Gamma and X-ray: "Same but Different".* White paper IBA, 2016. URL http://iiaglobal.com/uploads/documents/IBA.white_paper_-_x-ray_vs_gamma.pdf.

[37] B. Dodd and R. J. Vetter. *Replacement of 137Cs Irradiators with X-ray Irradiators.* Operational Radiation Safety, 2009. doi: http://dx.doi.org/10.1097/01.HP.0000334555.78657.bc.

[38] I. G. Draganic and Z. D. Draganic. *The Radiation Chemistry of Water.* Academic Press, 1971. ISBN 9780323158787.

[39] G. R. Eaton, S. S. Eaton, D. P. Barr, and R. T. Weber. *Quantitative EPR.* Springer, 2010. ISBN 978-3-211-92947-6.

[40] S. J. et al. *GATE: a simulation toolkit for PET and SPECT.* Physics in Medicine and Biology, 2004.

[41] FAO and WHO. *General Standard for Irradiated Foods - CODEX STAN 106-1983, REV.1-2003.* Food and Agriculture Organization of the United Nations (FAO) and the World Health Organization (WHO), 2003.

[42] FAO and WHO. *Code of Practice for Radiation Processing of Food - CAC/RCP 19-1979.* Food and Agriculture Organization of the United Nations (FAO) and the World Health Organization (WHO), 2011.

[43] P. Follett. *Phytosanitary irradiation for fresh horticultural commodities: generic treatments, current issues, and next steps.* Stewart Postharvest Review, 2014. ISBN 1745-9656.

[44] B. A. Goodman, N. Worasith, S. Ninlaphruk, H. Mungpayaban, and W. Deng. *Radiation Dosimetry Using Alanine and Electron Paramagnetic Resonance (EPR) Spectroscopy: A New Look at an Old Topic.* Applied Magnetic Resonance, 2016. doi: https://doi.org/10.1007/s00723-016-0855-8.

[45] R. Hajj, R. E. Hage, R. Sonnier, B. Otazaghine, B. Gallard, S. Rouif, M. Nakhl, and J.-M. Lopez-Cuesta. *Grafting of phosphorus flame retardants on flax fabrics: Comparison between two routes.* Polymer Degradation and Stability, 2017. doi: https://doi.org/10.1016/j.polymdegradstab.2017.11.006.

[46] L. A. Harrah. *Chemical Dosimetry with Doped Poly(halostyrene) Film.* Radiation Research, 1970. doi: https://doi.org/10.2307/3572873.

[47] J. Helt-Hansen, A. Miller, and P. Sharpe. *Dose response of thin-film dosimeters irradiated with 80–120 keV electrons.* Radiation Physics and Chemistry, 2005. doi: https://doi.org/10.1016/j.radphyschem.2005.06.004.

[48] M. Z. Heydari, E. Malinen, E. O. Hole, and E. Sagstuen. *Alanine Radicals. 2. The Composite Polycrystalline Alanine EPR Spectrum Studied byENDOR, Thermal Annealing, and Spectrum Simulations.* Physical Chemistry A, 2002. doi: https://doi.org/10.1021/jp026023c.

[49] R. Hill, B. Healy, L. Holloway, Z. Kuncic, D. Thwaites, and C. Baldock. *Advances in kilovoltage x-ray beam dosimetry.* Physics in Medicine and Biology, 2014. doi: https://dx.doi.org/2F10.1088/2F0031-9155/2F59/2F6/2FR183.

[50] J. G. Hjørringgaard, C. Ankjærgaard, M. Bailey, and A. Miller. *Alanine pellet dosimeter efficiency in a 40 k V x-ray beam relative to cobalt-60.* Radiation Measurements, 2020. doi: https://doi.org/10.1016/j.radmeas.2020.106374.

[51] A. S. Hoffman. *Applications of radiation processing in biomedical engineering — A review of the preparation and properties of novel biomaterials.* Radiation Physics and Chemistry, 1977. doi: https://doi.org/10.1016/0146-5724(77)90080-2.

[52] A. Horsfield, J. Morton, and D. Whiffen. *The electron spin resonance spectrum of CH3ĊHCOOH at 77°K in L-alpha-alanine.* Molecular Physics, 1962. doi: https://doi.org/10.1080/00268976100100591.

[53] A. Horsfield, J. Morton, and D. Whiffen. *The electron spin resonance spectrum of CH3ĊH(CO2H) between 100°K and 200°K.* Molecular Physics, 1962. doi: https://doi.org/10.1080/00268976200100121.

[54] J. H. Hubbell and S. M. Seltzer. *Tables of X-ray mass attenuation coefficients and mass energy-absorption coefficients 1 keV to 20 MeV for elements z = 1 to 92 and 48 additional substances of dosimetric interest.* National Institute of Standards and Technology (NIST), 1995. doi: http://dx.doi.org/10.18434/T4D01F.

[55] IAEA. *The Development of X-ray Machines for Food Irradiation.* International Atomic Energy Agency, 1995. URL http://www-naweb.iaea.org/nafa/fep/public/x-ray.pdf.

[56] IAEA. *Absorbed Dose Determination in Photon and Electron Beams - An International Code of Practice - 2nd Edition.* International Atomic Energy Agency, 1997. ISBN 92-0-100597-0.

[57] IAEA. *Dosimetry for Radiation Processing.* International Atomic Energy Agency, 2000. ISBN 1011-4289.

[58] IAEA. *Technical Report Series No. 398: Absorbed dose determination in external beam radiotherapy: An international code of practice for dosimetry based on standards of absorbed dose to water.* International Atomic Energy Agency, 2001. ISBN 92-0-102200-X.

[59] IAEA. *Dosimetry system for SIT - Manual of Gafchromic® film.* International Atomic Energy Agency, 2004.

[60] IAEA. *Diagnostic Radiology Physics: A Handbook for Teachers and Students.* International Atomic Energy Agency, 2006. ISBN 978-92-0-131010-1.

[61] ICRU. *ICRU report no. 10b - Physical Aspects of Irradiation.* International Commission on Radiation Units and Measurements, 1964. doi: https://doi.org/10.1093/jicru/os6.1.Report10b.

[62] ICRU. *ICRU report no. 14 - Radiation Dosimetry: X-Rays and Gamma Rays with Maximum Photon Energies between 0.6 and 50 MeV.* International Commission on Radiation Units and Measurements, 1969. doi: https://doi.org/10.1093/jicru/os8.1.Report14.

[63] ICRU. *ICRU report no. 16 - Linear Energy Transfer.* International Commission on Radiation Units and Measurements, 1970. doi: https://doi.org/10.1093/jicru/os9.1.Report16.

[64] ICRU. *ICRU report no. 17 - Radiation Dosimetry: X Rays Generated at potentials of 5 to 150 kV.* International Commission on Radiation Units and Measurements, 1970. doi: https://doi.org/10.1093/jicru/os9.2.Report17.

[65] ICRU. *ICRU report no. 21 - Radiation Dosimetry: Electrons with Initial Energies between 1 and 50 MeV.* International Commission on Radiation Units and Measurements, 1972. doi: https://doi.org/10.1093/jicru/os11.2.Report21.

[66] ICRU. *ICRU report no. 33 - Radiation Quantities and Units.* International Commission on Radiation Units and Measurements, 1980. doi: https://doi.org/10.1002/jlcr.2580180918.

[67] ICRU. *ICRU report no. 80 - Dosimetry Systems for Use in Radiation Processing.* International Commission on Radiation Units and Measurements, 2008. doi: https://doi.org/10.1093/jicru/8.2.Report80.

[68] S. Incerti. *Geant4-DNA overview.* 2015 Geant4-DNA Tutorial, 2015.

[69] S. Incerti and al. *The Geant4-DNA Project.* International Journal of Modeling, Simulation,and Scientific Computing, 2010. doi: https://doi.org/10.1142/S1793962310000122.

[70] S. INCERTI and al. *Comparison of Geant4 very low energy cross section models with experimental data in water.* Journal of Medical Physics, 2010. doi: https://doi.org/10.1118/1.3476457.

[71] S. Incerti and al. *Geant4-DNA example applications for track structure simulations in liquid water: a report from the Geant4-DNA Project.* Journal of Medical Physics, 2018. doi: https://doi.org/10.1002/mp.13048.

[72] ISO. *ISO 11137-1:2006 Sterilization of health care products — Radiation — Part 1: Requirements for development, validation and routine control of a sterilization process for medical devices.* ISO, 2006.

[73] ISO. *ISO 11137-2:2013 Sterilization of health care products — Radiation — Part 2: Establishing the sterilization dose.* ISO, 2013.

[74] ISO. *ISO 11137-3:2017 Sterilization of health care products — Radiation — Part 3: Guidance on dosimetric aspects of development, validation and routine control.* ISO, 2017.

[75] ISO. *ISO 11137-4:2020 Sterilization of health care products — Radiation — Part 4: Guidance on process control.* ISO, 2020.

[76] ISO and ASTM. *ISO/ASTM standard 51608: Standard Practice for Dosimetry in an X-Ray (Bremsstrahlung) Facility for Radiation Processing.* ISO/ASTM, 2005.

[77] ISO and ASTM. *ISO/ASTM standard 51205: Standard Practice for Use of a Ceric-Cerous Sulfate Dosimetry System.* ISO/ASTM, 2009.

[78] ISO and ASTM. *ISO/ASTM standard 51276: Standard Practice for Use of a Polymethylmethacrylate Dosimetry System.* ISO/ASTM, 2012.

[79] ISO and ASTM. *ISO/ASTM standard 51261: Standard Practice for Calibration of routine Dosimetry systems for Radiation Processing.* ISO/ASTM, 2013.

[80] ISO and ASTM. *ISO/ASTM standard 51275: Standard Practice for Use of a Radiochromic Film Dosimetry System.* ISO/ASTM, 2013.

[81] ISO and ASTM. *ISO/ASTM standard 51607: Standard Practice for Use of an Alanine-EPR Dosimetry System.* ISO/ASTM, 2013.

[82] ISO and ASTM. *ISO/ASTM standard 51650: Standard Practice for Use of a Cellulose Triacetate Dosimetry System.* ISO/ASTM, 2013.

[83] ISO and ASTM. *ISO/ASTM standard 51818: Standard Practice for Dosimetry in an Electron Beam Facility for Radiation Processing at Energies Between 80 and 300 keV.....* ISO/ASTM, 2013.

[84] ISO and ASTM. *ISO/ASTM standard 51940: Standard Guide for Dosimetry for Sterile Insect Release Programs.* ISO/ASTM, 2013.

[85] ISO and ASTM. *ISO/ASTM standard 51707: Standard Guide for Estimation of Measurement Uncertainty in Dosimetry for Radiation Processing.* ISO/ASTM, 2014.

[86] ISO and ASTM. *ISO/ASTM standard 51649: Standard Practice for Dosimetry in an Electron Beam Facility for Radiation Processing at Energies Between 300 keV and 25 MeV.* ISO/ASTM, 2014.

[87] ISO and ASTM. *ISO/ASTM standard 51939: Standard Practice for Blood Irradiation Dosimetry.* ISO/ASTM, 2017.

[88] ISO and ASTM. *ISO/ASTM standard 51631: Standard Practice for Use of Calorimetric Dosimetry Systems for Dose Measurements and Routine Dosimetry System Calibration in Electron Beams.* ISO/ASTM, 2020.

[89] ISO and ASTM. *ISO/ASTM standard 52628: Standard Practice for Dosimetry in Radiation Processing.* ISO/ASTM, 2020.

[90] K. Janatpour, L. Denning, K. Nelson, B. Betlach, M. MacKenzie, and P. Holland. *Comparison of X-ray vs. gamma irradiation of CPDA-1 red cells.* Vox Sanguinis, 2005. doi: https://doi.org/10.1111/j.1423-0410.2005.00699.x.

[91] JCGM. *International vocabulary of metrology – Basic and general concepts and associated terms (VIM).* JCGM WorkGroup 2, 2012. URL https://www.bipm.org/utils/common/documents/jcgm/JCGM_200_2012.pdf.

[92] JPAC. *X-ray irradiation of blood components.* Joint United Kingdom (UK) Blood Transfusion and Tissue Transplantation Services Professional Advisory Committee, 2008.

[93] M. Karamitros and al. *Modeling Radiation Chemistry in the Geant4 Toolkit.* Progress in Nuclear Science and Technology, 2011. doi: http://dx.doi.org/10.15669/pnst.2.503.

[94] I. Kawrakow, E. Mainegra-Hing, D. Rogers, F. Tessier, and B. Walters. *The EGSnrc Code System: Monte Carlo Simulation of Electron and Photon Transport.* National Research Council Canada, 2020. URL https://nrc-cnrc.github.io/EGSnrc/doc/pirs701-egsnrc.pdf.

[95] H. Khoury, E. da Silva Jr, K. Mehta, V. de Barros, V. Asfora, P. Guzzo, and A. Parker. *Alanine-EPR as a transfer standard dosimetry system for low energy X radiation.* Radiations Physics and Chemistry, 2015. doi: https://doi.org/10.1016/j.radphyschem.2015.03.015.

[96] R. E. Kirk and D. F. Gorzen. *X-ray tube with cylindrical anode.* US patent number US7346147B2, 2005.

[97] S. C. Klevenhagen, R. J. Aukett, R. M. Harrison, C. Moretti, A. E. Nahum, and K. E. Rosser. *The IPEMB code of practice for the determination of absorbed dose for x-rays below 300 kV generating potential (0.035 mm Al–4 mm Cu HVL; 10–300 kV generating potential).* Physics in Medicine and Biology, 1996. doi: https://doi.org/10.1088/0031-9155/41/12/002.

[98] G. F. Knoll. *Radiation Detection and Measurements.* Wiley, 2010. ISBN 978-0-470-13148-0.

[99] J. LaVerne. *OH Radicals and Oxidizing Products in the Gamma Radiolysis of Water.* Radiation Research, 2000. doi: https://doi.org/10.1667/0033-7587(2000)153[0196:oraopi]2.0.co;2.

[100] N. Ludwig. *Modification d'acides aminés et de protéines en milieu aqueux sous faisceau d'ions.* Ph. D Thesis - University of Strasbourg, 2018.

[101] Magnettech. *Manual and documentation MiniScope MS 5000 and MS 5000X EPR spectrometer with scientific grade performance.* Freiberg Instruments, 2019.

[102] K. Makuuchi and S. Cheng. *Chapter 10: Curing of Composites and Adhesives, from the book: Radiation Processing of Polymer Materials and its Industrial Applications.* Wiley, 2010. ISBN 9780470587690.

[103] K. Makuuchi and S. Cheng. *Radiation Processing of Polymer Materials and its Industrial Applications.* Wiley, 2012. doi: 10.1002/9781118162798.

[104] E. Malinen, M. Z. Heydari, E. Sagstuen, and E. O. Hole. *Alanine Radicals, Part 3: Properties of the Components Contributing tothe EPR Spectrum of X-Irradiated Alanine Dosimeters.* Radiation Research, 2003. doi: https://doi.org/10.1667/0033-7587(2003)159[0023:arppot]2.0.co;2.

[105] E. Malinen, E. A. Hult, E. O. Hole, and E. Sagstuen. *Alanine Radicals, Part 4: Relative Amounts of Radical Species inAlanine Dosimeters after Exposure to 6–19 MeV Electrons and10 kV–15 MV Photons.* Radiation Research, 2003. doi: https://doi.org/10.1667/0033-7587(2003)159[0149:arprao]2.0.co;2.

[106] E. Marchioni, J.-Y. Pabst, and F. Kuntz. *Characterization and application of two kinds of ESR dosimeters.* Radiation Physics and Chemistry, 2002. doi: https://doi.org/10.1016/S0969-806X(02)00199-8.

[107] T. Mastrangelo, A. G. Parker, A. Jessup, R. Pereira, D. O.-D. Vila, A. Islam, T. Dammalage, and J. M. M. Walder. *A New Generation of X Ray Irradiators for Insect Sterilization.* Journal of Economic Entomology, 2010. doi: https://doi.org/10.1603/EC09139.

[108] W. L. McLaughlin, J. C. Humphreys, B. B. Radak, A. Miller, and T. A. Olejnik. *The response of plastic dosimeters to gamma rays and electrons at high absorbed dose rates.* Radiation Physics and Chemistry, 1979. doi: https://doi.org/10.1016/0146-5724(79)90090-6.

[109] W. L. McLaughlin, M. M. Kosaníc, V. M. Markovíc, M. T. Nenadovíc, J. Holcman, and K. Sehested. *The kinetics of dye formation by pulse radiolysis of pararosaniline cyanide in aqueousorganic solution.* Risø National Laboratory, 1979. ISBN 87-550-0630-2.

[110] K. Mehta. *Chapter 2: Electron Accelerators for Radiation Sterilization, from the book: Trends in Radiation Sterilization of Health Care Products.* International Atomic Energy Agency, 2008. ISBN 978–92–0–111007–7.

[111] K. Mehta and A. Parker. *Characterization and dosimetry of a practical X-ray alternative to self-shielded gamma irradiators.* Radiation Physics and Chemistry, 2011. doi: https://doi.org/10.1016/j.radphyschem.2010.08.011.

[112] A. Miller. *Polystyrene Calorimeter for Electron Beam Dose Measurements.* Radiation Physics and Chemistry, 1995. doi: https://doi.org/10.1016/0969-806X(95)00361-Z.

[113] A. Miller and A. Kovacs. *Calorimetry at Industrial Electron Accelerators.* Nuclear Instruments and Methods in Physics Research B, 1985. doi: https://doi.org/10.1016/0168-583X(85)90156-9.

[114] A. Miller and A. Kovacs. *Application of Calorimeters for Routine and Reference Dosimetry at 4-10 MeV Industrial Electron Accelerators.* Radiation Physics and Chemistry, 1990. doi: https://doi.org/10.1016/1359-0197(90)90314-8.

[115] A. Miller, A. Kovacs, and F. Kuntz. *Development of polystyrene calorimeter for application atelectron energies down to 1.5 MeV.* Radiation Physics and Chemistry, 2002. doi: https://doi.org/10.1016/S0969-806X(01)00661-2.

[116] R. B. Miller. *Electronic Irradiation of Foods.* Springer, 2005. ISBN 978-0-387-28386-9.

[117] I. Miyagawa and W. Gordy. *Electron Spin Resonance of an Irradiated Single Crystal of Alanine: Second-Order Effects in Free Radical Resonances.* Chemical Physics, 1960. doi: https://doi.org/10.1063/1.1700912.

[118] L. MOUAWAD. *Monte Carlo simulations and a theoratical study of the damage induced by ionizing particles at the macroscopic scale as well as the moleculat scale.* Ph. D Thesis - University of Strasbourg, 2017.

[119] A. Mozumder and J. L. Magee. *Model of Tracks of Ionizing Radiations for Radical Reaction Mechanisms.* Radiation Research, 1966.

[120] V. Y. Nagy and M. F. Desrosiers. *A complex time dependence of the EPR signal of irradiated L-alpha-alanine.* Applied Radiation Isotopes, 1996. doi: https://doi.org/10.1016/0969-8043(96)00053-X.

[121] V. Y. Nagy, J. Puhl, and M. F. Desrosiers. *Advancements in Accuracy of the Alanine Dosimetry System. Part 2. The Influence of Irradiation Temperature.* Radiation Physics and Chemistry, 2000. doi: https://doi.org/10.1016/S0969-806X(99)00339-4.

[122] A. Nasreddine, F. Kuntz, and Z. E. Bitar. *Absorbed dose to water determination for kilovoltage X-rays using alanine/EPR dosimetry systems.* Radiation Physics and Chemistry, 2020. doi: https://doi.org/10.1016/j.radphyschem.2020.108938.

[123] G. L. Newton and J. R. Milligan. *Fluorescence detection of hydroxyl radicals.* Radiation Physics and Chemistry, 2006. doi: https://doi.org/10.1016/j.radphyschem.2005.10.011.

[124] P. Olko. *Calculation of the Relative Effectiveness of Alanine Detectors to X-rays and Heavy Charged Particles Using Microdosimetric One-Hit Detector Model.* Radiation Protection Dosimetry, 1999. doi: https://doi.org/10.1093/oxfordjournals.rpd.a032798.

[125] P. Olko. *The microdosimetric one-hit detector model for calculating the response of solid state detectors.* Radiation Measurements, 2002. doi: https://doi.org/10.1016/S1350-4487(01)00292-X.

[126] P. Olko and M. P. R. Wligorski. *Microdosimetric One Hit Detector Model for Calculation of Dose and Energy Response of Some Solid State Detectors.* Radiation Protection Dosimetry, 2002. doi: https://doi.org/10.1093/oxfordjournals.rpd.a006811.

[127] PANEL. *Guide on Establishing the Sterilisation Dose in ISO 11137 Part 2.* Panel on Gamma and Electron Irradiation, 2012. URL https://www.irradiationpanel.org/app/download/3781179/Guide+Establishing+Sterilisation+Dose+11137-2+2012.pdf.

[128] PANEL. *Guide on the establishment of the maximum acceptable dose (Dmax,acc) for a product.* Panel on Gamma and Electron Irradiation, 2016. URL https://www.irradiationpanel.org/app/download/5791309/Guide+establish+Dmaxacc.pdf.

[129] B. J. Parsons. *Chapter 3: Sterilisation of healthcare products by ionising radiation: principles and standards, fromthe book: Sterilization of biomaterials and medical devices.* Woodhead Publishing Limited, 2012. ISBN 978-1-84569-932-1.

[130] E. D. B. Pelowitz. *MCNPX Users Manual Version 2.7.0.* Los Alamos National Laboratory, 2011.

[131] G. Poludniowski, G. Landry, F. DeBlois, P. M. Evans, and F. Verhaegen. *SpekCalc: a program to calculate photon spectra from tungsten anode x-ray tubes.* Physics in Medicine and Biology, 2009. doi: https://doi.org/10.1088/0031-9155/54/19/n01.

[132] RADSOURCE. *RS3400 blood irradiator.* RADSOURCE. URL https://www.radsource.com/blood-irradiator-rs3400/.

[133] D. F. Regulla and U. Deffner. *Dosimetry by ESR Spectroscopy of Alanine.* Applied Radiation and Isotopes, 1982. doi: https://doi.org/10.1016/0020-708X(82)90238-1.

[134] S. Saglam, A. Cakir, and S. Kuter. *Blood irradiation, from the book: Modern Approaches To Quality Control.* InTech, 2011. ISBN 978-953-307-971-4.

[135] E. Sagstuen, E. O. Hole, S. R. Haugedal, and W. H. Nelson. *Alanine Radicals: Structure Determination by EPR and ENDOR of Single Crystals X-Irradiated at 295K.* Physical Chemistry A, 1997. doi: https://doi.org/10.1021/jp972158k.

[136] P. Sharpe. *Progress Report on Radiation Dosimetry at NPL.* National Physical Laboratory, 2003. URL https://www1.bipm.org/cc/CCRI(I)/Allowed/16/CCRI(I)03-14.pdf.

[137] P. H. G. Sharpe, A. Miller, J. P. Sephton, C. A. Gouldstone, M. Bailey, and J. Helt-Hansen. *The Effect of Irradiation Temperatures between Ambient and 80 ˚C on the Response of Alanine Dosimeters.* Radiation Physics and Chemistry, 2009. doi: https://doi.org/10.1016/j.radphyschem.2009.03.028.

[138] W.-G. Shin, J. Ramos-Mendez, B. Faddegon, H. N. Tran, Y. P. C. Villagrasa, S. Okada, M. Karamitros, D. Emfietzoglou, I. Kyriakou, M. C. Bordage, D. Sakata, S. Guatelli, H. J. Choi, C. H.Min, S. B. Lee, and S. Incerti. *Evaluation of the influence of physical and chemical parameters on water radiolysis simulations under MeV electron irradiation using Geant4-DNA.* Journal of Applied Physics, 2019. doi: https://doi.org/10.1063/1.5107511.

[139] A. Sinclair. *X-ray versus gamma irradiation of blood components for prevention of transfusion-associated graft versus host disease.* Technology Assessment Unit of the McGill University Health Centre (MUHC), 2011. URL http://www.mcgill.ca/tau/files/tau/IrradiatedBlood_FINAL_12Apr11.pdf.

[140] O. F. Sleptchonok, V. Y. Nagy, and M. F. Desrosiers. *Advancements in Accuracy of the Alanine Dosimetry System. Part 1. The Effects of Environmental Humidity.* Radiation Physics and Chemistry, 2000. doi: https://doi.org/10.1016/S0969-806X(99)00338-2.

[141] Y. S. Soliman, P. Pellicioli, W. Beshir, A. A. Abdel-Fattah, R. A. Fahim, M. Krisch, and E. Bräuer-Krisch. *A comparative dosimetry study of an alanine dosimeter with a PTW PinPoint chamber at ultra-high dose rates of synchrotron radiation.* Physica Medica, 2020. doi: https://doi.org/10.1016/j.ejmp.2020.03.007.

[142] J. W. T. Spinks and R. J. Woods. *An Introduction to Radiation Chemistry.* Wiley, 1990. doi: https://doi.org/10.1002/bbpc.19910950346.

[143] M. G. Stabin. *Radiation Protection and Dosimetry.* Springer, 2007. ISBN 978-0-387-49983-3.

[144] K. Tadokoro, H. W. R. S. Panzer, A. Chabanel, G. Santailler, T. Guérin, D. Socquet, B. David, J. L. Labrune, C. K. Lin, W. C. Tsoi, M. Letowska, J. Antoniewicz-Papis, J. Naniewicz, K. Dudziak, E. Lachert, M. Lozano, K. Schneider, E. L. Snyder, and M. H. Champion. *Problems with Irradiators.* Vox Sanguinis, 2009. doi: https://doi.org/10.1111/j.1423-0410.2009.01244.x.

[145] R. Tanaka, S. Mitomo, and N. Tamura. *Effects of Temperature, Relative Humidity, and Dose Rate on the Sensitivity of Cellulose Triacetate Dosimeters to Electrons and gamma Rays.* International Journal of Applied Radiation Isotopes, 1984. doi: https://doi.org/10.1016/0020-708X(84)90024-3.

[146] H. Tomita, M. Kai, T. Kusama, and A. Ito. *Monte Carlo simulation of physicochemical processes of liquid water radiolysis The effects of dissolved oxygen and OH scavenger.* Radiation and Environmental Biophysics, 1997. doi: https://doi.org/10.1007/s004110050061.

[147] S. Uehara and H. Nikjoo. *Monte Carlo Simulation of Water Radiolysis for Low-energy Charged Particles.* Radiation Reseach, 2006. doi: https://doi.org/10.1269/jrr.47.69.

[148] S. Uehara, H. Nikjoo, and D. T. Goodhead. *Cross-sections for water vapour for the Monte Carlo electron track structure code from 10 eV to the MeV region.* Physics in Medicine and Biology, 1993. doi: 10.1088/0031-9155/38/12/010.

[149] E. Waldeland and E. Malinen. *Review of the dose-to-water energy dependence of alanine and lithium formate EPR dosimeters and LiF TL-dosimeters e Comparison with Monte Carlo simulations.* Radiations Measurements, 2011. doi: https://doi.org/10.1118/1.3432567.

[150] E. Waldeland, E. Olaug, E. Sagstuen, and E. Malinen. *The energy dependence of lithium formate and alanine EPR dosimeters for medium energy x rays.* Medical Physics, 2010. doi: https://doi.org/10.1118/1.3432567.

[151] R. Watanabe and K. Saito. *Monte Carlo simulation of water radiolysis in oxygenated condition for monoenergetic electrons from 100 eV to 1MeV.* Radiation Physics and Chemistry, 2001. doi: https://doi.org/10.1016/S0969-806X(01)00195-5.

[152] S. Yamashita, G. Baldacchino, T. Maeyama, M. Taguchi, Y. Muroya, M. Lin, A. Kimura, T. Murakami, and Y. Katsumura. *Mechanism of radiation-induced reactions in aqueous solution of coumarin-3-carboxylic acid: Effects of concentration, gas and additive on fluorescent product yield.* Free Radical Research, 2012. doi: https://doi.org/10.3109/10715762.2012.684879.

[153] G. Zeng and J. McCaffrey. *The response of alanine to a 150 keV X-ray beam.* Radiation Physics and Chemistry, 2005. doi: https://doi.org/10.1016/j.radphyschem.2004.05.044.

[154] G. G. Zeng, M. R. McEwen, D. W. O. Rogers, and N. V. Klassen. *An experimental and Monte Carlo investigation of the energy dependence of alanine/EPR dosimetry: I. Clinical x-ray beams.* Physics in Medicine and Biology, 2004. doi: https://doi.org/10.1088/0031-9155/49/2/006.

[155] G. G. Zeng, M. R. McEwen, D. W. O. Rogers, and N. V. Klassen. *An experimental and Monte Carlo investigation of the energy dependence of alanine/EPR dosimetry: II. Clinical electron beams.* Physics in Medicine and Biology, 2005. doi: https://doi.org/10.1088/0031-9155/50/6/006.

Appendix A - Comparison of ion chamber measurements of absorbed dose to water between Aerial and NPL

Introduction

A comparison of ion chamber measurements of absorbed dose to water between Aerial and NPL was carried out at NPL in April 2019. The goal of this comparison was to measure absorbed dose to water with different ion chambers based on different codes of practices. For Aerial, a PTW Farmer 30013 ion chamber was used. Absorbed dose to water was measured according to the IAEA TRS 398 code of practice[58]. A PTW Farmer 30012 ion chamber was used by Dr. Anna Subiel (NPL) to measure absorbed dose to water based on the IPEMB[97] code of practice. More details about absorbed dose to water measurement formalisms, proposed by the IAEA TRS 398 and the IPEMB codes of practices, are presented in section 5.

X-ray irradiations

Ion chambers were irradiated using four different X-ray beam qualities, which details are listed in table 6.12. Each ion chamber was placed in a water equivalent phantom made of Solid Water® material (density 1.04 g/cm^3) at a depth of 2 cm. For each beam quality, five irradiations of 30 s each were carried out and the cumulated absorbed dose to water was measured. Figure 6.10 shows the experimental setup of irradiations.

Ambient temperature as well as atmospheric pressure were monitored throughout the entire irradiations. This is very important to correct the response of ion chambers due to the differences of current temperature and pressure conditions compared to ones during the calibration of each chamber. A monitoring ion chamber was placed just next to the beam shutter in order to ensure that the dose rate is stable throughout the entire irradiations. A correction of the dose rate could be applied to ion chamber measurements if a dose rate variability is observed.

	Added filtration			HVL_1		
HV [kV]	**Al [mm]**	**Cu [mm]**	**Sn [mm]**	**Al [mm]**	**Cu [mm]**	E_{eff} **[keV]**
135	1.2	0.27	0	8.8	0.5	58.9
180	1	0.54	0	12.3	1	75.8
220	0.9	1.4	0	16.1	2	101
280	1	0.26	1.5	20	4	168

TABLE 6.12: Details of beam qualities used for irradiations of Aerial and NPL's ion chambers.

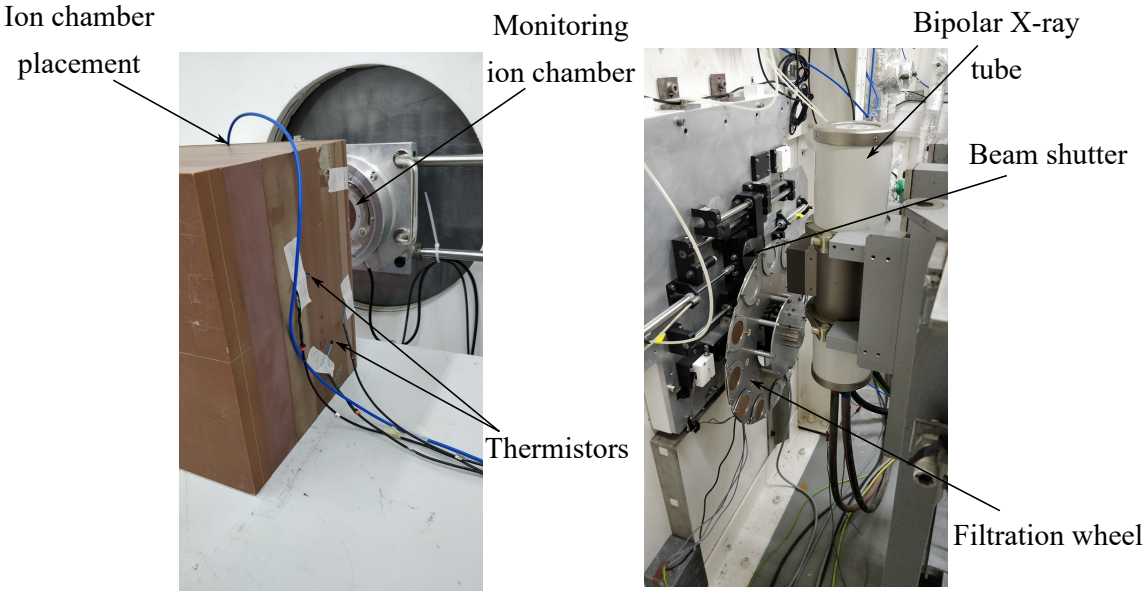

FIGURE 6.10: Left image: experimental setup of irradiations carried out at NPL. Right image: X-ray installation.

Measurements formalisms

According to the IAEA TRS 398 protocol, the absorbed dose to water at the reference depth in water, for and X-ray beam of quality Q is given by the following equation:

$$D_w^Q = M^Q \,.\, N_{D_w}^{Q_0} \,.\, k^{Q,Q_0} \tag{6.13}$$

where D_w^Q is the measured absorbed dose to water for the beam quality Q, M^Q is the corrected ion chamber reading expressed in Coulomb $[C]$, $N_{D_w}^{Q_0}$ is the calibration coefficient of the ion chamber for a reference quality Q_0 and is equal to 5.351 $\times$ 10^7 Gy/C, and k^{Q,Q_0} is the beam quality correction factor given by the calibration laboratory.

The ion chamber reading M needs to be corrected for the influence quantities: temperature and pressure, polarity and the electrometer calibration. Thus, the corrected ion chamber reading, for a certain beam quality Q can be expressed as such:

$$M^Q = M \,.\, k_{T,P} \,.\, k_{pol} \,.\, k_{elec} \tag{6.14}$$

where $k_{T,P}$ is the temperature and pressure correction factor, k_{pol} is the polarity correction factor and k_{elec} is the electrometer calibration factor. These factors are expressed as:

$$k_{T,P} = \frac{(273.2 + T)}{(273.2 + T_0)} \times \frac{P_0}{P} \tag{6.15}$$

with T being the irradiation temperature, T_0 is the irradiation temperature during calibration, P is the ambient air pressure during the irradiation and P_0 is the ambient air pressure during calibration.

$$k_{pol} = \frac{|M_+| + |M_-|}{2M} \tag{6.16}$$

where M_+ is the ion chamber reading when the positive polarization voltage is applied and M_- is the ion chamber reading when the negative polarization voltage is applied. According to the calibration certificate of Aerial's PTW 30013 ion chamber, the polarity effect was found to be less than 0.2 %, thus it was not taken into account for ion chamber reading correction. k_{elec} is given by the calibration laboratory, and for Aerial's PTW 30013 ion chamber $k_{elec} = 1.000 \pm 0.5\%$.

According to the IPEMB code of practice using the in-phantom method[97], the absorbed dose to water for an X-ray beam of quality Q is determined as follows:

$$D_{w,z=2cm} = M \,.\, N_k \,.\, k_{ch} \,.\, \left[\left(\frac{\bar{\mu}_{en}}{\rho}\right)_{w/air}\right]_{z=2,\phi} \tag{6.17}$$

where $D_{w,z=2cm}$ is the absorbed dose to water measured at a water depth of 2 cm for a beam quality Q, M is the ion chamber reading corrected for temperature and pressure differences, polarity and electrometer calibration, N_k is the air-kerma calibration coefficient for a beam quality Q, k_{ch} is the factor that accounts for the change in the response of the ion chamber between calibration in air and measurement in a water phantom and finally, $\left(\frac{\bar{\mu}_{en}}{\rho}\right)_{w/air}$ is the mass-energy absorption coefficient ratio, water to air, averaged over the photon spectrum at 2 cm depth of water and field diameter ϕ.

Results and discussion

Absorbed dose measurements with both ion chambers are listed in table 6.13. One can notice that there exists a difference between measured absorbed doses over the studied energy range. However, this difference decreases with increasing effective energy.

	HVL$_1$			**Aerial**		**NPL**		
HV [kV]	**Al [mm]**	**Cu [mm]**	E_{eff} **[keV]**	D_W **[Gy]**	u_{D_w} **[Gy]**	D_W **[Gy]**	u_{D_w} **[Gy]**	D_w^{Aerial}/D_wNPL
135	8.8	0.5	58.9	50.06	1.13	53.35	1.17	0.9383
180	12.3	1	75.8	75.48	1.71	77.12	1.70	0.9788
220	16.1	2	101	72.23	1.63	73.77	1.62	0.9791
280	20	4	168	68.32	1.54	69.35	1.53	0.9852

TABLE 6.13: Comparison of absorbed doses to water measured with both ion chambers.

During the study of the relative response of Aerial's alanine pellets to kV X-rays (section 5.3.1, alanine dosimeters were irradiated, at different absorbed doses, with two of NPL's X-ray beam qualities (135 and 280 kV). The absorbed dose to water that was delivered to alanine dosimeters was measured with NPL's ion chamber, yet, absorbed dose to water that was delivered to alanine pellets irradiated at Aerial was measured with Aerial's ion chamber. Thus, a correction factor needs to be applied to the absorbed dose to water measured by NPL's ion chamber, in order to have a more realistic comparison between results of irradiations carried out at Aerial and NPL. In other terms, the EPR response of irradiated alanine dosimeters needs to be compared, always, to absorbed dose to water measured with the same reference instrument, which in our study, is Aerial's ion chamber. Thus, the dose ratios, that are listed in the last column of table 6.13, were used as correction factors to the absorbed dose to water measured by NPL's ion chamber.

Abbas NASREDDINE

Alanine/EPR dosimetry for low to medium energy X-ray radiation processing control

Résumé

L'irradiation par des rayons X de faible à moyenne énergie devient de plus en plus une technique répandue qui remplace des irradiations réalisées par des sources radioactives pour différentes applications telles que l'irradiation du sang, les traitements Sterile Insect Technology et la décontamination des produits alimentaires.

Afin de s'assurer que la bonne dose est délivrée au produit, un dosimètre est placé sur ce dernier. Un type de dosimètres utilisé pour ces applications est le dosimètre à l'alanine, qui est équivalent à l'eau dans le cas des photons d'énergie supérieure à 200 keV.

Cette thèse présente l'utilisation de l'alanine pour le control et la validation des process d'irradiations réalisés avec des rayons X de faible à moyenne énergie, ainsi que différentes méthodes développées pour déterminer des facteurs correctifs à appliquer à la réponse de ce dosimètre. Ces méthodes reposent sur des mesures expérimentales, des simulations Monte Carlo et des calculs analytiques.

Mots clés : alanine/RPE, dose absorbée dans l'eau, simulations Monte Carlo, rayons X, dosimétrie.

Résumé en anglais

Nowadays, low to medium energy X-ray irradiators are starting to replace irradiators using radioactive sources, mainly in the fields of blood irradiations, Sterile Insect Technique and food irradiations.

A dosimeter is placed on the irradiated product to ensure that the desired dose is well delivered. One of the dosimetry systems that is used in radiation processing is the alanine/EPR dosimetry system. Alanine is considered as water equivalent, from a dosimetric point of view for photon energies that are higher than 200 keV. However, it loses its water equivalency for lower photon energies.

This thesis presents the use of alanine for the control and validation of irradiation processes performed with low to medium energy X-rays, as well as different methods developed to determine corrective factors to be applied to the response of this dosimeter. These methods are based on experimental measurements, Monte Carlo simulations and analytical calculations.

Keywords: alanine/EPR, absorbed dose to water, Monte Carlo simulations, X-rays, dosimetry.